Development of human induced pluripotent stem cell-derived neural cultures for seizure-liability testing

Alastair Iain Grainger

Doctor of Philosophy

Aston University

August 2020

Aston University

Development of human induced pluripotent stem cell-derived neural cultures for seizure-liability testing

Alastair Iain Grainger

Doctor of Philosophy

August 2020

Thesis Summary

Drug-induced seizure is a major reason for compound attrition during drug development, hence testing the potential of novel agents to induce such neurotoxic events is a vital process. Currently, *in vivo* and *in vitro* animal assays are used for seizure-liability studies; yet controversy over the relevance, efficacy and cost of these methodologies has led to interest in the development of human based models, for increased translatability and data extrapolation.

Human induced pluripotent stem cells (iPSCs) are a revolutionary platform for neurotoxicity testing. However, considerable variation in culturing protocols, growth media and analytical techniques exists, with no validated standard for drug-induced seizure-liability testing.

In this thesis, this cutting-edge iPSC technology, in combination with concurrent morphological and functional analysis has considered several methods for generation of a robust, reproducible human seizure-liability model, capable of responding to ionic and pharmacological stimuli.

Spontaneously differentiated neural cultures display electrical activity, but sporadic epileptiform activity, as observed with fluorescent calcium imaging. Moreover, weak functional activity and longevity and the absence of characteristic seizure-like activity was observed in isolated monocultures of neurons and astrocytes. Various co-culture protocols were developed and tested, displaying greater baseline activity, network interconnectivity and responses to pro-convulsant conditions than spontaneously differentiated cultures; highlighting the absolute requirement for both cell types to be present in culture. Final experiments introduced interneuronal populations to the established co-culture protocol; with preliminary results highly suggestive of providing a robust system which can be used for widespread seizure-liability assessment.

This thesis provides the first comparison of iPSC-derived culture methods for seizure-liability testing, whilst factoring in several variables which currently exist in the literature; including growth medium, duration of differentiation and methods to control cell proliferation. In addition, a proposal for a validatory panel of pro-convulsant conditions for the inclusion of human iPSC-derived platforms in safety pharmacology studies is presented.

Keywords: Seizure, Neuron, iPSC, Astrocyte, Co-culture

Acknowledgements

I would like to thank Professor Mike Coleman for his selfless scientific and incredibly generous financial support. Thank you for teaching me that cynicism and humour is just as important as knowledge. Dr. Eric Hill has been an invaluable mentor for both academic and pastoral support. Thank you for your enthusiasm, encouragement, constant willingness to chat and remarkable ability to come up with a million ideas. I must thank Dr. Rhein Parri for his brutal scientific mind and for terrifying me with all things electrophysiology and Dr. David Nagel for teaching me how to perform virtually every single technique.

This thesis would not have been possible if not for the Humane Research Trust, so I would like to thank them for giving us an audience before I was appointed and subsequently providing me with the funding to carry out this research.

Thank you, Marianne, James and Adele, whose collaboration and regular discussions over beer and chicken wings made everything better. Dave Jenkins, whose complete lack of maturity made the lab and office a genuinely outstanding place to be.

Without the financial and moral support from Mom, Dad and Nan, I would not have been able to complete my studies, so thank you for providing me with the opportunity to contribute to science and follow the ambitions from that picture I drew 20 years ago. Cal, thank you for proof-reading the thesis. Fez, you helped me in absolutely no way, so I shall not thank you, but I have to include you, as you are my brother.

Arguably most importantly of all, I would like to thank Greggs, McDonald's, Cadbury's, PG Tips and heavy metal for always being there for me.

Last, but in no way least, thank you Prilly. Thank you for your support, your encouragement and for sticking by me whilst I became a fat, miserable, poor student. You are a constant source of motivation and inspiration and hopefully now I can repay your patience and support and I eagerly await you to start your PhD journey so I can sit there and repeatedly laugh 'I told you so'.

Contents

List of Abbreviations

0 Mg	Zero-magnesium
4-AP	4-aminopyridine
ACM	Astrocyte-conditioned medium
aCSF	Artificial cerebrospinal fluid
ADR	Adverse drug reaction
AED	Anti-epileptic drug
AMPA	Amino-3-hydroxy-5-methyl-4-isoxalepropionic acid
AP	Action potential
AQP4	Aquaporin 4
AraC	Cytosine arabinoside
BBB	Blood-brain barrier
BDNF	Brain-derived neurotrophic factor
BMP	Bone morphogenetic protein
CBD	Cannabidiol
CNS	Central nervous system
CNTF	Ciliary neurotrophic factor
DAPT	N-[N-(3,5-Difluorophenacetyl)-L-alanyl]-S-phenylglycine t-butyl ester
DIV	Days *in vitro*
DMEM	Dulbecco's modified eagle medium
DS	Dravet's syndrome
EGFR	Epidermal growth factor
EPSC	Excitatory postsynaptic current
EPSP	Excitatory postsynaptic potential
ES	Embryonic stem cell
GABA	γ-aminobutryic acid
GABAR	GABA receptor
GDNF	Glia-derived neurotrophic factor
GEFS	Genetic epilepsy with febrile seizures
GIN	GABAergic interneuron
High K	High potassium
HS	Hippocampal slice
ICC	Immunochemistry
ILAE	International league against Epilepsy
iPSC	Induced pluripotent stem cell
MEA	Multi-electrode array
NMDA	N-methyl-d-aspartate
NPC	Neural progenitor stem cell
NSC	Neural stem cell
OS	Organotypic slice
PCR	Polymerase chain reaction
PDLO	Poly-d-l-ornithine
PDS	Paroxysmal depolarising shift
PEI	Polyethyleneimine
PIP3	Phosphatidylinositol (3,4,5)-triphosphate
PORN	Poly-l-ornithine
PSL	Pre-clinical seizure-liability
PTX	Picrotoxin
ROI	Region of interest
SCT	StemCell Technologies
SLE	Seizure-like event
TTX	Tetrodotoxin
VG	Voltage-gated
VPA	Sodium valproate
WIV	Weeks *in vitro*

List of Figures, Tables and Supplementary Video Files

Figures

Tables

Videos

Chapter 1

1: GENERAL INTRODUCTION

1.1 Introduction

The human brain is the most complex organ in the body, controlling our highest functions, as well as regulating myriad processes which incorporate the entire physiological system. The brain is vulnerable to damage by physical trauma and a multitude of injurious agents, including pathogens, pharmaceuticals and toxins. Physiological and anatomical protection and regulation for the controlled environment of the brain is provided by the blood-brain barrier (BBB). This consists of brain endothelia, astrocytes and pericytes, providing a system of tight endothelial junctions where selective permeability to water, some gases and fuel sources such as glucose and amino acids can be modulated (Daneman & Prat, 2015). The presence of glial cells in particular regulates the ionic and nutrient composition of fluid surrounding neurons (Prat et al., 2001). Should these mechanisms fail, brain functionality can be compromised. Indeed, seizure is one such severe neurological complication that can present from several circumstances, ranging from an adverse drug reaction (ADR), to infection or as a result of trauma (Koseki et al., 2014; Vaughan & Delanty, 2003).

1.2 Definitions: Seizures and Epilepsy

A seizure is the defining symptom of epilepsy, which is one of the most common chronic neurological disorders, estimated to affect 65 million individuals worldwide (Thurman et al., 2011). 'Epilepsy' encompasses multiple syndromes which predispose the individual to generation of epileptic seizures (Fisher et al., 2005). A seizure itself is defined as an abnormal, transient discharge of neurons in the brain (Fisher et al., 2005), and is broadly characterised by neuronal hyperexcitability and hypersynchrony (Jiruska et al., 2013). If an individual suffers a single event with no recurrence, they are said to have suffered a *seizure*. If multiple consecutive

and/or recurring seizures are experienced, the patient may be diagnosed with *epilepsy* (Scharfman, 2007).

In a clinical/research context, seizures are referred to as 'ictal events', with the period leading up to seizure termed *pre-ictal*, the period following seizure termed *post-ictal* and for individuals with recurrent seizures, the period between each event is known as the *interictal state* (Fisher et al., 2014). *Epileptogenesis* describes the processes which render a healthy system capable of generating seizures, whilst also establishing the condition, hence making recurrent seizures more likely (Blauwblomme et al., 2014; Pitkänen, 2010). *Ictogenesis* refers to the transition between the interictal state to the ictal state in an already hyperexcitable brain (Dichter, 2009). This thesis makes frequent reference to 'seizurogenesis', which in this context describes the generation of seizures in reference to pharmacological/ionic stimuli.

Patients suffering from seizures experience different effects depending on the brain region involved. The International League Against Epilepsy (ILAE) classify seizures into four categories: focal, generalised, those of an unknown onset (formerly classified as epileptic spasms) and unclassified – where insufficient data exists to categorise the seizure (Fisher et al., 2017). Focal seizures originate in neuronal networks in one part of the cerebral hemisphere, whereas generalised seizures begin and spread bilaterally to incorporate the entire brain, explaining the variety of symptoms and often loss of consciousness which results (Stafstrom & Carmant, 2015). It is worth highlighting that the classification of seizures and epilepsy is a very dynamic process, with revisions to the terminology published almost annually. An expanded description of the most recent classification is shown in Figure 1.1. Symptoms of seizures may include changes in cognition, paraesthesia, or the experience of flashing lights or unusual odours. Convulsions are commonly observed, which can be accompanied by various combinations of muscle rigidity (tonic) and jerking limb (clonic) activity. Atonic seizures, also called 'drop attacks' are associated

with a sudden loss of muscle tone, with patients often collapsing. They are characteristic of focal seizure types and more common in the adult population (Baraldi et al., 2015).

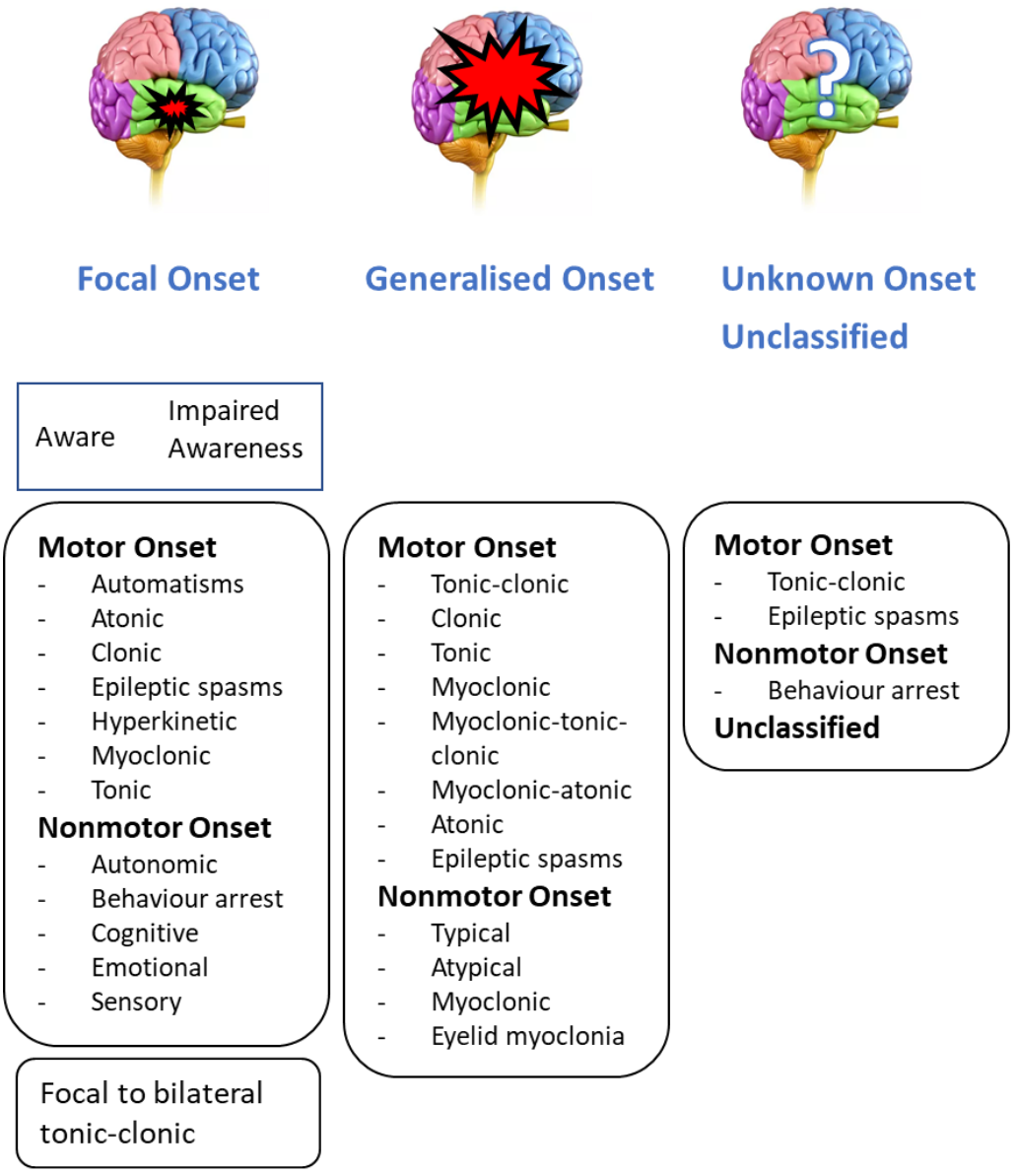

Figure 1.1: ILAE classification of seizures and their major symptoms. Adapted from Fisher et al., (2017).

Although seizure is the defining symptom of the epilepsies, only about 25% of patients who suffer seizure have an epilepsy syndrome (Stasiukyniene et al., 2009). The remaining patients suffer seizures from the major causes listed above, as well as neonatal occurrences amongst

infants. These seizures may be described as *provoked* or *acute symptomatic*, as they are not the result of established or enduring brain alterations; but rather occur in an acute and transient manner (Fisher et al., 2005; Thurman et al., 2011). The potential severity of induced seizures makes them an important metric for the necessity for predictive neurotoxicity assays.

1.3 Mechanisms of Seizure Induction

Seizurogenesis falls under the broad umbrella of epileptogenesis – modifications in the brain to support seizure development. It is likely that epileptogenic mechanisms occur before, throughout and following seizurogenesis to support seizure propagation, leading to changes within the brain which are receptive to seizurogenesis before a seizure occurs (Blauwblomme et al., 2014). However, neither of these processes are entirely understood and both seizurogenesis and epileptogenesis can arise from multiple mechanisms, which adds increased complexity. On the most elementary level, one can consider seizurogenesis to be the result of perturbation to the delicate balance between neuronal excitation and inhibition, mediated by ion flux and ion channels. Indeed, suppressing inhibition and enhancing excitation are both criteria for epileptic discharges (Lerche et al., 2001).

1.3.1 Healthy neuronal activity

Neurons are excitable cells. At rest, a membrane potential of roughly -70 mV is established by the ionic gradient which exists between sodium (Na^+), potassium (K^+), chloride (Cl^-) and organic cations in the cellular environment. This resting membrane potential (RMP) arises from higher intracellular K^+ and higher Na^+ in the extracellular space and is maintained by a series of voltage-gated channels, the sodium-potassium ATPase active transporter (Na^+-K^+ pump) (Chrysafides & Sharma, 2019) and leak channels, of which the neuron has considerably more, allowing the passage of K^+ (Lesage, 2003). When excited, the membrane potential is depolarised, primarily due to the opening of sodium channels and influx of Na^+ to reach the action potential (AP) firing threshold. The repolarisation phase involves the efflux K^+ to return to the RMP and prevent repetitive stimulation (Raimondo et al., 2015).

As the Na^+-K^+ pump plays such a vital role in maintaining resting neurons, if dysfunctional, the RMP may not be established. As a result, the neuron can depolarise to the point where the electrochemical balance becomes unstable and hence, neurons become hyperexcitable (Funck et al., 2015). Indeed, it has been shown that partial inhibition of the Na^+-K^+ pump induces epileptiform burst-firing (Vaillend et al., 2002). Dysfunction of the Na^+-K^+ pump may also be associated with provoked neonatal seizures in infants, based on evidence that in rodents, the development of this protein is delayed after birth. It may be possible that the same process, or alteration to the corresponding protein occurs in humans who are predisposed to neonatal seizure (Scharfman, 2007).

1.3.2 Potassium

Neuronal cells are highly permeable to K^+ movement through membrane ion channels, making K^+ the principle regulator of neuronal excitability. Action potentials lead to increased extracellular potassium concentrations ($[K^+]_e$), which are returned to a resting state following the opening of potassium channels, the Na^+/K^+ pump and glial cell K^+ uptake (Larsen et al., 2016). Normally, the accumulation of K^+_e is prevented to avoid widespread depolarisation, which can lead to increased firing and burst-firing, facilitating seizurogenesis. Exceeding an extracellular concentration of 2.7 – 3.5 mM can have effects on either nerve terminals (whose depolarisation results in neurotransmitter release) or neurons themselves (whose depolarisation leads to AP discharge). Mild depolarisation increases excitability by moving towards the more positive firing threshold. If the $[K^+]_e$ exceeds 10 mM, 'persistent', slowly inactivating Na^+ currents increase the likelihood of recurrent seizure (Somjen, 2002). Baseline K^+_e has been shown to be approximately 25-fold lower than intracellular K^+, which means a small efflux of K^+ can generate large changes in the transmembrane K^+ gradient (Jiang & Haddad, 1991) and furthermore, significant membrane depolarisation (Lesage, 2003).

As K^+ plays such an integral role in excitability and the movement of K^+ is enabled by various channels and transporters, it is not surprising that mutations in and dysfunction of ion channels

can directly affect brain excitability and induce seizure activity (Steinlein et al., 2001). Potassium channels are the most widely distributed neuronal and glial ion channels in the nervous system, comprising voltage-gated (VG), calcium-dependent and sodium-activated channels (de Curtis et al., 2018). VG channels are involved in repolarisation following AP (Gutman et al., 2005), calcium-dependent are sensitive to changes in intracellular [Ca^{2+}] following AP and are involved in setting the RMP (Marrion & Tavalin, 1998) and sodium-activated potassium channels mediate the outward current, regulating neuronal excitability during repetitive AP's (Bhattacharjee & Kaczmarek, 2005). Unregulated activity in any of these channels can provide an ionic basis for the generation of hyperexcitability and repetitive AP discharge, which is typical of a seizure. Indeed, the inherited epileptic syndrome 'benign familial neonatal convulsions' is associated with the mutation of two potassium channels: *KCNQ2* and *KCNQ3*, which normally contribute to repolarisation of the neuron during action potentials (Lerche et al., 1999).

Whilst perturbation of normal ionic gradients can lead to seizurogenesis, seizures themselves also affect the ionic environment and can generate conditions which promote seizure recurrence. During seizure, $[K^+]_e$ increases and extracellular sodium and calcium ($[Na^+]_e$/$[Ca^{2+}]_e$) decreases, due to neuronal release and uptake, respectively (Feldberg & Sherwood, 1957; Somjen, 2002). This can create a cycle of depolarisation, promoting further AP discharge from continuous excitation (Sypert & Ward, 1974). Experiments with canine and feline models as early as the 1940's showed the seizurogenic effects of elevated K^+_e and that neurons release excess K^+ during electrical stimulation and seizure (Cicardo & Torino, 1942; Feldberg & Sherwood, 1957). The accumulation of K^+_e as a result of seizure is undisputed, however, whether this alone causes seizure is a topic of debate. The 'potassium accumulation hypothesis' theory (Fröhlich et al., 2008) suggests that seizure-induced K^+_e accumulation triggers the onset of seizure and leads to a positive-feedback cycle, only slowed when a depolarisation block occurs. Depolarisation blocks are a result of Na^+ channels becoming inactivated following severe depolarisation (Raimondo et al., 2015). Irrespective of the debate, it is widely accepted that K^+

is an integral ion in maintaining neuronal ionic homeostasis and conditions of hyperexcitability. In Chapter 4, experimental means of modulating K^+_e are discussed in detail.

1.3.3 Sodium

Alongside the undisputed importance of K^+ flux, neurons would be unable to initiate or propagate AP's without Na^+. Similarly to K^+ flux, Na^+ currents are established by the passage of Na^+ via a series of ion channels which open, close or inactivate, depending upon the membrane potential. Na^+ currents can participate in epileptiform firing (Stafstrom, 2007) due to their effect on membrane depolarisation and hence, excitability. Such effects can result through modulation of sodium ion channels. Decreased inactivation and increased activation and opening times, for example, would all support the influx of Na^+ and the subsequent continued depolarisation of the neuron.

Mutations in three genes encoding sodium channels (*SCN1A, SCN2A* and *SCN1B*) can result in various epilepsy syndromes (Escayg & Goldin, 2010). Mutations to *SCN1/2A* leads to genetic epilepsy with febrile seizures plus (GEFS+), characterised by febrile seizures in infants, persisting beyond 6 years of age (Wallace et al., 1998). In addition, mutations to *SCN1B* have also been reported in GEFS+ patients (Wallace et al., 2001).

Dravet's syndrome (DS, Severe myoclonic epilepsy of infancy) is another inherited epilepsy syndrome, the hallmarks of which include febrile seizures during the first year of life and impaired psychomotor development (Dravet & Bureau, 1981). Furthermore, seizures observed in DS often do not respond to anticonvulsant treatment (Lossin, 2009). Mutations in *SCN1A* are observed in 33%-100% of patients with DS (Tonekaboni et al., 2013). Mutations of sodium channels have been shown to promote a gain-of-function effect, leading to hyperexcitability of neurons, however whether this mechanism is consistent between mutations to other sodium channels is yet to be determined (Lossin, 2009).

In combination with section 1.3.2, mutations to sodium-activated potassium channel 'KCNT1' can result in severe epileptic encephalopathies, via faster recovery from AP discharge, leading to rapid firing (Quraishi et al., 2019).

1.3.4 Chloride

Chloride (Cl^-) is the most abundant negatively charged ion in the body, and its homeostasis is regulated predominantly by membrane Cl^- channels and transporters, particularly the Cl^- extruder: potassium-chloride co-transporter (KCC2) (Chamma et al., 2012). Cl^- in the CNS plays crucial roles in neurotransmitter uptake and moderating neuronal excitability by determining the responses of the inhibitory neurotransmitters γ-aminobutyric acid (GABA) and glycine on post-synaptic cells (Ben-Ari et al., 2007). In particular, Cl^- modulates inhibitory responses from activation of $GABA_A$ receptors to reduce neuronal excitability via the maintenance of hyperpolarising GABAergic transmission (Di Cristo et al., 2018; Rahmati et al., 2018). With relevance to epilepsy, KCC2 mutations have been found to attenuate Cl^- movement and hence, impairs inhibition, leading to neuronal excitation (Duy et al., 2019).

1.3.5 Neurotransmitter involvement in seizure

Synaptic transmission involves the release of neurotransmitter from a pre-synaptic nerve terminal across a synapse to receptors on the post-synaptic neuronal membrane. Neurotransmitters are an absolute requirement for brain function at every level, hence they can play integral roles in seizurogenesis. Glutamate and GABA are the major excitatory and inhibitory neurotransmitters in the mammalian CNS, respectively.

1.3.5.1 Glutamate and excitation

Glutamate is the main excitatory neurotransmitter in the human brain. Put simply, depolarisation (excitation) is mediated by synaptic currents resulting from glutamatergic transmission. Glutamate and its associated receptor agonist subtypes can stimulate a variety of ionotropic and metabotropic receptors to exert its excitatory effects. The N-methyl-D-aspartate (NMDA) and amino-3-hydroxy-5-methyl-4-isoxazolepropionic acid (AMPA) receptors are

particularly important in seizure and activation of multiple NMDA receptors (NMDAR) further depolarises the cell and promotes increased Ca^{2+} influx (Vaughan & Delanty, 2003). At resting potential, NMDAR are blocked by magnesium (Ruppersberg et al., 1994), which can be rapidly removed via depolarisation (Mayer et al., 1984). Increased depolarisation during seizure can lead to increased NMDAR activation and hence, NMDA and AMPA receptor antagonists are well-known to suppress seizurogenesis (Blauwblomme et al., 2014). AMPA receptor activation enables K^+ and Na^+ flux into the cell, generating a fast excitatory postsynaptic current (EPSC). The flow of ions from the EPSC generates an excitatory postsynaptic potential (EPSP), which increases the likelihood of reaching the threshold for AP firing. EPSCs are also generated by NMDA and kainate receptor agonism, however, the kinetics of NMDAR pore unblocking are complex and consist of both rapid and slower components, resulting from the magnesium pore block (Vargas-Caballero & Robinson, 2003). The strength of the EPSCs can vary between receptors, however, small EPSCs can integrate excitatory inputs over a large time period so could still lead to AP discharge (Lerma, 2003).

1.3.5.2 GABA and inhibition

γ-aminobutyric acid (GABA) is the principle inhibitory neurotransmitter and as such, plays an important role in counterbalancing neuronal excitation and excessive AP discharge. GABA antagonism is a major mechanism of seizurogenesis, as the inhibition of GABA's inhibitory mode of action results in excitation. This is supported by common GABA agonists such as benzodiazepines and barbiturates, which are known to be anti-convulsive and function by enhancing the inhibitory effect of GABA (Wong et al., 2010). Similarly, antagonistic agents which block GABA synthesis (such as isoniazid) are documented pro-convulsants (Treiman, 2001). In this context, GABA acts upon either the $GABA_A$ or $GABA_B$ receptor (GABAR), regulating Cl^- entry or increasing K^+ conductance, respectively. $GABA_A$ are postsynaptic receptors, whereas $GABA_B$ are found presynaptically (Bromfield et al., 2006). GABAergic transmission mostly results in hyperpolarisation (making AP discharge less likely) and GABAergic synapses are most abundant

in GABAergic interneurons (discussed below). Cl^- currents hyperpolarise neurons as they enter the cell, reducing the likelihood that threshold will be reached for AP discharge. Stimulation of metabotropic $GABA_B$ receptors decreases Ca^{2+} entry to the presynaptic cell, reducing neurotransmitter release (Treiman, 2001).

1.3.6 Interneurons and their role in seizure

Despite the seemingly well-understood evidence of inhibitory neurotransmission, the effects of $GABA_A$ receptor-mediation are paradoxical. GABAergic interneurons (GIN) are a diverse subset of neurons, widely expressed throughout the CNS, which function predominantly as inhibitory cell types. However, depending on the brain region and disease conditions, the effects of GIN may also be excitatory (Snodgrass, 1992; Ye & Kaszuba, 2017). Whilst interneurons hyperpolarise roughly 80% of pyramidal neurons in the cortex (Benes & Berretta, 2001), the remaining 20% become depolarised (Blauwblomme et al., 2014; Neske et al., 2015), challenging the popular tenet that GIN are consistently inhibitory in nature.

The past decade has seen an increase in evidence that $GABA_A$ receptor-mediated mechanisms and GIN in particular, are involved in seizurogenesis (Huberfeld et al., 2015) and that the onset of seizure correlates with reduced neuronal firing and enhanced GABAergic interneuronal network activity (Librizzi et al., 2017). Moreover, in the absence of ionotropic glutamatergic transmission, enhanced GABAergic activity alone is sufficient to result in epileptiform activity in *in vitro* experimental slice preparations and synchronised burst firing of pyramidal neurons (Lévesque et al., 2016; Uusisaari et al., 2002). Interestingly, depolarising effects of GABA are seen in developing cortical networks alongside chronic epileptic brains, due to reduced capability of the neuronal Cl^- transporter KCC2 (discussed above), which renders neurons with a high intracellular chloride concentration. A different transporter (NKCC1), imports Cl^- into the immature cells, resulting in Cl^- efflux, which depolarises the membrane and leads to excitation (Wang & Kriegstein, 2009). During seizure, excessive inhibitory currents may overload KCC2's

function to maintain low intracellular [Cl^-], resulting in depolarising, $GABA_A$ receptor-mediated potentials.

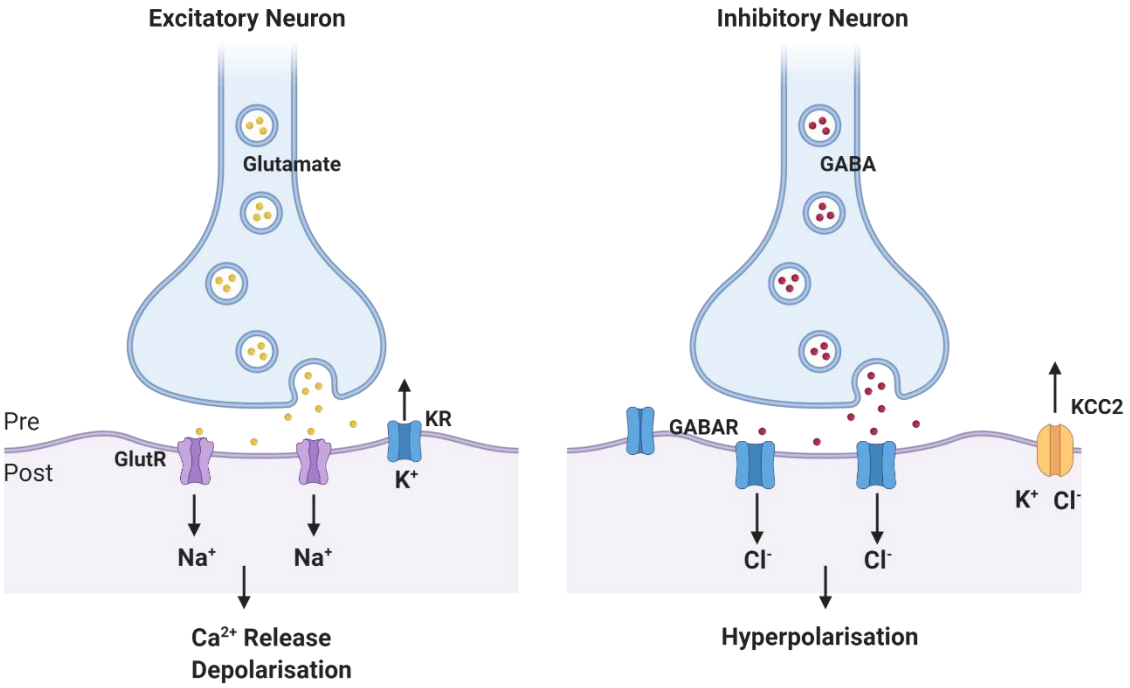

Figure 1.2: Ion transmission at excitatory and inhibitory synapses. Glutamate release from excitatory presynaptic cells binds to various glutamate receptors (GluR) on the postsynaptic membrane, resulting in sodium influx and subsequent calcium increase and depolarisation. Potassium efflux occurs via potassium receptors (KR), leading to an overall increase in potential in the postsynaptic cell. GABA release from inhibitory neurons binds $GABA_A$ subtype receptors (GABAR), leading to chloride influx, resulting in a decrease in membrane potential and hyperpolarisation. The potassium chloride transporter 2 (KCC2) facilitates flux of chloride and potassium to restore baseline potential.

Whilst the precise mechanisms of GIN-mediated excitatory effects are not entirely understood, several suggested mechanisms have been postulated. Firstly, GIN can excite post-synaptic neurons due to the raised reversal potential of GABAR in post-synaptic cells. Secondly, the continuous activity of GIN could lead to reduction in GABA levels, preventing their inhibitory mode of action on excitatory pyramidal cells. Excessive depolarisation of GIN can result in a depolarisation block and subsequent failure to fire AP (Trevelyan & Schevon, 2013). Thirdly, GIN can synchronise network activity during seizure activity and in addition, GIN can disinhibit other

GIN, leading to excitation (Ye & Kaszuba, 2017; Zhu et al., 2018). Furthermore, GABAR antagonism results in more rapid spread of seizure activity suggesting interneurons provide an inhibitory restraint on seizure propagation (Wenzel et al., 2017) and breakdown of feed-forward inhibition occurs during the spread of seizure activity across the cortex (Trevelyan et al., 2006, 2007), which is likely due to membrane depolarisation of GIN (Cammarota et al., 2013). As such, the roles which GIN function and dysfunction play in seizure are myriad, complex and not fully understood.

Synchronisation of neurons is essential for seizure activity, and interconnectivity between neuronal subtypes in the cortex supports network synchronisation, mediated by GIN (Magloire et al., 2019). It has been demonstrated that synchronisation and hyperexcitation observed in seizures can result from altered GIN activity (Avoli & de Curtis, 2011; Dinocourt et al., 2003; Hedrich et al., 2014). Pyramidal cells in all layers of the cortex project locally and distally to other pyramidal cells, as well as GIN. Each cortical neuron receives thousands of excitatory synaptic inputs, and as functionally related areas are particularly highly interconnected, neuronal activity can spread very rapidly between these densely unified regions (McCormick & Contreras, 2001). GIN such as the basket cells innervate pyramidal neurons and as they are distributed throughout the cortex and cerebellum and are multipolar, they connect to many surrounding cells. As a result, discharge of a single GIN can result in the synchronous hyperpolarisation of the surrounding population of pyramidal cells and characteristic epileptiform activity.

The effects of GIN-mediated seizure activity can also affect ion currents. As the inhibition depletes and the cell begins to depolarise, currents such as the T-type Ca^{2+} current become active, which are regarded as pivotal mechanisms underlying the generation of neuronal burst-firing (Cain & Snutch, 2013). Whilst relatively inactive at RMP, hyperpolarisation relieves inhibition and influx of Ca^{2+} occurs. T-type Ca^{2+} channels require only low-threshold depolarisations for bursts of action potentials and are the first to respond to small

depolarisations, with their activity leading to further depolarisation of the cell. Indeed, blockade of the voltage-gated Ca^{2+} channel can prevent burst-firing activity of neurons, which normally result in seizure. In fact, this is the mechanism of action of ethosuximide, which is used as an anticonvulsant (Leresche et al., 1998). Finally, gap junctions facilitate low-resistance movement of current between cells; particularly between GIN in the cortex and other GABAergic cell types. This promotes rapid and effective synchronisation between local networks (Scharfman, 2007). In summary, the roles of interneurons in controlling and indeed, in generating seizures are a highly significant complicating factor in epilepsy and seizure, hence, their inclusion is essential for a heterogenous epileptic model.

1.3.7 Astrocytes and their role in seizure

Many studies of seizures describe properties of excitatory and inhibitory neurons and the resulting networks which form from their interaction. However, glial cells such as astrocytes, oligodendrocytes, microglia and Schwann cells perform vital tasks in the nervous system. It has been shown that the neuron:glia ratio varies considerably throughout areas of the brain (von Bartheld et al., 2016). In the cerebellum, glial cells make up only 18.9% of cells, whilst in the rest of brain this figure can increase to 91.7% (Herculano-Houzel, 2014). Despite this very significant quantity, it is only relatively recently that astrocytes have been studied in sufficient depth to appreciate the full diversity of their roles in the brain and seizure.

There are several ways in which astrocytes are actively involved in transmission at synapses and consequent excitation of neurons and as such, their typical neuronal-supportive function is to protect against hyperexcitation and seizure activity (Volman et al., 2012). Excessive glutamatergic excitation of neurons can cause excitotoxicity, resulting in damage to, and the eventual death of the neuron (Maragakis et al., 2004). Astrocytes take up excess ammonia and glutamate from the synaptic cleft via the GLT1 (EAAT2) transporter (Maragakis et al., 2004) and use glutamine synthetase to convert it to glutamine via a condensation reaction (Choi, 1987). Inhibition of astrocytic glutamine synthetase has been implicated in multiple neurodegenerative

disorders, including epilepsy (Eid et al., 2013). Furthermore, GLT1 knockout rats have an increase in neuronal cell death and in extracellular glutamate concentration, characteristic of excitotoxicity (Rothstein et al., 1996). Alongside glutamate, astrocytes can affect extracellular GABA levels. Increase of GAT3, the astrocytic GABA transporter, reduces extracellular GABA prior to seizure onset (Lee et al., 2006).

In addition to neurotransmitter levels, healthy astrocytes also regulate the extracellular concentration of Na^+, K^+, Cl^- and Ca^{2+}, determining the reversal potentials of these ions in neighbouring neurons. Indeed, alteration to the reversal potential has a direct effect on cell excitability (Annunziato et al., 2013). In particular, astrocyte membranes are highly permeable to K^+, as they contain many potassium channels along with sodium/potassium ATPases, which together normally prevents hyperexcitability of neurons (Carmignoto & Haydon, 2012). In rodent models, these transporters are responsible for maintaining low extracellular K^+ levels and importantly, restore resting levels of K^+ following epileptiform activity (Coulter & Steinhäuser, 2015). Dysfunction of astrocytic uptake of extracellular K^+ and astrocytic uncoupling can lead to the generation and propagation of seizure (Bedner et al., 2015).

Interestingly, astrocytes can regulate osmotic homeostasis via selective membrane water channels called aquaporins (AQP). AQP4 is highly expressed in the end-feet of astrocytes, surrounding capillaries and the BBB, and is highly abundant at sites of fluid transport (Hubbard et al., 2015). There is an increasing body of evidence for the ability of astrocytes to affect K^+-mediated epileptiform activity by regulating extracellular cerebrospinal fluid (CSF) volumes. This was hypothesised following the observation that astrocytic AQP4 is often co-localised with Kir4.1 potassium channels (Nagelhus et al., 2004) and that in AQP4 knockout mice, decreased water permeability (Solenov et al., 2004) and significantly impaired K^+ clearance was reported (Binder et al., 2006).

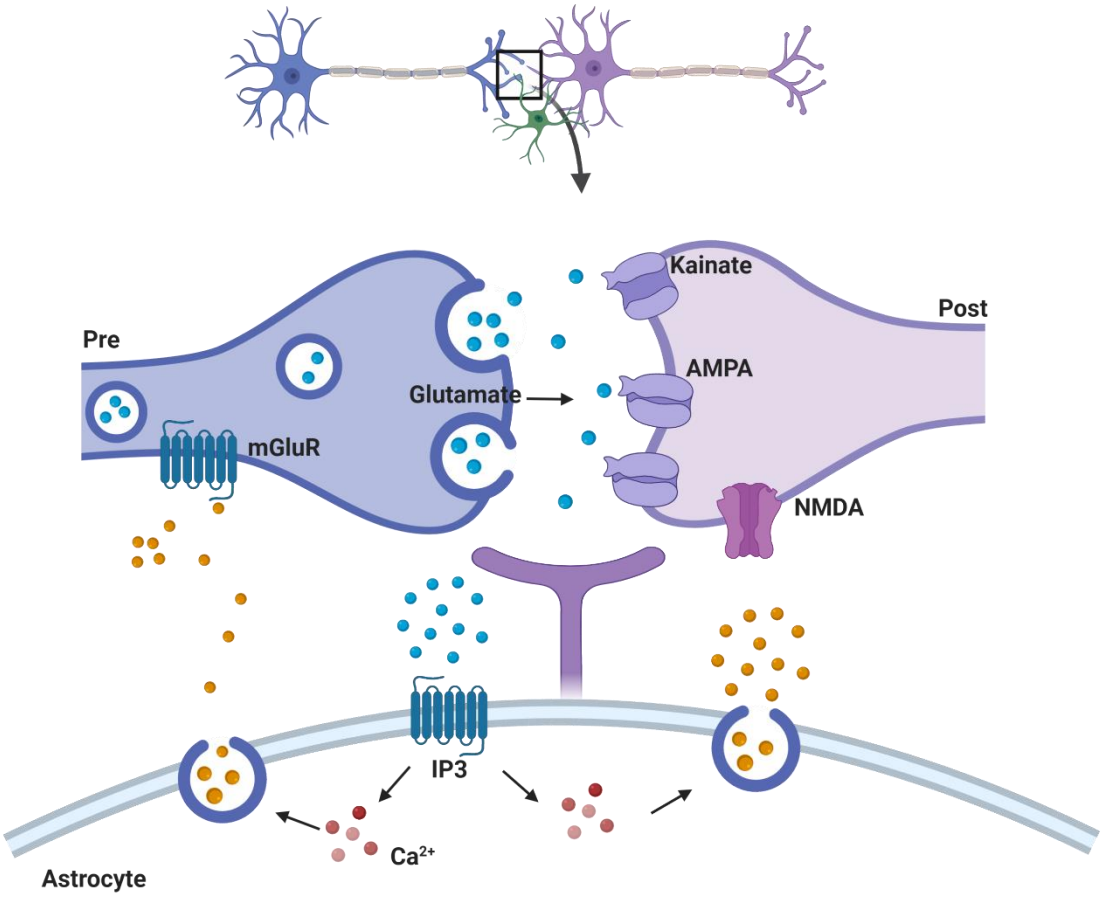

Figure 1.3: Excitatory tripartite synapse and the role of astrocytes in excitability. The tripartite synapse is formed between the pre and postsynaptic nerve terminals and the close proximity of astrocytic end feet. Upon depolarisation and release of neurotransmitter at the presynaptic terminal (blue dots), some glutamate can diffuse to metabotropic glutamate receptors (mGluR) on astrocytes. Stimulation of astrocytic mGluR results in elevation of inositol trisphosphate (IP3) and subsequent calcium release (pink dots). This increased astrocytic calcium can cause release of astrocytic glutamate (orange dots). Release of intracellular astrocytic calcium can lead to glutamate release, affecting presynaptic mGluR and postsynaptic NMDA receptors, enhancing presynaptic release or postsynaptic excitability, respectively.

Moreover, in these knockout models, the duration of seizure activity was increased (Binder et al., 2006). The evidence suggests that astrocytic regulation of fluid in the extracellular environment can lead to depolarisation of astrocytes from K^+ accumulation, activating a sodium-bicarbonate cotransporter, which leads to a surge in intracellular osmolarity. As a result, water intake into the astrocytes via AQP4 increases, leading to swelling of the cell and shrinkage of its

surrounding extracellular space. The decrease in extracellular space reduces the distribution area for extracellular K^+, lowering the seizure threshold and promoting excitability (Volman et al., 2012).

Astrocytes can release glutamate and ATP via calcium-dependent gliotransmission, which in turn, can regulate neuronal activity (Hubbard & Binder, 2016), including synchronisation of neurons in the hippocampus (Angulo et al., 2004). Furthermore, application of ATP analogues has been shown to evoke neuronal excitation and promote seizure activity (Rassendren & Audinat, 2016). Alongside gliotransmitter release and ion buffering and uptake, connectivity between astrocytes and neurons can influence seizure dynamics. It is now accepted that neurons and astrocytes communicate bidirectionally, and that their interaction is achieved by close physical proximity of the pre-synaptic membrane, post-synaptic membrane and glia, termed the 'tri-partite synapse' (Figure 1.3). Whilst neurons are synaptically connected, astrocytes communicate through gap junctions, via calcium signalling, which enables them to redistribute neuro/gliotransmitters and ions released by neurons in the tripartite synapse (Perea et al., 2009). During preictal activity, astrocytes are highly active and display synchronised activity across large brain distances, independent of neuronal activity. In addition, glial activity surges during seizurogenesis, and consequently produces a strong increase in neuronal network activity (Nikolic et al., 2019) via a rapid increase in extracellular glutamate and gap junction signalling (Diaz Verdugo et al., 2019). The roles of astrocytes in a healthy system and in seizure activity warrant their inclusion in studies of disease and epileptogenesis. Their ability to influence neuronal excitation and integrate into healthy and epileptic networks highlights their absolute relevance to seizure activity and may provide previously unconsidered contributions to initiation and propagation of seizures.

1.4 Anti-epileptic drugs

Despite the prevalence of epilepsy globally, the same anti-epileptic drugs (AED) have been used for several decades (Dichter & Brodie, 1996). Although there are roughly 25 AED licensed for clinical use, many patients find themselves on a combination of established medication, termed 'rational polytherapy', as roughly 30% of patients have drug refractory epilepsy (Perucca et al., 2007). In turn, rational polytherapy increases the occurrence of ADR. Recent years have seen the development and clinical use of numerous new AEDs, which are superior in their reduction of ADR and teratogenicity and have increased target specificity. However, despite these obvious benefits, the new classes of drugs offer no improved anti-epileptic effect compared with traditional AEDs (Hanaya & Arita, 2016), even though newer AEDs presented with novel mechanisms of action (Shih et al., 2013).

Many first-generation agents, including phenytoin and benzodiazepines, modulate sodium channels to prevent neuronal depolarisation and excitability, or function as GABA agonists to increase inhibition, respectively. Whilst new agents would seem a welcome inclusion to treatment of seizure and epilepsy, Perampanel (Fycompa), a clinically approved novel inhibitor of AMPA-induced intracellular Ca^{2+} increases, has potential for abuse and addiction (Shih et al., 2013). There exists a delicate balance between anti-epileptic effect and ADR for even the newer AEDs, suggesting that the development of AEDs with a high safety profile that is also efficacious is a significant challenge.

A compound gaining significant media attention and notoriety is cannabidiol (CBD), that has demonstrated anticonvulsant properties via modulation of G protein-coupled receptor 55 at excitatory synapses. It is believed to reduce intracellular Ca^{2+}, alongside adenosine-mediated signalling (Nichols & Kaplan, 2020). Its notoriety arises from its derivation from cannabis plants, currently categorised as a Class B controlled substance in the UK, however, CBD can also be produced synthetically and does not act directly upon the cannabinoid receptors (Lattanzi et al., 2018). As such, the psychoactive side effects reported from illegal cannabis use is not of concern

when taking CBD therapeutically. Whilst currently licensed for use in severe epilepsy cases, further study into this seemingly safe, efficacious compound is required before widespread prescription can be expected.

The exact mechanisms of action of all AED are beyond the scope of this thesis, with the exception of the first-generation AED sodium valproate, which is discussed in detail in Chapter 6.1. Figure 1.4 briefly summarises the action of many AED.

Figure 1.4: Mechanisms of action of anti-epileptic drugs. AEDs display diverse mechanisms of action, affecting both inhibitory and excitatory nerve terminals. GAT-1: sodium and chloride-dependent GABA transporter 1, SV2A: synaptic vesicle glycoprotein 2A. Modified from Shih et al., 2013.

1.5 Current animal models of seizure-liability

CNS toxicity testing of any new pharmaceutical is a vital procedure and a legal requirement for safety pharmacology studies (ICH, 2000). A drug-induced seizure is an example of a potentially fatal ADR and is the most commonly encountered CNS-related issue during the drug development process (Authier et al., 2016). Pre-clinical seizure liability (PSL) testing is essential to identify such ADRs, however these tests usually occur late in the drug development process (Figure 1.5) (Easter et al., 2007). Despite the severity of drug-induced seizure, there are no official guidelines outlining how this issue should be tested and regulated (Easter et al., 2009; Will et al., 2016). *In vitro* and *in vivo* models enable potential side effects to be discovered earlier, thereby saving time, cost and resources. However, current models are hindered by limitations such as low-throughput capabilities, heavy reliance on animal studies and arguable relevance to man, whilst often incurring considerable financial expense. Furthermore, with relevance to *in vivo* PSL testing, the severity of assays frequently requires specialist practitioners, further increasing costs and decreasing throughput. In 2018, the UK performed a total of 474,000 procedures on animals for regulatory testing, of which toxicity testing comprised 31%. In addition, over 200,000 procedures were carried out for basic nervous system research (21% of all basic research) (Home Office, 2018). There is increasing pressure to reduce the numbers of animals used, without sacrificing on the quality of information provided by such tests.

Current effective *in vitro* models include rodent brain tissue slices and CNS cell cultures. These have been employed for decades and are credited with the discovery of mechanisms pertinent to seizure, epilepsy and neurobiology in general. Animal-based models of seizure are important for defining epileptogenic and ictogenic activity, as well as providing a reference point for the more recent human-based research. Whilst *seizure* describes a full ictal event *in vivo*, the term 'seizure-like event' (SLE) more accurately describes the effects seen in *in vitro* and predictive *in silico* models.

There are many animal-based *in vitro* and *in vivo* models for seizure-liability testing. For simplicity, the following section will focus on the models most commonly used in toxicity screening. Most current models employ rodents, as the rodent brain develops incredibly rapidly, with a gestation period of 18-24 days and tissue can be ready for neurological experimentation from Day 7-10 postnatal; compared with 9 months gestation for humans, followed by years of maturation (Murray et al., 2010; Semple et al., 2013).

1.5.1 *In vivo* methods

It has been estimated that a single compound requires several hundred rodents and approximately £1 million for complete assessment of neurotoxicity and seizure liability (Moser, 2011; OECD, 2006; Smirnova et al., 2014), due in part to the low-throughput capabilities and specialised tests performed on whole animals. Whilst the range of species used is considerable, varying from zebrafish to baboons, there exists no standard platform for which all methods of inducing seizure *in vivo* can be applied.

Despite this considerable expense, there are many established *in vivo* models for modelling epilepsy and PSL, ranging from the cortical implantation of metals known to induce seizure, to drugs known to modulate GABA inhibitory activity, to electroshock and implanted electrode models (Rubio et al., 2012). These models were classified according to their method of epileptogenesis (Fisher, 1989), summarised in Table 1.1. Discussion of these is beyond the scope of this thesis, however an excellent review into *in vivo* models of epilepsy and seizure is available (Rubio et al., 2012)

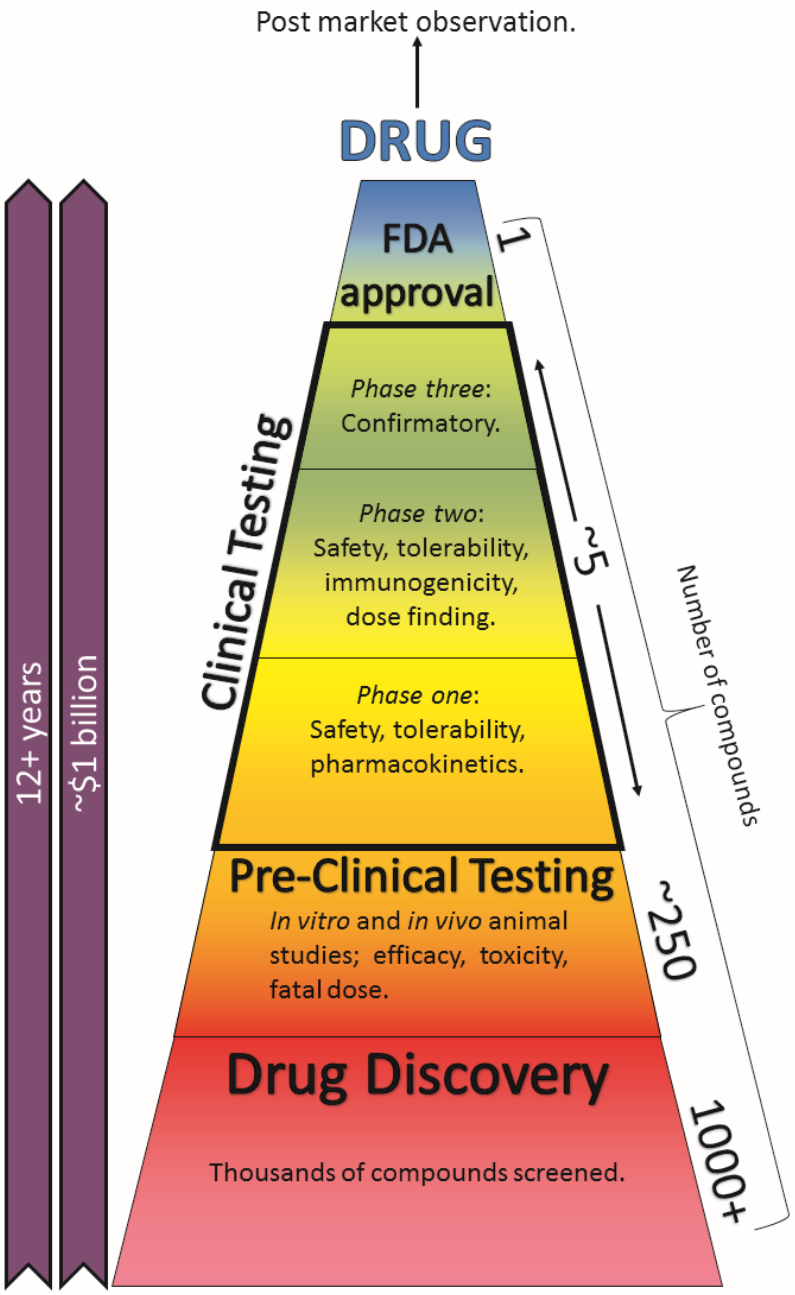

Figure 1.5: The drug development process (Grainger et al., 2018). Taking anywhere up to 15 years and a cost of ~$1.7 Billion, the process can be separated into pre-clinical and clinical testing. Pre-clinical studies consist of *in silico, in vitro* and *in vivo* animal and cell-based assays. Post-market surveillance continues indefinitely (Paul et al., 2010). Reducing these studies or finding better alternatives can save time, cost and resources.

Table 1.1: Classification of *in vivo* models of epileptogenesis, based on ILAE guidelines (Fisher, 1989; Rubio et al., 2012).

Simple partial seizure models	Cortically implanted metals
	Aluminium, Cobalt, Zinc
Complex partial seizure Model	Kainic Acid administration
	Repetitive electrical stimulation (Kindling)
	Tetanic Toxin administration
Generalised tonic-clonic seizure models	Maximum electroshock
	Pentylenetetrazol
	Flutotyl
Generalised partial seizure models	Penicillin
	GABA
	Bicuculline
Generalised absence seizure models	Audiogenic seizures in mice
	Genetic: Photosensitive baboons
Status epilepticus	Pilocarpine

1.5.2 *In vitro* methods

Whilst *in vivo* methods ensure a living, complete system and provide insights not only into the cellular effects of seizure induction, but also behavioural and physical aspects, they are not high-throughput systems, are very expensive and raise considerable ethical concerns. *In vitro* models are often used as complements to whole animals, beneficial for their increased throughput and less specialised tests. A comparison of the most common methods of PSL using *in vitro* models is given in Table 1.2.

1.5.2.1 Acute slice assays

In a 2016 industrial survey of nervous system safety pharmacology, the rat *ex vivo* hippocampal slice assay was found to be most commonly used for seizure-liability testing (Authier et al., 2016). Slices can be obtained from any region of any species with a complex brain. Hippocampal slices (HS) are useful *in vitro* models as they retain a defined cytoarchitecture and relevant receptors and constituents of the full brain system, including inter-area connectivity. This is of great importance, as the cause of seizures and epileptiform activity can be complex and interlinked with multiple hierarchical levels of the CNS (Scharfman, 2007). External conditions can be precisely controlled and manipulated with HS. Indeed, slice assays typically involve manipulation of the extracellular ionic milieu to induce SLE, discussed in Chapter 4.1. Furthermore, the mechanisms by which different agents induce SLE is highly variable. With tissue slices, it is more likely that all necessary cell types and receptors to respond to diverse pharmacological agents are present. Acute slices are harvested from adult rodent brain, intended for experimentation on the same day to study individual neurons or neuronal circuits (Lein et al., 2011). However, difficulties in inter-species extrapolation reduces the utility of the platforms and inevitably, slice preparations undergo important cellular and environmental changes including ischaemia and severing of projection neurons that would have connected the slice to the rest of the system.

Obviously, human brain tissue is problematic to obtain (except for limited excised epileptic tissue), so efforts to refine the commonly used rodent HS or replace with non-human primates have been attempted (Easter et al., 2007). Once removed from the animal, slices rapidly begin to deteriorate, making them an expensive and low-throughput model system; however, a semi-automated platform has been validated for use in pre-clinical testing, allowing multiple slices per animal to be perfused simultaneously, thus, increasing the throughput capabilities of the platform (Easter et al., 2007).

1.5.2.2 Organotypic slice assays

In contrast to acute slice preparations, organotypic slices (OS) are derived from neonatal rodents and are maintained *in vitro* for several weeks (Lein et al., 2011). Compared with acute slices, OS require more time and resources; in particular, culture medium which can provide essential growth factors, hormones and metabolites; which may or may not include serum. As variability between culture media can frequently be attributed to serum, chemically defined media have also been developed and have been shown to support OS culture and more importantly, facilitate seizurogenesis (Liu et al., 2017).

Organotypic slices are representative of their respective *in vivo* counterpart. They contain most of the neuronal subtypes present in the brain and retain local intrinsic connective properties of the tissue. As previously mentioned, excision of acute slices leads to cellular damage, ischaemia and an altered metabolic state, however OS can recover from these insults during culture and have been shown to exhibit synaptogenesis and early studies demonstrated the formation of new functional contacts (Chen et al., 2008; Robain et al., 1994; Sato et al., 2007). Furthermore, any necrotic cells or debris disappears after several weeks in culture (Lein et al., 2011). OS are particularly useful for assessing long-term effects of agents or SLEs, as they can be further incubated following experimentation.

Despite the supposed benefits of OS, there are limitations in using them as models, *cf* acute slices. There is concern that as the tissue is harvested from neonates, that this is not entirely representative of adult tissue. Whilst any acute damage to OS rectifies itself, synaptic reorganisation and axonal/dendritic remodelling can occur from destruction of afferent connections of neurons – a process termed deafferentation (Gutiérrez & Heinemann, 1999). The trauma of slicing can also activate glial cells, leading to the formation of an astrocytic scar, which was believed to prevent axon regeneration; although this is now disputed (Anderson et al., 2016; Lein et al., 2011).

1.5.2.3 Primary cell culture assays

The second most commonly used model system for seizure-liability studies is primary neuronal cell cultures (Authier et al., 2016). Similarly to slice models, primary rodent CNS cultures can contain most, if not all, of the components of intact cortex, which bear a true resemblance to the cells *in vivo*. However, the structure and three-dimensional nature of the brain is lost. Unlike slice assays, cell cultures are typically higher throughput, but do take several weeks in culture to reach maturity, as is the case with OS.

Whilst neurons are an absolute requirement for seizure activity, they are not the only cell type involved (Section 1.3.7). Indeed, omitting other cell types, or culturing ratios of subtypes not representative of *in vivo* ratios could affect the validity of such models. There is also concern that certain receptors or channels may not appear in cultured neurons, which may or may not influence the outcome of experiments (Dichter & Pollard, 2006). Despite this, primary cell culture assays can reliably and consistently predict seizure-liability. Recent literature has produced a comprehensive *in vitro* screen for seizure-liability using primary rat cortical neurons, including ratios of neurons and astrocytes observed in the intact rat brain (Bradley et al., 2018). In addition, the predictive capability of rat cortical models from cultures containing both excitatory and inhibitory neuronal subtypes has been demonstrated (Kreir et al., 2018). In both instances, rodent cells were shown to be able to respond to a large group of agents known to induce SLEs, with consideration of multiple neural activity markers. However, like OS, there is controversy over when the cultured cells reach maturity and at which point they should be used for seizure-liability studies so that they are as representative of the living system as possible. Arguably, the most important consideration for epileptiform studies is the capability of cells to evolve network functionality, which can develop, propagate and sustain SLEs.

1.6 Human neurotoxicity models

Just as many animal-based models have been developed and widely used for disease modelling and drug testing, there exists several human cell models which have been used as animal alternatives for some time. Whilst these models have the benefit of being human derivatives and are rapidly cultured with relatively low expense, these methods are outdated and inferior compared to animal models. Two particular human cancer cell-derived models are most well-known: the neuroblastoma SH-SY5Y cell line and the embryonal carcinoma NT2/D1 line.

1.6.1 SH-SY5Y Neuroblastoma line

The subclone of neuroblastoma line SK-N-SH, SH-SY5Y neuroblast-like cells can be differentiated in the presence of retinoids, to form neuronal-like cultures, possessing a similar karyotype to human cells (Biedler & Schachner, 1978; Yusuf et al., 2013). SH-SY5Y cells are mostly used for studies with dopaminergic pathologies, such as Parkinson's disease, owing to their tendency to generate dopaminergic neurons (Shipley et al., 2016). Despite the publishing of protocols to differentiate SH-SY5Y into adrenergic-like and cholinergic-like subtypes (Shipley et al., 2016), the author is unaware of any reliable protocol for the generation of cortex-specific neurons; likely a result of SH-SY5Y not being precursors to any specific cell fate. Moreover, functional studies have been performed using SH-SY5Y cultures, wherein changes in K^+ conductance to known seizurogenic agents were not observed and electrophysiological properties were highly variable (Tosetti et al., 1998). SH-SY5Y are not an appropriate system for studying seizure-liability, owed to their lack of heterogeneity, their functional inactivity and the display of several genetic aberrations, typical of a cancer cell origin (Xicoy et al., 2017).

1.6.2 NT2/D1 Embryocarcinoma cell line

In contrast, the NTERA-2 cl. D1 (NT2/D1) cell line has been widely used to generate both neurons (Andrews, 1984) and functional astrocytes, following retinoid treatment and mitotic inhibition (Bani-Yaghoub et al., 1999). Compared with SH-SY5Y, the individual cell types are functional, displaying complex network activity including wave propagation and respond to various

compounds with increases or cessation of calcium-mediated activity, where appropriate (Hill et al., 2012). Further research in our laboratory has confirmed these culture models are effective as platforms for toxicological investigations and pharmacological interrogation (Hill et al., 2012; Tarczyluk et al., 2015; Woehrling et al., 2006, 2007, 2010, 2011, 2013).

NT2 D1 differentiate to form co-cultures of functional neurons and astrocytes within 2 months, without the need for expensive or specialised growth medium considerations. The differentiation process is reproducible and faster than other stem cell models, making them an attractive model system. However, as with SH-SY5Y cultures, NT2 cells originate from a cancer cell, which can preclude their usage when other, non-cancerous cell types are available. Indeed, NT2's have been shown to contain a highly variable karyotype of up to 60 chromosomes in a large percentage of cells (Mostert et al., 1996).

1.6.3 Human tissue

Current research into the mechanisms and treatment of drug-refractory epilepsy is using resected human tissue from patients. This condition is diagnosed when seizures cannot be controlled by at least two or three anti-convulsants appropriate for the epilepsy syndrome (Tang et al., 2017). The possibilities for human tissue range from histopathological analyses, to modulation of SLE in drug-resistant tissue and the testing of novel anti-convulsant compounds and electrophysiological investigation (Gabriel et al., 2004; Hsiao et al., 2015; Klaft et al., 2016). Furthermore, several methods are now available that increase the longevity of the resected tissue, enabling increased throughput of investigations (Schwarz et al., 2017; Wickham et al., 2018). However, it is unlikely that enough human tissue will ever be available for high-throughput compound screening. Furthermore, the tissue is often in a diseased state, which may demonstrate different responses to otherwise healthy tissue.

Ethical considerations and consent also need to be obtained to use human tissue, further complicating an already limited process. Human stem cells could provide a viable alternative to

human tissue, allowing researchers to generate functional neuronal networks for high throughput drug testing.

It is also possible to obtain human cerebrospinal fluid (hCSF) from patients, which has been shown to have a protective effect on resected human tissue, promoting longevity compared with culture medium (Schwarz et al., 2017). Furthermore, preservation of electrophysiological properties, including network-level activity is observed. Whilst it appears unlikely that hCSF would be readily available in the quantities necessary to culture and assess iPSC-derived neural models, it would nevertheless be interesting to determine what effects, if any, this composition has on the electrophysiological activity of the cultures.

1.7 Requirements for a human *in vitro* model of seizure-liability testing

As discussed above, an ideal model system for *in vitro* PSL testing should therefore be able to recapitulate the information existing models provide and address some of their limitations. The most obvious shortcoming for current platforms used for seizure-liability testing is that they use animals. An ideal platform would therefore be relevant to humans, using cells which are phenotypically human, expressing human receptor proteins with which current convulsant and anti-convulsant compounds can interact. The cells should also be able to form functional neurophysiological networks, containing the various cell types seen in the intact brain, with brain region specificity, as opposed to current generic models. Importantly, the platform must be capable of pharmacological interrogation, of displaying phenotypic human seizure-like activity and of sensitivity to known therapeutic anti-convulsants. The system should also be robust and amenable to high-throughput testing and predictive of the effects of diverse neuroactive compounds. A human-based *in vitro* seizure-liability platform for pre-clinical neurotoxicity testing should in theory and practice, **fundamentally** perform as existing animal models do, whilst improving species translation with human seizure activity.

1.8 Human induced pluripotent stem cells

Induced pluripotent stem cell (iPSC) technology (Takahashi & Yamanaka, 2006) is a ground-breaking, revolutionary method, with considerable potential for toxicity testing and disease modelling, allowing the generation, growth and study of human cells without the need for invasive isolation procedures or extensive ethical approval. Previously, sources of human stem cells were primarily embryos, causing considerable political and moral controversy. In addition, the use of embryonic stem cells (ESC) in the clinic is limited by the rejection of the transplanted cells by the patient's immune system (Park et al., 2008).

Similarly to ESCs, human iPSCs can differentiate into any cell type generated by the three germ layers which develop *in utero* and retain the ability to propagate in culture indefinitely (Robinton & Daley, 2012). Pioneering work reprogrammed murine (Takahashi & Yamanaka, 2006) and human (Yu et al., 2007) fibroblasts via retroviral transduction of transcription factors: c-Myc, Oct4, Klf4 and Sox2; now referred to as the 'Yamanaka Factors'. Since the original methods of reverting adult cells to a state of pluripotency, there have been considerable advances and refinements in the process, moving from viral methods (which typically have large footprints, with viral vector sequences integrating into the genome) to episomal and mRNA-based reprogramming with typically lower footprints, which may be less efficient (Malik & Rao, 2013).

The application of iPSCs extends from neurotoxicity testing and disease modelling to drug-screening and cell-based therapies (Jung et al., 2012; Kumar et al., 2012). Neuronal cultures which are derived from human iPSC could be a suitable addition to PSL testing, as the systems are closer to humans than a primary rodent-derived cell line. In addition, a remarkable benefit of iPSCs is that they retain the genotype of the original fibroblast cell and indeed, any cell then generated from iPSCs also shares that genetic background. This is invaluable in disease research, as cells taken from both patients and controls can be studied and compared.

1.8.1 iPSC-derived neural seizure-liability models

The foremost aim of *in vitro* neurotoxicity tests, including iPSC-derived PSL models, should be to replicate the *in vivo* morphology and functionality as closely as possible. Diseases of the cerebral cortex are major causes of morbidity and mortality. Hence, iPSC-derived cortical neuronal systems could provide a reliable predictive base for PSL testing and are conceptually more relevant to toxicity testing than animal tissue, as they are human cells. Indeed, the cortex of primates is considerably different to that of rodents, with a marked increase in size relative to the rest of the CNS and its complexity (Shi et al., 2012a). Moreover, diversity of the neurons within the layers of the cortex and their respective developing stem cell populations means a truly representative model needs to use human stem cells to follow this pattern of differentiation.

Protocols for the development of iPSC-derived cortical neurons and characterisation of cortical neurogenesis and terminal differentiation to achieve mature electrophysiological properties and functional excitatory synapses have been developed, as shown in Figure 1.6 (Chambers et al., 2009; Shi et al., 2012b). Neural induction methods for generating NPCs from iPSCs are classified into 3D spheroid-based and 2D monolayer protocols. Irrespective of the culture method used, the process is largely the same and it was found that both methods produce neurons with similar electrophysiological properties and similar morphological endpoints, with subtle differences in neurite length and proportion of progenitor cell expression (Chandrasekaran et al., 2017). 2D culture methods (Chambers et al., 2009; Shi et al, 2012b) produced more SOX1 positive cells, with smaller neurite extensions, whereas 3D floating sphere methods (Gunhanlar et al., 2017) produced cells with higher levels of PAX6 expression. In addition, 3D methods form neurons with longer neurite extensions, which may be advantageous for the production of forebrain cortical neurons (Chandrasekaran et al., 2017).

In either case, the protocols are largely similar and involve the culturing of iPSCs on a gelatinous protein substrate, reminiscent of the basement membrane matrix. Neural induction involves

the suppression of epidermal fate, as opposed to the induction of a neural fate, meaning the default state of naïve ectoderm is neural (Colas & Schoenwolf, 2001). The inhibition of epidermal fate is achieved by the inhibition of SMAD signalling – which are a family of proteins that function as the main signal transducers for TGFβ and bone morphogenetic proteins (BMP) and are essential cytokines for development of the nervous system (Chambers et al., 2009). Inhibition is achieved via the synergistic action of two inhibitors (SB431542 and Noggin) which induces rapid and complete neural conversion of >80% of human stem cells under monolayer, adherent conditions (Chambers et al., 2009). Specifically, SB43142 is a small molecule which enhances neural induction via TGFβ inhibition and Noggin inhibits BMP.

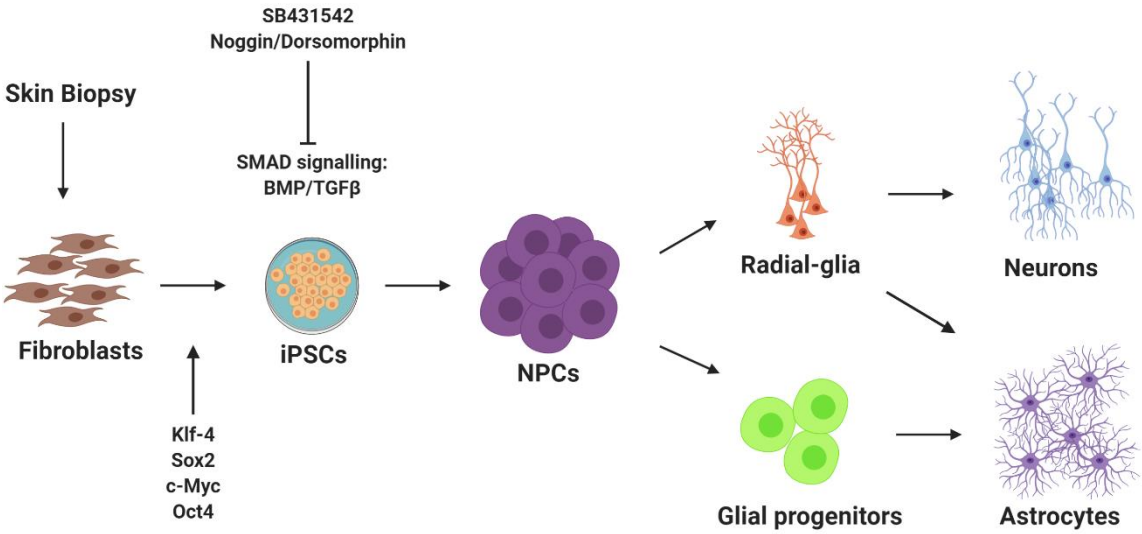

Figure 1.6: Neural induction of iPSCs to form neural subtypes. Patient fibroblasts are reprogrammed with the Yamanaka factors Klf-4, Sox2, c-Myc and Oct4 to a state of pluripotency. Dual SMAD inhibition of iPSCs via the small molecule SB431542 and Noggin/dorsomorphin can then induce the iPSCs to a neural fate, leading to the generation of neural precursor stem cells (NPCs), typically arranged in a cortical rosette structure. Defined growth medium and differentiation of NPCs leads to the generation of radial glia and glial progenitor cells, both of which can generate astrocytes. Neurons result following radial glia formation. Modified from Grainger et al., 2018.

Following the work of Shi et al., (2012a,b), it was found that vitamin A derivatives are crucial for induction of *in vitro* cortical neurogenesis, as is reported *in vivo* (Kim et al., 2010) and the use of retinoids, combined with an alternative small molecule SMAD inhibitor to Noggin (dorsomorphin) greatly reduces variation in cortical induction and increases efficiency of conversion to near 100% (Shi et al., 2012b).

The development of iPSC-derived cortical cultures should demonstrate the presence of cortical neuronal markers, astrocytes and populations of excitatory and inhibitory neurons (which exist at roughly 80% to 20% in the human cortex, respectively (Shi et al., 2012a). Indeed, the cortical induction method proposed by Shi et al., (2012b) showed the generation of astrocytes following spontaneous differentiation. Moreover, it has been shown that human iPSCs can also be differentiated exclusively into astrocytes (Shaltouki et al., 2013) and interneurons (Kim et al., 2014; Liu et al., 2013). This is of critical importance when considering the seizurogenic potential of novel compounds. An entirely excitatory or inhibitory culture is not a representative system and accurate drug responses may not be observed without inclusion of both major neural subtypes. Efforts have been made to determine the presence of excitatory and inhibitory neuronal populations and neuron/astrocyte ratios and it would appear that immunostaining for morphological assessment and pharmacological interrogation can suggest the presence/absence of such neuronal subtypes and astrocytes (Gunhanlar et al., 2017; Kuijlaars et al., 2016; Tukker et al., 2016). A complete, demonstrative, heterogenous system must include all subtypes and at ratios close to those observed *in vivo*. Furthermore, assessing the effects of compounds on astrocytes will provide increased accuracy and validity, particularly as astrocyte-specific agents can be tested and monitored in mixed cultures (Hill et al., 2012).

Table 1.2: Comparison of current major seizure-liability testing platforms. Modified from Grainger et al., (2018).

Model	Benefits	Limitations
Acute slice assay	• Representative of *in vivo* adult rodent brain • Same day experimentation • Validated for use • Defined cytoarchitecture • Current 'gold standard' • Forms functional network	• Difficulty in inter-species extrapolation • Preparations undergo cellular changes and damage • Projection neurons severed • Typically low throughput
Organotypic slice culture	• Representative of *in vivo* rodent • Retain connective properties of the tissue • Forms functional network • Can recover from damage from slicing • Can assess long-term effects of neuroactive chemicals	• Difficulty in inter-species extrapolation • Derived from neonates, so may not be predictive of matured system • More time consuming than acute slices • Requires supportive culture medium • Synaptic reorganisation/remodelling
Primary CNS culture	• Representative of cell subtypes *in vivo,* as derived from intact system • Predictive model validated • Higher throughput than slices	• Difficulty in inter-species extrapolation • Loss of structure and 3-dimensionality • More time consuming • Do cultured cells reach maturity? • Often cultured in absence of astrocytes or other neural cells
iPSC-derived culture	• Human-based • Exhibit humanoid morphology • No ethical considerations • Amenable to high throughput • Retain genotype of original fibroblast, so they can be used to model genetic components of human epilepsies	• Expensive • Time consuming • Research still in infancy, lacking validation • No defined ultrastructure • No standard protocol • No guarantee of presence of desired cell types, unless co-cultured

1.9 Functional analysis of iPSC-derived cultures

Whilst there are now many emerging disease platforms and investigative models using iPSC-derived neurons, research using human iPSC neural networks for the express purposes of drug screening is still in its infancy. It has been shown that iPSC-derived neurons respond appropriately to convulsant and pro-convulsant agents and could be utilised in PSL testing (Ishii et al., 2017; Odawara et al., 2014; Tukker et al., 2016). Whilst typical endpoints for current PSL tests include assessment of biochemical, morphological and physiological endpoints, the throughput capabilities of these assays are too low for toxicity screening. Changes to ion channels, calcium changes and network responses are implicated in many toxicity pathways and functional techniques used must be able to detect these changes. Convulsant compounds affect the nervous system and neuronal excitability as discussed in depth in Chapter 4. These disruptions in turn affect nervous system physiology, often preceeding or occuring in the absence of the typical morphological/biochemical changes. Furthermore, some existing methods fail to record the most rapid events, such as action potentials, or are not amenable to high-throughput testing, making them less desirable for toxicity screening. Therefore, methods used with iPSC-derived neural models must demonstate a relatively high-throughput capability, without compromising on the quality of the information obtained. Techniques enabling network-wide effects to be recorded and visualised would provide relevant endpoints to monitor drug induced SLEs.

In many cases, gold-standard electrophysiological techniques such as patch clamping are employed to accurately monitor electrical activity and responses, however, these are invasive and are traditionally limited to measurement of a single cell. Individual manual patch clamping is also a very technically demanding and precise method and requires a high-level of expertise. However, there is potential to increase throughput capacity via automated patching systems, which can measure several neurons simultaneously (Kodandaramaiah et al., 2012) and indeed, recent developments have enabled multiple-cell patch clamping to be used in industrial

applications (Vardi et al., 2016). Whilst patch clamping is a particularly efficient and accurate method of studying ionic currents, its use for large-scale toxicity screening is not practical.

1.9.1 Calcium Imaging

Calcium imaging is a well-established technique which enables visualisation of free intracellular Ca^{2+} from populations of cells. Calcium indicators are sensitive to calcium movement and can be loaded in a non-invasive manner to neuronal cells, although, prolonged exposure to the dye is toxic. Fluorescent dyes can either be single wavelength or ratiometric. Fluorescent calcium imaging enables the researcher to explore the role calcium is playing in the cell, due to specific calcium-mediated processes occuring over different time periods. For example, calcium-mediated neurotransmitter release occurs much more rapidly than calcium-mediated gene expression in the nucleus (Grienberger & Konnerth, 2012).

With regards to PSL, calcium imaging can be used to detect responses to electrical activity, oscillatory activity, synchrony and network activity, making it a very useful tool for assessing neural circuitry and drug responses (Smetters et al., 1999). This approach has been used in an effort to characterise the development and maturation of iPSC-derived neural calcium activity and to study network responses to neurotransmitters/drugs (Kirwan et al., 2015; Tukker et al., 2016). These studies have demonstrated maturation of oscillatory calcium activity and increased activity when exposed to excitatory compounds. However, to the author's knowledge, the use of calcium imaging as a method for PSL testing in iPSC-derived neural networks has not yet been demonstrated, despite preliminary work showing the capability of iPSC-derived neurons to respond to the GABA antagonist picrotoxin with increased synchronised activity (Kuijlaars et al., 2016). In contrast, the response of primary rodent neural cultures to a panel of neurotransmitters and convulsants has been shown by multi-well calcium imaging (Pacico & Meur, 2014), with large increases in repetitive calcium-mediated activity observed in the presence of pro-convulsants, suggesting that calcium imaging as a method for viewing SLE is

valid. Whilst the author in this case opted for a non-optical method of calcium imaging, the ability to visualise cell calcium activity in near real-time is extremely advantageous.

Ultimately, optical fluorescent calcium imaging allows for greater resolution at a cellular level, as opposed to single cell patches which can miss considerable amounts of data and not necessarily inform on the activity of the entire network. Fluorescent calcium imaging of iPSC-derived neural networks for seizure-liability testing has not previously been performed and as such, there is scope for this technique and platform to incorporate into the existing strategies for toxicity testing.

1.9.2 Multi-electrode array recordings

Multi-electrode array (MEA) systems are increasingly used with iPSC-derived cultures to assess spontaneous electrical activity, synchronous epileptiform bursting activity, drug-responses and network mechanisms, such as long-term potentiation and depression (Matsuda et al., 2018; Odawara et al., 2014, 2016a, 2016b; Seidel et al., 2017). MEAs take advantage of the generation of neuronal ion currents and membrane action potential firing. MEAs transduce this ionic voltage change to electronic current, which can then be detected and analysed by a wide range of commerically available and custom-made software.

This cutting-edge technology is non-invasive, enabling the real-time analysis of activity in multiple locations in cultured neurons and recording of extracellular potentials and basic measures such as spiking and bursting activity and network responses (Johnstone et al., 2010). The use of primary rat cortical neurons on the MEA is well characterised, with extensive neural activity endpoints. The parameters and results from primary models are important for providing a comparative system for emerging iPSC-derived MEA data (Bradley et al., 2018). A number of studies have been carried out to determine whether MEA analysis of iPSC-derived neural networks is a viable option for toxicity screening. Furthermore, a broad panel of drugs have been evaluated, and results suggest that MEAs are a useful tool in screening compounds with

diverse mechanisms of action (Kasteel & Westerink, 2017; McConnell et al., 2012; Valdivia et al., 2014). In addition, over the past several years, multi-well MEAs have emerged, with capacity of upwards of 300-1000 recording electrodes. These systems significantly increase the throughput capabilities of primary cell culture and slice assays, further making them attractive systems for predictive toxicity tests and drug screening.

As the throughput capabilities of MEAs increase and their usage in toxicity screening becomes more widespread, it will be important to generate standard protocols and definitions of SLEs in iPSC-derived models. A recent study by Bradley et al., (2018) has assessed a wide variety of endpoints to demonstrate epileptiform activity and network functionality, providing a comprehensive predictive primary rodent model. Whilst there are some commonalities between approaches, each group using MEAs for neurotoxicity screening assess different endpoints based upon their respective experimental design. For example, a common endpoint to consider is the number of spikes in a burst, with bursts being typical of epileptiform activity. However, the definitions set on burst parameters have large variation and as such, analysis is specific to particular cell lines, which makes standardisation difficult. Despite this, recent literature has suggested a stepwise method for detection of synchronised burst firings in iPSC-derived neural cultures (Matsuda et al., 2018). This is a positive move towards standard protocols for assessing epileptiform activity using the MEA with human iPSC-derived cultures, with a particular emphasis on toxicity testing, especially as many difficulties in MEA analysis have presented themselves with this modern technique. Moreover, as this technology is a recent introduction to the field, there are challenges with culturing cells for experimentation, as historically MEA studies utilised slice assays, which do not require a specialised culturing protocol.

Compared to traditional electrophysiological techniques, the MEA enables network electrical activity to be monitored, especially in the recent high-throughput systems. This means

substantially more data can be derived than for equivalent patch/ current clamp recordings, is more rapid and for epileptiform studies in particular, network activity visualisation is more beneficial than individual cells. A benefit of using these established techniques is that several software packages are available for data acquisition and analysis, many with user-friendly interfaces. However, for newer technology, software is limited and analysis is more complex.

Presenting a novel method of seizure-liability testing of iPSC-derived neural cultures must include a suitable analytical protocol, so that meaningful data can be generated from the studies.

1.10 Aims and Objectives

The current methods of pre-clinical seizure-liability testing are heavily reliant upon animal-based platforms. Human induced pluripotent stem cell technology has revolutionised regenerative medicine, providing an essential tool for generating human cells in a non-invasive and ethically sound manner. The generation of morphologically distinct, functionally active, pharmacologically responsive neural cells from iPSC could supplement existing strategies in drug development, with more relevance to man, whilst removing doubts from inter-species extrapolation. To date, the inclusion of human-based platforms as models for seizure-liability is extremely limited, due to a lack of a complete, robust system. Furthermore, the methods used to assess seizure-liability in these cultures are developments in progress. Consequently, this thesis aims to contribute to the cutting-edge platforms of iPSC-derived toxicity testing.

To that end, the overall aim of this thesis is to develop a protocol for the differentiation of human iPSC-derived cortical cultures which can respond to pro-ictogenic compounds with increased activity and synchrony and interface with a high-throughput analytical technique.

In order to achieve this aim, the following objectives will be considered:

1) To generate morphologically distinctive cortical cell types in culture, consisting of neurons, astrocytes, cortical layers and synapses, assessed via immunostaining and qPCR
2) To produce electrically functional cultures, which can generate action potentials, network activity and respond to excitatory stimuli, via fluorescent calcium imaging and multi-electrode array analysis
3) To induce hyperexcitable and hypersynchronous activity in culture, via addition of ionic and pharmacological manipulations widely used as convulsants in toxicity testing and observe said activity using optical and MEA approaches
4) To establish a suitable analytical protocol for functional assessments

Chapter 2

2: MATERIALS AND METHODS

All reagents were purchased from Sigma-Aldrich (Poole, UK) unless otherwise stated.

2.1 Cell culture

2.1.1 Coatings

Cultureware was pre-treated to improve the hydrophilicity of surfaces to enhance adherence of cells for long-term culture. All mentions of incubation refer to a humidified 5% CO_2 incubator at 37°C, unless otherwise stated.

2.1.1.1 Plastic multi-well plates

Plastic 6-well, 12-well and 96-well plates (Corning, CA, USA) were coated with 200 µL/cm^2 of 20 µg/mL poly-L-ornithine (PORN) and incubated for 4 hours, followed by two sterile dH_2O washes. Laminin was dissolved in sterile dH_2O to a 10 µg/mL working solution and coated at 200 µL/cm^2, then incubated overnight. Prior to cell seeding, wells were washed with D-PBS without magnesium or calcium.

2.1.1.2 Glass coverslips

For immunocytochemistry and calcium imaging experiments, glass coverslips (13 mm thickness, VWR) were sterilised in 70% ethanol and dried overnight in the laminar flow hood to ensure evaporation. Coverslips were then placed in 6-well and 12-well plates and treated with PORN-laminin as described in 2.1.1.1.

2.1.1.3 Multi-electrode array planar chips

Platinum and carbon-coated MED-P515A planar multielectrode array (MEA) chips were purchased from Alpha Med Scientific (Osaka, Japan). The arrays comprised a 10 mm culture depth with 64 electrodes in an 8 x 8 grid arrangement with 150 µm spacing between electrodes. Arrays were rinsed in sterile dH_20 and gently submerged in 70% ethanol for a maximum of 15

minutes for sterilisation. Ethanol was aspirated and the array left to dry in the laminar flow hood under UV irradiation for 60 minutes. Arrays were coated with 100 µL 20 µg/mL PORN and incubated for 6 hours. PORN was aspirated and arrays were rinsed with sterile dH_20, before 20 µL of 10 µg/mL laminin was pipetted directly over the electrodes. Arrays were incubated for 30 minutes and laminin aspirated ready for immediate cell seeding. After seeding, cells were left to adhere for 1 hour, before gently being flooded with cell culture medium (2.1.2.1).

2.1.2 Neural precursor stem cell differentiation

2.1.2.1 Cell culture medium

Axol: Axol Neural Maintenance Medium and Supplement Kit, Ax0031 (Axol Bioscience, Cambridge, UK).

SCT: BrainPhys™ Basal medium, 2% (v/v) SM1 supplement, 1% (v/v) N2A supplement, 100 µg/mL brain-derived neurotrophic factor (BDNF), 100 µg/mL glia-derived neurotrophic factor (GDNF), 100 mg/mL cyclic adenosine monophosphate, sodium salt (cAMP) and 50 µg/mL *L*-ascorbic acid (all components from StemCell Technologies, Cambridge, UK).

Astrocyte medium: ScienCell Astrocyte medium, 2% (v/v) foetal bovine serum, 1% (v/v) penicillin-streptomycin and 1% (v/v) astrocyte growth supplement (all components from ScienCell Research Laboratories, CA, USA).

Sync SCT: BrainPhys™ Basal medium, 2% (v/v) SM1 supplement, 1% (v/v) N2A supplement, 100 µg/mL BDNF and 100 µg/mL GDNF.

2.1.2.2 Spontaneous differentiation

Cryopreserved Ax0013 neural precursor cells (NPCs) from cord blood $CD34^+$ cells of a healthy, newborn male donor were purchased from Axol Bioscience (Cambridge, UK). Cells were fast-thawed in a 37°C water bath, resuspended in Axol media and centrifuged for 5 minutes at 200 x *g*. The cell pellet was resuspended in Axol and a sample taken for haemocytometer counting.

Cells were seeded at a density of 50,000/cm^2 onto pre-treated PORN-laminin culture plates, glass coverslips and MEA chips as described in 2.1.1. Spontaneously differentiating cells were fed with Axol every other day, with a complete media change. Neuronal differentiation and confluency were monitored via daily phase contrast microscopy images using the EVOS XL Core Imaging System (Life Technologies, UK). Once cells reached ~80% confluency, they were passaged by discarding spent media from the culture and rinsing with D-PBS without magnesium or calcium.

To detach the cells, 100 µL/cm^2 accutase (Thermo Fisher, MA, USA) was distributed over the cell layer and incubated for 5 minutes. Four times the accutase volume of Axol was added to each well to neutralise the dissociation reaction. Dissociated cells were centrifuged at 200 x *g* for 5 minutes and the cell pellet was resuspended in Axol, before a sample was taken for cell counting. Cells were seeded as above. Cells were expanded through 3-5 passages, for final plating for spontaneous differentiation experiments at passage 6.

Passage 6 cells were fed with either Axol or SCT, as described in 2.1.2.1. Every other day, a complete Axol and half SCT media exchange was done. Cells were differentiated over various timepoints, being monitored daily using phase contrast imaging, as mentioned previously.

2.1.2.3 Synchronised neural differentiation

Cryopreserved Ax0013 were fast-thawed, plated and expanded to passage 6, as described in 2.1.2.1. However, for final plating to passage 6, cells were seeded at 100,000 cells/cm^2 and cultured in Sync SCT media. Cells were incubated overnight and the following day, a full media change was performed, adding 10 µM N-[N-(3,5-Difluorophenacetyl)-L-alanyl]-S-phenylglycine t-butyl ester (DAPT; Abcam, ab120633) to enable all neurons to exit the cell cycle at the same time. Full Sync SCT media changes with 10 µM DAPT were done every other day, so the cells were incubated with DAPT for a total of 7 days. On day 8, cells were returned to Sync SCT media without DAPT and media replaced every other day until day 14. On day 14, BDNF and GDNF

were removed from the media and the cells were fed every other day with half media changes of SCT with SM1. Synchronised differentiating cells were cultured over 8 weeks, monitored via phase image microscopy as above.

2.1.2.4 Astrocyte differentiation

Cryopreserved, 11-week-old iPSC-derived astrocytes (Ax0015; Axol Bioscience) from cord blood $CD34^+$ of a healthy newborn male donor were fast-thawed in a 37°C water bath, resuspended in astrocyte media (AM) and centrifuged for 5 minutes at 400 x *g*. The cell pellet was resuspended in AM and a sample taken for haemocytometer counting. Cells were seeded at a density of 12,000/cm^2 onto pre-treated PORN-laminin culture plates and glass coverslips as described in 2.1.1. Astrocyte cultures were fed with AM every other day, with a half media change and passaged as described for 2.1.2.2 (albeit at 400 x *g* centrifugation).

For synchronised astrocyte studies, following passaging, astrocytes were recovered for 24 hours in AM, then treated with 10 µM cytosine arabinoside (AraC) for 24 hours, before recovery in AM. Astrocytes were then cultured for 4 weeks for experimental study.

2.1.2.5 Co-cultures of neurons and astrocytes

Ax0013 neurons and Ax0015 astrocytes were synchronised using 10 µM DAPT and AraC, respectively, as described in 2.1.2.3/4.

Final ratios of neurons to astrocytes were 20:1, respectively. Cultures were matured for 10 weeks following astrocyte addition (co-cultured astrocytes final age 21 weeks).

Table 2.1 describes the protocol for co-culturing synchronised neurons and astrocytes for co-culture studies.

Table 2.1: Process of co-culturing neurons and astrocytes together, including media requirements and seeding densities.

Day	Neurons procedure	Astrocytes procedure
0	Passage Ax0013 NPCs and plate at 100,000/cm^2	
1	Recovery	
2	Sync SCT media with 10 µM DAPT	
3		
4	Sync SCT media with 10 µM DAPT	Plate Ax0015 astrocytes at 12,000/cm^2
5		
6	Sync SCT media with 10 µM DAPT	Astrocyte media
7		
8	Sync SCT media with 10 µM DAPT	Astrocyte media
9	Remove DAPT. Sync SCT media.	Passage Ax0015 astrocytes
10		Recovery
11	Sync SCT media	Inhibit astrocytes with 10 µM AraC
12		Recovery
13		Passage astrocytes onto neurons 5,000/cm^2
14	Recovery	
15	Recovery	
16+	SCT + SM1 feed every 2-3 days	

2.1.2.6 Co-cultures with interneurons

Co-cultures of Ax0013 NPC's and Ax0015 astrocytes were synchronised and differentiated as described in 2.1.2.5, with the addition of Ax0665 interneurons (Axol Biosciences, Cambridge, UK). Cryopreserved interneurons were fast-thawed in a 37°C water bath, resuspended in Axol media and centrifuged for 5 minutes at 200 x *g*. The cell pellet was resuspended in Axol and a sample taken for haemocytometer counting. A seeding density of 16,000 interneurons/cm^2 were added to the co-cultures at Day 9 (prior to the addition of astrocytes).

2.2 Immunofluorescent staining

Incubation periods for immunofluorescent staining were all performed at room temperature.

2.2.1 General staining method

Cultured cells for immunocytochemistry studies were fixed in an equal volume of culture media and 4% (v/v) paraformaldehyde (PFA) in PBS for 5 minutes at room temperature. The solution was removed, and cells were treated with PFA only for 5 minutes, then washed twice in PBS and incubated for 5 minutes in permeabilisation buffer (PBS with 0.2% (v/v) Triton X-100), then permeabilised again for 5 minutes. Cells were then blocked for 1 hour in block buffer (BB) (PBS with 0.2% (v/v) Triton X-100 and 2% (w/v) bovine serum albumin) on a stationary rocker at low speed. Cells were either single-stained or co-stained with a maximum of two primary antibodies dissolved in BB for 1 hour (see Table 2.2). Cells were washed 3 x 5 minutes in BB to remove excess antibody. For secondary antibody staining, coverslips were protected from light and secondary antibody dissolved in BB (1:500) was added for 1 hour (Table 2.2). The BB wash steps were repeated and the cells rinsed in dH_20 before being inverted onto a droplet of mountant containing the nuclear stain DAPI (Vectashield, UK) on glass microslides. Coverslips were protected from light and allowed to dry overnight, for storage at 4°C.

2.2.2 Synaptic staining method

For staining of sensitive synapses, an amended protocol was used. Cells were fixed as described in 2.2.1. To quench auto-fluorescence, fixed cells were rinsed three times and incubated for 5 minutes in 50 mM ammonium chloride in PBS. Cells were then incubated for 10 minutes in synaptic permeabilisation buffer (0.1% (w/v) saponin in PBS), followed by 30 minutes in synaptic block buffer (SBB) (0.1% (w/v) saponin, 3% bovine serum albumin in PBS). Primary antibodies (Table 2.2) were dissolved in SBB and the cells incubated for 1 hour, under gentle agitation. Cells were then rinsed twice and incubated for 10 minutes in SBB. Secondary antibodies were dissolved in SBB and incubated for 1 hour, followed by two rinses in SBB, two PBS washes and a rinse with dH_2O. Cells were mounted and stored as described in 2.2.1.

Table 2.2: Primary and secondary antibodies used for ICC experiments. Antibodies frequently co-stained are indicated by matching colours.

Antibody	Expression	Dilution	Species	Secondary (all used 1:500)
Pax6 (Biolegend, 901301)	Neural progenitors	1:300	Rabbit	Goat Anti-Rabbit FITC (green) (Jackson ImmunoResearch, 127016)
Sox2 (R&D systems, MAB2018)	Pluripotency marker	1:100	Mouse	Donkey Anti-Mouse Rhodamine (red) (Jackson ImmunoResearch, 112581)
S100β (Dako, GA504)	Mature astrocytes	Pre-made solution	Rabbit	Goat Anti-Rabbit
Tuj1 (Abcam, ab7751)	Neuron-specific tubulin	1:500	Mouse	Donkey Anti-Mouse
Tbr1 (Abcam, ab18465)	Lower layer cortical neurons	1:200	Rabbit	Goat Anti-Rabbit
Satb2 (Abcam, ab51502)	Upper layer cortical neurons	1:25	Mouse	Donkey Anti-Mouse
VGlut1 (Synaptic systems, 135303)	Glutamatergic neurons	1:1000	Rabbit	Goat Anti-Rabbit
GAD67 (Abcam, ab26116)	GABAergic neurons	1:2000	Mouse	Donkey Anti-Mouse
Ki67 (Abcam, ab15580)	Cell proliferation	1:500	Rabbit	Goat Anti-Rabbit

2.2.3 Fluorescent microscopy acquisition and quantification

Immunofluorescently-labelled cells were imaged using a Zeiss Axiovert 200M epifluorescent microscope using Leica Application Suite Advanced Fluorescence (LASAF) microscopy software (Leica Microsystems, Milton Keynes, UK). Filter cubes optimised for the excitation and emission spectra of each fluorophore were used, alongside a 20x objective (Nikon) for cell staining and 63x oil-immersion objective (Nikon) for synaptic staining. Filter sets were as follows for all fluorescently imaged figures in the thesis:

Green FITC: excitation λ of 495 nm, emission λ of 519 nm,
Blue: excitation λ of 345 nm, emission λ of 455 nm,
Red DsRed: excitation λ of 588 nm, emission λ of 649 nm.

Several images were modified from green to grey post-acquisition to account for the author being colour vision-impaired and hence, unable to differentiate between pre-set colours.

For quantitative image analysis (Ki67 proliferation studies), each coverslip was imaged in three random areas, creating an overlay of each fluorophore and the nuclear stain. Images were separated and imported into ImageJ (Fiji, NIH). An automatic cell counting macro, developed in-house by Dr. Rachael Wood was used and optimised for cell sizes. Cell somas were automatically counted and the readout was extracted to Microsoft Excel (Microsoft, Redmond, USA). Averages of the three random regions were taken for each image. DAPI-positive cells were regarded as total cell number, and subsequent marker-positive data presented as a percentage of total cells.

2.3 Cell Viability Studies – MTT assay

3-(4,5-dimethyl-2-thiazolyl)-2,5-diphenyl-2H-tetrazolium bromide (MTT) was diluted in sterile PBS to a stock of 2.5 mg/mL.

Ax0015 astrocytes were seeded at a density of 3000 cells/well in 96-well plates (2.1) and treated with serial dilutions of AraC in astrocyte medium in triplicate and returned to the incubator for 24 hours. Media was aspirated, and the cells washed in PBS. MTT stock was diluted in AM to a

working concentration of 0.5 mg/mL and added to the cells and control wells, before incubation for 2 hours.

MTT was then aspirated and 50 µL dimethylsulfoxide (DMSO) added per well to permeabilise formazan crystals. DMSO was triturated and shaken at 500 rpm for 30 seconds, using a Stuart SSL3 gyro-rocker (Cole-Parmer, Staffordshire, UK), then returned to the incubator for a further 15 minutes. Absorbance values were then measured at 590/690 nm using a Multiskan-EX spectrophotometer (Thermo)**.**

2.4 Gene expression analysis

All reagents and kits were purchased from PrimerDesign (Hampshire, UK) unless otherwise stated.

2.4.1 RNA extraction

RNA was isolated from spontaneously differentiated cultures and co-cultures at various timepoints. RNA was extracted and purified in accordance with the manufacturer's instructions from the Qiagen RNeasy mini kit (Qiagen, Manchester, UK; 74104). An additional DNAse treatment was also performed, to reduce the potential of detection of contaminating genomic DNA (Qiagen, 79254). Quantification was performed using the Nanodrop 1000 (Thermo). If qPCR was not to be performed immediately, samples were stored at -80 °C until needed.

2.4.2 cDNA synthesis

Isolated RNA was thawed on ice and 100 ng total RNA made up to 9 µL in sterile DNA/RNAse-free water. 1 µL Oligo-dT primers were added to the RNA template.

The mixture was then annealed at 65 °C for 5 minutes using a Thermocycler PCR machine (Bio Techne, Abingdon, UK) and immediately cooled on ice. 10 µL of reverse transcription mastermix (containing deoxynucleoside triphosphates (dNTP's), reverse transcriptase, buffer and RNA/DNAse-free water) was added and the sample reverse transcribed using the Thermocycler with the following conditions: 20 minutes at 42 °C, 10 minutes at 75 °C and held at 4 °C.

2.4.3 qPCR

Qualitative PCR was performed according to manufacturer's instructions. Briefly, SYBR® green was added to cDNA samples alongside RNA/DNAse-free water to pre-validated primers for Pax6, Sox2, TUBB3, S100β and vGAT. The housekeeping genes GAPDH, ACTB, YWHAZ and 18S were assayed under the same conditions as for experimental primers. Samples were added to PCR plates with an optical film seal and spun in a plate spinner (Thermo) for 30 seconds to ensure the sample was sufficiently mixed. Plates were loaded into a Lightcycler (Thermo) and cycled as shown in Table 2.3.

Table 2.3: qPCR protocol including steps involved, temperature, duration and number of cycles for reaction.

Steps	Temperature	Time	Cycles
Initial Denaturation	95 °C	10 minutes	1
Denaturation	95 °C	15 seconds	40
Annealing/Extension	60 °C	1 minute	

2.4.3.1 qPCR analysis

Analysis of qPCR data was performed using Microsoft Excel and the ΔΔCt method. Both control samples (Week 0) and experimental samples were normalised to endogenous controls (Appendix Figure A9A) and ΔCt was calculated from the difference in CT value between the target gene and the endogenous control, by subtracting the average control CT value from each replicate.

ΔΔCt was then calculated via ΔCt (experimental) – ΔCt (average control) and these values were used for statistical analysis (described in text). To generate a fold change in experimental gene expression relative to Time Week 0, $2^{-\Delta\Delta Ct}$ was computed and this value was represented in the figures throughout the thesis. In-text values refer to the ΔΔCt values from which statistical analysis was performed.

2.5 Fluorescent calcium imaging

2.5.1 Acquisition

Acquisition of calcium-mediated activity was achieved using a single-wavelength calcium sensitive dye and fluorescence imaging. Calcium signals were recorded under baseline (spontaneous) conditions, and evoked ionic and pharmacological conditions. 5 µM membrane-permeable Fluo4- acetoxymethyl ester (Fluo4-AM) (Molecular Probes, Eugene, Oregon, USA) dissolved in either Axol or SCT was added to the cells for 30 minutes and incubated at 37°C, followed by a recovery phase of media only, for 10 minutes. During incubation, respective media and artificial cerebrospinal fluid (aCSF) (containing, in mM: 126 NaCl, 26 $NaHCO_3$, 2.5 KCl, 1.25 KH_2PO_4, 10 $MgSO_4$, 2 $CaCl_2$, and 10 glucose) was heated to 37°C and bubbled with carbogen gas (95% O_2, 5% CO_2) to maintain pH.

Cells were imaged at a rate of 0.33 - 1 Hz over 5-40 minutes using a submersible 20X lens (Nikon, UK) and filter cube for Fluo4 (Chroma VT, USA). An Orca CCD camera (Hamamatsu, Japan) was used to acquire the images, allowing for the shutter to be controlled without the need to manually handle the microscope. A 65 ms exposure time and a bin value of 2 was used for experiments. Excitation of the fluorophore was done at 470 nm using an automated OptoLED power supply LED (Cairn, UK) and Optomorph software (Molecular Devices, US) was used for image acquisition of changes in intracellular calcium. Cells were mounted and perfused with either Axol, SCT or standard aCSF for several minutes before beginning the recording to allow the cultures to recover from any disturbances.

2.5.2 Evoked responses

After recording baseline activity for each coverslip, cells were subjected to a series of pharmacological and ionic manipulations (Table 2.4). Ionic manipulations involved modification of the standard aCSF recipe from 2.5.1. Drugs were dissolved in aCSF and continuously perfused

on to cultures at a low rate of 1 mL/min, avoiding the need for the recording to be paused or interrupted and limiting disruption.

Table 2.4: Variety of pharmacological and ionic manipulations used throughout the thesis.

Treatment	Class	Concentration used
Glutamate	Excitatory neurotransmitter	100 µM
Tetrodotoxin	Sodium channel blocker	1 µM
4-aminopyridine	Potassium channel blocker	100 µM
Picrotoxin	$GABA_A$ antagonist	100 µM
Valproate	Anticonvulsant	2 mM
Magnesium-free aCSF	Excitatory perfusate	0 mM $MgSO_4$
High potassium aCSF	Excitatory perfusate	7.5 mM KCl

2.5.3 Calcium Analysis

2.5.3.1 Video preparation and region of interest determination

Images were stacked, aligned and processed into video files using ImageJ. Continuous imaging over several minutes led to minor frameshift in some recordings, therefore stacks were aligned using the plugin: template matching - align slices in stack. Brightness and contrast were adjusted and videos were imported into Matlab software (Mathworks, 2018b), running NETCAL© network analysis software (www.itsnetcal.com, ©Javier Orlandi, 2017). Regions of interest (ROI) were automatically detected and manually reviewed, and from each ROI a fluorescence trace was generated. The data from each trace was exported to Microsoft Excel and GraphPad Prism (Version 8) to determine active cells, number of calcium events and bursting frequencies.

2.5.3.2 Active cell and calcium event classification

The size of a calcium event was calculated via: $\frac{\Delta F}{F} = \frac{F-F0}{F0}$ where F0 is the first frame in a video file. A cell was identified as being active if the ΔF/F peak value was greater than three times the standard deviation of the baseline noise, which was manually determined for each cell. These were regarded as spontaneous events. For synchronised events, cells were regarded as synchronous if their initiation was within 1 frame of another spontaneous event within the

video. Most recordings were acquired at 0.33 Hz, meaning a gap of one frame is equal to three seconds.

2.5.3.3 Experimental calculations

To calculate peaks per cell, burst frequency and active cells, each individual trace was manually reviewed and the peak values including number of peaks per cell, time of peaks and peaks per minute recorded using Microsoft Excel.

In order to quantify synchrony between cells of the population, the percentage of synchronised cells was calculated between active cells. To reduce the possibility of false positive reporting, events in which only two neurons were synchronised were dismissed, meaning a minimum of three neurons had to display the same response to be described as synchronised (Pirttimaki et al., 2017). Additionally, Pearson's correlation was performed on all individual active cell traces, compared to an average population trace (Cornelissen et al., 2013; Kuijlaars et al., 2016).

2.6 Multi-electrode array (MEA)

2.6.1 MEA acquisition

Planar MEA chips were prepared and cells seeded as described in sections 2.1 and 2.2. Cultures on MEA chips were recorded on a heated stage (Alpha Med Scientific, Osaka, Japan) whilst in a 37°C humidified incubator, with 5% CO_2, as extracellular MEA activity is sensitive to pH levels (maintained by CO_2 concentration). Extracellular signals were recorded in all 64 electrodes simultaneously at 1 kHz acquisition using MED64 Mobius Toolkit software (Alpha Med Scientific) using a 'basic-recording' template. Recordings typically lasted for 10 minutes, following a few minutes unrecorded initial measurement, to allow cells to recover. Signals detected were amplified using an Amadeus 64-channel amplifier (Alpha Med Scientific). Signals were low-pass filtered at 100 Hz and sampled at 20 kHz/channel (Odawara et al., 2016b).

2.6.2 MEA analysis

For MEA analysis, recordings obtained were ran through Mobius spike detection software (Alpha Med Scientific). Thresholds were set at 500 % standard deviation from baseline to ensure spikes were detected and not background noise. Extracted spike data was assessed visually for each 64 channels to determine whether the recorded data was in fact spike activity, and not noise. Once confirmed, frequency analyses, number of spikes/burst and burst duration were calculated using Mobius software.

Parameter values for analysis were set using an active MEA example as a basis for (Table 2.5).

Table 2.5: Burst detection parameters for MEA analysis

Parameter	Value
Max Interval to start burst (ms)	300
Max interval to end burst (ms)	350
Min number of spikes in a burst	3
Min duration of a burst (ms)	50
Min interval between bursts (ms)	100

2.7 Statistical analysis

All statistical analyses were performed using GraphPad Prism Version 8; the author is grateful to Professor Alan Nevill (Wolverhampton University, UK) for his advice whilst using this package. Bars on graphs and descriptions in-text represent mean values and error bars indicate ± standard error of the mean (SEM). For many graphs, box plots were selected to show the distribution of data.

Data-sets were considered un-paired and the Shapiro-Wilk normality test was performed to assess the distribution of data, followed by the appropriate statistical test: 1-way and 2-way analysis of variance (ANOVA) or student's T-test, with Tukey's post hoc test for multiple comparisons. The test used is indicated in-text.

Statistical analysis was complicated for percentage of active cell datasets in Figure 3.11 and Figure A3, due to an array of unequal sample sizes, combined with the data not satisfying Gaussian distribution, even after log transformation. As a result, individual one-way ANOVAs were performed (Appendix A3) and non-parametric t-tests of individual timepoints (Figure 3.11).

For non-normally distributed data undergoing 2-way ANOVA, the data was first log transformed to satisfy the requirements of normality. Datasets which underwent transformations are indicated in text.

For quantitative synchronised calcium-mediated activity, a Pearson's correlation was performed as described in 2.4.3. However, to generate an average R value for each experiment, a Fisher's *z*-transformation was applied to each individual R value. The mean of the z values was then calculated and this number back-transformed using Fisher's back-transformation. This provided an average R value for the experiment.

N numbers reported in figure legends refer to the number of biological differentiations, whereas those in text refer to the total number of technical repeats from all biological differentiations.

Statistical significance depicted in figures was reported as: *$p < 0.05$, **$p < 0.01$, ***$p < 0.001$, ****$p < 0.0001$.

Chapter 3

3: MORPHOLOGICAL AND FUNCTIONAL CHARACTERISATION OF SPONTANEOUSLY DIFFERENTIATED NEURAL CULTURES

3.1 Introduction

The human brain is a bewilderingly complex structure, comprised of a remarkable number of two principle cell types: neurons and glia. The cerebral cortex is the executive computational centre of the mammalian CNS, containing dozens of neuronal subtypes (Anderson & Vanderhaeghen, 2014). Neurons are electrically excitable cells, arranged in the cortex in six distinct layers and their extensive interconnectivity provides the processing capability that governs all physiological and psychological processes that we experience. Of particular relevance to this thesis is a basic feature of the cerebral cortex, which is how it is prone to generating synchronous, large bursts of activity which facilitates seizurogenesis (Bromfield et al., 2006). The role of glia and their various subtypes (namely astrocytes) has been markedly under-investigated, despite the brain being unable to function without both cell types. This forms the basis of the investigation in this Chapter.

3.1.1 *In vitro* and *in vivo* neurogenesis

An incredible and unique quality of iPSCs is their ability to form human neural cells in a relatively efficient and non-invasive manner (Takahashi & Yamanaka, 2006). The process of converting iPSCs to neural precursor stem cells (NPCs) is referred to as 'neuralisation'. Several neural differentiation protocols exist, which ultimately enables the production of neural subtypes (Chambers et al., 2009; Shi et al., 2012a;2012b). Each method has subtle differences, but largely the same outcome: functional, morphological human neural subtypes.

For an iPSC-derived model to fully recapitulate *in vivo* neurogenesis, there must be a degree of similarity and developmental processes in the *in vitro* environment. Shi et al., (2012a)

demonstrated that iPSCs follow an extended period of cortical neurogenesis (lasting several weeks) – that is more representative of the human *in vivo* environment *cf* rodent neurogenesis, which occurs over a matter of days. For example, during human development, neurulation involves the formation of the neural tube, which develops *in utero* into the brain and spinal cord (Sadler, 2005). The development of radially organised columnar epithelial cells *in vitro* gives rise to the characteristic cortical neural rosettes, which mirrors this neurulation process (Elkabetz & Studer, 2008).

In addition to distinctive morphology, cells undergoing *in vitro* cortical neurogenesis should contain markers for neural progenitor transcription factors (Shi et al., 2012a) and the generation of cortical neuronal layers (Pasca et al., 2015). Upper and lower cortical layer transcription factors have been identified during *in vitro* development, with the emergence of lower layer neurons occurring first and the layers developing in an 'inside-out' manner (Anderson & Vanderrhaeghen, 2014). This correlates with mammalian neocortical development, wherein NPCs sequentially give rise to lower layer and upper layer neurons during embryonic stages (Bansod et al., 2017).

Further characterisation of the temporal development of neural subtypes can also be monitored, particularly as radial glia form quite readily, followed by neuronal subtypes, before a switch from neurogenesis to gliogenesis. *In vivo*, the switch from neurogenesis to gliogenesis occurs at the perinatal states, and a delayed arrival of astrocytes is also observed *in vitro* (Shi et al., 2012a; Bansod et al., 2017). Consequently, the late arrival of astrocytes after neurons is a reliable indicator of cortical differentiation. As mentioned above, *in vivo* neural activity is dependent upon both neurons and astrocytes. However, protocols exist for the generation of individual neural subtypes, including neurons and astrocytes. Shaltouki et al, (2013) showed the exclusive generation of iPSCs into matured astrocytes using a defined media formulation.

3.1.2 Functional considerations

Whilst monitoring the emergence of and assessing for the presence of neural subtypes during cortical differentiation is an invaluable tool, these results alone are of little or no indication of cell function. Many cells in culture may morphologically resemble cells *in vivo,* but that is not an accurate assessment of their identity. As neurons are electrically excitable cells and indeed, astrocytes are capable of functional activity, the best assessment of a successful neural differentiation is to verify the functional capability of the cells.

In vivo, neurons are active cells, firing AP and eliciting neurotransmission. This functionality arises due to a difference in ionic potential that exists between the intracellular and extracellular spaces. To replicate *in vivo* activity, human iPSC-derived cultures should be able to generate AP *in vitro* and respond to neurotransmitters, as happens in the intact brain.

3.1.3 Growth medium considerations

The first stage of any project intended to develop a reliable protocol for applying iPSCs to use in neural models, is to optimise the basic conditions for growth and differentiation, as these conditions can influence the above structural and functional endpoints. Growth media is the most important determinant of these outcomes, as culture conditions for stem cell-derived neurons do not necessarily mirror those observed *in vivo* (Rocktäschel et al., 2019). Evidently, as the cell culture itself should be as representative of the *in vivo* state as possible, all integrated factors such as the media should also aim to mimic *in vivo* compositions. Multiple companies and institutions are now producing their own media formulations and whilst often based on neurobasal/DMEM recipes, the added supplements and factors has led to great variation within the field.

Interestingly, very high concentrations of glucose (up to 25 mM) are commonly observed in culture media compositions, where this value should be closer to 5 mM to be physiologically relevant and promote translatability of stem cell models (Rocktäschel et al., 2019). A specialised

neuronal medium was developed in 2015 which serves to mimic human *in vivo* compositions as closely as possible (Bardy et al., 2015). Indeed, they recognised the hyperglycaemic condition of many neurobasal/DMEM recipes and amended theirs to prevent abnormal glucose homeostasis affecting the cultures, as has been shown with several brain disorders (Mergenthaler et al., 2013). Moreover, It has been shown that concentrations of salts (in particular, NaCl) and the presence of serum may directly influence certain electrical activity (Bardy et al., 2015), which creates another issue for functional studies, as groups are testing their cells using different fluid compositions. In addition to glucose, salts and osmolarity, the neuronal supplements used for growth media have also been assessed (Sünwoldt et al., 2017). Commonly used supplements including B27 and N2 were found to elicit variable effects on neuronal cultures and negatively alter glucose metabolism, respectively. B27 is serum-free and highly dense in nutrients and hormones, ranging from insulin to progesterone. B27 in many cases is neuroprotective, contributing to neuronal growth and neurite extension (Chen et al., 2008). However, the advent of serum-free media compositions intended to reduce the variability which can occur from serum-containing solutions and indeed, modifications to B27 recipes have resulted in an optimised, more physiological supplement (NS21) (Chen et al., 2008). N2 supplement is a widely-used, chemically defined serum-free supplement recommended for growth of post-mitotic neurons; however, the modern alternative (GS21) was found to positively affect energy metabolism in neuronal cultures (Sunwoldt et al., 2017).

Artificial cerebrospinal fluid (aCSF) is a mimic of the fluid surrounding the brain *in vivo* and whilst devoid of neuromodulators found in human CSF, it contains the necessary salts and pH to function as a perfusate and bathing solution (Wickham et al., 2020). Indeed, aCSF is widely used for *ex vivo* slice assays and primary cultures and for inducing and assessing epileptiform activity. Due to the range of medium available for iPSC culture, it may be that a defined aCSF formulation should be used for functional studies to create a standard protocol for iPSC-derived neural toxicity testing. Despite its widespread use as a perfusate in rodent *in vivo, in vitro* and human

in vitro models, aCSF does not promote neuronal survival for longer than a few days and hence, is an unsuitable medium for maintaining cells long-term (Bardy et al., 2015).

As the role of growth medium is so influential, the effects of two different commercially available growth media (Axol Biosciences: Axol Neural Maintenance medium; Shi et al., 2012b and StemCell Technologies: BrainPhys™; Bardy et al., 2015) have been compared in this chapter, to assess the differences in their ability to generate morphologically and functionally matured neural cultures.

The aims of this Chapter are to:

1) **Assess the morphological expression of spontaneously differentiated neural cultures via cell specific biomarkers of: neural progenitors, cortical layers, excitatory and inhibitory neurons and glia; using fluorescence microscopy**
2) **Determine the functional capability of spontaneously differentiated cultures, including the ability to fire action potentials and respond to neurotransmitters, using fluorescent calcium imaging and multi-electrode array recordings**
3) **Compare the effects of Axol and SCT media on their respective abilities to generate functionally and morphologically matured neural cultures**

3.2 Results

3.2.1 Characterisation of spontaneous differentiation

Human iPSC-derived NPCs were spontaneously differentiated in Axol and SCT over 18 weeks *in vitro* (WIV). In order to determine whether neural cultures can generate expected neural subtypes, immunocytochemistry (ICC) and qualitative polymerase chain reaction (qPCR) were performed over 18 WIV. 18 WIV was designated as a cut-off point, as the viability of SCT cells post W18 were severely impacted. Indeed, widespread detachment of fasciculated neurons was observed in all W18 SCT cultures (Appendix Figure A1). Whilst cells were cultured past 21 WIV, experimentation became highly problematic, with large reductions in activity and very poor resolution from microscopy.

Cells in both media conditions produced morphologically distinctive neural cortical rosettes by 1 WIV, positive for both Pax6 and Sox2 neural progenitor markers, which were distributed in a radial fashion (Figure 3.1, n=9 coverslips (cs)). Pax6 and Sox2 gene expression was assessed using qPCR. Results indicate that Pax6 expression was significantly upregulated in Axol media at 4 WIV ($p= 0.046$, Figure 3.2A). Whilst SCT observed a difference in values of Pax6 expression, relative to control, these did not attain statistical significance. The expression of Sox2 was significantly downregulated in SCT media at W4 and W8 compared to control ($p<0.0001$, Figure 3.2B) but Sox2 was significantly upregulated at W12, compared with earlier experimental timepoints ($\Delta\Delta$Ct W12: 1.87 ± 0.64; W4: 5.31 ± 0.47, $p= 0.0008$, W8: 4.20 ± 0.19, $p= 0.0278$).

To monitor the emergence of distinct neural subtypes, neuron-specific class III β-tubulin (Tuj1) and calcium-binding protein S100β were used to stain neurons and astrocytes, respectively. At 4 WIV, both conditions were negative for S100β staining (Figure 3.3B), however, both displayed an interconnected array of $Tuj1^+$ neurons, developing by 8 WIV to aggregated clusters of neuronal cell bodies (Figure 3.3C, n=9 cs). By 8 WIV, both Axol and SCT displayed $S100\beta^+$ staining, however, the staining was localised to the soma, correlating with the $DAPI^+$ nuclei also observed (Figure 3.3A,B).

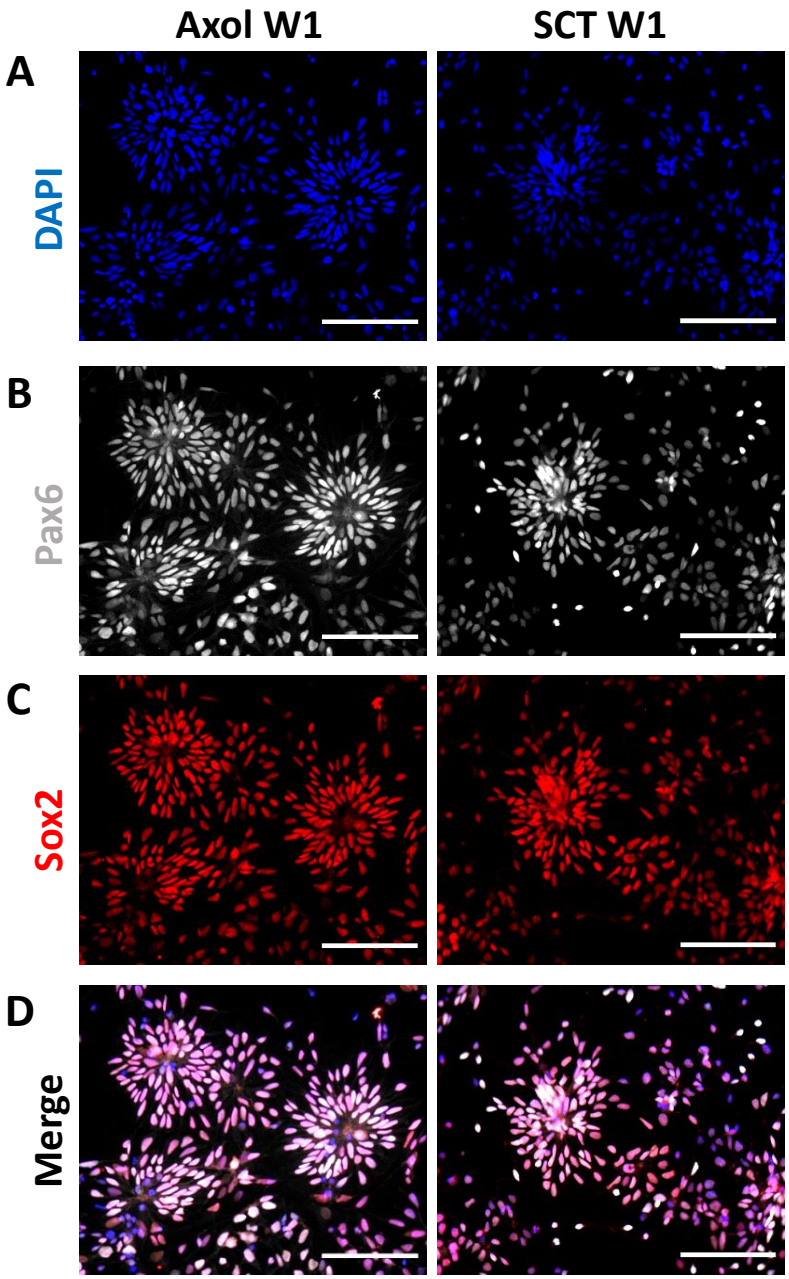

Figure 3.1: Spontaneously differentiated neural precursor cells (NPC's) form cortical rosettes in Axol and SCT media. iPSC-derived neural precursors were differentiated in Axol or SCT media over 1 week and immunocytochemistry was performed to assess the presence of neural progenitor markers. (**A**) Nuclei stained with DAPI (Blue, excitation λ 345 nm, emission λ 455 nm). (**B**) Pax6 neural progenitor staining (Grey, excitation λ 495 nm, emission λ 519 nm). (**C**) Sox2 neural progenitor staining (Red, excitation λ 588 nm, emission λ 648 nm). (**D**) Merged images of A,B,C. N=3. Scale bar: 100 µm.

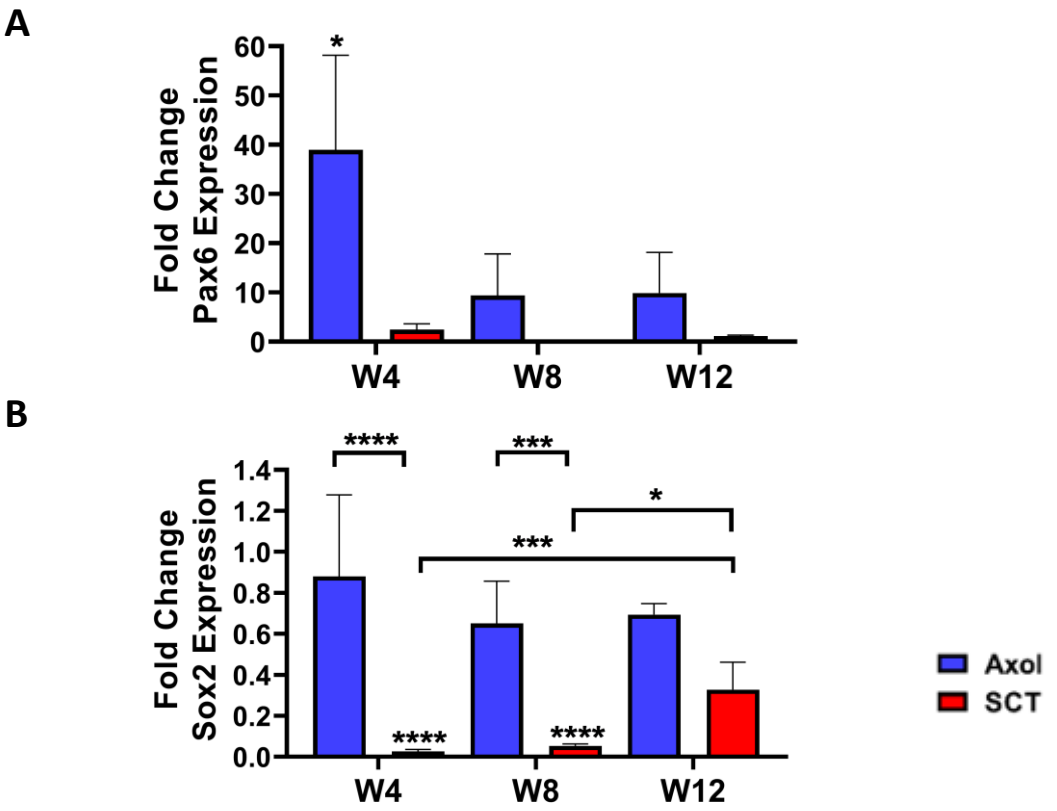

Figure 3.2: Spontaneously differentiated NPCs express Pax6 and Sox2 progenitor genes in Axol and SCT media. iPSC-derived neural precursors were differentiated in Axol or SCT media over 12 weeks and qPCR was performed to assess the expression of genes associated with neural progenitors. (**A**) Fold change in Pax6 expression over 12 WIV relative to control expression at W0 (not indicated on graph). (**B**) Fold change in Sox2 expression over 12 WIV. Data is displayed as mean ± SEM. N=3 separate biological differentiations. *p< 0.05, 2-way ANOVA with Tukey's multiple comparisons test.

At 12 WIV, morphologically distinct S100β^{+} astrocytes were observed in both conditions (Figure 3.4C, n=9 cs. In addition, by 12 WIV, the staining appeared to show an even distribution of astrocytes and neurons, closely intertwined in both media conditions, with more astrocytes visible by 18 WIV (Figure 3.4). Furthermore, the size of astrocytes in the Axol cultured cells' field of view at 18 WIV were more comparable to those of the SCT astrocytes. The discrepancy between sizes of astrocytes was observed in both media conditions at 12 and 18 WIV, showing that different types and sizes of astrocytes were generated throughout the spontaneous differentiation (n=9 cs). In addition, there were several regions of each W18 coverslip where the cultures appeared entirely astrocytic (Appendix Figure A2).

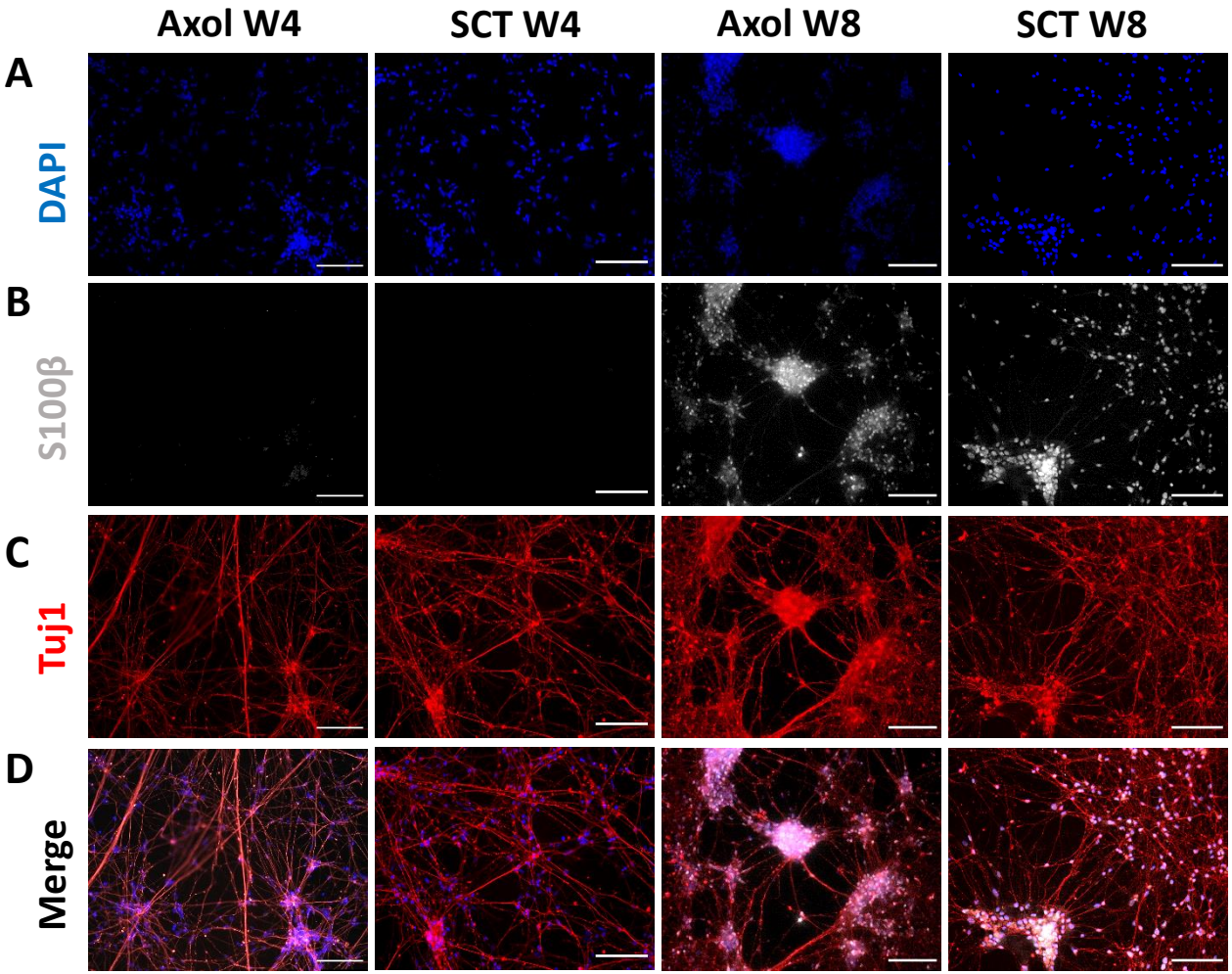

Figure 3.3: Astrocytes emerge following 8 WIV spontaneous differentiation of human iPSC-derived neural precursors. Neural cultures were differentiated in either Axol legacy or SCT BrainPhys media over 8 weeks and immunocytochemistry was performed to assess the emergence of neurons (Tuj1) and astrocytes (S100β). (**A**) Nuclei stained with DAPI (Blue, excitation λ 345 nm, emission λ 455 nm). (**B**) S100β astrocytic staining (Grey, excitation λ 495 nm, emission λ 519 nm). (**C**) Tuj1 neuronal staining (Red, excitation λ 588 nm, emission λ 649 nm). (**D**) Merged image of A,B,C. N=3. Scale bar: 100 µm.

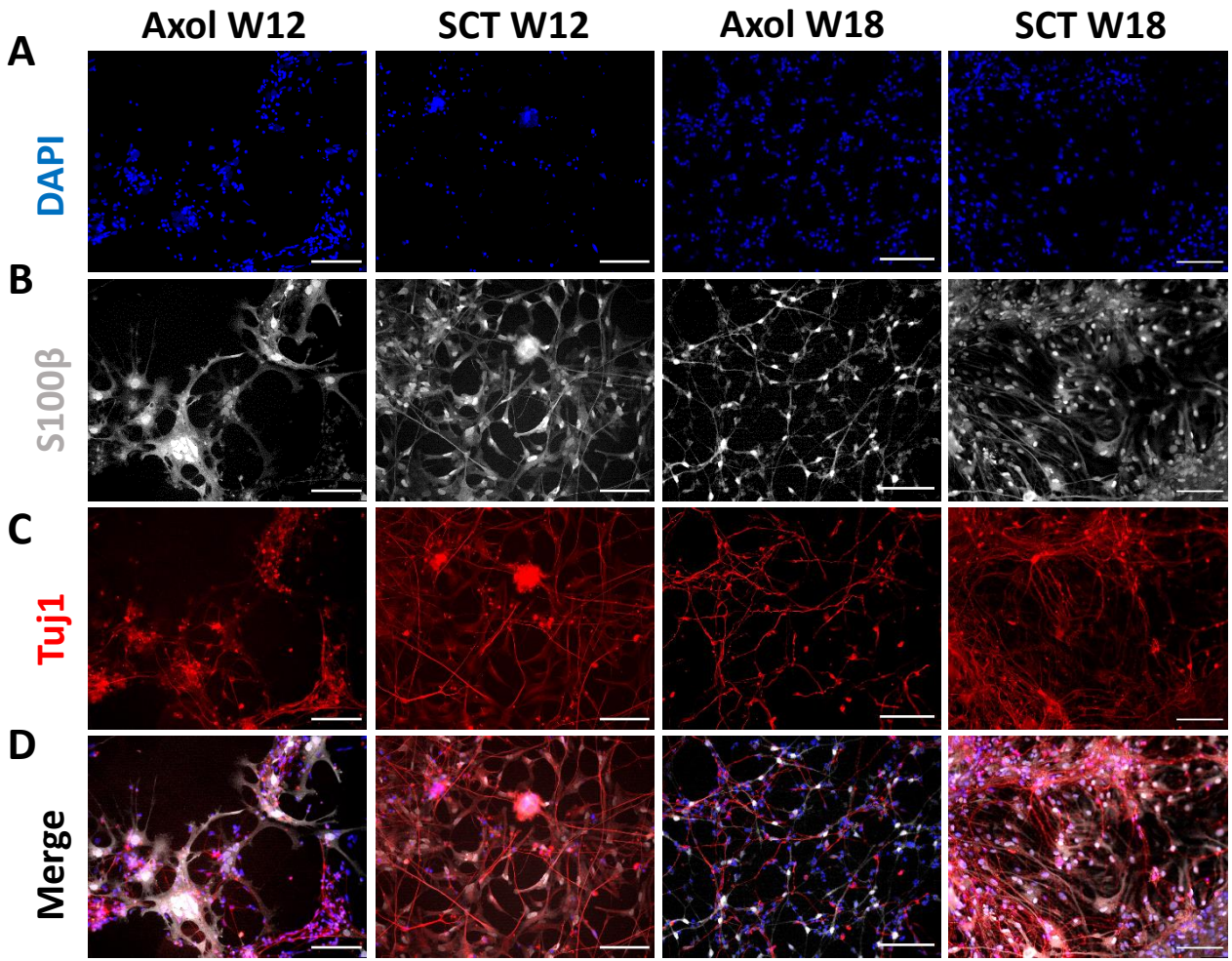

Figure 3.4: Human iPSC-derived NPCs form neurons and morphologically distinct astrocytes by 12 WIV. Neural cultures were differentiated in either Axol legacy or SCT BrainPhys media over 18 weeks and immunocytochemistry was performed to assess the emergence of neurons (Tuj1) and astrocytes (S100β). (**A**) Nuclei stained with DAPI (Blue, excitation λ 345 nm, emission λ 455 nm). (**B**) S100β astrocytic staining (Grey, excitation λ 495 nm, emission λ 519 nm). (**C**) Tuj1 neuronal staining (Red, excitation λ 588 nm, emission λ 649 nm). (**D**) Merged image of A,B,C. N=3. Scale bar: 100 µm.

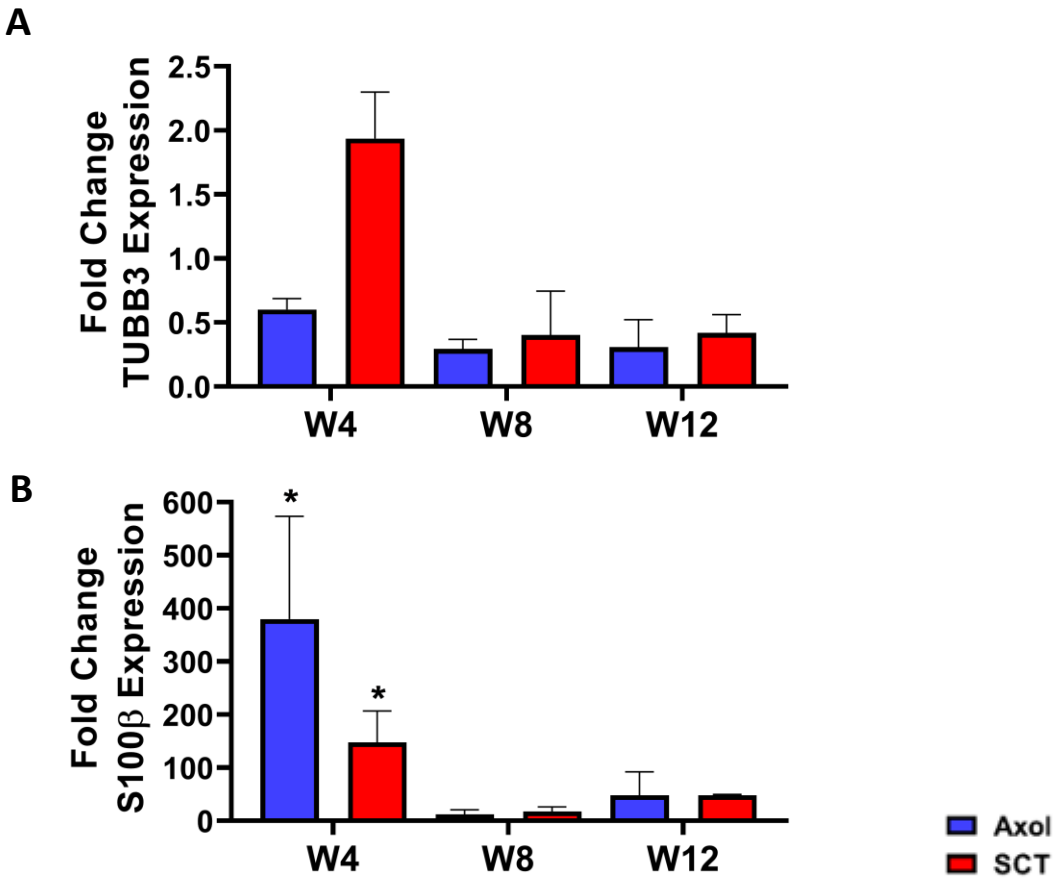

Figure 3.5: Spontaneously differentiated NPCs express TUBB3 and S100β over 12 WIV in Axol and SCT media. iPSC-derived neural precursors were differentiated in Axol or SCT media over 12 weeks and qPCR performed to assess the expression of genes associated with neurons (TUBB3) and astrocytes (S100β). (**A**) Fold change in TUBB3 expression over 12 WIV relative to control expression at W0 (not indicated on graph). **B)** Fold change in S100β expression over 12 WIV. Data is displayed as mean ± SEM. N=3. *p< 0.05, 2-way ANOVA with Tukey's multiple comparisons test.

There was no significant difference in TUBB3 expression (gene encoding *Tuj1*) at any timepoint in both Axol and SCT media compared to control (Figure 3.5A). In contrast, at W4 fold S100β expression in both Axol and SCT was significantly increased *cf* control (Axol: p= 0.0192, SCT: p= 0.0193, Figure 3.5B).

Roughly 80% of the mammalian cerebral cortex is comprised of excitatory neurons (Marik et al., 2010). The presence of excitatory vesicles (VGlut1) was therefore of great importance. Figure 3.6 shows that both Axol and SCT at 4 WIV generated characteristic punctate synaptic staining.

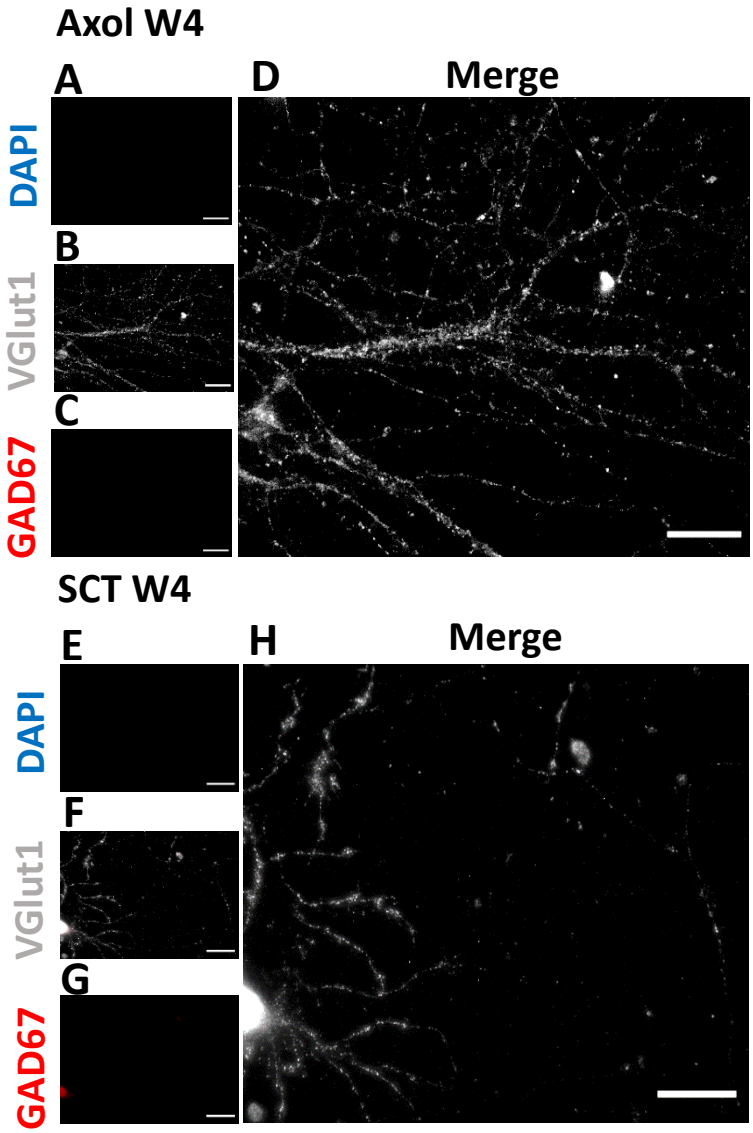

Figure 3.6: Spontaneously differentiated NPCs form excitatory, but not inhibitory synapses in Axol and SCT media. iPSC-derived NPCs were differentiated over 4 weeks and immunocytochemistry performed to assess excitatory and inhibitory synapse formation. (**A-D**) Cultures differentiated in Axol media. (**E-H**) Cultures differentiated in SCT media. (**A,E**) Nuclei stained with DAPI (Blue, excitation λ 345 nm, emission λ 455 nm). (**B,F**) VGlut1 excitatory vesicle staining (Grey, excitation λ 495 nm, emission λ 519 nm). (**C,G**) GAD67 inhibitory staining (Red, excitation λ 588 nm, emission λ 649 nm). (**D,H**) Merged images. N=3. Scale bar: 25 µm

The absence of $DAPI^+$ cells (Figure 3.6A,E) is due to the magnification used. Using the 63x objective, $DAPI^+$ nuclei covered most of the field of view, therefore a region of interest was selected where no DAPI signal was obtained. Vesicular glutamate transporter-1 (VGlut1) is associated with membranes of synaptic vesicles and preferentially transports glutamate. VGlut1 is often used to indicate the presence of excitatory neurons (Wojcik et al., 2004).

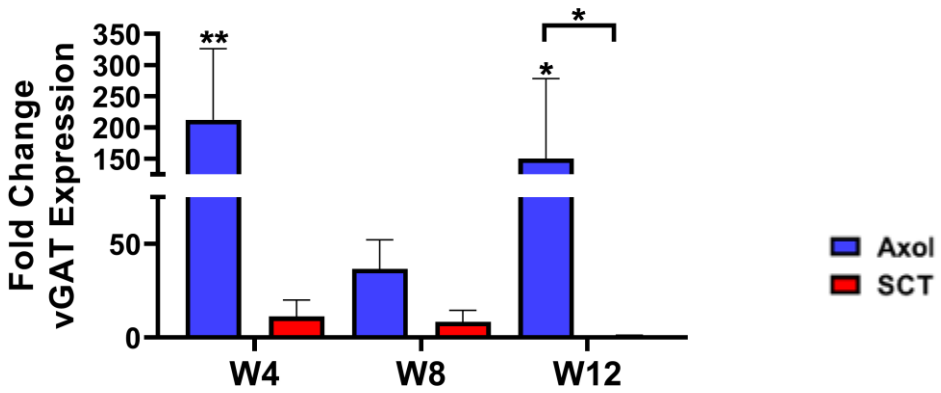

Figure 3.7: Spontaneously differentiated NPCs express vGAT over 12 WIV in Axol and SCT media. iPSC-derived neural precursors were differentiated in Axol or SCT media over 12 weeks and qPCR performed to assess the expression of inhibitory amino acid transporter vGAT. Fold change in vGAT expression over 12 WIV relative to control expression at W0 (not indicated on graph).. Data is displayed as mean ± SEM. N=3. *p< 0.05, **p< 0.01, 2-way ANOVA with Tukey's multiple comparisons test.

In contrast, glutamic acid decarboxylase 67 kDa (GAD67) is an enzyme catalysing the decarboxylation of glutamate to GABA, widely expressed in GABAergic neuronal populations (Rudy et al., 2011). GAD67 was therefore used as a marker for inhibitory neuronal populations.

Figure 3.6C,G shows a complete absence of $GAD67^{+}$ staining at 4 WIV. Staining for GAD67 was also performed at W8, W12 and W18 and $GAD67^{+}$ staining was consistently absent in both conditions (data not shown). As synaptic vesicular staining is a sensitive process, the ICC results of GAD67 were supplemented with qPCR analysis of a secondary gene (SLC32A1) encoding the vesicular inhibitory amino acid transporter vGAT, which is highly concentrated in the nerve terminals of GABAergic neurons (Chaudhry et al., 1998). Figure 3.7 shows a significant increase in fold vGAT expression at 4 and 12 WIV in Axol *cf* control (W4: p= 0.0043, W12: p= 0.0267). There was no significant change in expression of vGAT at any point in time during differentiation in SCT media.

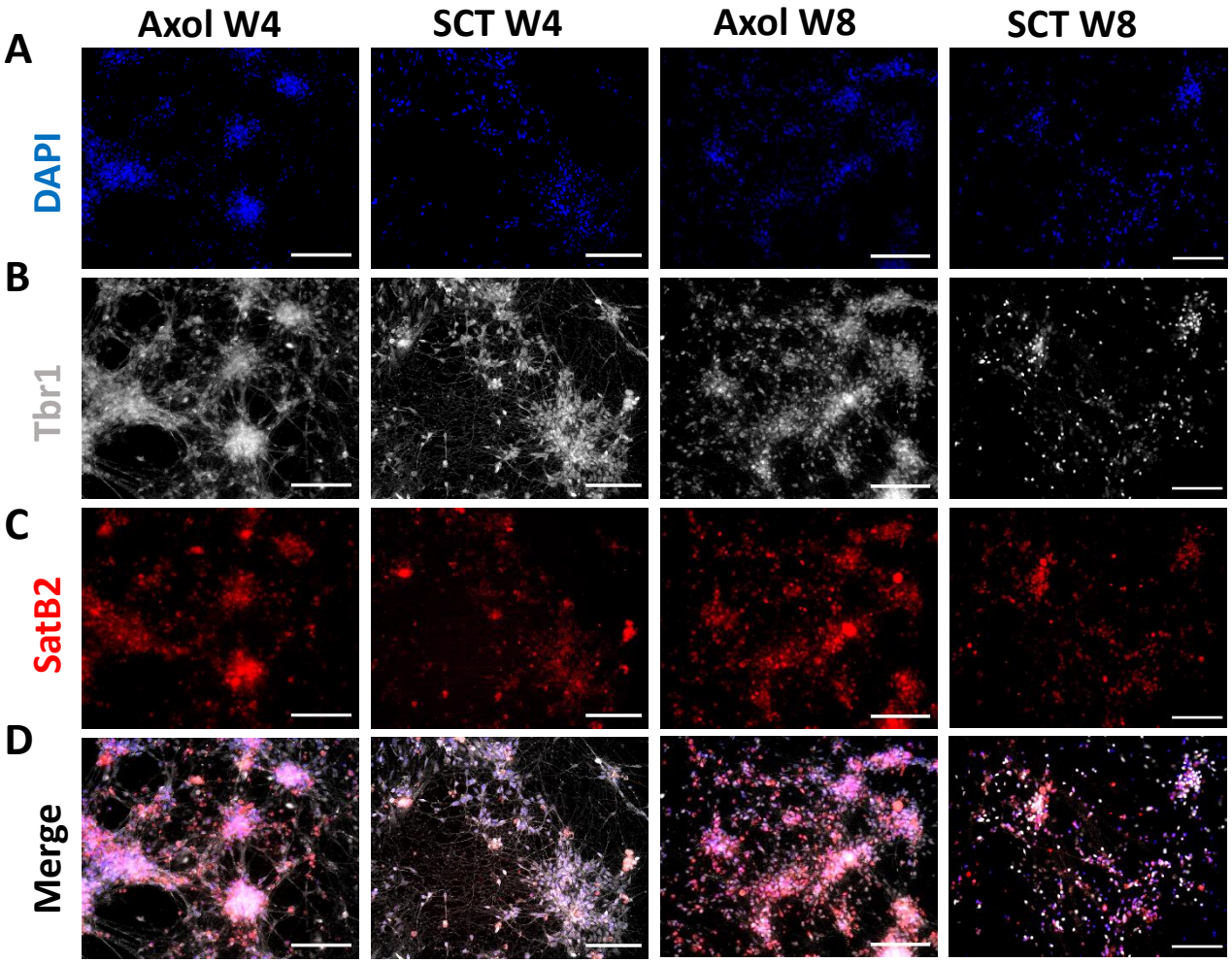

Figure 3.8: Human iPSC-derived NPCs form upper and lower cortical neurons when spontaneously differentiated after 4 weeks. Neural cultures were differentiated in either Axol legacy or SCT BrainPhys media over 8 weeks and immunocytochemistry was performed to assess the emergence of lower layer cortical neurons (Tbr1) and upper layer cortical neurons (SatB2). (**A**) Nuclei stained with DAPI (Blue, excitation λ 345 nm, emission λ 455 nm). (**B**) Lower layer cortical neurons (Grey, excitation λ 495 nm, emission λ 519 nm). (**C**) Upper layer cortical neurons (Red, excitation λ 588 nm, emission λ 649 nm). (**D**) Merged image of A,B,C. N=3. Scale bar: 100μm.

Alongside neurons and astrocytes, the intention for spontaneous differentiation was to commit to cortical neurogenesis. To test this, immunocytochemistry (ICC) was done to assess for the emergence of cortical layer markers. Transcription factors T-box brain-1 (Tbr1) and special AT-rich sequence-binding protein-2 (SatB2) encode lower and upper layer cortical neurons, respectively. In both conditions, the level of Tbr1 expression appeared constant at all timepoints. Images from W4 and W8 are displayed, as the resolution of W12 onwards decreased considerably as the density of cultures increased. W4 Axol appears to show a greater proportion of $SatB2^+$ cells, compared to W4 SCT (Figure 3.8). In addition, SatB2 expression between W4 and W8 Axol appears the same, whereas there appears to be an increase in SatB2 expression between W4 and W8 SCT (n=9 cs).

3.2.2 Functional calcium activity in spontaneously differentiated cultures

Having performed experiments to assess the presence of morphologically relevant neural subtypes and cortical markers, the next important question was whether the cells could display functional activity and basic drug responses. This question was addressed via single-wavelength fluorescent calcium imaging using Fluo4-AM and multi-electrode array (MEA) analysis. Spontaneous cultures were cultured as described (Chapter 2) for the above ICC/qPCR studies and assessed at the same timepoints for their functional properties.

A standard principle in electrophysiology is the use of artificial cerebrospinal fluid for functional studies. However, as Bardy et al., (2015) claim their media is superior for functional studies, the effect of each respective media as a perfusate on electrical activity was considered (Figure 3.9). There was no significant difference between the use of Axol and SCT media as perfusates (n=5/6 cs, p= 0.99). However, the use of both medias induced a significantly lower percentage of active cells compared with the same cultures perfused with aCSF (Axol Media: 4.08 ± 1.75%, n=6 cs, Axol aCSF: 11.77 ± 1.60%, n=9 cs, p= 0.03; SCT Media: 3.86 ± 1.18%, n=5 cs, SCT aCSF: 14.48 ± 2.00%, n=9 cs, p= 0.003).

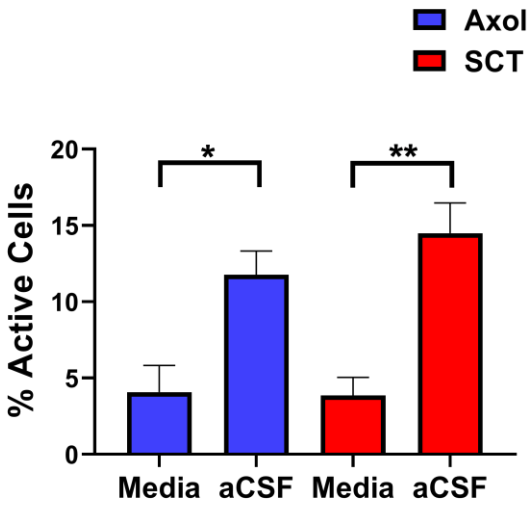

Figure: 3.9 Artificial cerebrospinal fluid is the optimal perfusate for fluorescent (Fluo4-AM) calcium imaging of neural cultures. Human iPSC-derived neural cultures were spontaneously differentiated over 8 weeks in either Axol or SCT media. Cultures were then fluorescently calcium imaged in respective growth media and in artificial cerebrospinal fluid. The percentage of active cells calculated as those with ≥ one peak of calcium activity. Data is displayed as mean ± SEM. N=3. *p< 0.05, **p< 0.01, ANOVA with Tukey's multiple comparisons test.

Following the assessment of perfusates, aCSF was selected to continue functional studies. The responses of W8 cultures to 1 µM tetrodotoxin (TTX) and 100 µM glutamate are shown in Figure 3.10 and Video 3.1. In both instances, the cultures were spontaneously active in all randomly selected example cells. The addition of TTX is an established method for blocking Na^+ channels and preventing the subsequent sodium-mediated depolarisations necessary for action potential generation (Wasserstrom & Salata, 1988). In both cultures, TTX addition inactivated the baseline spontaneous calcium responses. This spontaneous calcium activity was then recovered by the addition of the excitatory neurotransmitter glutamate, with representative cells responding with large amplitude fluorescence increases of ≥0.5 ΔF/F in 8/10 traces for SCT and 7/10 traces for Axol. In all experiments, spontaneously active cells were inactivated by the addition of TTX and excited by glutamate (n=9 cs). In the representative example in Figure 3.10, the average

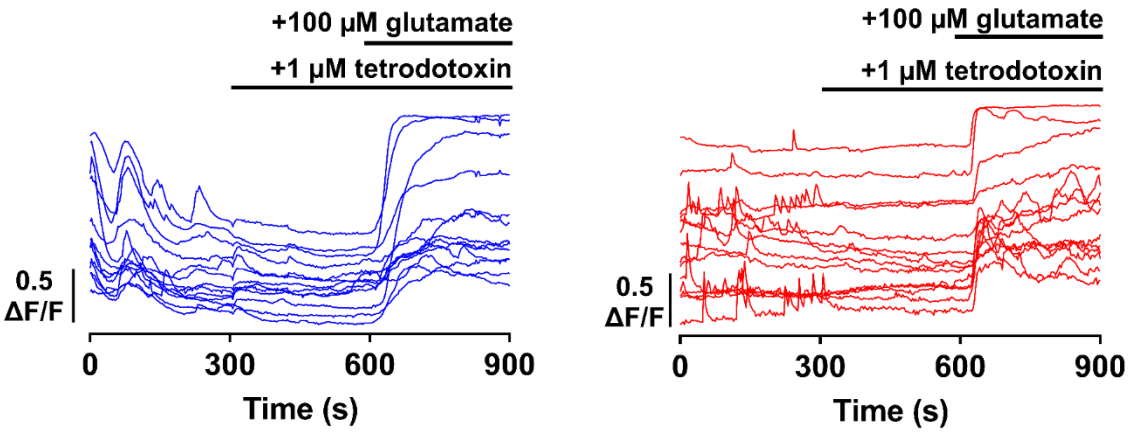

Figure 3.10: Responses of Axol and SCT spontaneously differentiated cultures to 1 µM tetrodotoxin (TTX) and 100 µM glutamate. Human iPSC-derived neural cultures were spontaneously differentiated over 8 weeks in either Axol (Blue; left) or SCT (Red; right) media. Cultures were then fluorescently calcium imaged using Fluo4-AM in aCSF to record baseline activity, then treated with TTX and glutamate. N= ≥6 coverslips from ≥2 biological differentiations. Solid black bar indicates the addition of respective condition.

change in fluorescence during spontaneous recordings were 107.95 ΔF/F and 125.29 ΔF/F for Axol and SCT, respectively.

Treatment with TTX reduced the average fluorescence amplitude values of Axol to 90.77 ΔF/F and SCT to 121.24 ΔF/F, with glutamate causing large increases in fluorescence value to 140.24 ΔF/F and 155.11 ΔF/F, respectively.

Following initial investigation of functional calcium activity/responses, spontaneously differentiated cultures were assessed at each timepoint for baseline calcium activity. SCT had no significant effect on the percentage of active neurons at any timepoint (p= 0.1016, Appendix Figure A3). In contrast, Axol cells were significantly more active at 18 WIV compared with every other timepoint (W4: 3.40 ± 0.58%, n=18 cs, p< 0.0001; W8: 14.57 ± 1.77%, n=27, p= 0.0013; W12: 7.59 ± 0.75%, n=36 cs, p< 0.0001; W18: 26.76 ± 4.93%, n=18, Appendix Figure A3). At 4 WIV, cultures differentiated in SCT displayed significantly more active cells than Axol cultures (Axol: 3.399 ± 0.58%, SCT: 11.22 ± 1.27%, n=18 cs, p< 0.0001, Figure 3.11A). However, at 8 WIV, there was no significant difference observed between media groups (n=27 cs, p=0.36, Figure

3.11B). Figure 3.11C shows that SCT was significantly more active than Axol at W12 (Axol: 7.59 ± 0.75%, n=36 cs, p< 0.0001). In contrast, W18 displayed no significant difference between either media condition (n=18 cs, p= 0.4619, Figure 3.11).

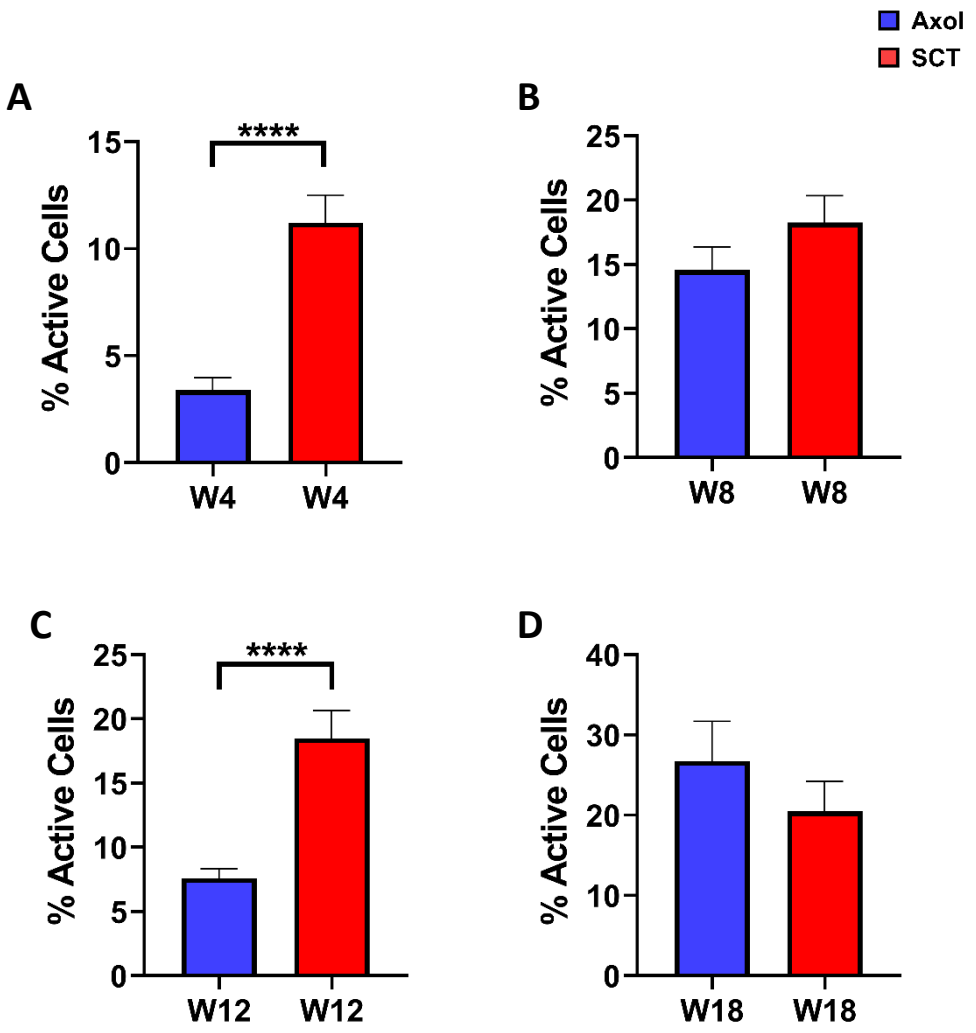

Figure: 3.11 Comparisons of spontaneously differentiated cultures over 18 WIV. Human iPSC-derived spontaneous neural cultures were differentiated over 12 weeks. Cultures were then fluorescently calcium imaged in aCSF to record baseline activity. Active cells were determined as those with a minimum of one peak of calcium-mediated activity (peak > 3x s.d baseline noise). (**A**) W4 Axol and SCT. (**B**) W8 Axol and SCT. (**C**) W12 Axol and SCT. (**D**) W18 Axol and SCT. Data is displayed as mean ± SEM. N=3. ****p< 0.0001, unpaired, Mann-Whitney.

3.2.3 Multi-electrode array recordings

Whilst fluorescent calcium imaging is an invaluable optical method for monitoring cellular activity and responses to drug treatments, multi-electrode arrays (MEA) are a non-invasive, real-time, multi-point measurement of putative action potentials and moreover, they yield an impression of network activity. Combined with calcium imaging, this gives a strong indication of the true responses of cultured cells. Spontaneous cultures were plated onto MEAs and their adherence monitored over time.

Cells detached at various timepoints in every repeat (n=>40 MEA chips), with cells forming aggregates and fasciculation of neurites over extended periods in culture. Interestingly, the cells appeared to migrate back over the electrodes at some timepoints after initially detaching; however, there was a marked reduction in the number of electrodes underneath cultured neurons. Figure 3.12 shows that at 2 WIV, all 64 electrodes were covered, reducing to 21 electrodes by 4 WIV. By 8 WIV this number had increased to 53 electrodes, however by 12 WIV, the entire culture had detached, with 0 electrodes covered. To combat the issue of adherence, two different MEA chips were purchased: carbon-based and platinum-based.

In addition, MEAs were coated with several biological substrates: polyethyleneimine (PEI), poly-d-*L*-ornithine (PDLO) and poly-*L*-ornithine (PORN) (Amin et al., 2016), on both chip types. Cells were seeded and differentiated over time. PORN on carbon-based MEA chips was found to be the most adherent coating substrate and this was used for all future experiments (data not shown). Despite the adherent properties of PORN *cf* PEI and PDLO, cell activity could only be assessed at W4 and W8 for 1 successful repeat (Figure 3.13).

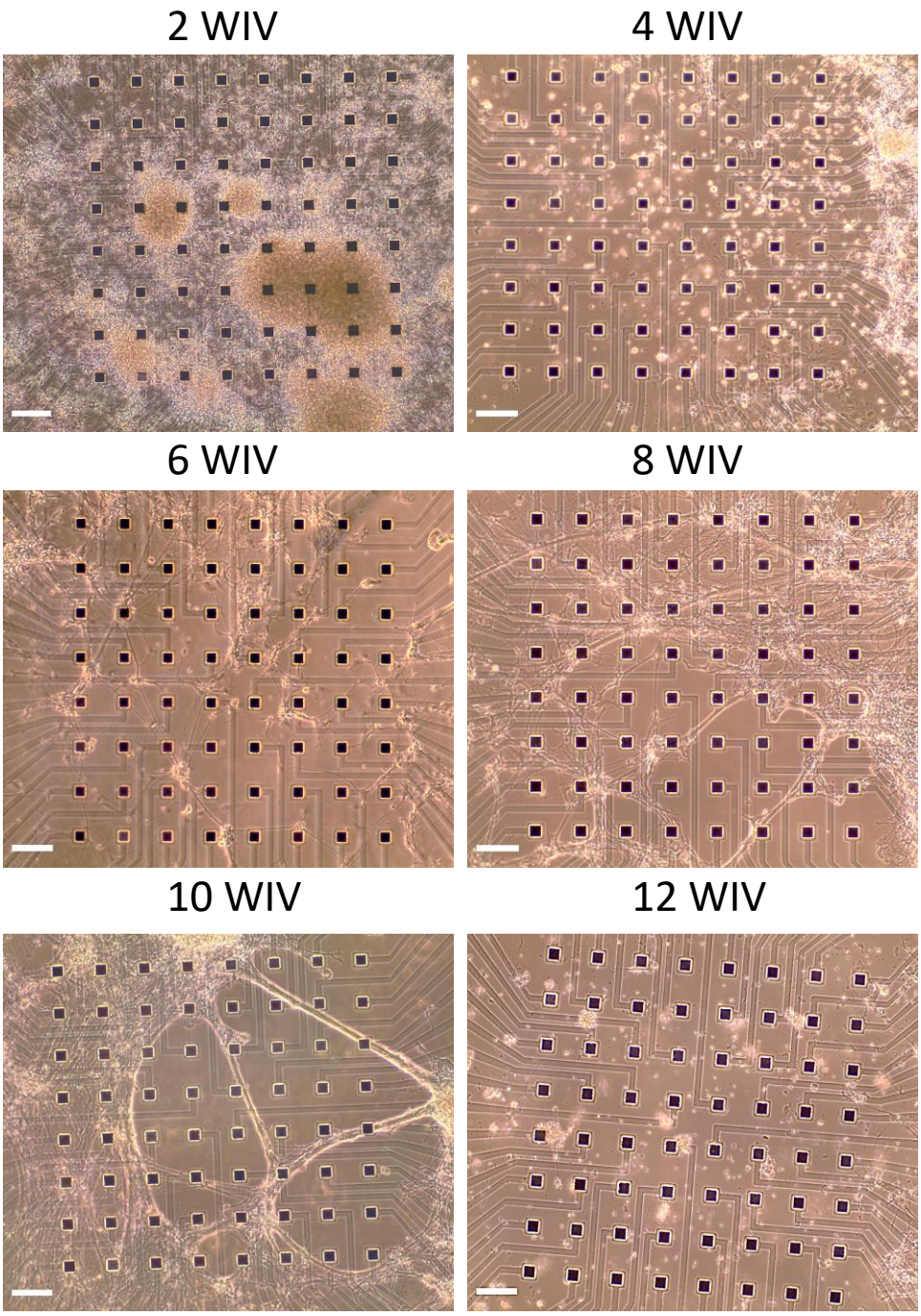

Figure 3.12: Spontaneously differentiated NPCs over 12 WIV on planar MEA chips. Representative phase contrast images display the same cultured 64 carbon-coated electrodes over 12 weeks. WIV refers to number of weeks *in vitro* differentiation. N=10. Scale bar: 200 µm.

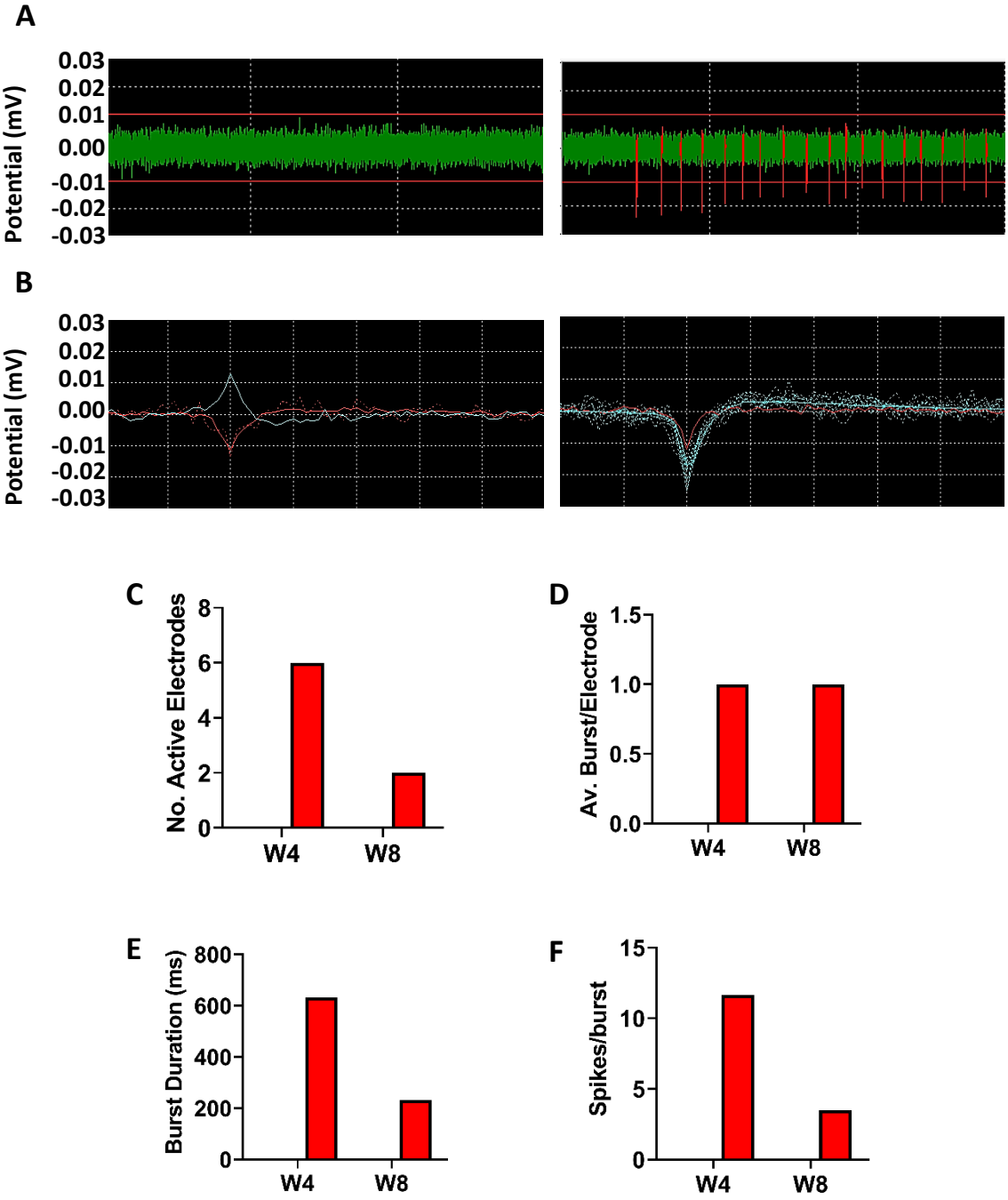

Figure 3.13: Spontaneous multi-electrode array responses of Axol and SCT- cultured cells at 4 and 8 WIV. Cells were seeded and differentiated on carbon MEA chips over 8 weeks and baseline activity assessed using MEA analysis. (**A**) Traces of spiking activity, -0.015 mV was the minimum potential to denote action potential activity, whilst red lines above/below show 5 x standard deviation threshold. (**B**) Clustered activity relating to traces in A. (Left: Axol, Right: SCT). (**C**) Number of active electrodes where spikes recorded. (**D**) Average number of bursts per active electrode. (**E**) Duration of burst in each electrode. F) Average number of spikes/burst. N=1 in each condition.

3.3 Discussion

In this Chapter, the morphological and functional characterisation of iPSC-derived spontaneously differentiated cultures has been achieved through ICC, qPCR, fluorescent calcium imaging and MEA analysis.

Spontaneously differentiated cultures generate neurons, astrocytes, cortical cells and excitatory synapses

The decision to present only qualitative ICC data arose from the realisation that as cultures matured, they became extremely dense. This culminated in the formation of large 3-dimensional aggregates which were impossible to image using available fluorescent and confocal imaging (Appendix Figure A4). This is a common theme within this field and throughout our laboratory (Personal communication, Dr. Eric Hill). Only qualitative results for iPSC neuronal differentiations are usually presented (Odawara et al., 2014). Quantitation was possible for some early timepoints with some staining, but the results from one timepoint were of very little value, as comparisons with later timepoints was not possible. To maintain consistency throughout ICC experiments, a qualitative, rather than quantitative approach was preferred.

The formation of distinctive neural rosettes in Axol and SCT media shows the potential of each media for neural differentiation and serves as a reliable indicator that cells have committed to a cortical, neuronal lineage (Shi et al., 2012a). Pax6 controls cortical development and is a reliable marker of cortical neurogenesis (Manuel et al., 2015), whereas Sox2 regulates iPSCs neural commitment and is highly expressed in proliferating neural progenitor cells (Zhang, 2014). Whilst the ICC results show the relatively equal staining of both neural progenitors, differences were observed in the expression of Pax6 at W4, with Axol expressing significantly increased levels *cf* control, using qPCR. The expression of Sox2 decreased over 8 WIV compared to control in both conditions, consistent with the expectation that as cultures mature and cells terminally differentiate, the pool of progenitor stem cells should reduce from the earliest timepoints. Indeed, it has been demonstrated that constitutive expression of Sox2 results in the

maintenance of progenitor characteristics and inhibits neuronal differentiation (Graham et al., 2003; Packard et al., 2016). An increase in Sox2 expression was observed with both growth medium at W12, which is likely due to the presence of matured astrocytes, as astrocytes are known to express Sox2 (Niu et al., 2015). There also exists the possibility that Pax6 expression in SCT was lower only at the timepoints recorded; Pax6 expression could have been higher between W0-W4, then reduced before levels were measured at W4. In either scenario, the expression of progenitors in both conditions, coupled with the positive ICC markers and cortical rosette formation, are strong indicators of a cortical neural differentiation.

Cortical fate was confirmed with ICC of cortical layer markers. The presence of both $Tbr1^+$ and $SatB2^+$ cells complemented the results seen for early cortical neurogenesis. Whilst the qualitative results appear to show an increase in SatB2 expression for SCT, by W8, both cultures appear to have a similar expression of cortical layers. This suggests that both conditions can generate distinctive cortical cells as seen *in vivo* and agrees with the timeframes reported *in vitro* (Kuijlaars et al., 2016; Shi et al., 2012a)

Despite the differences in neural progenitor expression in both media, it appears to have no effect on neuronal differentiation. Both media generated $Tuj1^+$ neurons by 4 WIV, irrespective of their progenitor expression. qPCR indicates a reduction over time in TUBB3 expression, which could correlate with the emergence of neurons early in development. In both instances, $Tuj1^+$ cells were observed from W4 throughout, displaying characteristic connective arrangements. Whilst $DAPI^+$ nuclei can be observed throughout the culture, they occupy a very small area of the field of view, compared with the neurite extensions. It was not possible to assign a neural process to a cell body, particularly as the interconnectivity displayed made it impractical to distinguish between neurites of different cells.

It is understood that gliogenesis occurs following neurogenesis *in vivo* (Tchieu et al., 2019) and this has been recapitulated *in vitro* (Shi et al., 2012a). For this reason, it was expected that the

emergence of S100β$^+$ astrocytes would occur later than neurons. S100β expression is associated with a matured developmental stage in astrocyte development (Raponi et al., 2007), which is desirable in these cultures, as the endpoint is a mature neural culture. The results demonstrate an absence of astrocytes at W4, with the emergence of immature astrocytes at W8. The immaturity was confirmed by a lack of characteristic astrocytic morphology. Astrocytes are large cells, with distinctive processes, however, prior to W12, all S100β$^+$ staining was localised to the nucleus, with no processes visible. By 12 WIV, both cultures were generating morphologically matured S100β$^+$ astrocytes, which agrees with the results reported for spontaneous neural differentiations (Gunhanlar et al., 2017; Kuijlaars et al., 2016; Shi et al., 2012a). A significant increase in both Axol and SCT at 4 WIV for S100β expression could be suggestive of the cultures preparing for gliogenesis. This could also explain why the values decrease by W8, when immature astrocytes are beginning to be expressed. It was concluded that prior to W8, the cultures were morphologically immature as only neurons were present.

Both cultures formed VGlut1$^+$ excitatory synaptic vesicles within 4 weeks and continued to do so over the timepoints tested. It is understood that inhibitory GABAergic and glycinergic synaptogenesis precedes excitatory synaptogenesis *in vivo* (Soto et al., 2011) and GAD67 and vGAT were used to determine whether cultures expressed inhibitory cell types. Interneurons have been reported in spontaneously differentiated cortical cultures, albeit in small amounts (Gunhanlar et al., 2017; Kirwan et al., 2015; Shi et al., 2012a). The presence of interneurons in this instance is a paradoxical result, as interneurons do not develop in the cortex *in vivo*, but rather migrate in from the medial ganglionic eminence during neural development (Martini et al., 2009). As the 2D culture environment lacks any external brain region input, the presence of representative quantities of GABAergic cell types was not anticipated. In this instance, cultures were GAD67 negative for ICC at all timepoints, however, the qPCR expression data does suggest the presence of inhibitory subtypes, with statistical significance, which could be accounted for by the cellular system preparing for inhibitory synaptogenesis and the fact that excitatory

neurons can still express functional GABA receptors (Kirwan et al., 2015). It has been shown that if interneurons are present following spontaneous differentiation, they develop following excitatory neurons (Gunhanlar et al., 2017). However, interneurons may typically develop during extended periods of culture, or arrive and die out in the intermediate timepoints between the experiments in this Chapter. Indeed, increases in vGAT expression over time were observed and in addition, supplementary experiments were performed at 18 WIV, with only one repeat, due to apparatus failure. These preliminary expression results of Axol W18 were >5-fold higher than all other timepoints (Appendix Figure A5), suggesting the development of interneurons occurs at later timepoints in culture.

A key parameter for assessing which media is superior was the emergence of different neural development markers, particularly matured astrocytes, as these appear at later stages of differentiation *in vivo*. However, the data conclusively shows that both Axol and SCT media differentiate cells into all expected cell subtypes at the same timepoints and that the absence of astrocytes in these cultures would constitute an immature system, prior to 8 WIV. Whilst ICC can qualitatively suggest the presence and morphology of cell types, it offers no consideration of functionality. Development of this assay requires cells which not only resemble their *in vivo* counterparts, but demonstrate functional activity and drug responses also.

Both Axol and SCT media produced functionally active cultures

Calcium imaging and MEA analysis were used to assess functional responses. Both conditions displayed more spontaneous activity when perfused with aCSF, therefore aCSF was chosen as the perfusate for all subsequent calcium imaging studies. These results disagree with those reported by Bardy et al., (2015), and further reflects the differences between cells in different culture systems. Whilst cells appeared responsive, eliciting asynchronous calcium-mediated activity, there was no evidence that the activity was electrical. In order to test this, TTX was added to the cultures, resulting in the immediate cessation of spontaneous activity.

Collectively, these results suggest that the activity observed which was blocked by TTX is a secondary effect of sodium-dependent action potentials, and confirms the cells are functionally active (Hill et al., 2012). Whilst these results give insight into the electrical ability of the cells, they provide no information on the receptors which the cultures may be expressing. Glutamate is the principal excitatory neurotransmitter in the mammalian CNS, with a wide range of ionotropic and metabotropic targets (Goodwani et al., 2017). Application of glutamate resulted in large fluorescence increases, indicating that the cultures became excited in response and hence, they express functional glutamatergic receptors. It was beyond the scope of this investigation to determine precisely which receptors were expressed.

Having established that both cell conditions respond to different classes of pharmacological agent, the assessment of spontaneous activity over W4 to W18 was initiated, to determine if this identified an optimal differentiation medium. SCT-differentiated cultures were found to be significantly more active at W4 and W12, indicating a potential for SCT to be the better choice of growth medium.

Optimisation of MEA experiments was a challenge, with different electrodes and coating reagents tested. Unfortunately, in every condition, the cells detached and recordings were not possible after early timepoints. As laminin is a component of the extracellular matrix and is necessary for cell adhesion and differentiation (Baur et al., 1995), various concentrations of laminin were also tested to see if adherence could be improved. Preliminary studies assessed functional responses when cultures were dense (WIV 1-3), although, as expected there was a lack of activity, probably due to cell immaturity (data not shown).

The single successful recordings completed at W4 and W8 showed a lack of activity with Axol and low activity with SCT, even at W8, which is not in agreement with the literature. Odawara et al., (2014) showed that responses of iPSC-derived neurons increased from 3 WIV, with robust activity observed from 4 WIV. However, as only one repeat was successful, this was very

preliminary. It is important to clarify that MEA experiments were not performed in aCSF, but rather, in the respective growth medium. In contrast to calcium imaging experiments, for MEA studies, the same chips can be assessed over time, as the recordings are made in the incubator, in a sterile atmosphere and the technique is completely non-invasive. As the cells were still differentiating and MEA recordings were done at multiple timepoints, the sterile growth medium was chosen to study activity, rather than aCSF, which would have required filter sterilisation and would have posed a risk to culture sterility. Bardy et al., (2015) showed that SCT media was superior to standard media recipes for functional analyses, potentially due to physiologically-relevant concentrations of salts and factors as discussed above. Their work suggested neurobasal and DMEM recipes did not have representative concentrations of such components, and hence, produced weaker functional responses. Whilst the data generated here is very preliminary, it could be inferred that SCT might hold more promise than Axol medium for MEA recordings.

PORN was found to be the ideal coating reagent for adherence and differentiation of iPSC-derived NPCs. It was also preferable to use the same coating conditions as were used for calcium imaging, for consistency. As there was no issue with detachment of cells on glass coverslips, or on culture ware, it was concluded that the issue with MEA adherence was highly likely to be due to the MEA chips themselves. Indeed, a supplementary experiment was performed wherein MEA chips for a different MEA system were obtained and cultures were more adherent in this instance. These results differ to those of Amin et al., (2016), who found PDLO was the ideal substrate for MEA adherence. However, the results agree with the observation that PORN results in aggregation and fasciculation of neural cells over time (Amin et al., 2016).

As the difference in medium was only presented following measurements of functionality, it was decided that the data required to determine a better medium needed to be more robust than just the morphological and basic functional results generated in this Chapter. Although SCT

MEA measurements appeared superior, only one experiment could be conducted. For these reasons, it could not be concluded with confidence which medium was better for spontaneous neural differentiation. In Chapter 4, a side-by-side comparison was performed to determine which condition led to more responsive cultures, and hence, which media would be an ideal option for development of the assay.

The results of this chapter indicate that two leading growth media can successful generate excitatory cortical culture cells over 12 WIV differentiation. Moreover, as both conditions elicited action potential-dependent activity and excitatory neurotransmission, they were both assessed for their ability to generate seizure-like activity in Chapter 4.

Chapter 4

4. INVESTIGATING THE ABILITY OF SPONTANEOUSLY DIFFERENTIATED iPSC-DERIVED NEURAL CULTURES TO GENERATE EPILEPTIFORM ACTIVITY

4.1 Introduction

Existing assays used to study epileptiform activity and seizure-like events (SLE) manipulate cellular processes in otherwise healthy tissue, in order to initiate seizurogenesis and generate SLE (Chapter 1.5). The induction of SLE is well-established in primary rodent *in vitro* models and brain slice assays, using agents which alter ion flux, neurotransmission and affect the whole electrical network (Accardi et al., 2018; Debanne et al., 2006; Easter et al., 2007; Gabriel et al., 2004; Gonzalez-Sulser et al., 2011; Igelström et al., 2011; Pena & Tapia, 2000; Yaari et al., 1983, 1986). In order to generate SLE, the system must form receptors/drug targets for the pro-ictogenic conditions to exert their effects. In this Chapter, responses to a variety of ionic and pharmacological manipulations frequently used in rodent *in vitro* epilepsy studies were used to assess whether the system could respond to these conditions, as well as displaying 'normal' baseline activity.

4.1.1 Manipulating cell excitability via ion flux

Neuronal excitability is controlled by ion gradients (Chapter 1). The manipulation of ion levels in neurons can result in increased activity, leading to SLE. Changes to potassium (K^+) and magnesium (Mg^{2+}) levels are typically achieved by modulation of the bathing solution used to perfuse the cell/tissue for the experiment. In these studies, aCSF was the most appropriate perfusate for all conditions (Chapter 3).

Elevated extracellular potassium concentrations ($[K^+]_e$) can lead to depolarisation, increased firing and burst-firing, all of which facilitate seizurogenesis. Furthermore, during seizure, $[K^+]_e$ increases and extracellular sodium and calcium ($[Na^+]_e$/$[Ca^{2+}]_e$) decreases, due to neuronal

release and uptake, respectively (Raimondo et al., 2015). This can create a cycle of depolarisation, promoting further action potential discharge. Increasing potassium levels is an established method for generating SLE *in vitro* (Traynelis & Dingledine, 1988; Yaari et al., 1986). In addition, it has been demonstrated that iPSC-derived neurons can respond to high potassium solutions, with increased calcium-mediated activity (Tukker et al., 2016).

Lowering the concentration of Mg^{2+} can affect the system at the network level, leading to recurrent SLE (Igelström et al., 2011; Pacico & Meur, 2014). 'Normal' matured activity is asynchronous, so for seizures to occur, multiple neurons need to be recruited in an unusually hypersynchronous manner (Jiruska et al., 2013; Vaughan & Delanty, 2003). Bursts are generated by sustained recurrent excitation, elicited by clusters of glutamatergic pyramidal neurons in the cortex, and followed by a period of hyperpolarisation. Recurrent excitation via NMDA and non-NMDA glutamatergic receptor activation can further recruit and synchronise neurons into the seizurogenic activity (Debanne et al., 2006; McCormick & Contreras, 2001)**.** This sequence of events is termed the paroxysmal depolarising shift (PDS). Normally, Mg^{2+} blocks the pore of the NMDA receptor. During the PDS, the membrane becomes depolarised to the point where the voltage-dependent Mg^{2+} block of NMDA receptors is released. When Mg^{2+} is lowered, NMDA receptors become permeable to Ca^{2+} which, alongside voltage-gated Na^{+} activation, induces long-lasting potentiation of glutamatergic transmission at pyramidal cell synapses (Staley & Dudek, 2006). Activation of multiple NMDA receptors further depolarises the cell and promotes increased Ca^{2+} influx (Vaughan & Delanty, 2003). Indeed, NMDA and AMPA receptor antagonists are known to suppress seizurogenesis (Rogawski, 1992). In this Chapter, magnesium was removed from the aCSF to attempt to induce increases in activity, via NMDA-receptor mediated excitation.

4.1.2 Pharmacological induction of SLE

SLE can also be induced pharmacologically in rodent seizure models, with chemical and biological agents promoting increased bursts of activity from release of excitatory and inhibitory neurotransmitters, as discussed in Chapter 1.

4.1.2.1 4-aminopyridine

An agent now used in the therapy of multiple sclerosis, 4-aminopyridine (4-AP), is also an experimental compound widely used to induce SLE and increase neuronal activity in rodent models, however the mechanism of action is not entirely understood (Accardi et al., 2018; Bradley et al., 2018; Easter et al., 2007; Gonzalez-Sulser et al., 2011; Hongo et al., 2015; Kreir et al., 2018; Pena & Tapia, 2000). In addition, 4-AP has been shown to elicit recurrent depolarisations in human iPSC-derived networks (Matsuda et al., 2018; Pruunsild et al., 2017).

Proposed mechanisms of 4-AP are all based on the evidence that it blocks transient K^+ currents via antagonism of potassium channels. More specifically, 4-AP enters the Shaker family of potassium channels and will then only exit when the activation gate is open (Loboda & Armstrong, 2001). However, when 4-AP is inside the channel, its primary effect is to bias the activation gate towards the closed conformation, thus blocking the movement of K^+ currents and prolonging action potentials by inhibiting repolarisation. The consequence of this is increased release of glutamate from nerve endings, causing overactivation of glutamate receptors. Paradoxically, under these conditions, GABA-mediated transmission may increase excitation and consequently, generate epileptiform activity (Pena & Tapia, 2000)

This mechanism can also affect interneuronal populations. The K^+-interneuron accumulation hypothesis (Perreault & Avoli, 1991) suggests that the firing of interneurons transiently increases the $[K^+]_e$, via K^+ repolarising conductances. However, this extracellular change will cause other interneurons to fire AP, with increased K^+_e accumulation enhancing the excitability

of neighbouring interneurons. This promotes a cycle of positive feedback, the result of which is increased neuronal discharges (González et al., 2018).

4.1.2.2 Picrotoxin

GABA antagonism is a major mechanism of seizurogenesis, as the inhibition of GABA's inhibitory mode of action results in increased excitation (Olsen & DeLorey, 2012). A variety of $GABA_A$ receptor antagonists can be selected to cause SLE. Commonly used are: gabazine, picrotoxin (PTX), bicuculline and pentylenetetrazol (Bradley et al., 2018; Easter et al., 2007; Fan et al., 2019; Hongo et al., 2015). Although mainly used to induce SLE *in vivo*, pentylenetetrazol is also used *in vitro* (Easter et al., 2009). Gabazine is a competitive antagonist of GABA receptors (Ueno et al., 1997) and has also been used in iPSC-derived neural cultures to assess network activity (Kuijlaars et al., 2016) and to generate epileptiform activity (Ishii et al., 2017). Although several GABA antagonists with pro-ictogenic effects exist, not all mechanisms are understood. In this study, PTX was selected for GABA antagonism, as it has a well-understood mode of action: non-competitive $GABA_A$ receptor chloride antagonism, binding preferentially to an agonist bound state (open/closed or both conformations) (Newland & Cull-Candy, 1992). In addition, PTX has been shown to elicit increased activity in iPSC cultures (Kuijlaars et al., 2016; Tukker et al., 2018; Verheyen et al., 2015; Zhang et al., 2016) and as such, provided an ideal antagonist for comparison in the iPSC-derived cultures in this thesis.

4.1.3 Proposal for a panel of agents for seizure-liability testing

As the fundamental aim of iPSC-derived seizure liability models (including the work of this thesis), is to provide a suitable addition to pre-clinical toxicity testing, a validatory panel of agents, which should be considered for all methods attempting to test seizure-liability, is proposed (Table 4.1). This panel is based on previous neurotoxicity screening studies performed on rodent cultures (Bradley et al., 2018; Easter et al., 2007, 2009; Fan et al., 2019; Mack et al., 2014).

The panel chosen reflects commonly used compounds for inducing SLE and to the author's knowledge, no iPSC-derived models have been tested and have responded to all of these conditions. It would also be advantageous to determine the effects of ionic manipulation on cultures, particularly as these are widely used for *in vitro* seizure studies, however, these are not routinely used in drug screening.

In support of the inclusion of human models in the battery of pre-clinical safety pharmacology tests, all models should be able to generate epileptiform activity in response to these drugs as a minimum attribute, as has been shown reproducibly in several validated rodent systems.

Table 4.1: Proposed panel of seizurogenic drugs for validation of iPSC-derived seizure-liability testing platforms. VG = voltage-gated. The exact mechanism of action of PTZ is unknown, however it has been shown to act upon GABA receptors (Bradley et al., 2018).

Condition	Class	Target	References
4-aminopyridine (4-AP)	VG-Potassium channel blocker	Potassium channels	Easter et al., 2007/9; Bradley et al., 2018; Fan et al., 2019
Picrotoxin (PTX)	GABA A antagonist (non-competitive)	GABA A Receptor	Easter et al., 2007; Mack et al., 2014; Bradley et al., 2018; Fan et al., 2019
Pentylenetetrazol (PTZ)	Convulsant	GABA receptor (expected)	Easter et al., 2007/9; Bradley et al., 2018; Fan et al., 2019
Bicuculline	GABA antagonist (competitive)	GABA A receptor	Mack et al., 2014; Bradley et al., 2018; Fan et al., 2019

The aims of this Chapter are to:

1) **Assess whether iPSC-derived spontaneously differentiated neural cultures respond to 4-aminopyridine, picrotoxin and zero magnesium/high potassium aCSF with increased and synchronised activity, using fluorescent calcium imaging.**
2) **Determine to what extent different growth medium (Axol and SCT) influences the above outcomes.**

4.2 Results

The results of Chapter 3 indicate that spontaneously differentiated human iPSC-derived neural cultures in Axol and SCT media are capable of generating various neural subtypes, which elicit basic functional responses to the excitatory neurotransmitter glutamate and also display action potential-dependent activity, as demonstrated by TTX addition. In order to determine whether these cultures were capable of epileptiform activity, cells were spontaneously differentiated over 18 weeks *in vitro* (WIV) and assessed periodically at the same timepoints as Chapter 3, as the results of Chapter 3 indicated cultures differentiated in both Axol and SCT media generated excitatory synapses and displayed functional calcium-mediated activity by 4 WIV. Fluorescent calcium imaging was chosen as the technique of assessing seizure induction, as far as can be determined, this is a novel approach to testing seizure-like activity in human iPSC-derived cultures.

At each time point, cultures were perfused with different pro-ictogenic conditions of diverse mechanisms of action (as per Chapter 4.1). For all timepoints and drug conditions, the data is displayed in the same way, comprising a representative fluorescently-stained snapshot of the cultures with associated regions of interest (ROI), example traces from the ROI, raster plots of example spike data and various other parameters of epileptiform activity.

4.2.1 4 WIV Testing

Cells cultured in Axol medium did not respond significantly to 100 µM 4-aminopyridine (4-AP) in percentage active cells, peaks per cell, burst frequency, percentage synchronised elevations or R value (Figure 4.1). However, the percentage of responding cells of SCT-differentiated cultures to 100 µM 4-AP was significantly increased (Control: 14.17 ± 1.61%, 4-AP: 23.85 ± 4.29%, n=9 coverslips from 3 differentiations (cs), p= 0.0395). In addition, there was an increase in R value observed for SCT (Control: -1.20 ± 0.02, 4-AP: -0.47 ± 0.26, n=9 cs, p= 0.0178, Figure 4.1H).

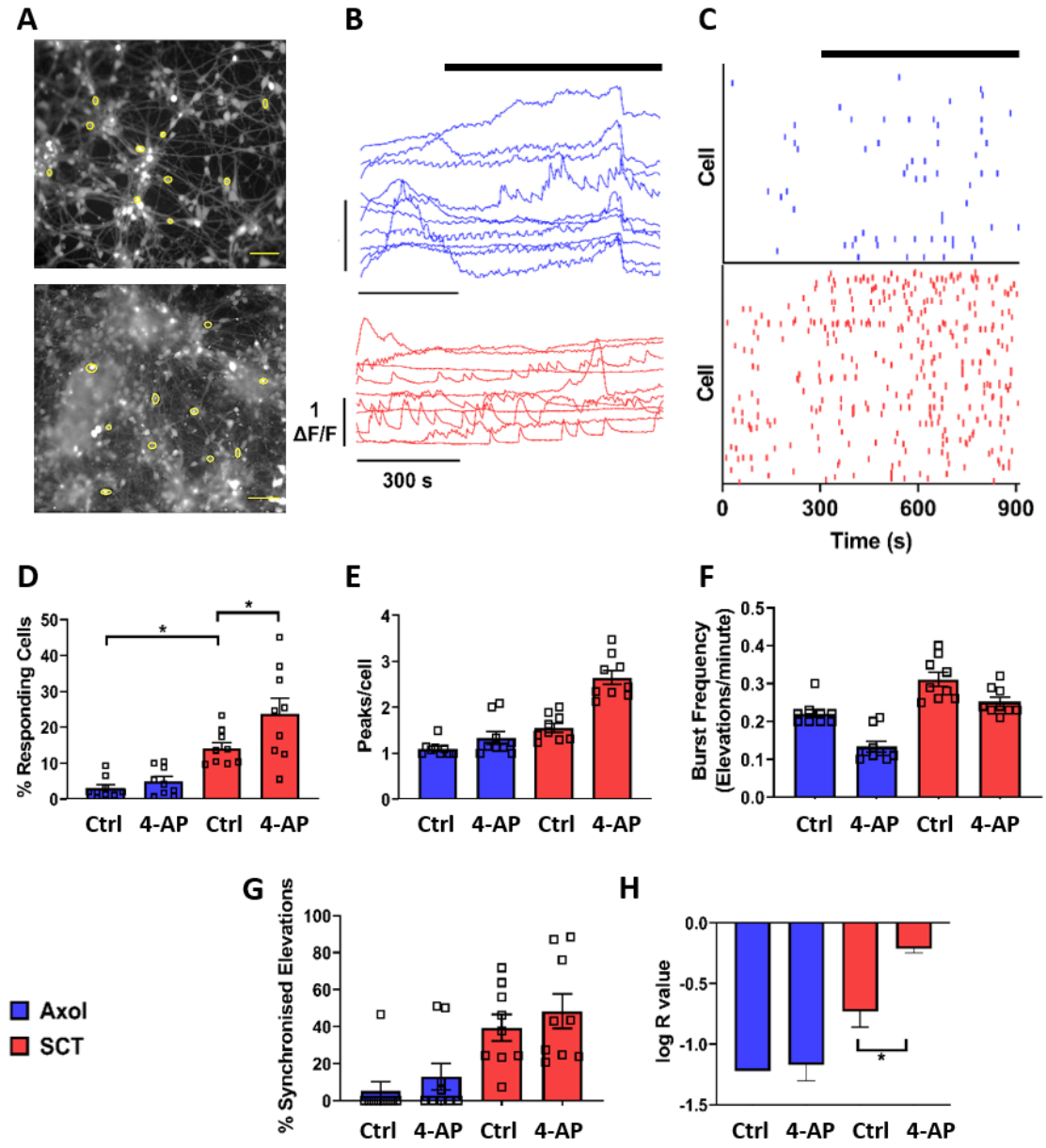

Figure 4.1: **Fluorescent calcium imaging responses of spontaneously differentiated human iPSC-derived neural cultures to 4-aminopyridine at 4 WIV.** (**A**) Cells cultured in either Axol (upper, blue throughout) or SCT (lower, red throughout) media were loaded with 5 μM Fluo4-AM for imaging. (**B**) Time-lapse videos were recorded at 0.33 Hz, with representative figures showing 10 example, random fluorescent traces related to yellow regions of interest in (A). (**C**) Representative Raster plot. Spikes were identified manually and plotted over time to identify synchronised events. (**D**) Responding cells were determined as those with ≥ one peak of calcium activity. (**E**) Calcium peaks per active cell. (**F**) Frequency of calcium events per minute. (**G-H**) Quantitative measures of synchrony. (**G**) % synchronised cells relating to (C). (**H**) Average R value was calculated by performing a Pearson's correlation of the spike data generated for (C), then performing a Fisher's *z*-transformation. Data in D-H is displayed as mean ± SEM from N=3 separate neural differentiations. *p< 0.05, 2-way ANOVA with Tukey's multiple comparisons test. Scale bar: 5 μm. Solid black bar in B-C indicates addition of 100 µM 4-AP.

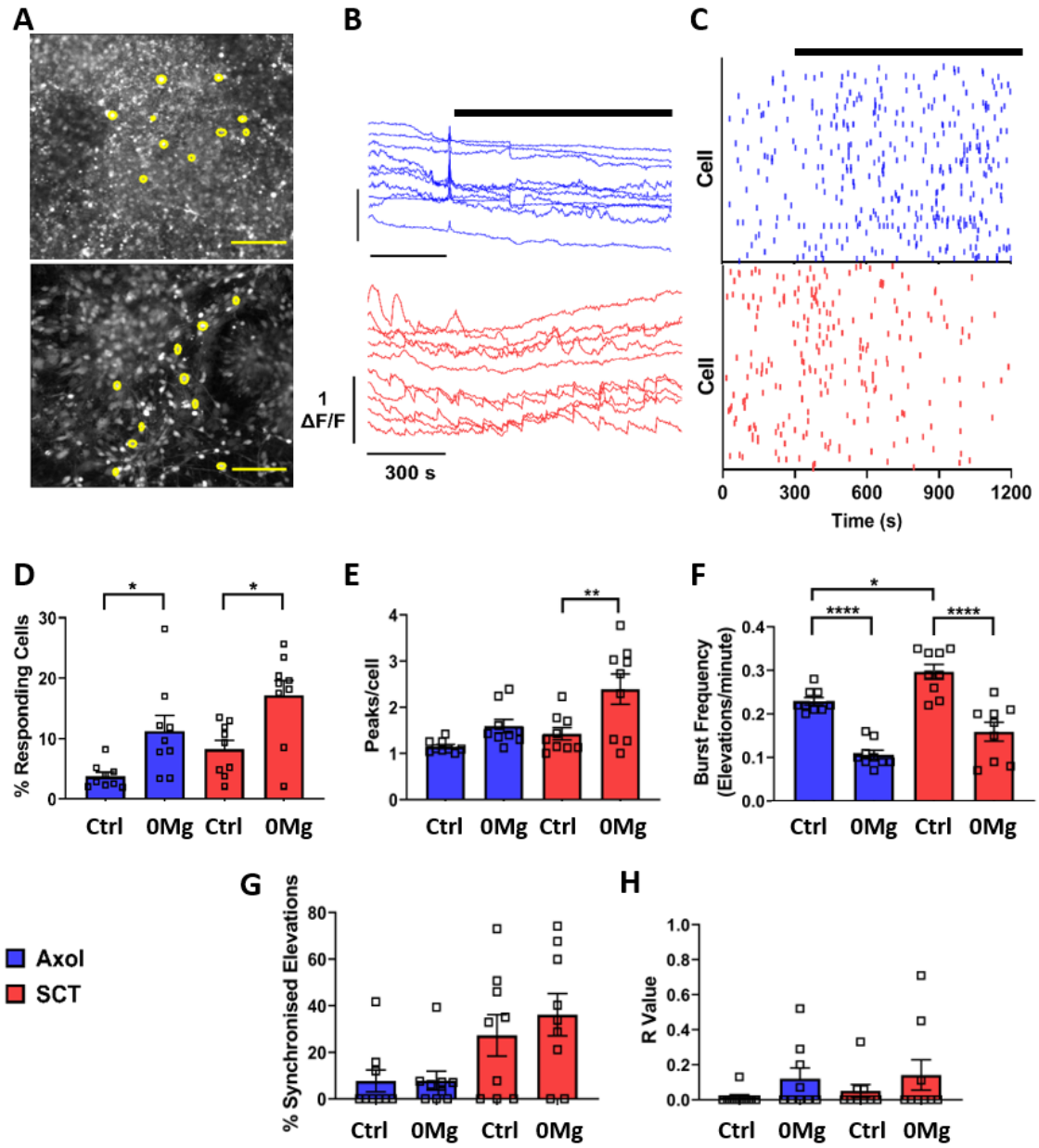

Figure 4.2: **Fluorescent calcium imaging responses of spontaneously differentiated human iPSC-derived neural cultures to zero-magnesium aCSF perfusion at 4 WIV.** (**A**) Cells cultured in either Axol (upper) or SCT (lower) media were loaded with 5 μM Fluo4-AM for imaging. (**B**) Time-lapse videos were recorded at 0.33 Hz, with representative figures showing 10 example, random fluorescent traces related to yellow regions of interest in (A). (**C**) Representative Raster plot. Spikes were identified manually and plotted over time to identify synchronised events. (**D**) Responding cells were determined as those with ≥ one peak of calcium activity. (**E**) Calcium peaks per active cell. (**F**) Frequency of calcium events per minute. (**G-H**) Quantitative measures of synchrony. (**G**) % synchronised cells relating to (C). (**H**) Average R value of the spike data generated for (C). Data in D-H is displayed as mean ± SEM. N=3. *p< 0.05, ****p< 0.0001, 2-way ANOVA with Tukey's multiple comparisons test. Scale bar: 5 μm. Solid black bar in B-C indicates addition of 0 Mg^{2+} aCSF.

Indeed, the percentage of responding cells in SCT was statistically greater than that of cells cultured in Axol media (Axol: 3.07 ± 0.98%; SCT: 14.17 ± 1.61%, n=9 cs, p= 0.0145, Figure 4.1D). Moreover, whilst largely statistically insignificant, the average responses of Axol and SCT to 4-AP increased in every instance, with the exception of burst frequency, where a non-significant decrease was observed in both conditions (Figure 4.1F). The control values for each parameter were consistently higher in SCT than that of Axol and in addition, the response to drug was higher in SCT than that of Axol (Figure 4.1D-H).

Axol and SCT cultures displayed a significant increase in percentage of responding cells to zero-magnesium aCSF perfusion (0 Mg) (Axol Control: 3.73 ± 0.68, 0 Mg: 11.27 ± 2.56, n=9 cs, p= 0.0459; SCT Control: 8.26 ±1.44, 0 Mg: 17.18 ± 2.46, n=9 cs, p= 0.0138, Figure 4.2D). 0 Mg aCSF perfusion also significantly increased the number of peaks per cell for SCT at 4 WIV (Control: 1.43 ± 0.13, 0Mg: 2.39 ± 0.33, n=9 cs, p= 0.0063, Figure 4.2E) and both conditions presented a highly significant reduction in burst frequency, despite the increase in other markers of activity (Axol Control: 0.23 ± 0.01, 0 Mg: 0.11 ± 0.01, n=9 cs, p = <0.0001; SCT Control: 0.30 ± 0.02, 0 Mg: 0.16 ± 0.02, n=9 cs, p< 0.0001, Figure 4.2F).

4.2.2 8 WIV Testing

Similarly to 4 WIV, at 8 WIV Axol cultures did not present any significant response to 4-AP, despite increases compared with control in all metrics of activity except burst frequency, which again decreased (Figure 4.3D-H). In contrast, SCT cultures displayed a significant increase in number of peaks per cell (Control: 1.61 ± 0.16, 4-AP: 2.86 ± 0.42, n=9 cs, p= 0.005, Figure 4.3E).

SCT culture responses to 0 Mg also resulted in significant increases in the percentage of responding cells (Control: 17.00 ± 4.14, 0Mg: 34.04 ± 2.58, n=9 cs, p= 0.004, Figure 4.4D) and peaks per cell (Control: 1.55 ± 0.16, 0Mg: 2.81 ± 0.38, n=9 cs, p= 0.002, Figure 4.4E).

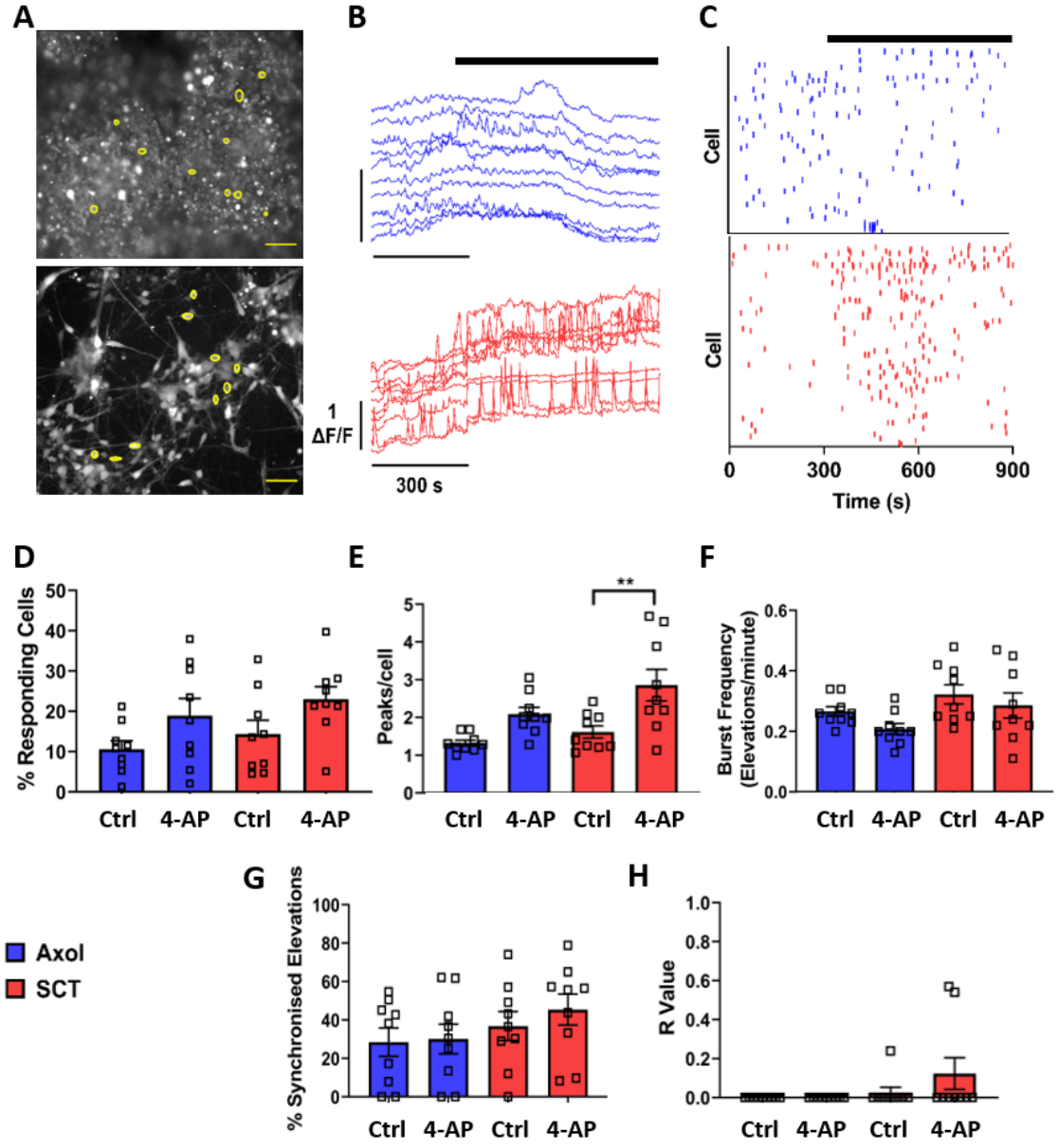

Figure 4.3: **Fluorescent calcium imaging responses of spontaneously differentiated human iPSC-derived neural cultures to 4-aminopyridine perfusion at 8 WIV.** (**A**) Cells cultured in either Axol (upper) or SCT (lower) media were loaded with Fluo4-AM for imaging. (**B**) Time-lapse videos were recorded at 0.33 Hz, with representative figures showing 10 example, random fluorescent traces related to yellow regions of interest in (A). (**C**) Representative Raster plot. Spikes were identified manually and plotted over time to identify synchronised events. (**D**) Responding cells were determined as those with ≥ one peak of calcium activity. (**E**) Calcium peaks per active cell. (**F**) Frequency of calcium events per minute. (**G-H**) Quantitative measures of synchrony. (**G**) % synchronised cells relating to (C). (**H**) Average R value of the spike data generated for (C). Data in D-H is displayed as mean ± SEM. N=3. **p< 0.01, 2-way ANOVA with Tukey's multiple comparisons test. Scale bar: 5 μm. Solid black bar in B-C indicates addition of 100 µM 4-AP.

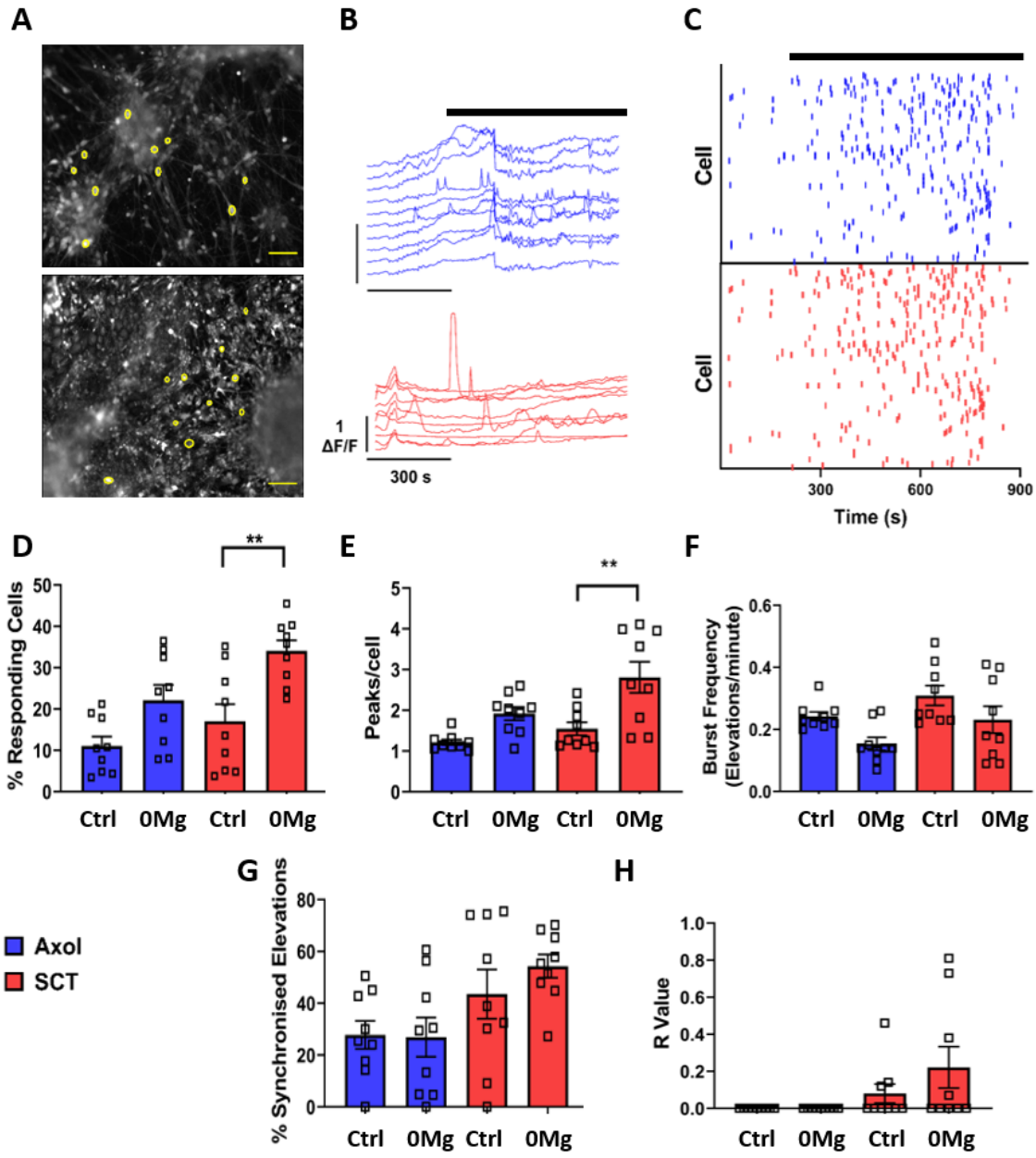

Figure 4.4: Fluorescent calcium imaging responses of spontaneously differentiated human iPSC-derived neural cultures to zero-magnesium aCSF perfusion at 8 WIV. (**A**) Cells cultured in either Axol (upper) or SCT (lower) media were loaded with 5 μM Fluo4-AM for imaging. (**B**) Time-lapse videos were recorded at 0.33 Hz, with representative figures showing 10 example, random fluorescent traces related to yellow regions of interest in (A). (**C**) Representative Raster plot. Spikes were identified manually and plotted over time to identify synchronised events. (**D**) Responding cells were determined as those with ≥ one peak of calcium activity. (**E**) Calcium peaks per active cell. (**F**) Frequency of calcium events per minute. (**G-H**) Quantitative measures of synchrony. (**G**) % synchronised cells relating to (C). (**H**) Average R value of the spike data generated for (C). Data in D-H is displayed as mean ± SEM. N=3. **p< 0.01, 2-way ANOVA with Tukey's multiple comparisons test. Scale bar: 5 μm. Solid black bar in B-C indicates addition of 0 Mg^{2+} aCSF.

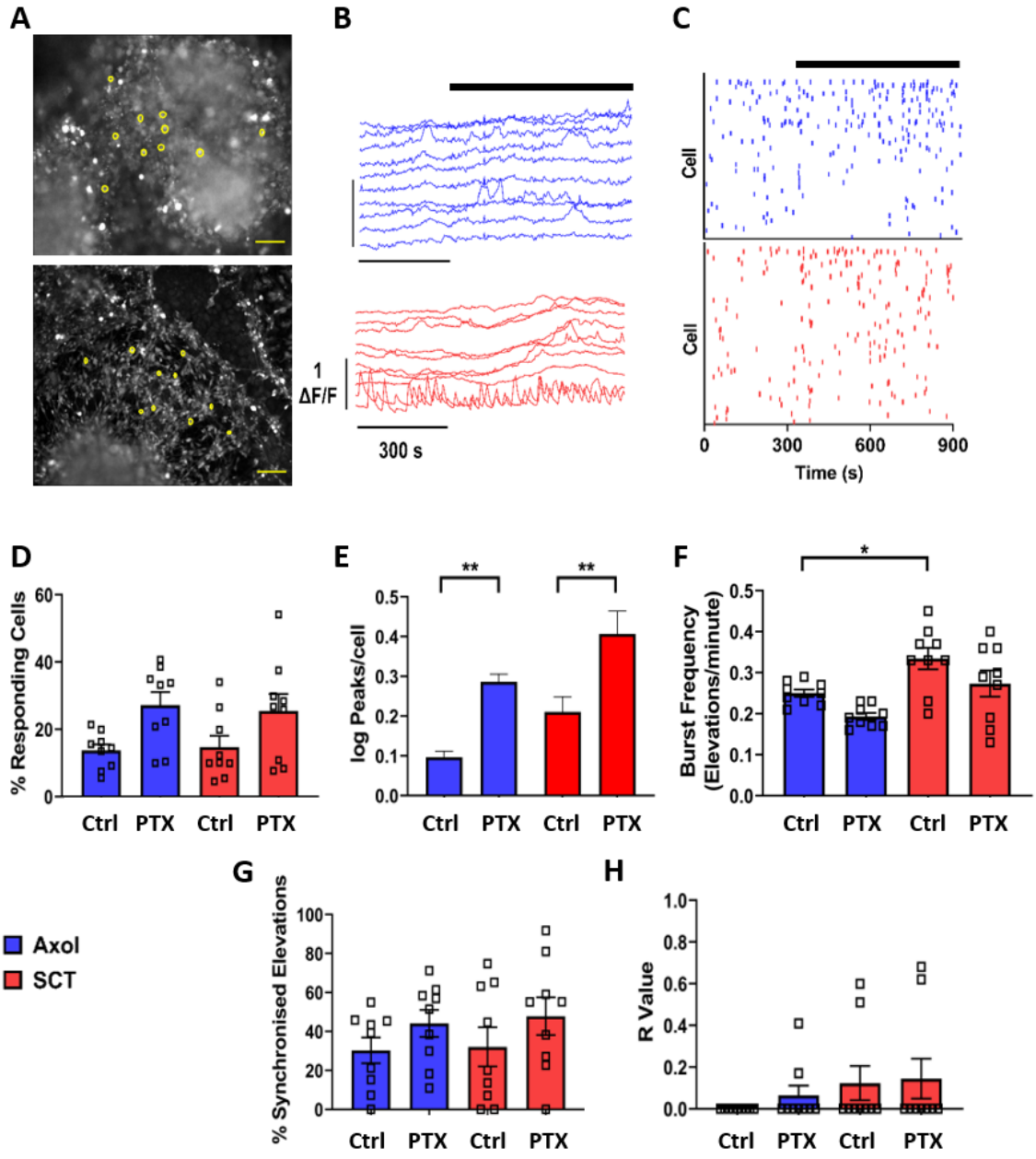

Figure 4.5: **Fluorescent calcium imaging responses of spontaneously differentiated human iPSC-derived neural cultures to picrotoxin at 8 WIV.** (**A**) Cells cultured in either Axol (upper) or SCT (lower) media were loaded with 5 μM Fluo4-AM for imaging. (**B**) Time-lapse videos were recorded at 0.33 Hz, with representative figures showing 10 example, random fluorescent traces related to yellow regions of interest in (A). (**C**) Representative Raster plot. Spikes were identified manually and plotted over time to identify synchronised events. (**D**) Responding cells were determined as those with ≥ one peak of calcium activity. (**E**) Calcium peaks per active cell. (**F**) Frequency of calcium events per minute. (**G-H**) Quantitative measures of synchrony. (**G**) % synchronised cells relating to (C). (**H**) Average R value of the spike data generated for (C). Data in D-H is displayed as mean ± SEM. N=3. *p< 0.05, **p< 0.01, 2-way ANOVA with Tukey's multiple comparisons test. Scale bar: 5 μm. Solid black bar in B-C indicates addition of 100 μM PTX.

The addition of 100 µM picrotoxin (PTX) at 8 WIV increased the number of peaks per cell in both conditions (Axol control: 0.01 ± 0.02, PTX: 0.29 ± 0.02, n=9 cs, p= 0.005; SCT control: 0.21 ± 0.04, PTX: 0.41 ± 0.06, n=9 cs, p= 0.0034, Figure 4.5E). Additionally, SCT control displayed a significant increase in burst frequency compared to Axol control (Axol: 0.25 ± 0.01, SCT: 0.33 ± 0.03, n=9 cs, p= 0.043, Figure 4.5F).

Neither condition significantly increased synchronised activity in any ictogenic conditions tested at 8 WIV (Figures 4.3-5). R values for all Axol control and 4-AP repeats were zero (Figure 4.3H). In addition, the burst frequency response for all conditions at 8 WIV was not statistically different (Figures 4.3/4/5H).

4.2.3 12 WIV Testing

4-AP treatment at 12 WIV resulted in an increase in peaks per cell for SCT (Control: 1.61 ± 0.19, 4-AP: 2.75 ± 0.46, n=9 cs, p= 0.017, Figure 4.6E), whereas the only significant effect on Axol cultures was the reduction in burst frequency compared wth control (Control: -0.67 ± 0.02, 4-AP: -0.86 ± 0.03, n=9 cs, p= 0.024, Figure 4.6F).

Axol cultures responded significantly to 0 Mg aCSF with an increase in percentage of responding cells (Control: 0.93 ± 0.09%, 0Mg: 1.29 ± 0.11%, n=9 cs, p= 0.05, Figure 4.7D). Neither culture displayed significant increases in percentage of synchronised elevations (Figure 4.7G), however SCT produced a significant increase in log R value (Control: -1.35 ± 0.05, 0Mg: -0.32 ± 0.13, n=9 cs, p= 0.001, Figure 4.7H).

PTX elicited a significant response in percentage of responding cells from Axol (Control: 6.83 ± 1.31%, PTX: 18.19 ± 2.21%, n=9 cs, p= 0.01, Figure 4.8D). In contrast, SCT showed no significant response to PTX, with the exception of a signficant reduction in burst frequency (Control: 0.29 ± 0.03, PTX: 0.17 ± 0.02, n=9 cs, p= 0.002, Figure 4.8F).

High potassium aCSF perfusion (>K^+) was chosen as an additional test for 12 WIV, intended to excite the morphologically matured system, as Chapter 3 indicated all cellular subtypes were

present by this stage. Whilst the only statistically significant result from >K^+ perfusion was the percentage of responding cells in Axol (Control: 0.89 ± 0.10%, >K^+: 1.37 ± 0.03%, n=9 cs, p= 0.0014, Figure 4.9D), >K^+ resulted in the greatest percentage of synchronised cells and peaks per cell values seen throughout W12 testing (Figures 4.6-9). Of particular importance is the distribution of data observed throughout Figure 4.9D-H for SCT cultures. For all studies, (excluding log-tranformed data in E), the distribution shows an isolated 'anomalous' value higher than the normal distribution. This is discussed in section 4.2.5.

Continuing the trend of W4 and W8, SCT controls were higher than those of Axol controls throughout all W12 treatments, with the sole exception of the R values generated in >K^+ (Figure 4.9H). Importantly, all of these comparisons again were not statistically significant.

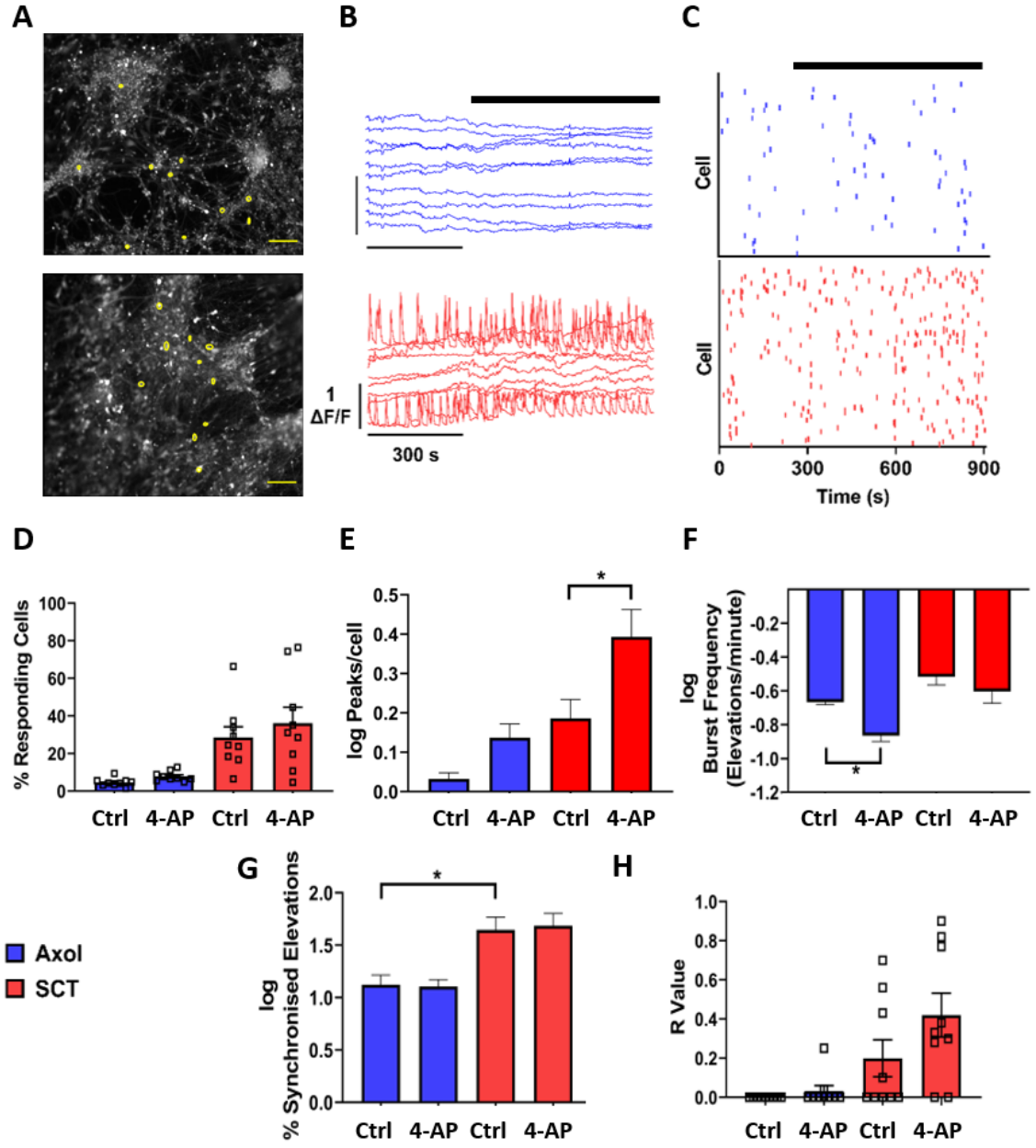

Figure 4.6: **Fluorescent calcium imaging responses of spontaneously differentiated human iPSC-derived neural cultures to 4-aminopyridine at 12 WIV.** (**A**) Cells cultured in either Axol (upper) or SCT (lower) media were loaded with 5 μM Fluo4-AM for imaging. (**B**) Time-lapse videos were recorded at 0.33 Hz, with representative figures showing 10 example, random fluorescent traces related to yellow regions of interest in (A). (**C**) Representative Raster plot. Spikes were identified manually and plotted over time to identify synchronised events. (**D**) Responding cells were determined as those with ≥ one peak of calcium activity. (**E**) Calcium peaks per active cell. (**F**) Frequency of calcium events per minute. (**G-H**) Quantitative measures of synchrony. (**G**) % synchronised cells relating to (C). (**H**) Average R value of the spike data generated for (C). Data in D-H is displayed as mean ± SEM. N=3.*p< 0.05, 2-way ANOVA with Tukey's multiple comparisons test. Scale bar: 5 μm. Solid black bar in B-C indicates addition of 100 μM 4-AP.

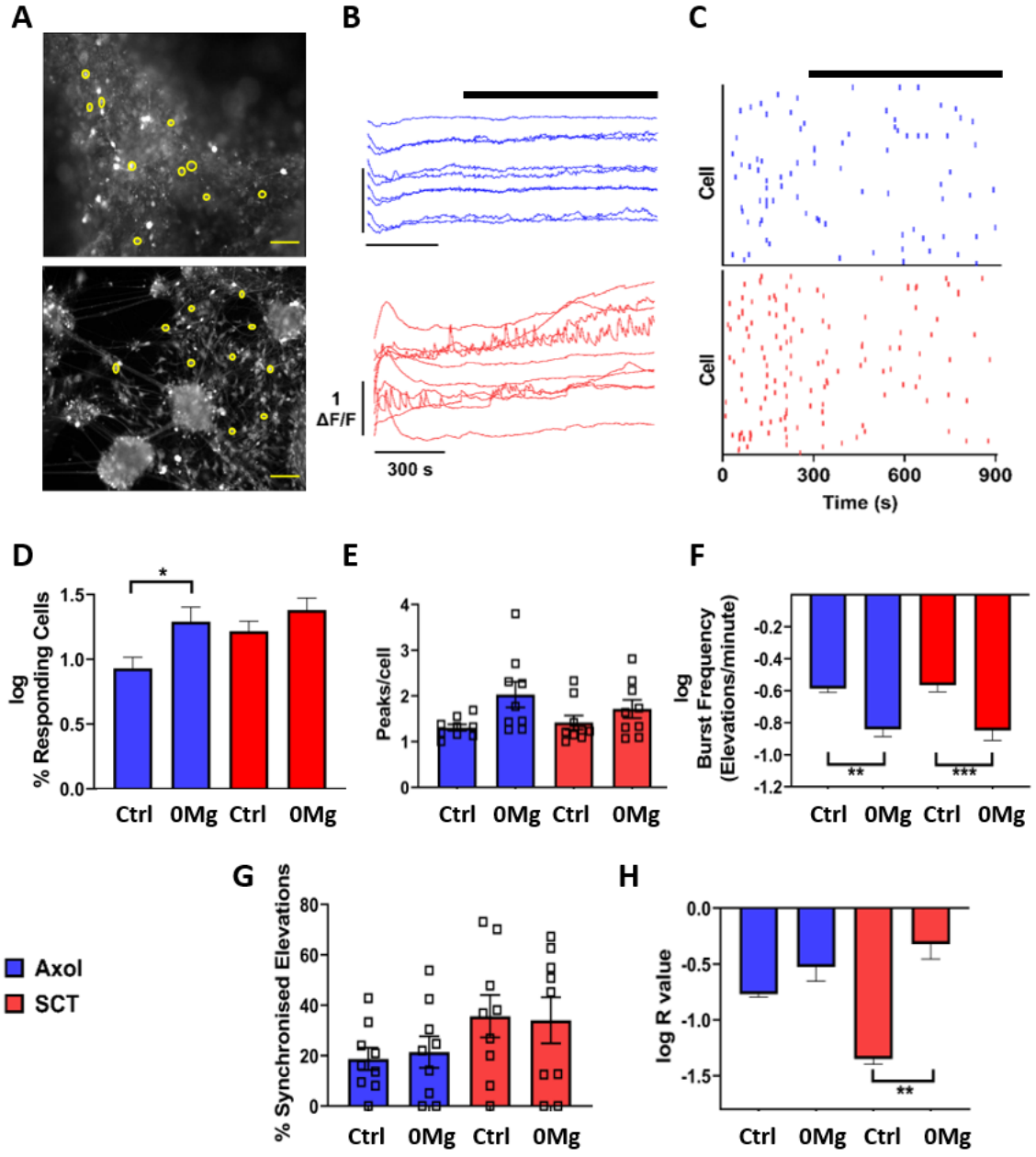

Figure 4.7: **Fluorescent calcium imaging responses of spontaneously differentiated human iPSC-derived neural cultures to zero-magnesium aCSF perfusion at 12 WIV.** (**A**) Cells cultured in either Axol (upper) or SCT (lower) media were loaded with Fluo4-AM for imaging. (**B**) Time-lapse videos were recorded at 0.33 Hz, with representative figures showing 10 example, random fluorescent traces related to yellow regions of interest in (A). (**C**) Representative Raster plot. Spikes were identified manually and plotted over time to identify synchronised events. (**D**) Responding cells were determined as those with ≥ one peak of calcium activity. (**E**) Calcium peaks per active cell. (**F**) Frequency of calcium events per minute. (**G-H**) Quantitative measures of synchrony. (**G**) % synchronised cells relating to (C). (**H**) Average R value of the spike data generated for (C). Data in D-H is displayed as mean ± SEM. N=3. *p< 0.05, **p <0.01, ***p< 0.001, 2-way ANOVA with Tukey's multiple comparisons test. Scale bar: 5 μm. Solid black bar in B-C indicates addition of 0 Mg^{2+} aCSF.

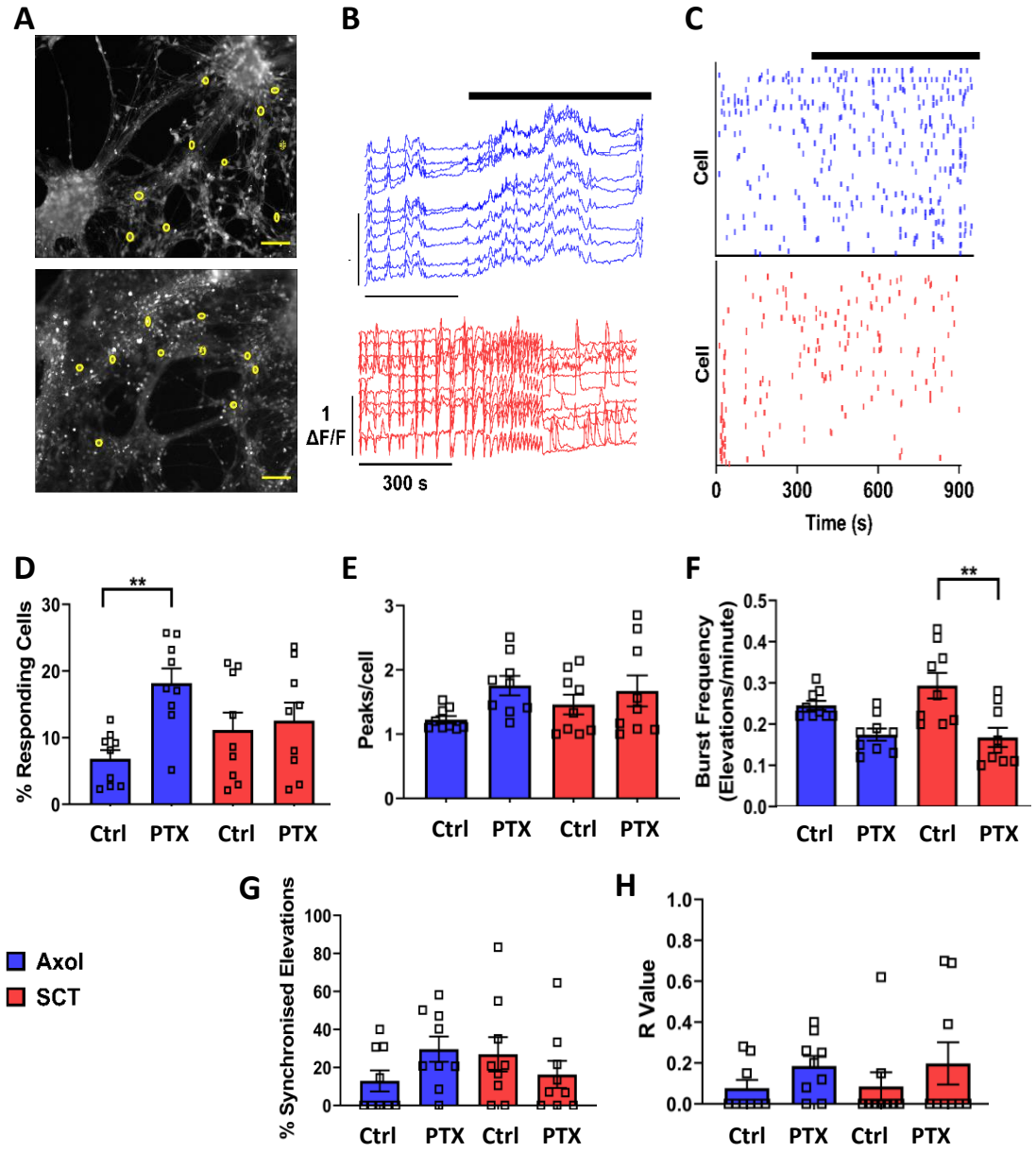

Figure 4.8: **Fluorescent calcium imaging responses of spontaneously differentiated human iPSC-derived neural cultures to picrotoxin at 12 WIV.** (**A**) Cells cultured in either Axol (upper) or SCT (lower) media were loaded with 5 µM Fluo4-AM for imaging. (**B**) Time-lapse videos were recorded at 0.33 Hz, with representative figures showing 10 example, random fluorescent traces related to yellow regions of interest in (A). (**C**) Representative Raster plot. Spikes were identified manually and plotted over time to identify synchronised events. (**D**) Responding cells were determined as those with ≥ one peak of calcium activity. (**E**) Calcium peaks per active cell. (**F**) Frequency of calcium events per minute. (**G-H**) Quantitative measures of synchrony. (**G**) % synchronised cells relating to (C). (**H**) Average R value was of the spike data generated for (C). N=3. **p< 0.01, 2-way ANOVA with Tukey's multiple comparisons test. Scale bar: 5 μm. Solid black bar in B-C indicates addition of 100 µM PTX.

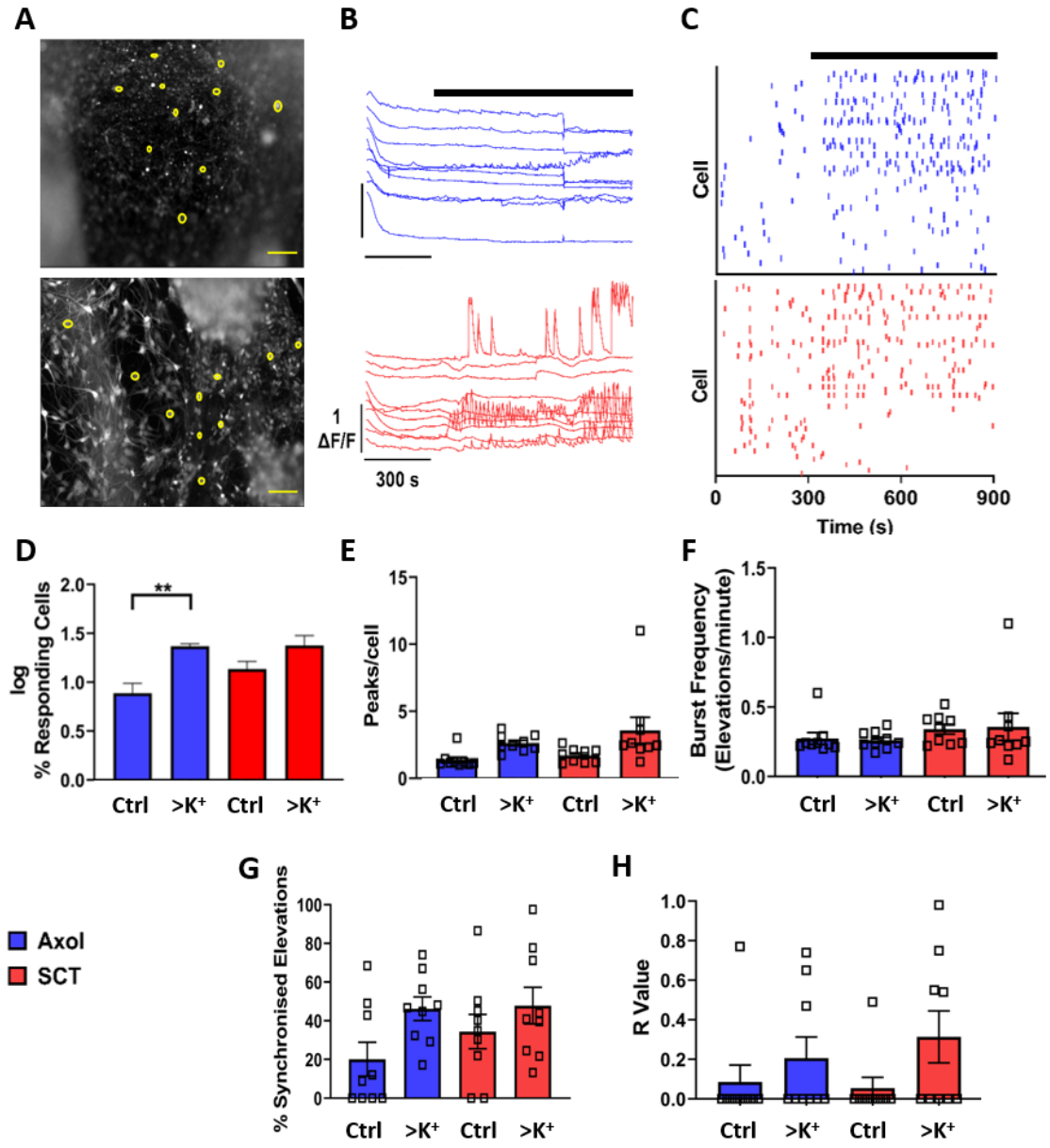

Figure 4.9: **Fluorescent calcium imaging responses of spontaneously differentiated human iPSC-derived neural cultures to high potassium (>K$^+$) aCSF perfusion at 12 WIV.** (**A**) Cells cultured in either Axol (upper) or SCT (lower) media were loaded with 5 μM Fluo4-AM for imaging. (**B**) Time-lapse videos were recorded at 0.33 Hz, with representative figures showing 10 example, random fluorescent traces related to yellow regions of interest in (A). (**C**) Representative Raster plot. Spikes were identified manually and plotted over time to identify synchronised events. (**D**) Responding cells were determined as those with ≥ one peak of calcium activity. (**E**) Calcium peaks per active cell. (**F**) Frequency of calcium events per minute. (**G-H**) Quantitative measures of synchrony. (**G**) % synchronised cells relating to (C). (**H**) Average R value was calculated by performing a Pearson's correlation of the spike data generated for (C). Data in D-H is displayed as mean ± SEM. N=3. **p< 0.01, 2-way ANOVA with Tukey's multiple comparisons test. Scale bar: 5 μm. Solid black bar in B-C indicates addition of elevated potassium aCSF.

4.2.4 18 WIV Testing

18 WIV cultures did not display statistically significant responses to 4-AP, however in both media conditions, a significant decrease in burst frequency was observed (Axol control: 0.29 ± 0.03, 4-AP: 0.16 ± 0.02, n=9 cs, p= 0.0007; SCT control: 0.27 ± 0.02, n=9 cs, 4-AP: 0.16 ± 0.02, n=9 cs, p= 0.0041, Figure 4.10F). Interestingly, the SCT culture control values were all lower *cf* Axol culture control values, except for R value (Figure 4.10D-H), which was different to all previous experiments.

0 Mg elicited significant responses in percentage responding cells (Control: 14.69 ± 3.5%, 0Mg: 32.08 ± 5.85%, n=6 cs, p= 0.037, Figure 4.11D) and peaks per cell (Control: 1.23 ± 0.08, 0Mg: 1.75 ± 0.9, n=6 cs, p= 0.032, Figure 4.11E) for Axol cultures, whilst SCT did not display any significant increases. Interestingly, both cultures significantly decreased bursting frequency whilst in drug (Axol Control: 0.25 ± 0.02, 0Mg: 0.15 ± 0.02, n=6 cs, p= 0.03; SCT Control: 0.3 ± 0.03, 0Mg: 0.14 ± 0.02, n=6 cs, p= 0.0006, Figure 4.11F).

When PTX was perfused to W18 cultures, peaks per cell were significantly increased for SCT cultures (Control: 1.4 ± 0.17, PTX: 2.21 ± 0.26, n=6 cs, p= 0.001, Figure 4.12E), and significant decreases observed for burst frequency in Axol (Control: 0.23 ± 0.01, PTX: 0.12 ± 0.01, n=6 cs, p= 0.03, Figure 4.12F). Both cultures displayed a lack of synchronised activity. Axol control and PTX R values were all zero (Figure 4.12H).

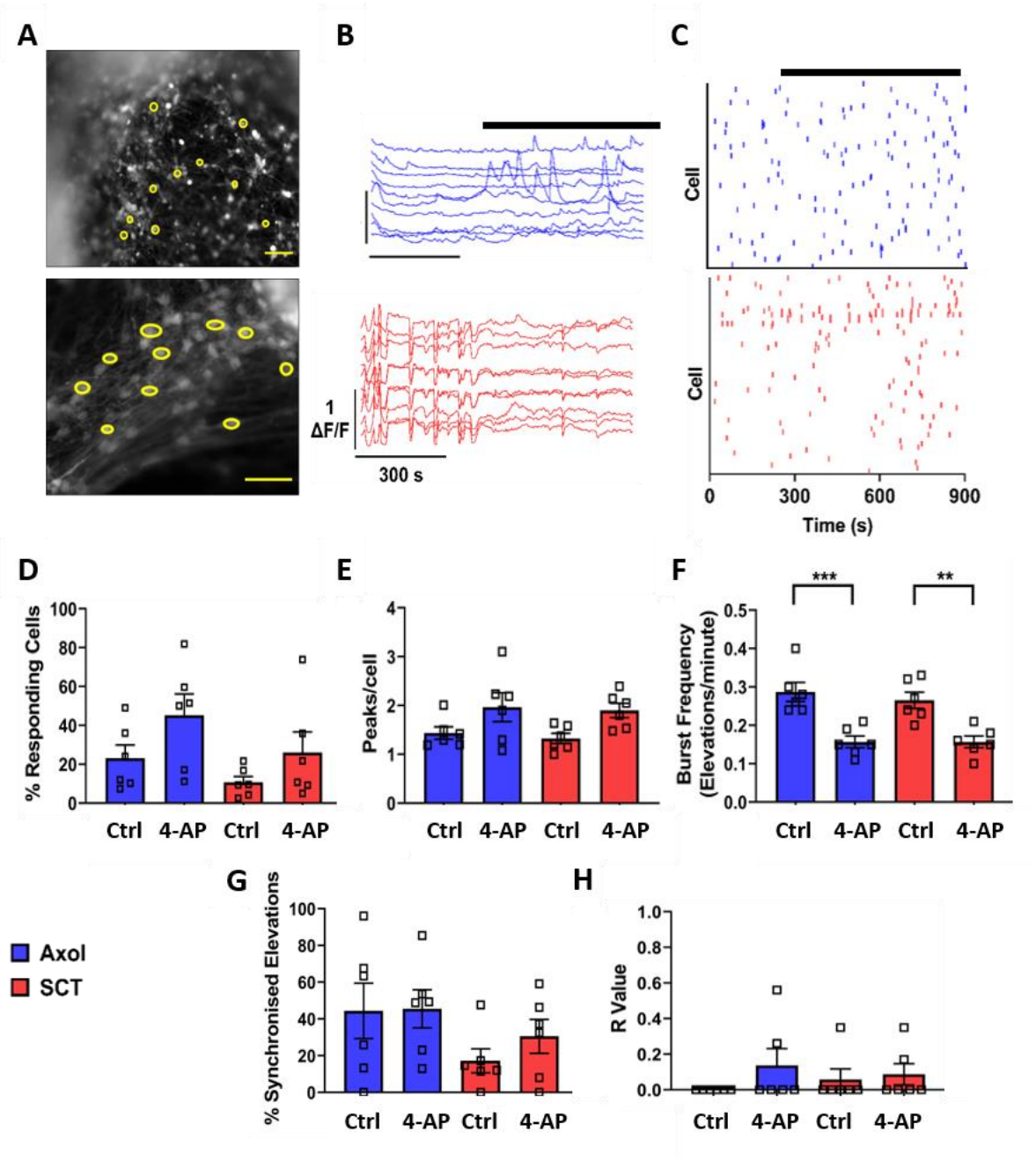

Figure 4.10: **Fluorescent calcium imaging responses of spontaneously differentiated human iPSC-derived neural cultures to 4-aminopyridine perfusion at 18 WIV.** (**A**) Cells cultured in either Axol (upper) or SCT (lower) media were loaded with 5 μM Fluo4-AM for imaging. (**B**) Time-lapse videos were recorded at 0.33 Hz, with representative figures showing 10 example, random fluorescent traces related to yellow regions of interest in (A). (**C**) Representative Raster plot. Spikes were identified manually and plotted over time to identify synchronised events. (**D**) Responding cells were determined as those with ≥ one peak of calcium activity. (**E**) Calcium peaks per active cell. (**F**) Frequency of calcium events per minute. (**G-H**) Quantitative measures of synchrony. (**G**) % synchronised cells relating to (C). (**H**) Average R value of the spike data generated for (C). Data in D-H is displayed as mean ± SEM from N=2 separate neural differentiations. **p< 0.01, ***p< 0.001, 2-way ANOVA with Tukey's multiple comparisons test. Scale bar: 5 μm. Solid black bar in B-C indicates addition of 100 µM 4-AP.

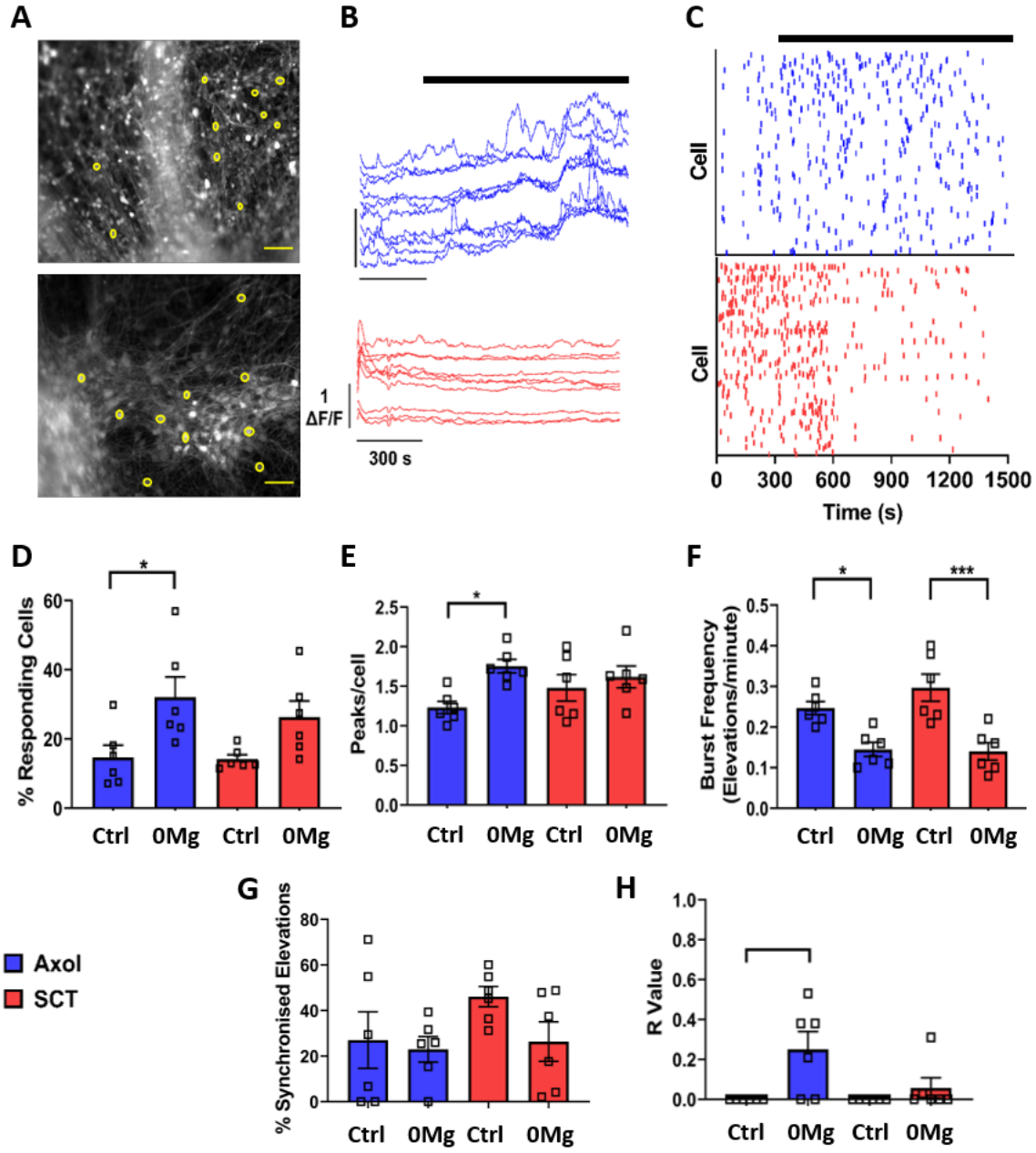

Figure 4.11: **Fluorescent calcium imaging responses of spontaneously differentiated human iPSC-derived neural cultures to zero-magnesium aCSF perfusion at 18 WIV.** (**A**) Cells cultured in either Axol (upper) or SCT (lower) media were loaded with 5 μM Fluo4-AM for imaging. (**B**) Time-lapse videos were recorded at 0.33 Hz, with representative figures showing 10 example, random fluorescent traces related to yellow regions of interest in (A). (**C**) Representative Raster plot. Spikes were identified manually and plotted over time to identify synchronised events. (**D**) Responding cells were determined as those with ≥ one peak of calcium activity. (**E**) Calcium peaks per active cell. (**F**) Frequency of calcium events per minute. (**G-H**) Quantitative measures of synchrony. (**G**) % synchronised cells relating to (C). (**H**) Average R value of the spike data generated for (C). Data in D-H is displayed as mean ± SEM. N=2. *p< 0.05, ***p< 0.001, 2-way ANOVA with Tukey's multiple comparisons test. Scale bar: 5 μm. Solid black bar in B-C indicates addition of 0 Mg^{2+} aCSF.

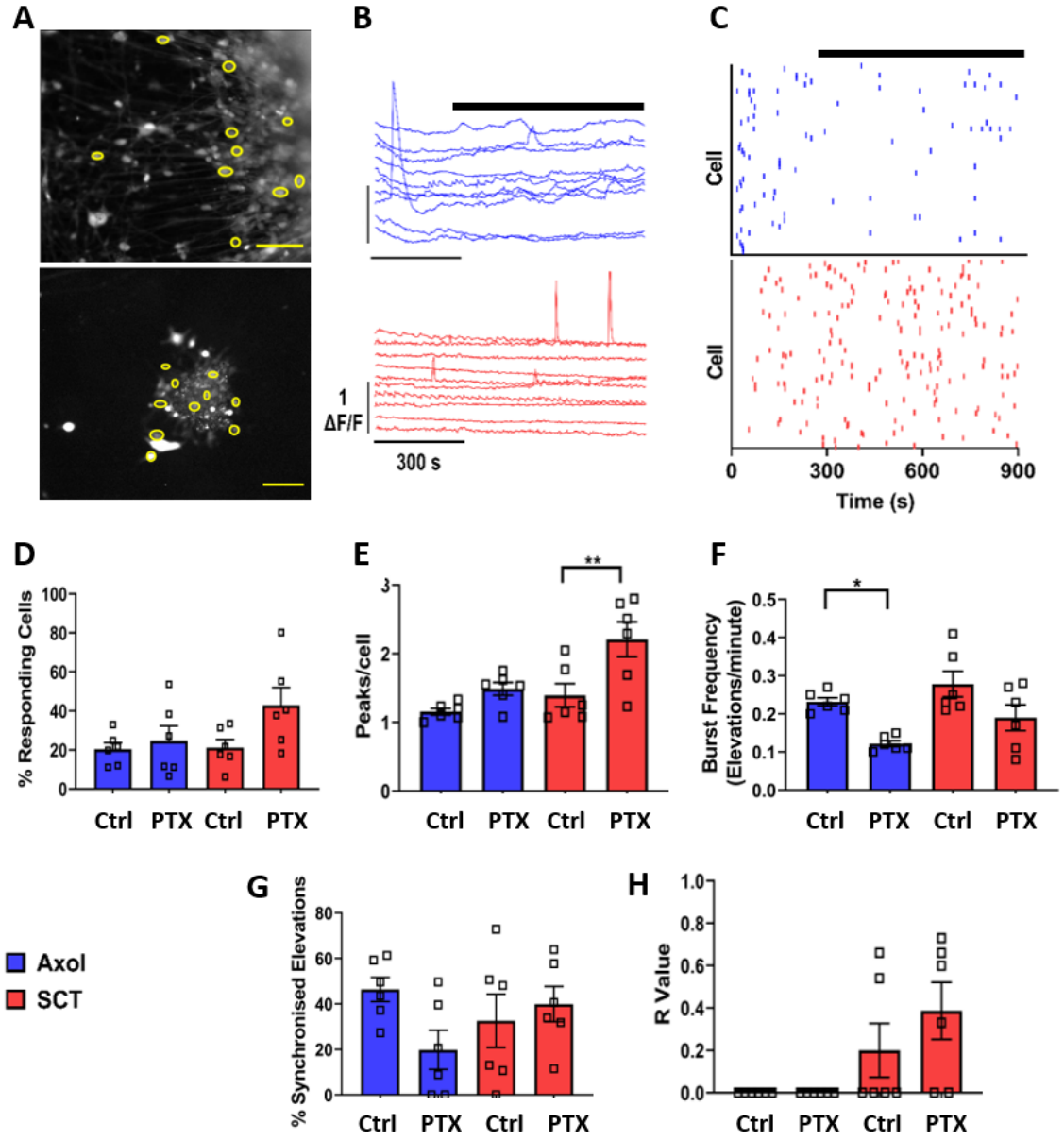

Figure 4.12: **Fluorescent calcium imaging responses of spontaneously differentiated human iPSC-derived neural cultures to picrotoxin at 18 WIV.** (**A**) Cells cultured in either Axol (upper) or SCT (lower) media were loaded with 5 μM Fluo4-AM for imaging. (**B**) Time-lapse videos were recorded at 0.33 Hz, with representative figures showing 10 example, random fluorescent traces related to yellow regions of interest in (A). (**C**) Representative Raster plot. Spikes were identified manually and plotted over time to identify synchronised events. (**D**) Responding cells were determined as those with ≥ one peak of calcium activity. (**E**) Calcium peaks per active cell. (**F**) Frequency of calcium events per minute. (**G-H**) Quantitative measures of synchrony. (**G**) % synchronised cells relating to (C). **(H)** Average R value of the spike data generated for (C). Data in D-H is displayed as mean ± SEM. N=2. *p< 0.05, **p< 0.01, 2-way ANOVA with Tukey's multiple comparisons test. Scale bar: 5 μm. Solid black bar in B-C indicates addition of 100 µM PTX.

4.2.5 'Anomalous' result from 12 WIV elevated potassium

As mentioned previously, a particular culture appeared to display a greater response in activity than the others tested. This result warranted an individual presentation of analysis, due to its obvious highly active, synchronised response to $>K^+$ aCSF. As this was an isolated culture, statistical analysis was not possible, however, due to the nature of the activity, a plethora of additional analyses fitting of epileptiform activity could be performed (Hongo et al., 2015). This culture can be found as 'Video 4.1' in the supplementary video files.

Figure 4.13B shows a clear increase in activity, with each randomly sampled ROI displaying elevations >1ΔF/F. The spike raster plot in Figure 4.13C also indicates a clear synchronisation amongst the cells in culture. Sparse activity is observed prior to $>K^+$ perfusion, then all cells display synchronised activity, depicted by the solid vertical lines.

In contrast to every other culture and condition, every single parameter saw an increased response from this culture. Of particular note is the burst frequency (Figure 4.13F), which displayed a 2.6-fold increase, which was not observed in any other culture tested. 94% of cells responded to the drug (Figure 4.13D), with 98% of these cells in the field of view displaying highly synchronised activity; further confirmed by an R value of 1.0 (Figure 4.13G-H).

More complex analysis was possible for this culture, given the magnitude of the responses. The area calcium events occupied and their amplitudes were both increased over 3-fold and 11-fold from control, respectively (Figure 4.13I-J). Moreover, duration of bursts decreased in the presence of $>K^+$ and the inter-burst-interval (IBI) ie, the time between events, was also decreased 1.6-fold in the presence of $>K^+$ (Figure 4.13K-L).

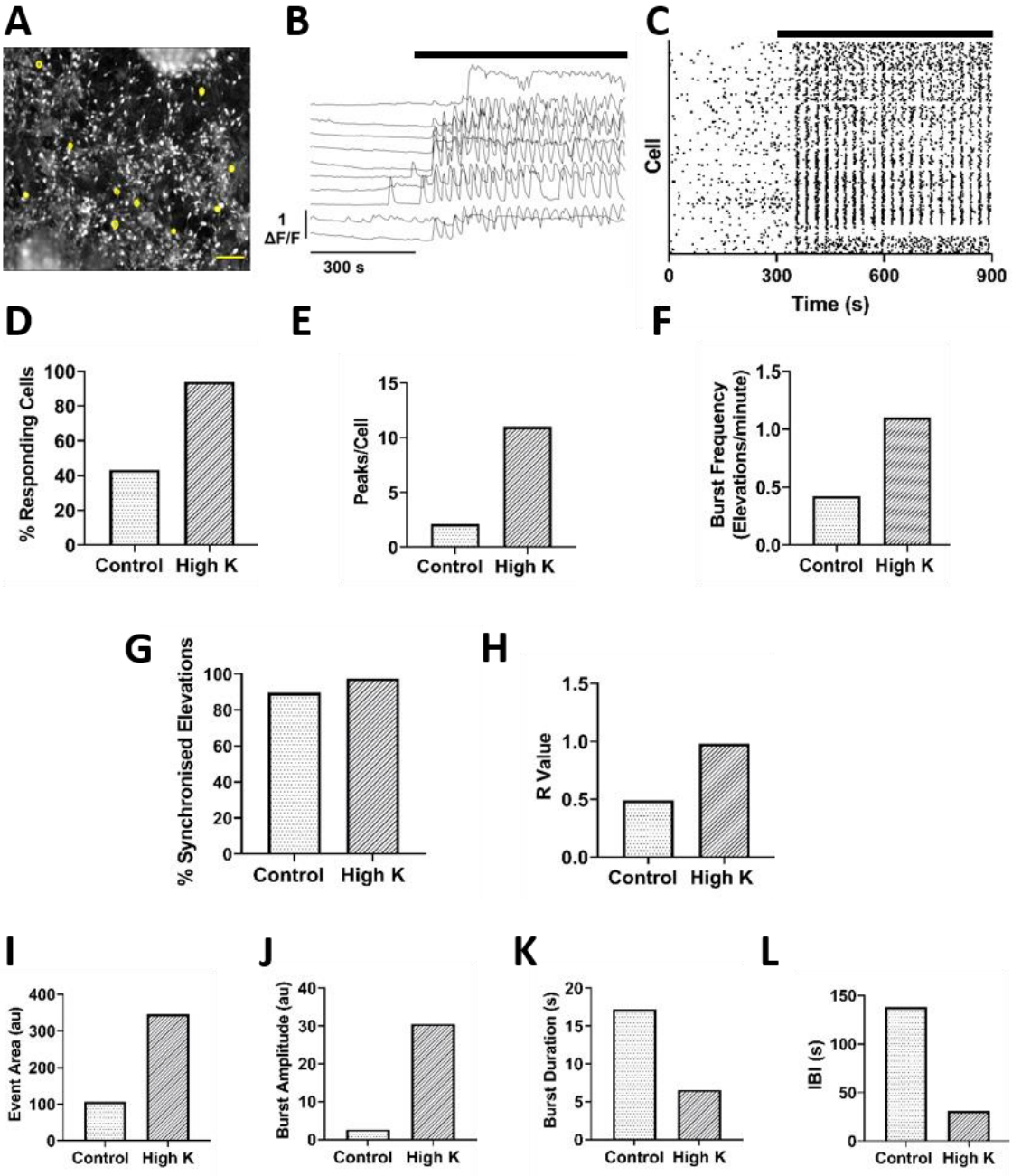

Figure 4.13 – Epileptiform response of SCT-cultured cells to >K^+ perfusion at 12 WIV. (**A**) Cells were cultured in SCT media for 12 weeks and loaded with 5 µM Fluo4-AM for fluorescent calcium imaging. (**B**) Time-lapse videos were recorded at 0.33 Hz, with representative figures showing 10 example, random fluorescent traces related to yellow regions of interest in (A). (**C**) Representative Raster plot. Spikes were identified manually and plotted over time to identify synchronised events. (**D**) Responding cells were determined as those with ≥ one peak of calcium activity. (**E**) Calcium peaks per active cell. (**F**) Frequency of calcium events per minute. (**G-H**) Quantitative measures of synchrony. (**G**) % synchronised cells relating to (C). (**H**) Average R Value. (**I**) Area calcium event occupied. (**J**) Amplitude of calcium events. (**K**) Duration of calcium events. (**L**) Time between calcium events. N=1. Scale bar: 5 µm. Solid black bar in B-C indicates addition of elevated potassium aCSF.

4.3 Discussion

The aim of this chapter was to determine whether spontaneously differentiated human neural precursor stem cells were capable of responding to pro-ictogenic conditions. The endpoints of the study assessed hyperexcitability, hypersynchrony and bursting: the hallmarks of epileptiform activity (Avoli & Jefferys, 2016). The use of fluorescent calcium imaging to test this presented an added benefit of enabling the visualisation of potential synchronised responses and interconnectivity of neural networks.

Cultures were tested from 4 to 18 WIV, as iPSC-derived cultures can fire AP as early as 3 WIV (Odawara et al., 2014) and indeed, functional calcium-mediated activity was observed in these cultures at 4 WIV (Chapter 3). For this reason, cultures and their responses to seizurogenic treatments were assessed from 4 WIV. From the outset, it was suspected that the responses would not be significant, due to an immature neuronal culture (Amin et al., 2016). Particularly for Axol cells, as 4 WIV was found to have significantly lower levels of activity *cf* later timepoints (Appendix Figure A3). Despite those suspicions, SCT cultured cells did display significant responses to both 4-AP and 0 Mg, albeit only in one parameter. As the criteria determined for epileptiform responses were both increased activity *and* synchrony, these responses were not, therefore, categorised as ictal.

Picrotoxin was not selected for experiments at 4 WIV. This decision was based on results of Chapter 3 indicating the total absence of $GAD67^{+}$ interneurons and the results of Gunhanlar et al., (2017), who reported the generation of $GAD67^{+}$ synapses from their spontaneous differentiation, but not until 6-8 WIV. This means that even if the spontaneous cultures did generate interneuronal populations, as has been reported in several instances (Gunhanlar et al., 2017; Kirwan et al., 2015; Shi et al., 2012a), 4 WIV would be too soon to see a response. Indeed, PTX did not generate epileptiform activity at any timepoint in either condition, which is likely due to the absence of GABAergic interneurons and inhibitory circuits; the primary target of PTX (Avoli & Jeffreys, 2016).

4-AP was selected for study due to its use as an epileptic agent (Avoli & Jeffreys, 2016). As the target of 4-AP is neuronal potassium channels, testing 4-AP from 4 WIV was decided, as theoretically, the cellular targets should have been present with the emergence of neurons. Over the 18 weeks, several isolated significant increases in parameters were observed, but no timepoint or media produced significant responses across the panel of endpoints. In fact, the only culture which appeared to respond with increased synchrony and increased activity metrics to 4-AP was 4 WIV SCT cultures. However, the number of peaks per cell and percentage of synchronised cells were not found to be significant, which would be expected from a highly active, synchronous culture displaying epileptiform activity. The slight discrepancy in values could be explained by the fact that more cells became active in the presence of 4-AP, but only displayed a single or very few peaks. This could account for the number of peaks not significantly increasing. Furthermore, the significance reported in R values could be an increase in synchrony between these few new peaks in the presence of drug. The absence of significant increases in percentage synchronised cells suggests that the newly active cells were displaying peaks randomly, not typical of epileptiform activity. Of interest was that the bursting frequency was reduced, which would not be expected in an epileptiform culture, as the bursts should be more frequent compared with control. Taken together, these results do confirm that SCT at 4 WIV responds to 4-AP, but not with epileptiform activity. This is most likely due to the immaturity of the culture and lack of refined synaptic circuits, which is a pre-requisite for synchronised epileptiform activity (Ishii et al., 2017).

0 Mg aCSF was selected as a pro-ictogenic condition, owed to its role in NMDA receptor-mediated excitation of cultures (Isaev et al., 2012). Similarly to 4-AP, some cultures and timepoints responded significantly to 0 Mg perfusion, but significant increases were not observed in all assessment endpoints in any experiment. Again, only one condition produced significant responses in activity and synchrony, which was Axol W18. Despite significant increases observed in peaks per cell, percentage responding cells and R value, the burst

frequency was significantly decreased, suggesting that whilst a response to 0 Mg was observed, epileptiform activity was not. 0 Mg acts on NMDA receptors, which are integral in functional excitatory synaptic transmission (Lutzu & Castillo, 2020). In human *in vivo* studies, synapse formation is believed to commence around week 9 (de Graaf-Peters & Hadders-Algra, 2006) and as NMDA receptor-mediated transmission is essential for the 0 Mg model, these results could suggest undeveloped synapses. This also explains why the condition which did respond to 0 Mg with increased activity and synchrony was 18 WIV.

The lack of epileptiform responses at W4 and W8 in particular, is potentially due to the absence of astrocytes in culture, as confirmed by immunostaining in Chapter 3. Astrocyte dysfunction is observed in epilepsy and seizure activity, the non-appearance of which prior to 8 WIV could provide an explanation as to why widespread synchrony was not observed (Tian et al., 2005; Wetherington et al., 2008). Furthermore, astrocytes are involved in establishment of neural circuitry and synaptogenesis (Christopherson et al., 2005). The lack of formation of a complete synaptically-connected network may explain the inability to form synchronous responses.

Interestingly, despite the conditions where significant responses in activity and synchrony were observed, for 11/12 experiments, the bursting frequency was lower in drug treatment *cf* controls, suggesting non-epileptiform activity. Furthermore, the reduction in burst frequency of 7 of these 11 conditions was significant. This is not consistent with epileptiform activity; bursting should actually increase as this is a characteristic response (Bradley et al., 2018). These results strengthen the argument that despite some experiments displaying increased activity and synchrony, this fundamental parameter indicates that activity in those responsive cultures was not epileptiform.

In addition, neither media at any timepoint or drug treatment elicited significant increases in the percentage of synchronised cells. This would be expected for ictal activity, as seizures synchronise populations of cells (Badea et al., 2001).

Whilst responses for many experiments were not statistically significant, the cultures did appear to respond to the various seizurogenic conditions, suggested by the mean drug response values increasing in almost every condition. It could be argued that more repeats could determine whether a significant response occurs, yet, the experimental design involved three repeats performed for three separate biological differentiations (total of 9 coverslips). However, the experimental design and sample size provided a reasonable opportunity for the cultures to display epileptiform activity and largely, they did not. The experimental design was applied consistently and results obtained at W4, W8 and W12 were considered indicative of the capability of the cultures. However, due to an equipment failure outside of the author's control, final biological repeats at W18 were lost, hence only 2 biological differentiations were perfomed (total of 6 coverslips). Therefore, 18 WIV experiments would benefit from an increased sample size. For this reason, the results at 18 WIV were not considered conclusive.

As the literature suggested 12 WIV is the point at which spontaneous cultures can display matured activity, high potassium aCSF perfusion (>K^+) was selected as an additional test for 12 WIV (Gunhanlar et al., 2017; Kirwan et al., 2015; Odawara et al., 2014, 2016b; Shi et al., 2012). Several repeats were also performed at week 18 (data not shown) with >K^+ aCSF, but due to time constraints and apparatus failure, insufficient repeats for statistical anaysis were obtained, and consequently, week 12 was preferentially chosen to ensure all repeats with >K^+ could be generated.

The single example presented shows that spontaneously differentiated cultures do possess the capacity to respond in a hypersynchronous and hyperexcited manner. As a result this culture was defined as having displayed epileptiform activity in response to >K^+ perfusion. However, this is isolated and hence, not robust or reliable. An R value of 1 indicates complete correlation and this was observed, alongside obvious increases in all other parameters of activity and synchrony. Whilst it can be concluded that spontaneously differentiated cultures can, therefore,

elicit epileptiform activity, 1 repeat of 18 different >K^+ aCSF experiments is not a clear indication that the cultures can respond in this way routinely and is not statistically significant. The ability for one culture to respond likely arises from the differences in cell densities and subtypes when cultures are allowed to differentiate spontaneously and without control. Despite careful seeding densities, cultures did vary coverslip to coverslip and batch to batch. It is this variation which probably precluded any successful and sustained observation of spontaneously differentiated cultures displaying repetitive seizure-like activity. This is also supported by the decision to present individual datapoints; which highlighted the large variance in the distribution of data, further confirming that spontaneous differentiation is unreliable as a method for generating consistent drug response data.

In conclusion, the experiments in this chapter support the contention that whilst spontaneously differentiated neural cultures in Axol and SCT media have the potential to respond to >K^+ aCSF perfusion with large increases in activity, synchrony and bursting, this is not a reliable or reproducible method for generating such activity. Furthermore, no epileptiform response was observed with 4-AP, PTX or 0 Mg aCSF– all of which routinely generate seizure-like events in rodent *in vivo* and *in vitro* models. The results suggest either an absence of relevant receptors/cell types or an immature neural network formation.

Regarding the question posed in Chapter 3, that was which growth medium (Axol or SCT) was more suitable to eliciting functional responses to these conditions, SCT appeared to create the superior culture conditions, due to significantly higher control percentages in several conditions, combined with the results of Chapter 3. This decision was strengthened by the observation that the only culture appearing to respond in an epileptiform manner was cultured in SCT medium.

The revelation that spontaneous differentiation is not suitable for seizure-liability led to the development of alternate culture models in the following chapters. Additionally, as SCT proved a superior growth medium, it was chosen for the proceeding investigations.

Chapter 5

5: OPTIMISATION OF HUMAN IPSC-DERIVED NEURONS AND ASTROCYTES IN A CO-CULTURE MODEL

5.1 Introduction

To the author's knowledge, no study has attempted to use spontaneous differentiation as a method for generating neural cultures for the express purposes of seizure-liability testing; as was demonstrated in Chapter 4. The results from Chapter 4, coupled with consideration of two commercially available growth media are suggestive of an immature neural network function, with limited ability to respond to pro-ictogenic pharmacological and ionic manipulations. A major limitation of spontaneous differentiation is the time taken for cultures to mature, both in terms of morphology (with emergence of astrocytes not occurring until 8 WIV) and functionality (Chapter 4.2, Shi et al., 2012a). Indeed, electrophysiological studies of spontaneously differentiated cultures suggest that neurons may take up to 23 WIV to reach maturity (Amin et al., 2016; Kirwan et al., 2015). In addition, variation was observed between cultures, with astrocytic overgrowth and high-density aggregation observed throughout in both growth media (Chapter 4.2, Appendix Figures A2/4).

5.1.1 Co-cultures of neurons and astrocytes

In contrast to a spontaneous differentiation protocol, many protocols exist for the co-culturing of rodent neurons with other cell types; predominantly astrocytes (Aebersold et al., 2018; El et al., 2018; Herzog et al., 2011; Jones et al., 2012). There have also been recent investigations which have attempted the seeding of human neurons and astrocytes together, in a neural 'co-culture'. Initial co-culture models seeded human iPSC-derived neurons with rodent astrocytes, or rodent astrocyte-conditioned media (Odawara et al., 2014, 2016a; Tang et al., 2013).

Odawara et al., (2014) showed that the co-culturing of human iPSC-derived neurons with rodent astrocytes results in greater, more rapid, functional and morphological maturity *cf* cultures without astrocytes. In an attempt to move to a more human-relevant system, with no inter-species extrapolation, an increasing number of studies have seeded iPSC-derived neurons with human iPSC-derived astrocytes in both short-term (de Rus Jacquet, 2019; Kayama et al., 2018; Matsuda et al., 2018; Tukker et al., 2016, 2018, 2019) and long-term cultures (Odawara et al., 2016b) and iPSC-derived neurons with primary human astrocytes (Kuijlaars et al., 2016).

Amongst their many functions, astrocytes are highly involved in the formation and maturation of excitatory and inhibitory synapses in the CNS, and also their degradation and removal to refine neural circuits (Nguyen et al., 2011). For example, rodent retinal ganglion cells form very few synapses when cultured alone, but the number is increased tenfold in the presence of astrocytes or astrocyte-conditioned media (ACM) (Pfrieger & Barres, 1997). The differences between rodent and human astrocytes are quite considerable, ranging from their size and function, to the presence of morphologically distinct astrocyte subtypes within the human brain and the cerebral cortex in particular (Oberheim et al., 2009). Despite these interspecies differences, studies using human iPSC-neurons and rodent astrocytes highlighted the importance of including astrocytes in culture. Human-neuronal and rodent-astrocytic co-cultures demonstrated enhanced and more rapid functional maturation, spiking activity and maintenance of long-term electrical activity *cf* neurons alone (Lischka et al., 2018; Odawara et al., 2014; Tang et al., 2013).

In addition, several recent studies have used co-culture protocols with a specific focus on seizure-liability testing (Ishii et al., 2017; Odawara et al., 2018; Tukker et al., 2019). These studies have shown that iPSC-derived neural co-cultures are capable of generating epileptiform activity in response to convulsants. This activity was achieved in 8 weeks, facilitated by the inclusion of iPSC-derived astrocytes, which is a far more rapid and practical developmental timeframe than

observed with spontaneously differentiated models, both in the literature (Gunhanlar et al., 2017; Kirwan et al., 2015; Shi, et al., 2012b) and in Chapters 3 and 4 of this thesis. An added benefit of the co-culture method *cf* spontaneous differentiation is that the seeding densities of each cell type can be precisely controlled, to promote the generation of a heterogenous neural model, with reduced variation between cultures.

Despite the obvious advantage of controlling cell ratios and the commercial availability of cells which have already been differentiated and karyotyped, a particular issue in the field is the tendancy for each group to use their own protocol, which differs widely with other literature. As such, there is no 'standard' as there is for rodent *in vitro* studies. Furthermore, commercial intellectual property issues prevent disclosure of precise media formulations and hence, neural induction methods used in the generation of the cells, and donors of the parent iPSC can be from a wide variety of patients. The methods used to generate iPSC derived co-cultures are diverse (Table 5.1). Differences in the supply of cells, ratios of subtypes, growth medium and surface coating reagent are considerable.

5.1.2 Monocultures of neurons and astrocytes

In order to generate a co-culture protocol, monocultures of neurons and astrocytes first had to be developed. In addition, the author is unaware of any group who have attempted seizure-liability studies on iPSC-derived astrocyte monocultures.

To generate neuronal monocultures, the small molecule DAPT was used. DAPT is an inhibitor of the γ-secretase complex, which is a key target of Notch (Nelson et al., 2007). Notch signalling plays a key role in neural connectivity, axon migration, synapse formation and synaptic maturation (Giniger, 2012) and maintains the progenitor pool in differentiating neural cultures; hence its inhibition leads to the progenitor pool exiting the cell cycle simultaneously. Indeed, DAPT has been used previously in iPSC-derived cultures to synchronise the differentiation of NPCs to generate enriched neuronal monocultures (Elkabetz & Studer, 2008; Kuijlaars et al.,

2016; Rhee et al., 2019; Wong et al., 2017), albeit at different concentrations and durations of treatment.

As discussed above, astrocytes are an integral component of neural cultures and indeed, experiments with stem cell-derived astrocytes have demonstrated that these cells are capable of exhibiting many of the functions of human *in vivo* astrocytes. These include: facilitating synaptic maturation, gliotransmission, protection of neurons from excitotoxicity and stress and astrocytic calcium activity (Hill et al., 2016). The recent emergence of this co-culture method was largely due to the advent of protocols for the exclusive generation of astrocytes from human iPSCs (Perriot et al., 2018; Serio et al., 2013; Shaltouki et al., 2013; Soubannier et al., 2019; TCW et al., 2017) and the recent commercial availability of iPSC-derived astrocytes.

The first efficient, relatively rapid protocol for astrocyte generation from iPSC was reported by Shaltouki et al., (2013). Astrocyte development can occur via two lineage pathways: via an intermediate precursor which expresses CD44 and an indirect pathway involving glial precursors which differentiate exclusively into astrocytes and oligodendrocytes (Shaltouki et al., 2013). Astrocytes can be generated from iPSC-derived NPCs, via the use of a defined differentiation medium. In this instance, treatment with the growth factors BMP2 and ciliary neurotrophic factor (CNTF) directs differentiation of NPCs to astrocytes (Shaltouki et al., 2013). BMPs can cause selective astroglial lineage from progenitor cells (Gross et al., 1996) and activation of the CNTF receptor has been shown to promote differentiation of cortical precursors into astrocytes and prevents cells committing to a neuronal lineage (Bonni et al., 1997). However, it was the inclusion of a splice variant of neuregulin known as 'heregulin' which was found to promote the highest efficiency of astrocyte differentiation. Neuregulins are cell adhesion molecules which act on the epidermal growth factor (EGFR) family of receptor tyrosine kinases to promote neural development. Heregulin has been shown to act in both paracrine and autocrine fashion, stimulating EGFR to activate downstream signalling pathways including the phosphatidylinositol

3-kinase/AKT pathway, important in regulating cell cycle and, involved with differentiation of stem cells to neurons and astrocytes (Otaegi et al., 2006). Astrocytes used in this Chapter have been differentiated using this method of defined differentiation medium (Shaltouki et al., 2013).

The aim of this Chapter was to compare different co-culture and monoculture methods using human iPSC-derived neurons and astrocytes, on their ability to respond to seizurogenic conditions with epileptiform activity.. The methods in this Chapter are represented in Figure 5.0.

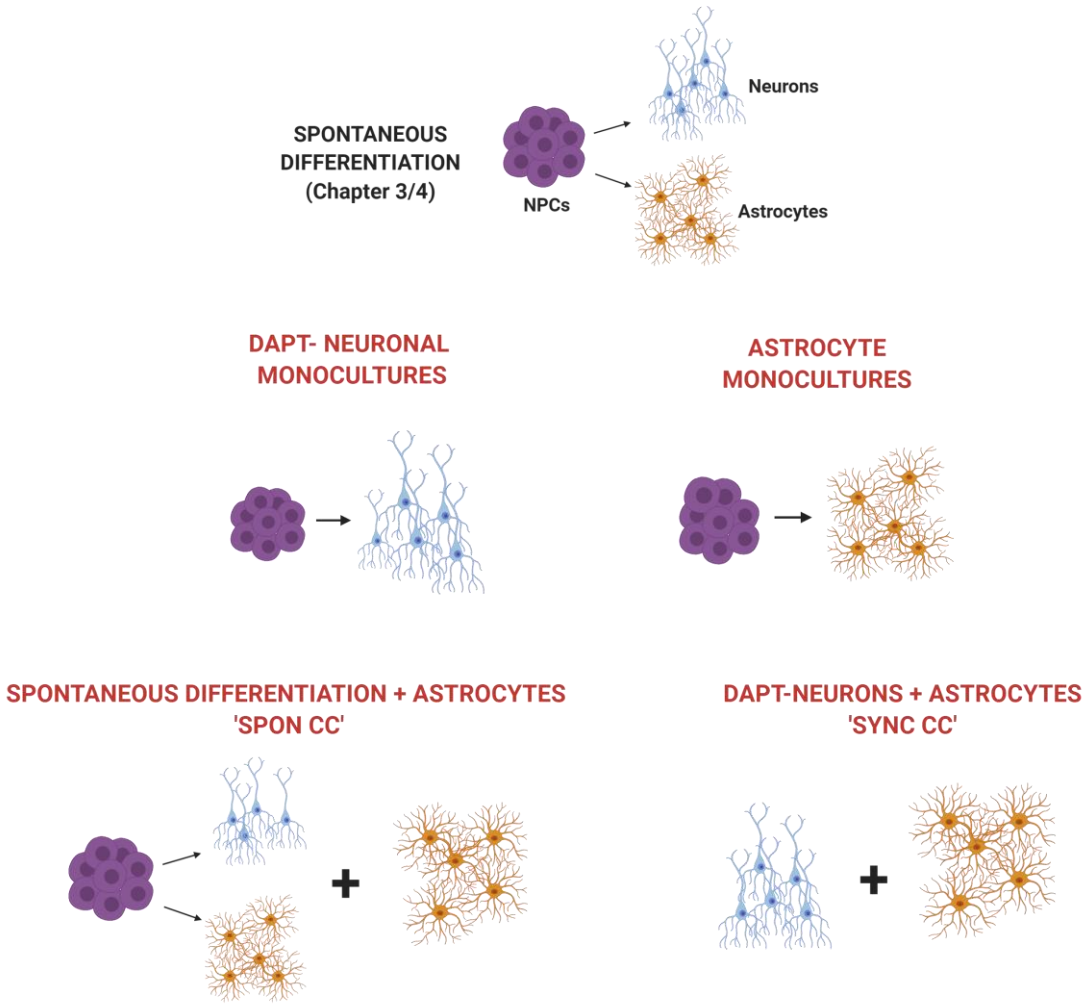

Figure 5.0: Representation of culture methods tested in Chapter 5. The monocultures and co-cultures highlighted in red text indicate those to be tested in this Chapter.

Table 5.1: Co-culture models of human iPSC-derived neural cells. Including seeding ratios of neurons to astrocytes, growth medium and method of co-culturing.

Neurons	Astrocytes	Ratio	Coating Reagent	Co-culture method	Culture Medium	Reference
Cellectis & Sigma DAPT treated	Primary Human	4:1	PORN-laminin	Together	N2/B27 with cAMP, BDNF, GDNF	Kuijlaars et al., 2016
iCell®	iCell	3:1	PORN-laminin	Neurons for 40 minutes, then astrocytes on top	iCell maintenance	Tukker et al., 2016
iCell® glutaneurons/ iCell® neurons	iCell	1:1	PEI-laminin	Together	SCT BrainPhys™	Tukker et al., 2018
iCell®/Synfire®	iCell	6:1	PEI-laminin	Together	SCT BrainPhys™ Neuro.4U®	Tukker et al., 2019
Cellular Dynamics	Cellular Dynamics	3:1	PEI-laminin	Together	iCell neuron maintenance and ScienCell astrocyte	Ishii et al., 2017
XCell Science cortical	XCell Science	10:1	PEI-laminin	Neurons for 8 days, then astrocytes	SCT BrainPhys™, removing BDNF/GDNF after astrocyte addition	Kayama et al., 2018
XCell Science cortical	XCell Science	10:1	PEI-laminin	Neurons for 8 days, then astrocytes	XCell neural maturation with SCT SM1 supplement	Odawara et al., 2018
XCell Science cortical Axol Bioscience Ax0019	XCell Science Axol Ax0084	16:1	Surebond-Readyset (Axol)	Neurons for 8 days, then astrocytes	SCT BrainPhys™, removing BDNF/GDNF after astrocyte addition	Matsuda et al., 2018

The aims of this chapter are to:

1) **Establish a suitable method for DAPT-synchronisation of iPSC-derived neurons using fluorescence microscopy**
2) **Assess the ability for cultures of astrocytes-only and neurons-only to form respective subtypes via immunostaining**
3) **Determine whether cultures of neurons and astrocytes-only can display epileptiform responses to 4-aminopyridine, picrotoxin and zero-magnesium aCSF, using fluorescent calcium imaging**
4) **Compare different co-culture methods to produce functional, robust cultures**
5) **Determine the ability for different co-culture methods to produce functional synapses and respond to zero-magnesium aCSF perfusion using fluorescent calcium imaging**

5.2 Results

5.2.1 Neuron and Astrocyte Monocultures

In order to determine the optimal method of synchronising human iPSC-derived neural stem cells (NPCs) to produce a pure neuronal population, NPCs were treated with the Notch signalling inhibitor DAPT over 7 days and the percentage of proliferating cells assessed via immunocytochemistry (ICC) using Ki67 – a nuclear protein necessary for and indicative of, cellular proliferation (Sun & Kaufman, 2018). This was supplemented in SCT medium, as previous results had shown SCT more effective for NPC differentiation than Axol neural maintenance medium (Chapters 3/4).

At all timepoints tested, DAPT-treated cells had a significantly lower percentage of Ki67-positive nuclei *cf* untreated cells: (D5: Control: 69.74 ± 6.46%, DAPT: 8.23 ± 4.25%, p= 0.0001; D6: Control: 63.21 ± 6.28%, DAPT: 7.97 ± 3.18%, p= 0.0003; D7: Control: 66.44 ± 9.20%, DAPT: 9.34 ± 4.90%, p= 0.0002, all n=9). The difference between DAPT treatments at Days 5-7 were not significant, with the largest difference being 1.37% between D5-D7. Whilst D7 had the highest percentage of $Ki67^{+}$ cells in DAPT, it did not have the highest number of proliferating cells in total (66.44%) which was lower than that of D5 (69.74%) (Figure 5.1A).

Alongside the duration of DAPT treatment, the initial seeding density was considered. Spontaneously differentiating cells in Chapter 3 were seeded at a density of 50,000 cells/cm^2, which was a sufficient protocol for spontaneous differentiation. However, as the proliferation of NPCs in DAPT-treated cultures were expected to be inhibited, a higher initial seeding density was selected to account for the reduction in cell proliferation (Figure 5.1B).

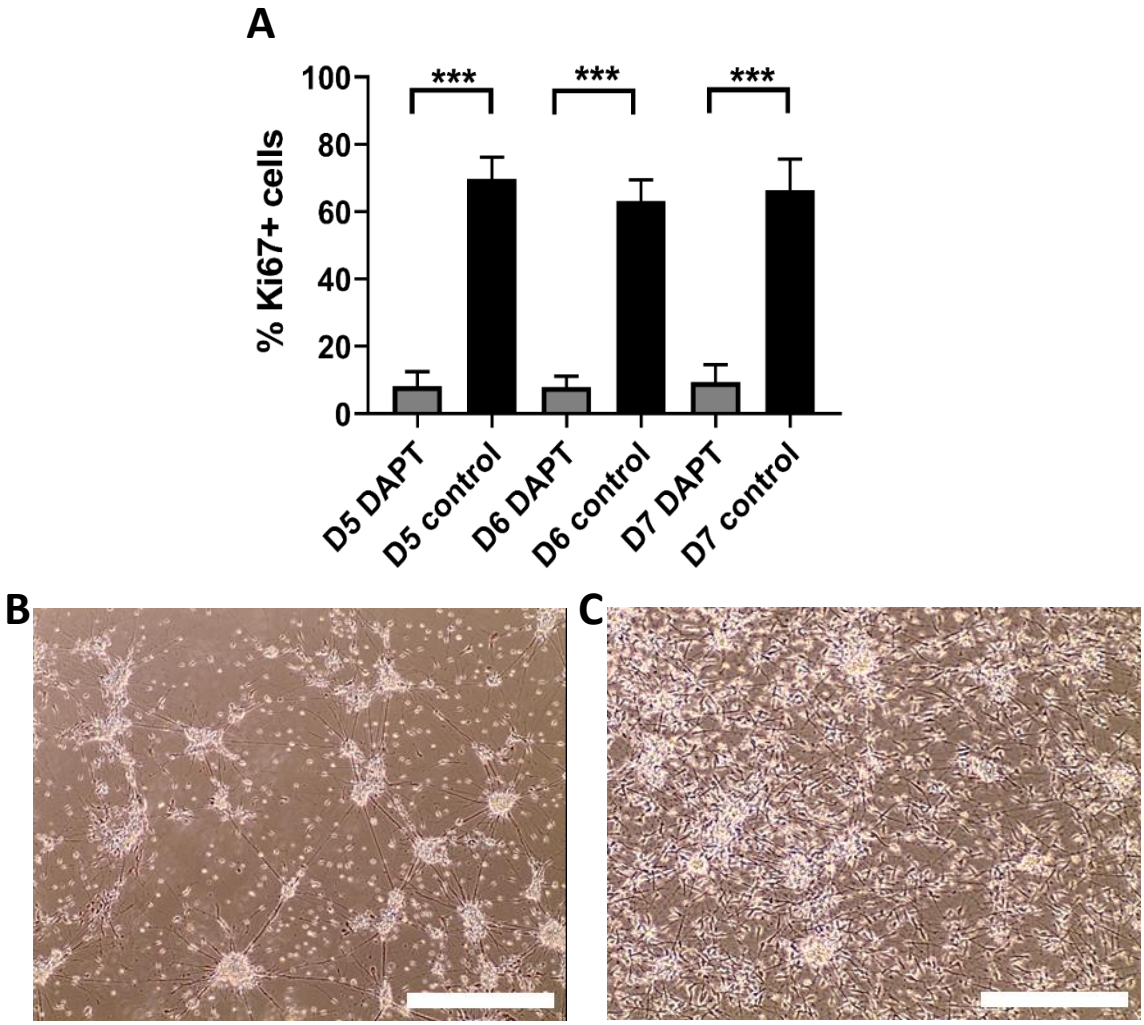

Figure 5.1: Determining optimal time course and seeding density for DAPT treatment of NPCs. Human iPSC-derived neural precursor stem cells were plated and allowed to recover for 24 hours, before being treated with 10 µM DAPT. (A) Cells were differentiated over 7 days with or without DAPT supplementation. Immunocytochemistry was performed and cells were stained for the cell proliferation marker Ki67. The percentage of $Ki67^+$ cells was determined from the total DAPI stained cells. (B-C) Representative phase contrast images of Day 7 DAPT seeding densities of 75,000 and 100,000 cells/cm^2, respectively. N=3. ***p< 0.001, 2-way ANOVA with Tukey's test. Scale bar: 100 µm.

Despite a 1.5-fold increase in cells *cf* spontaneous, a seeding density of 75,000 cells/cm^2 produced sparse cultures with poor viability; these showed extensive fasciculation of neurites and detachment from the culture surface by D7 (Figure 5.1B, n=3). The seeding density was subsequently increased to 100,000 cells/cm^2 and cells adopted an adhered, 2-dimensional orientation, with neurite extensions visible and reduced cell death (Figure 5.1C). 100,000

cells/cm^2 was selected as the optimal seeding density for cultures containing synchronised neurons.

Following establishment of an optimised synchronisation protocol, human iPSC-derived neurons and 11 WIV astrocytes were differentiated over 4 weeks and their morphology characterised via ICC (Figure 5.2-3). As per Chapter 3, neuron-specific class III β-tubulin (Tuj1) and calcium-binding protein S100β were used to label neurons and astrocytes, respectively. Results in this Chapter indicated that synchronised NPCs formed neural rosettes at 1 WIV, as with spontaneous differentiations (Figure 5.2, n=6 cs). Moreover, sync-neuron cultures generated Tuj1$^+$ neurons and were S100β negative (Figure 5.3, n=6 cs). In addition, the neurons presented a low degree of fasciculation, which remained constant throughout phase contrast monitoring (data not shown).

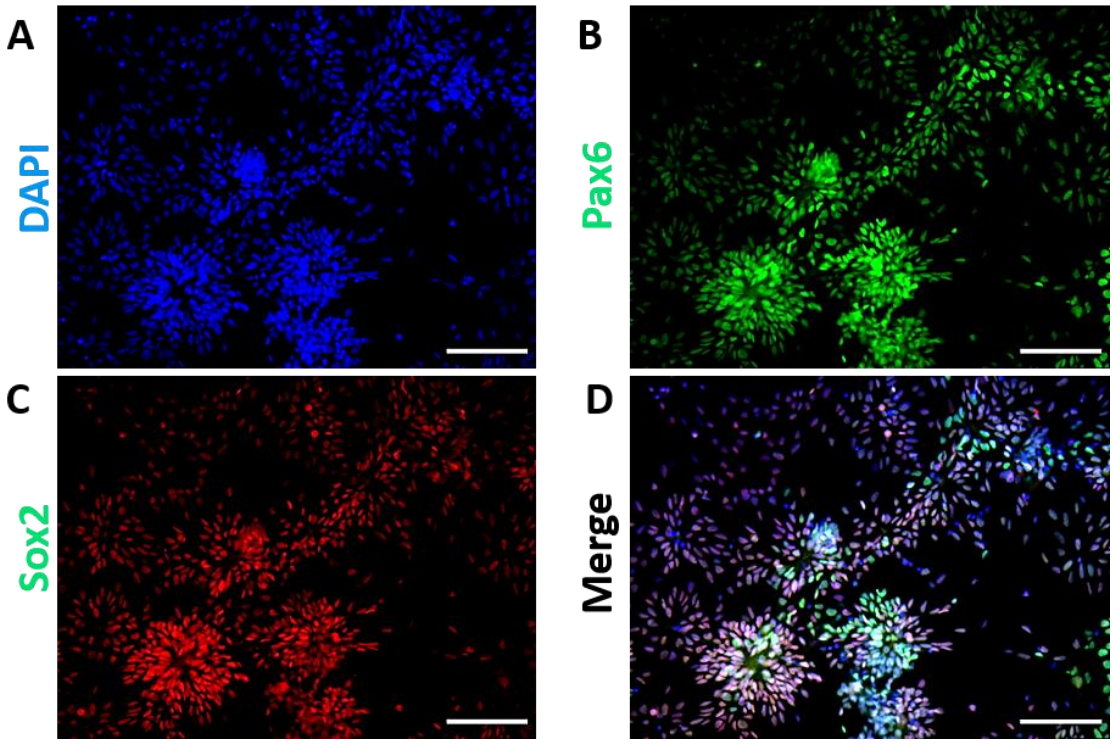

Figure 5.2: DAPT-synchronised NPCs form cortical rosettes at 1 WIV. iPSC-derived neural precursors were treated for 7 days with 10 µM DAPT and immunocytochemistry performed to assess the presence of neural progenitor markers. (A) Nuclei stained with DAPI (Blue, excitation λ 345 nm, emission λ 455 nm). (B) Pax6 neural progenitor staining (Green, excitation λ 495 nm, emission λ 519 nm). (C) Sox2 neural progenitor staining (Red, excitation λ 588 nm, emission λ 649 nm). (D) Merged images of A,B,C. N=3. Scale bar: 100 µm.

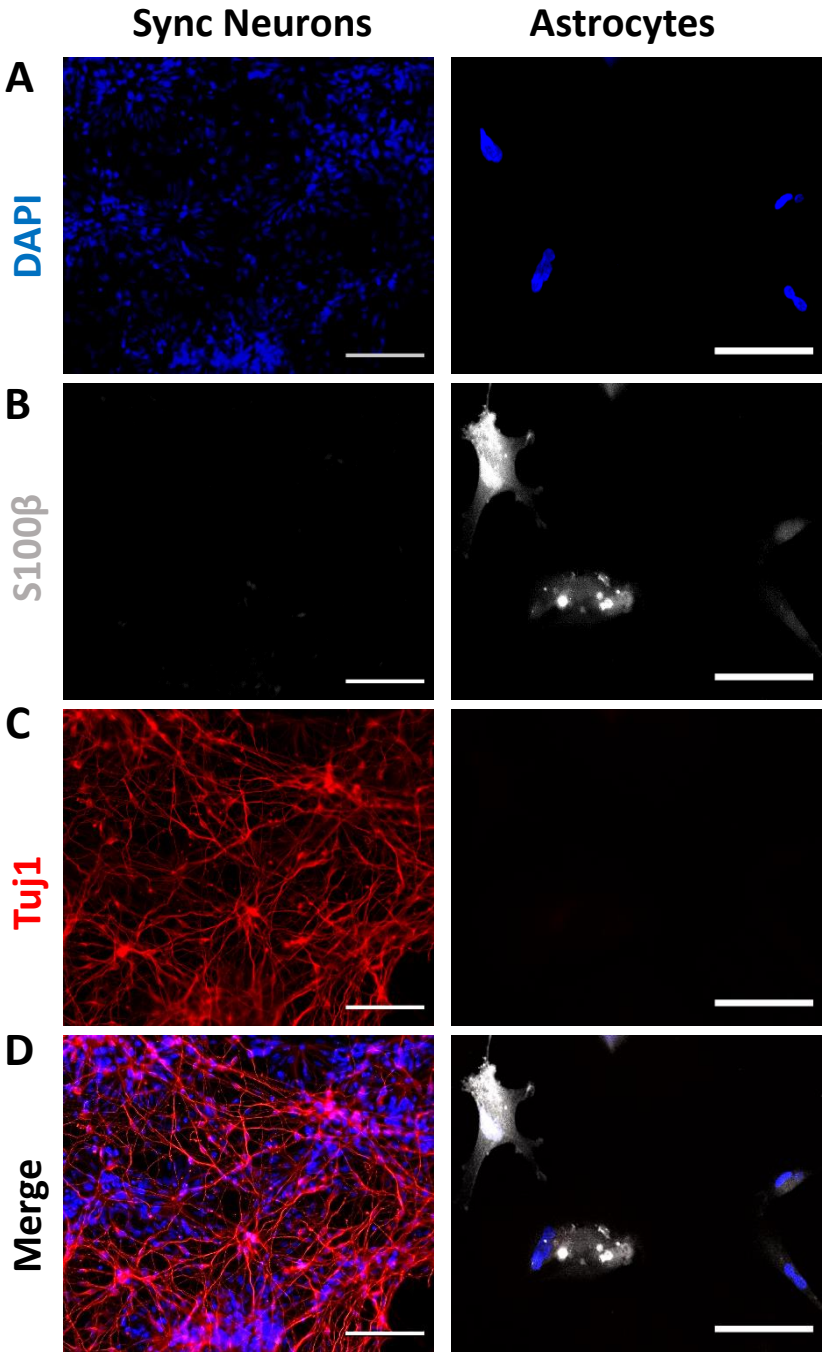

Figure 5.3: DAPT-treated NPCs do not generate S100β^{+} astrocytes and iPSC-derived astrocytes alone do not contain Tuj1^{+} neurons. iPSC-derived neural precursors were synchronously differentiated in SCT media with 10 µM DAPT (Left column) and 11-week old cryostored iPSC-derived astrocytes were cultured in ScienCell™ astrocyte media over 4 weeks. Immunocytochemistry performed to assess the presence of neuronal and astrocytic markers. (A) Nuclei stained with DAPI (Blue, excitation λ 345 nm, emission λ 455 nm). (B) S100β astrocytic staining (Grey, excitation λ 495 nm, emission λ 519 nm). (C) Tuj1 neuronal staining (Red, excitation λ 588 nm, emission λ 649 nm). (D) Merged image of A,B,C. N=3. Scale bar: 100 µm.

Sync-neuron cultures did not survive past ~7 WIV in any biological differentiation (Appendix Figure A6). In contrast, astrocyte-only cultures were S100β^{+} by 4 WIV (Figure 5.3B, n=6 cs) and did not contain Tuj1^{+} cells (n=6 cs). The relative size of the human iPSC-derived astrocytes were approximately 50-fold that of the neuronal cells (~100 µm versus ~2 µm).

5.2.2 Induction of epileptiform activity in monocultures

Having established a suitable synchronisation protocol and characterised the morphology of different culture types, respective cultures were perfused with a series of pro-ictogenic conditions as described in Chapter 4. Synchronised-neuronal monocultures at 4 WIV and 15 WIV astrocyte monocultures displayed no significant response in activity to 4-AP, 0 Mg^{2+} aCSF or PTX perfusion (Figures 5.4-6).

The peaks per cell values increased in all pro-ictogenic treatment (Figure 5.4-6F), however, this did not attain statistical significance. As with peaks per cell values, sync neurons exhibited higher control values *cf* astrocytes. For all treatments, the representative Fluo4-AM-loaded images supported the results of ICC in Figure 5.3, showing large (>100 µm) astrocytes and considerably smaller neurons (~2 µm) (5.4-6A,B).

Alongside metrics for activity, measures of synchrony were used to determine whether cultures of neurons and astrocytes alone could produce this characteristic epileptiform response. Neither neuron or astrocyte monocultures presented a significant response in terms of the percentage of synchronised cells (Figure 5.6G-I). However, in every instance, neuronal cultures showed an increase in percentage of synchronised elevations. Whilst astrocyte cultures also showed increases in synchronised elevations with 4-AP and 0 Mg perfusion, no synchronised events were detected in PTX (Figure 5.7I). Moreover, the R values reported for astrocyte cultures were all zero (Figure 5.7J-L). R values for neuronal cultures were also zero in each treatment, with the exception of a single repeat in 4-AP and 0 Mg (Figure 5.7J,K).

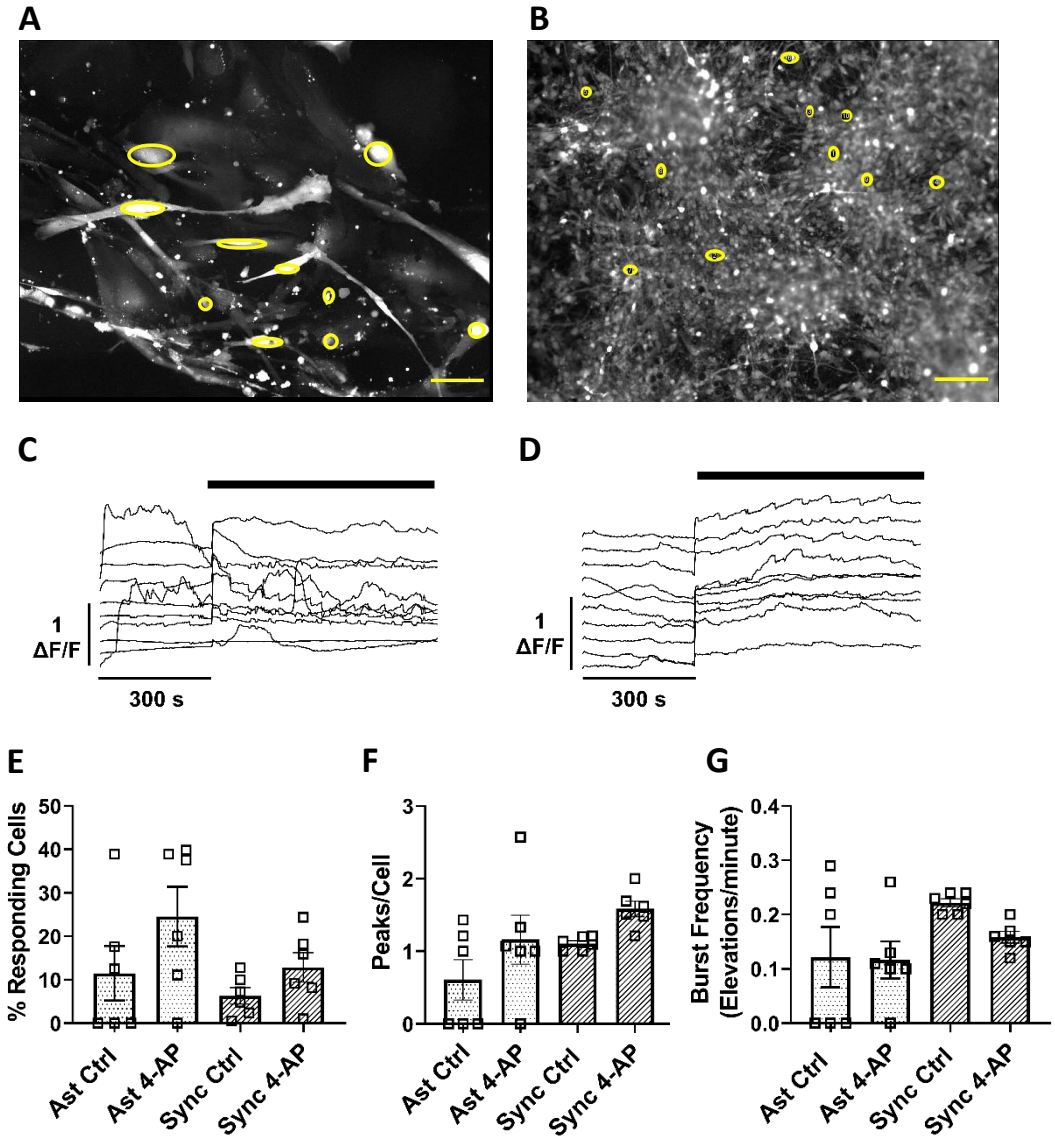

Figure 5.4: **Human iPSC-derived astrocyte and neuron monocultures do not respond to 4-aminopyridine perfusion.** (**A,B**) Astrocyte cultures (A) and neuronal cultures (B) were loaded with 5 µM Fluo4-AM for fluorescent calcium imaging, with time lapse videos recorded at 0.33 Hz. (**C-D**) Representative figures showing 10 example, random fluorescent traces related to yellow regions of interest in (A,B). (**E**) Responding cells were determined as those with ≥ one peak of calcium activity. (**F**) Calcium peaks per active cell. (**G**) Frequency of calcium events per minute. Data in E-G is displayed as mean ± SEM from N=3 separate differentiations. 2-way ANOVA with Tukey's multiple comparisons test. Scale bar: 5 µm. Solid black bar in C-D refers to addition of 100 µM 4-aminopyridine.

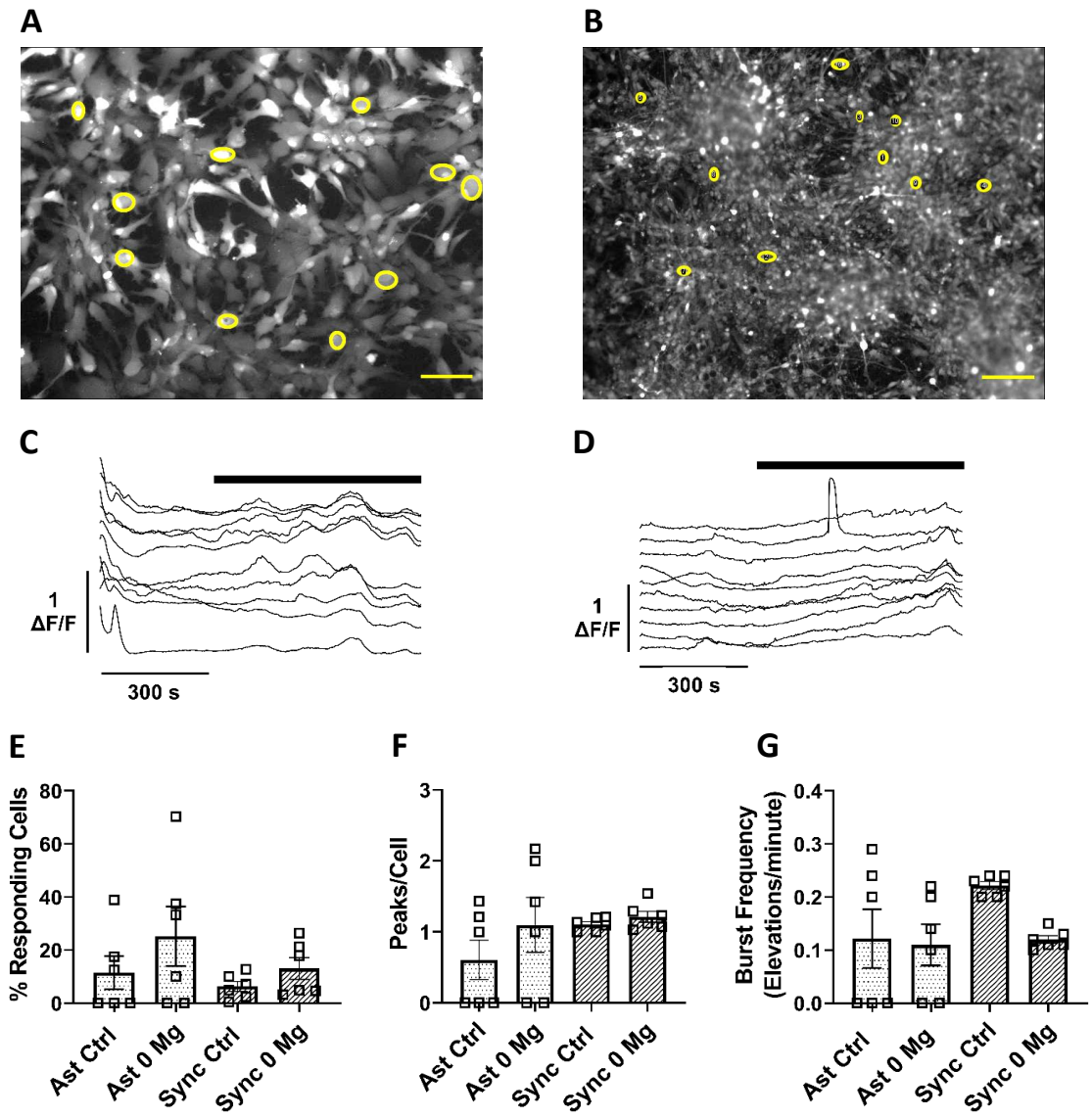

Figure 5.5: **Human iPSC-derived astrocyte and neuron monocultures do not respond to zero-magnesium aCSF perfusion.** (**A,B**) Astrocyte cultures (A) and neuronal cultures (B) were loaded with 5 µM Fluo4-AM for fluorescent calcium imaging, with time lapse videos recorded at 0.33 Hz. (**C-D**) Representative figures showing 10 example, random fluorescent traces related to yellow regions of interest in (A,B). (**E**) Responding cells were determined as those with ≥ one peak of calcium activity. (**F**) Calcium peaks per active cell. (**G**) Frequency of calcium events per minute. Data in E-G is displayed as mean ± SEM. N=3. 2-way ANOVA with Tukey's multiple comparisons test. Scale bar: 5 µm. Solid black bar in C-D refers to addition of magnesium-free aCSF.

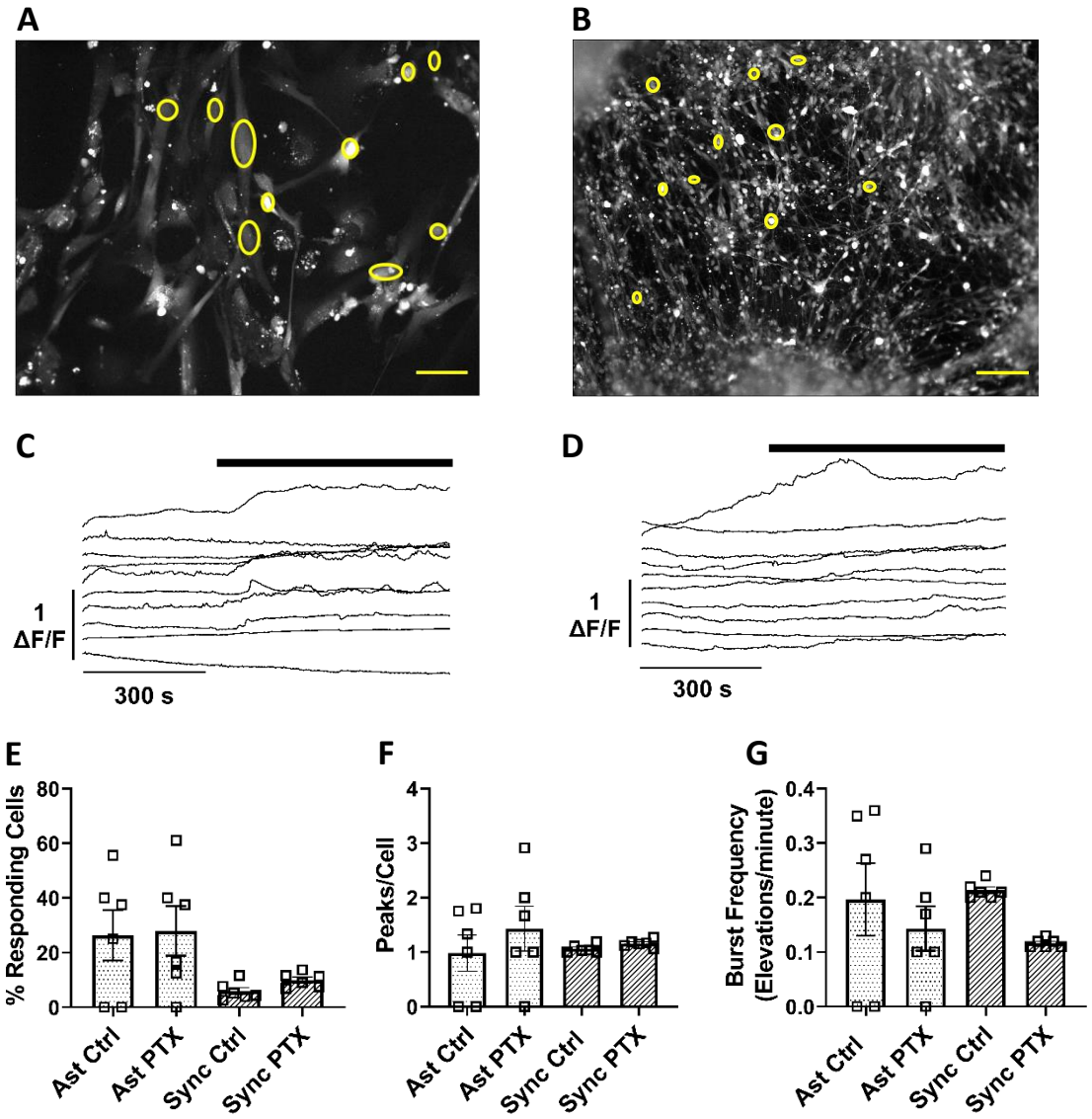

Figure 5.6: **Human iPSC-derived astrocyte and neuron monocultures do not respond to picrotoxin perfusion.** (**A,B**) Astrocyte cultures (A) and neuronal cultures (B) were loaded with 5 µM Fluo4-AM for fluorescent calcium imaging, with time lapse videos recorded at 0.33 Hz. (**C-D**) Representative figures showing 10 example, random fluorescent traces related to yellow regions of interest in (A,B). (**E**) Responding cells were determined as those with ≥ one peak of calcium activity. (**F**) Calcium peaks per active cell. (**G**) Frequency of calcium events per minute. Data in E-G is displayed as mean ± SEM. N=3. 2-way ANOVA with Tukey's multiple comparisons test. Scale bar: 5 µm. Solid black bar in C-D refers to addition of 100 µM picrotoxin.

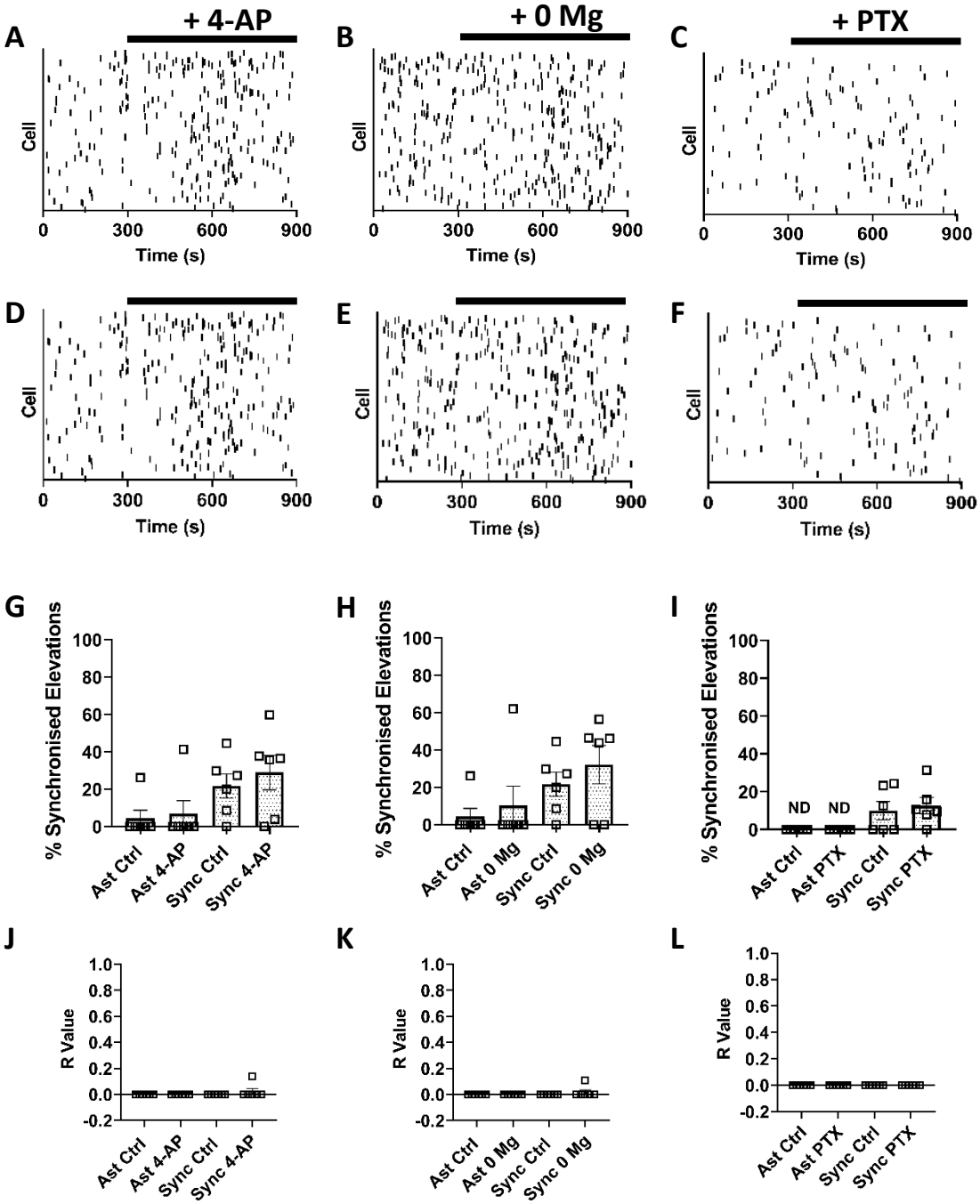

Figure 5.7: **Astrocyte and neuron monocultures do not display synchronous activity in response to pro-ictal conditions.** (**A-C**) Representative raster plots of astrocytic-only cultures in response to pro-ictal conditions. Spikes were manually identified and plotted over time to identify synchronised events. (**D-F**) Representative raster plots of neuron-only cultures. A,D: response to 100 µM 4-aminopyridine, B,E: zero-magnesium aCSF perfusion, C,F: 100 µM picrotoxin. (**G-I**) % synchronised cells of total active cells, relating to (A-F). (**J-L**) Average R value was calculated by performing a Pearson's correlation of the spike data generated for (G-I), then performing a Fishers-z transformation. Data in G-L is displayed as mean ± SEM. N=3. 2-way ANOVA with Tukey's multiple comparisons test. Solid black bar in A-F refers to addition of pro-ictal condition.

5.2.3 Co-culturing human iPSC-derived neurons and astrocytes together

Following studies with isolated cultures of neurons and astrocytes, the potential of co-cultured cells to display epileptiform responses when cultured together was attempted, as has been reported with other co-culture systems (Ishii et al., 2017; Matsuda et al., 2018; Odawara et al., 2018; Tukker et al., 2019). Initial co-culture experiments were performed using 0 Mg-aCSF perfusion, to assess whether synapse maturation and network functionality occurred more rapidly than spontaneously differentiated cultures. In order to determine this, several co-culture methods were assessed. Co-cultures were designated 'spontaneous' or 'synchronised', referring to the methods applied in the co-culture generation. Spontaneous co-cultures (Spon CC) comprised iPSC-derived NPCs and iPSC-derived astrocytes and synchronised co-cultures (Sync CC) comprised DAPT-synchronised iPSC-derived NPCs and iPSC-derived astrocytes (Figure 5.0).

Figure 5.8 shows that in both co-culture conditions, cells did not display significant increases in synchrony or activity when perfused with 0 Mg aCSF. Example traces from Spon CC indicate increased activity, with large fluorescence amplitude increases, compared with Sync CC (Figure 5.8B). The control values for percentage responding cells in Spon CC were higher than those for Sync CC, albeit not significantly (Spon CC: 15.47 ± 6.01, Sync CC: 10.54 ± 2.70; n=6 cs, p= 0.99). This was also true for peaks per cell, burst frequency and percentage of synchronised elevations, where the control values for Spon CC were not significantly higher than those for Sync CC.

Whilst Spon CC presented an increased response in responding cells and peaks, (Figure 5.8D,E), burst frequency and synchronised elevations decreased (Figure 5.8F,G), however none of these values attained statistical significance.

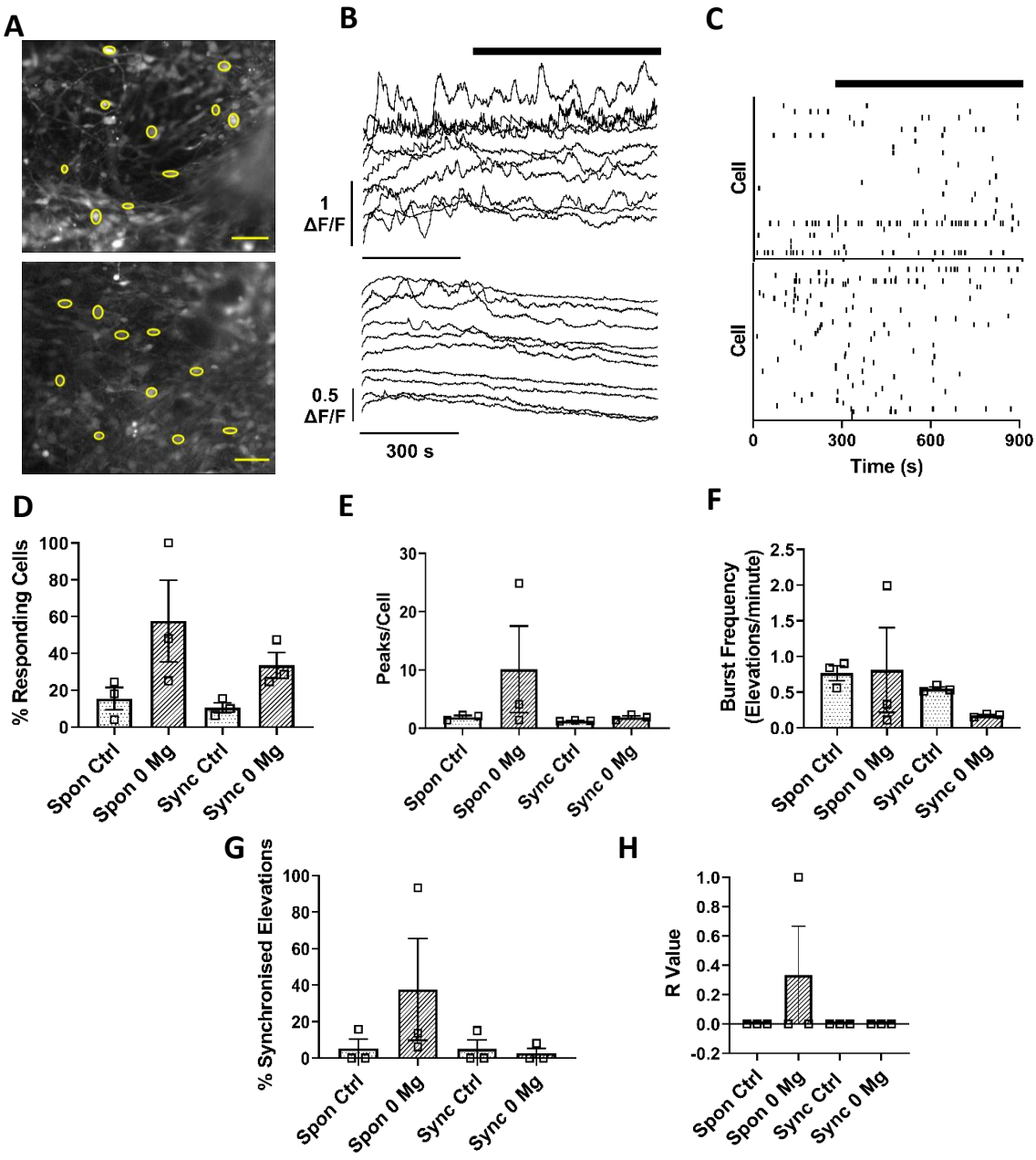

Figure 5.8: **Spontaneous and synchronous co-cultures responses to zero-magnesium aCSF perfusion.** (**A**) Upper: Spontaneously differentiated iPSC-derived neurons were cultured with iPSC-derived astrocytes over 8 weeks. Lower: Synchronously differentiated iPSC-derived neurons were cultured with iPSC-derived astrocytes over 8 weeks. Cultures were loaded with 5 µM Fluo4-AM for fluorescent calcium imaging. (**B**) Time-lapse videos were recorded at 0.33 Hz. Representative figures show 10 example, random fluorescent traces related to yellow regions of interest in (A). (**C**) Representative Raster plot. Spikes were identified manually and plotted over time to identify synchronised events. (**D**) Responding cells were determined as those with ≥ one peak of calcium activity. (**E**) Calcium peaks per active cell. (**F**) Frequency of calcium events. (**G-H**) Quantitative measures of synchrony. (**G**) % synchronised cells relating to (C). (**H**) Average R value was calculated by performing a Pearson's correlation of the spike data generated for (C), then performing a Fishers-z transformation. Data in D-H is displayed as mean ± SEM from N=3 separate co-cultures. 2-way ANOVA with Tukey's multiple comparisons test. Scale bar: 5 μm. Solid black bar in B-C indicates addition of zero-magnesium

In addition, in each assessment parameter, one Spon CC experiment skewed the distribution of data, with values considerably higher than others presented. This datapoint was analysed individually and is presented in Figure 5.10.

The responses of co-cultures to 0 Mg was also assessed at 18 WIV (Appendix Figure A7). Neither co-culture method displayed significantly increased responses to 0 Mg in any parameter. Furthermore, the values for responding cells and peaks per cell in both CC were lower at W18 than W8. In each parameter, the response to 0 Mg did not significantly increase, except for burst frequency, which displayed a significant decrease in value in Spon CC (Control: -0.38 ± 0.13, 0 Mg: -0.99 ± 0.02; n=3, p= 0.005). In addition, the morphology of both Spon CC and Sync CC at W18 appeared astrocytic, with approximately 5-fold increased soma diameter than other cells in culture (Appendix Figure A8).

Despite a lack of consistent response in spontaneously differentiated cultures in Chapter 3, MEA analysis was attempted for co-culture models, as the literature showed various groups had achieved adherent and active iPSC-derived co-cultures on MEAs (Ishii et al., 2017; Kayama et al., 2018; Matsuda et al., 2018; Odawara et al., 2018; Tukker et al., 2016, 2018, 2019). In contrast to the issues presented in Chapter 3, widespread detachment of cultures from MEAs was not observed in either co-culture model. Despite this, no activity was recorded in any of 9 MEA chips at W4, W12 and W18 for Spon CC cultures. At 8 WIV, a single MEA displayed activity in Sync CC, shown in Figure 5.9. As with previous MEA findings, statistical analysis was not possible as only one MEA of 9 showed electrophysiological activity. Again, although successful in adherence and recording activity, only 33 of 64 electrodes recorded signals which satisfied the minimum action potential classification of -0.015 mV potential (Figure 5.9B,C). The number of bursts per electrode was 1, with these lasting 351 ms on average and comprised of 44.36 spikes (Figure 5.9D-F).

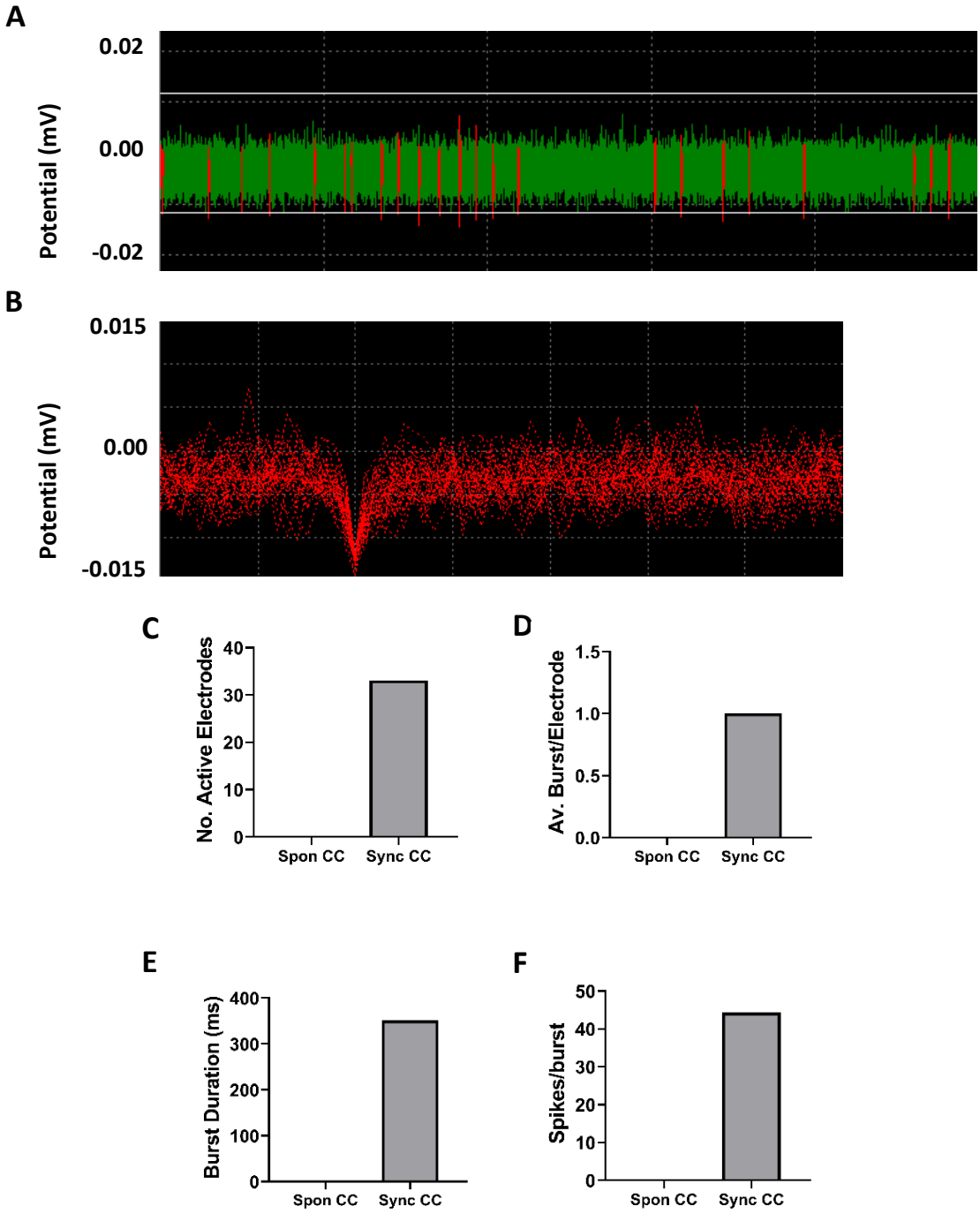

Figure 5.9: Multi-electrode array responses from spontaneous and synchronous co-culture models at 8 WIV. Co-cultures were differentiated on carbon MEA chips over 8 weeks and baseline activity assessed using MEA analysis. (A) Example snapshot of spiking activity, -0.015 mV was the minimum potential to denote action potential activity, whilst white lines above and below illustrate the standard deviation threshold. Vertical red lines which cross the threshold are detected signals. (B) Clustered spike analysis of all signals which reached the minimum potential for action potential classification, relating to the spikes from A. (C) Number of active electrodes where spikes were recorded. (D) Average number of bursts per active electrode. (E) Duration of bursts detected. (F) Average number of spikes/burst. N=1.

5.2.4 Individual datapoint from Spon CC

As presented above, the distribution of data for Spon CC was skewed by a single experiment (Figure 5.8). As seen with a previous isolated culture in Chapter 4, observation of this culture warranted an individual presentation of data alongside additional epileptiform analysis metrics (Hongo et al., 2015). This culture is represented as supplementary video file 'Video 5.1'.

Figure 5.10 shows the effects of 0 Mg perfusion on a Spon CC. Figure 5.10A shows that whilst many cells are visible in the field of view, cells are not overly dense and no aggregation can be seen. The example traces all show highly synchronised and increased activity when perfused with 0 Mg aCSF, each random trace displaying fluorescence amplitude increases of over 0.5ΔF/F compared with baseline (Figure 5.10B).

The percentage of responding cells increased over 4-fold in 0 Mg, from 24.39% to 100% of cells responding in the field of view (Figure 5.10D). Alongside this measurement of activity, peaks per cell increased 10-fold to 24.87 peaks per cell and the frequency of bursts was twice that of baseline (Control: 0.9 bursts per min, 0 Mg: 1.99 bursts per min) (Figure 5.10E,F).

The raster plot in Figure 5.10C very clearly shows the extent of synchronisation during perfusion with 0 Mg aCSF, beginning with asynchronous baseline activity. Indeed, the values of synchronised elevations indicate that 93.3% of cells in the field of view were synchronised in 0 Mg, compared to 0% at baseline (Figure 5.10G) and the R value of these active cells was 1 (Figure 5.10H).

Additional analyses of epileptiform activity revealed the amplitude and duration of bursts increased in 0 Mg, with the time between bursts of activity reduced *cf* baseline (Figure 5.10I-K).

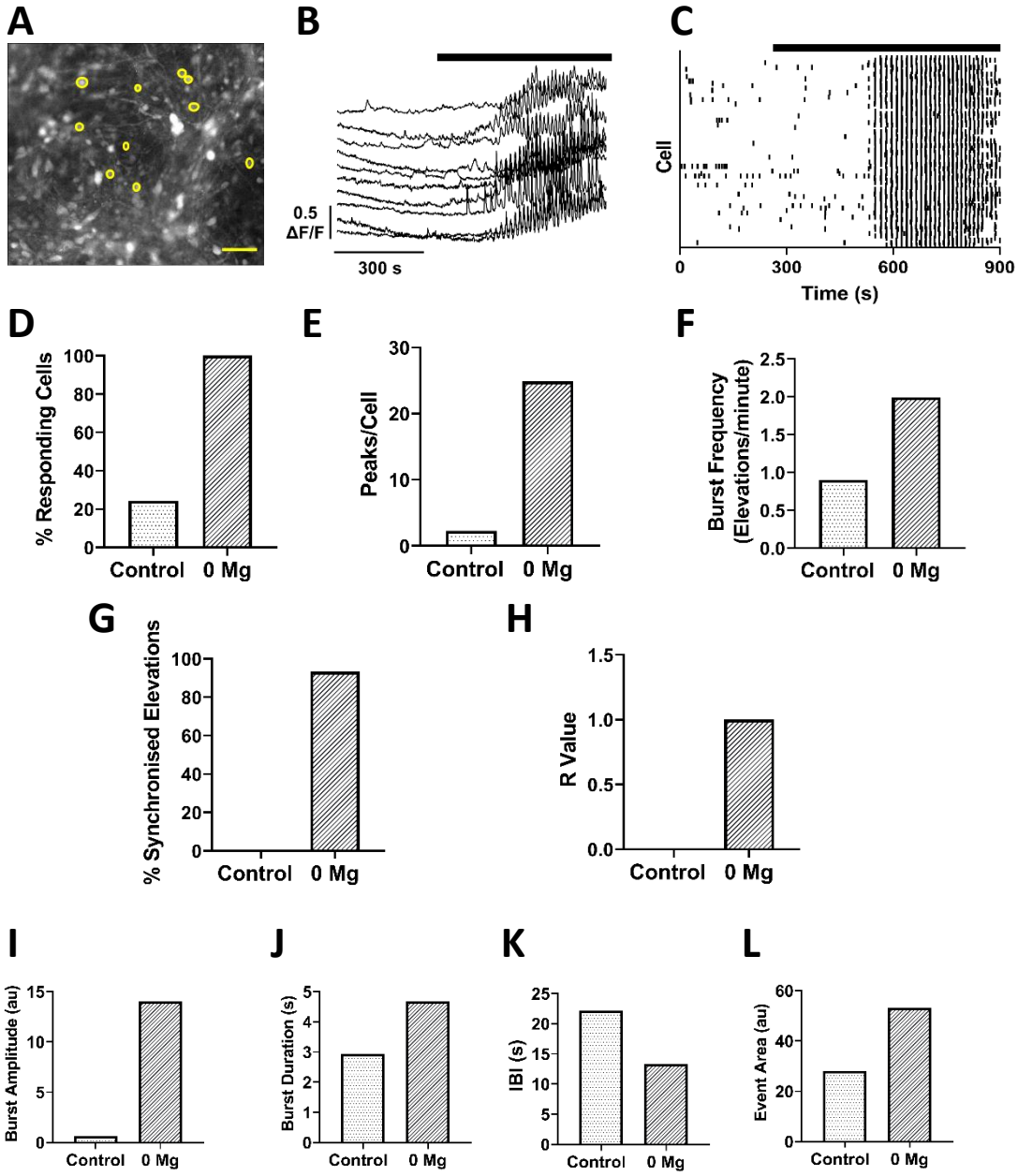

Figure 5.10 – Epileptiform response of spontaneous co-culture to zero-magnesium perfusion at 7 WIV. (**A**) Cultures were loaded with 5 µM Fluo4-AM for fluorescent calcium imaging. (**B**) Time-lapse videos were recorded at 1 Hz, with representative figures showing 10 example, random fluorescent traces related to yellow regions of interest in (A). (**C**) Representative Raster plot. Spikes were identified manually and plotted over time to identify synchronised events. (**D**) Responding cells were determined as those with ≥ one peak of calcium activity. (**E**) Calcium peaks per active cell. (**F**) Frequency of calcium events per minute. (**G-H**) Quantitative measures of synchrony. (**G**) % synchronised cells relating to (C). (**H**) Average R Value. (**I**) Amplitude of calcium events. (**J**) Duration of calcium events. (**K**) Time between calcium events. (**L**) Area calcium event occupied. N=1. Scale bar: 5 µm. Solid black bar in B-C indicates addition of zero-magnesium aCSF.

5.3 Discussion

As mentioned in 5.1, various methods exist for the co-culturing of neurons and astrocytes and this chapter sought to identify a standard method for producing co-cultures with this particular cellular system. It is important to note that there is a lack of literature agreement in terms of successful protocols for particular cell lines, so standardisation in human iPSC-derived models can be particularly difficult to achieve.

Monocultures do not display epileptiform activity

Firstly, individual cultures of the components which comprise mature co-culture systems were attempted (Chapter 5.2.1). As described in Chapters 3 and 4, spontaneous differentiation of NPCs generates co-cultures of both neurons and astrocytes over 8 WIV. However, overgrowth and extensive aggregation of cells was observed throughout spontaneous differentiation, alongside considerably more S100β^{+} astrocytes present over time (Appendix Figure A2, Chapter 3). For this reason, to generate neuronal monocultures, DAPT-synchronisation was utilised to force progenitors to exit the cell cycle simultaneously and differentiate solely into neurons. However, there is great variation in the application of DAPT for the purposes of neuronal synchronisation (Jun Rhee et al., 2019; Kuijlaars et al, 2016). As such, the densities of cells and concentration of DAPT used was carefully considered, to determine the most suitable conditions to generate pure neurons using this system.

Whilst the percentage of proliferating cells were lowest at 6 days *in vitro* (DIV), 7 DIV DAPT treatment was selected as the optimal method for use in co-cultures. In addition, the percentage of proliferating cells in the control condition at D7 indicated that by this point cells had begun to differentiate, as the value was lower than that of D6. As cells were already beginning their differentiation process, cells were treated with DAPT for the full duration of 7 days. Importantly, it has been observed in this cellular system and those within our laboratory (personal communications: Miss Marianne King, Mr James Crowe) that DAPT-synchronisation (and mitotic inhibition in general) does not target 100% of the cell population. As the emergence

of neurites was visible at D7, this suggests that DAPT had inhibited a significant proportion of the culture and that those cells had ceased proliferation and committed to a neural differentiation. Therefore, by treating the cells with DAPT as long as possible, it was assumed that this would target a higher percentage of total cells in culture, thereby producing the greatest response to Notch signalling inhibition.

It was tentatively assumed that as a result of NPCs exiting the progenitor pool and differentiating early in culture, maturity would occur more rapidly than seen for spontaneously differentiated cultures. However, the key morphological developmental timepoints were the same as seen in spontaneous differentiation (cortical rosettes present by 1 WIV, $Tuj1^+$ neurons present by 4 WIV), and the appearance of the neurons themselves was similar, with a low degree of fasciculation at 4 WIV. As expected, neuron-only cultures did not form astrocytes, due to the pool of progenitors being synchronised for terminal neuronal differentiation. Interestingly, low fasciculation of neurites continued throughout the following weeks, which was opposite to the aggregation observed in spontaneously differentiated cultures as they developed. It is likely, therefore, that the pool of progenitors at different stages of the cell cycle is likely the causative factor in fasciculation, aggregation and detachment observed previously (Chapter 3).

The proposed experimental protocol aimed to differentiate the neuronal monocultures over 8 weeks, to provide a secondary timepoint for comparison with the results of spontaneous differentiation in Chapters 3 and 4. This was achieved for astrocyte-only cultures, which were already 11 WIV at the time of initial seeding. The cells were GFAP and $S100\beta^+$ with characteristic astrocyte morphology by 4 WIV (personal communication; Marianne King, James Crowe). In addition, ICC data indicates that the control cultures were exclusively comprised of respective neural subtypes, with neuronal cultures S100β negative and astrocyte cultures Tuj1 negative throughout (Figure 5.3). Due to time constraints, qPCR was not performed on monocultures,

however, these cells were tested within the laboratory and expressed appropriate neuronal (TUBB3) and astrocytic markers (GFAP, S100β, ALDH) (personal communication, Marianne King).

Whilst monocultures of astrocytes survived indefinitely, this did not occur for neuronal monocultures, as complete detachment and cell death was observed around 7 WIV in all repeats (Appendix Figure A6, n=3). This is likely due to the absence of astrocytes and the protective functions they impart, including the prevention of neuronal cell death following insults including excitotoxicity and oxidative stress (Dhandapani et al., 2003). Whilst SCT medium was used to culture the cells, this media contained trophic factors BDNF and GDNF, which are secreted by astrocytes (Toyomoto et al., 2005; Wu et al., 2008). These results suggest that despite the growth medium containing astrocytic factors such as GDNF, the physical presence of astrocytes may be necessary to maintain neuronal viability. Indeed, it has been shown that physical contact between neurons and astrocytes is necessary for extended culture periods and that lack of physical contact between these cell types results in poor neuronal viability over time (Odawara et al., 2014). As the release of neurotrophic factors from astrocytes exerts protective effects on neurons in a paracrine fashion (Liu et al., 2017), the results in this chapter support those previously reported, i.e. that physical contact and paracrine signalling is necessary for neuronal viability, rather than solely the presence of growth factors.

From a morphological perspective, the emergence of neuronal markers was not affected by the absence of astrocytes in culture. In terms of functionality, neuronal monocultures displayed lower baseline activity than that of spontaneously differentiated cultures and furthermore, no significant responses were observed following treatment with pro-ictogenic conditions. This finding is supported by Odawara et al., (2014), who concluded that the presence of astrocytes in culture (whether human or rodent) is necessary for functional maturation of neurons. This is also further supported by numerous studies, which reported that neuronal monocultures are

an inferior model system for functional activity to those in contact with astrocytes (Ishii et al., 2017; Kuijlaars et al., 2016).

It is established that astrocytes, whilst not electrically excitable cells, communicate via intracellular calcium release and show both spontaneous and synchronous calcium-mediated activity (Carmignoto & Haydon, 2012; Parri & Crunelli, 2003; Pirttimaki et al., 2017; Volterra et al., 2014). In addition, no significant response was observed to any pro-ictogenic condition in astrocyte monocultures. These cultures also lacked synchronous activity. Interestingly, baseline activity of responding astrocytes was higher than that of neuronal monocultures, however this did not attain statistical significance. These results confirm the requirement of co-culture methods for long-term culture (Odawara et al., 2016a)

To the author's knowledge, this is the first study that has assessed the ability of monocultures of human iPSC-derived astrocytes to generate seizure-like activity *in vitro*. The data in this chapter confirms that separate cultures of neurons and astrocytes are much less robust models than those derived from spontaneous differentiation and fundamentally, they are an inappropriate model for seizure-liability testing.

Co-culturing neurons and astrocytes can produce epileptiform activity

Having established that monocultures are unsuitable models, initial co-culture models were attempted using methods reported in the literature, to assess whether this model system can be induced to generate seizure-like activity (Table 5.1). In comparison to monocultures, co-culturing of human iPSC-derived neurons and astrocytes produces viable, adherent cultures over time, as previously reported (Kayama et al., 2018; Kuijlaars et al., 2016; Matsuda et al., 2018; Odawara et al., 2016b; Tukker et al., 2016) and importantly, they possess the capability of epileptiform responses (Ishii et al., 2017; Odawara et al., 2018; Tukker et al., 2018, 2019).

The co-culture methods employed in this chapter were based on those previously described (Ishii et al., 2017; Matsuda et al., 2018), which assessed seizure-liability of co-cultures, wherein

both cell types were seeded simultaneously. Neither spontaneous or synchronised co-cultures showed significant responses to 0 Mg aCSF perfusion at timepoints tested. However, one spontaneous co-culture displayed a hypersynchronous and hyperexcitable response to 0 Mg. As with spontaneous differentiation in Chapter 4, the epileptiform response was an isolated non-repeatable experiment. As previously discussed, the high heterogeneity of response seen in spontaneously differentiating cultures could provide an explanation for this culture type being the responsive model out of the two tested.

Astrocytic overgrowth in long-term co-cultures

Calcium imaging results at W18 demonstrated very large cells, with typical astrocytic morphologies. Several video snapshots from each co-culture method displayed what appeared to be astrocytes throughout the entire culture (Appendix Figure A8). Whilst it is not possible to determine the cell type retrospectively, the low control calcium-mediated activity in these particular examples, coupled with visual identification of many cells with astrocytic appearance is suggestive of a large prepondrance of astrocytes observed in these cultures over time. This is despite the initial seeding ratio of neurons to astrocytes being in favour of neurons. As such, there exists the possibility that the pool of progenitors could be influenced by the higher initial number of astrocytes present from Day 1 with co-culture models, thus influencing the progenitor cell fate. Indeed, the fate of NPCs has been shown to be influenced by cytokine release from astrocytes (Gonzalez-Perez et al., 2012; Wang et al., 2011).

To further compare the co-culture methods, MEA recordings were attempted, as the cultures appeared considerably more adherent on MEAs than previously observed with spontaneous cultures (Figure 5.9). This could be due to astrocytes preferentially adhering to the culture surface as opposed to neurons. Indeed, studies using primary rodent models typically seed neurons on top of a layer of matured astrocytes to promote survival and adherence (Lange et al., 2012). Despite the adherence of the cultures, only one MEA recording displayed measurable spiking activity. The absence of activity could be explained by multiple reasons: firstly, astrocytes

themselves would not be detected by MEAs as they do not fire action potentials and secondly, even if neurons were present, by seeding simultaneously, there was an equal likelihood of astrocytes adhering on the recording electrodes, hence blocking signals from firing neurons. Indeed, when considering the development of astrocytes over time (Chapter 3), at earlier timepoints when MEA activity was successfully recorded in a synchronised co-culture, the astrocytes would not have overtaken neuronal proliferation to the same extent as they would have at 18 WIV. The increased astrocyte densities at 18 WIV compared to 8 WIV could explain the absence of detectable electrical activity over time.

Astrocyte proliferation in co-cultures

In collaboration with James Crowe (Parri Group, Aston University), it was shown that synchronous co-culture methods produced more active cells by 10 WIV when neuronal cells were seeded **prior** to astrocytes (Kayama et al,, 2018; Matsuda et al., 2018; Odawara et al., 2018) In this chapter, synchronised neurons and astrocytes were simultaneously seeded to generate co-cultures, as literature assessing seizure-liability of iPSC-derived co-cultures used this approach (Ishii et al., 2017; Kuijlaars et al., 2016; Tukker et al., 2016, 2019). Moreover, the astrocytes used in the co-culture tested by James Crowe were more matured than those in previous studies (Table 5.1). This approach was based on the evidence that mature astrocytes better support neuronal maturation (Hedegaard, 2019). As the differentiation process is very time-consuming, the use of matured astrocytes to hasten neuronal maturation is beneficial, both in terms of time and cost.

As seen in Chapter 3, astrocytic overgrowth was observed in each co-culture method in this chapter, and methods attempted by other members of the group (personal communication, James Crowe). The conclusions drawn from this chapter regarding the overgrowth of NPCs and astrocytes suggest that further refinement of the protocol was required. As such, the co-culture method selected for the final experimental chapter was based on the co-culture of

synchronously differentiated neurons and matured astrocytes, with careful consideration of the astrocytic component.

Chapter 6

6: INDUCTION OF EPILEPTIFORM ACTIVITY IN CO-CULTURES OF IPSC-DERIVED SYNCHRONISED NEURONS AND ASTROCYTES

6.1 Introduction

Results presented in Chapter 5, demonstrated that an increase in initial cell seeding density of NPCs and co-culturing with astrocytes was required to generate consistently functional cultures. Furthermore, the proliferative potential of NPCs and astrocytes was highlighted and suggested the need for further refinement of culture conditions to manage astrocytic overgrowth, especially as uncommitted cells can be influenced by the cell types in their surroundings (Gonzalez-Perez et al., 2012; Wang et al., 2011). Overgrowth of astrocytes in culture was observed for spontaneous differentiation (Chapter 3/4) and synchronous/spontaneous co-culture protocols (Chapter 5) and as such, methods to inhibit the proliferation of astrocytes were a focus of this chapter.

Cytosine arabinoside (AraC) has been previously used to control cellular proliferation of both neuronal and non-neuronal iPSC-derived and other human cells (Table 6.1). AraC incorporates into DNA, forming cleavage complexes and inhibiting replication. The formation of cleavage complexes results in DNA fragmentation and furthermore, AraC inhibits DNA polymerase, further decreasing DNA replication and repair of fragmentation (Sampath et al., 2006). AraC-induced mitotic inhibition has been found to be toxic to post-mitotic neurons (Martin et al., 1990). Hence, whilst AraC treatment would be unnecessarily toxic towards neurons, it was likely to be more effective than Notch signalling inhibition in potentially containing the growth of the highly proliferative astrocytes, although DAPT has also been used to inhibit proliferation of glial populations (Ma et al., 2019; Nagao et al., 2007).

There is no standard protocol for the use of AraC to inhibit astrocyte proliferation (Table 6.1). In agreement, De Rus Jacquet (2019) also stated that effective AraC treatment should be optimised for each cell line.

Table 6.1: Overview of human iPSC-derived and human primary cell types inhibited with AraC from recent literature.

Human Cell Type Targeted	[AraC, µM]	Duration AraC (days)	Reference
NPCs – Neurons	5	2	(Cheng et al., 2017)
Induced neurons	2	>10	(Pak et al., 2018)
NPCs – Glia	4	1	(Schwartzentruber et al., 2017)
Schwann Cells – Fibroblasts	5-10	Undisclosed	(Clark et al., 2017)
NPCs – Glia	5-8	1	(de Rus Jacquet, 2019)
Foetal brain tissue - all dividing cells	10	10	(Jana et al., 2007)

6.1.1 Interneurons

The co-culturing of neurons and astrocytes has been widely reported in *in vitro* primary and iPSC-derived models (Chapter 1/5). Whilst many of these cultures consist of excitatory neurons and astrocytes, the inclusion of inhibitory neuronal populations was less common (Tukker et al., 2016, 2018, 2019). Interneurons are essential for forming a complete neural network and play an integral role in seizure activity (Magloire et al., 2019). Immunostaining results from spontaneous differentiation (Chapter 3-4) were GAD67- at all timepoints and no significant response to the GABA-antagonist picrotoxin was observed. However, significant levels of vGAT expression were observed – consistent with the notion that interneurons may indeed be present, but in low numbers (Gunhanlar et al., 2017; Kirwan et al., 2015).

As previously discussed, there are several protocols for the generation of interneurons from iPSC (Chapter 1.3.6). Initially, the work of Shi et al., (2012a) demonstrated the presence of ventrally and caudally expressed transcription factors associated with the development of

GABAergic interneurons (GIN), which was confirmed with immunostaining of GAD67 inhibitory synapses. This was demonstrated only in the presence of the 'Sonic Hedgehog' (SHH) agonist purmorphamine (Shi et al., 2012b). SHH is a morphogen, critical in development of distinct brain regions (Rash & Grove, 2007) and mediates differentiation and maintenance of ventral GIN during neurogenesis (Xu et al., 2005, 2010).

Liu et al., (2013) then published a protocol for the direct differentiation of pure (~90%) populations of GIN, again using purmorphamine. They also found that early treatment with purmorphamine increased the efficiency of GIN induction (Liu et al., 2013). Subsequent protocols also used agonism of SHH signalling for GIN generation (Maroof et al., 2013; Nicholas et al., 2013; Tyson et al., 2015).

Despite several protocols for the generation of GIN, at the time of writing, the author was unaware of any group generating their own interneurons from iPSC/NPC to co-culture and for seizure-liability testing. Moreover, as several commercially available products have become available including excitatory and inhibitory neurons, at ratios representative of the *in vivo* environment, the need for generating components individually and 'assembling' the cultures, was apparently reduced. Most importantly, the addition of an inhibitory neuronal component to the system generates a heterogenous culture, wherein all main neural subtypes are present, thus generating a culture reflective of the intact cerebral cortex (Azzarelli et al., 2015). The generation of such a platform provides the potential for assessing seizure-liability of existing and novel compounds and also delivers a system for assessing existing and novel anti-epileptic agents to subdue such activity.

6.1.2 Sodium Valproate as an anti-epileptic

As outlined in Chapter 1, many anti-epileptic compounds exist with diverse mechanisms of action (Shih et al., 2013). Of these, one of the most widely prescribed anti-epileptic treatments is sodium valproate (VPA) (Chang et al., 2012). VPA is a preferential treatment in paediatric epilepsy, owing to its acceptable safety profile and broad mechanism of action (Ghodke-Puranik et al., 2013).

6.1.2.1 Effect of VPA on GABA and Neurotransmission

As discussed in Chapter 1, the synthesis and degradation of GABA is a multi-step process involving several enzymes. VPA has been shown to inhibit several enzymes involved in the degradation of GABA: GABA transaminase, succinic semialdehyde dehydrogenase and α-ketoglutarate dehydrogenase (Johannessen & Johannessen, 2003) and enhancement of those synthesising GABA such as GABA decarboxylase (Löscher, 1981). As a result, the levels of GABA in the brain increase and inhibition of activity is promoted.

6.1.2.2 Effect of VPA on Ion Channels

The blockade of ion channels prevents the hyperexcitability of neurons observed in seizures. Valproate is reported to block sodium channels (Englund et al., 2011; Rogawski et al., 2016), reducing the inward flow of Na^+ and preventing repetitive action potential firing. More recent evidence suggests it can also play a role in inhibiting low-threshold T-type calcium channels, inhibiting Ca^{2+} entry into the cell and hence, reducing neurotransmission (Broicher et al., 2007; Löscher, 2002). There is also evidence for VPA acting on potassium channels to reduce K^+ conductance and excitability, albeit only at higher drug concentrations than those used therapeutically (Franceschetti et al., 1986; Johannessen & Johannessen, 2003).

6.1.2.3 Effect of VPA on Histone deacetylases (HDACs)

In order for exceptionally long sequences of eukaryotic DNA to fit into the relatively small nucleus, the DNA structure has to be tightly packaged around histone proteins to form a structure called the nucleosome – the fundamental subunit of chromatin. Histone deacetylases

are a class of enzymes responsible for the regulation of gene expression via hydrolysis of acetylated lysines in the histone proteins which surround DNA. Histone modification is considered a major epigenetic mechanism for remodelling the chromatin structure – leading to alterations in gene expression, without direct modification to the genetic sequence (Xu et al., 2007). VPA has been identified as a class I HDAC inhibitor (Göttlicher et al., 2001) and with particular relevance to seizurogenesis, upregulation of BDNF and GDNF (which exerts neuroprotective effects) has been observed with VPA addition (Chen et al., 2006).

6.1.2.4 Effect of VPA on Phosphatidylinositol (3,4,5)-trisphosphate (PIP3)

PIP3 is formed as a result of tyrosine kinase signalling and PIP3 kinase phosphorylation. PIP3 functions as a second messenger to activate AKT to induce cellular proliferation and apoptosis (Wolff et al., 2014). With respect to neurons, PIP3 regulates synaptic transmission (Chang et al., 2014) and the PIP3/AKT pathway is implicated in seizure generation and epilepsy (Schick et al., 2006; Zhang & Wong, 2012). Depletion of PIP3 occurs during seizure, and can generate a positive feedback loop, promoting further seizure-like activity (Chang et al, 2014). VPA has been shown to reverse depletion of PIP3 following seizure, exerting a therapeutic effect (Chang et al., 2014).

The exact mechanism of action of VPA is still unclear, although several hypotheses have been published on the possible multi-factorial pharmacodynamics of VPA. This, alongside its use as a frontline treatment and its previous use in iPSC-derived neuronal cultures (Darville et al., 2016) prompted its use to determine its effect on potential seizure-like activity in this Chapter.

The aims of this chapter are to:

1) **Identify the optimal concentration of cytosine arabinoside for synchronisation of astrocytes, via the MTT cytotoxicity assay and measurements of cellular proliferation**
2) **Assess the ability for co-cultures of synchronised neurons and astrocytes to display epileptiform responses to 4-aminopyridine, high potassium aCSF and zero-magnesium aCSF conditions using fluorescent calcium imaging**
3) **Perform provisional experiments to determine whether the inclusion of commercially available iPSC-derived interneurons influences the ability of co-cultures to respond to the above manipulations, alongside picrotoxin**

6.2 Results

6.2.1 Synchronisation and Characterisation of co-cultures

The conclusions drawn from Chapter 5 indicated that astrocytic overgrowth exerted undesirable effects on the viability and function of neuronal co-cultures. Therefore, the first stage of this Chapter was to establish a suitable protocol for the mitotic inhibition of astrocytes. Cytosine arabinoside (AraC) was used for its ability to arrest growth of proliferating cells in iPSC-derived systems. Serial dilutions of AraC were tested for their effects on proliferation and cell viability. At each concentration tested, the percentage of $Ki67^+$ cells significantly decreased, with 10 µM AraC reducing proliferation furthest (Control: 32.26 ± 8.96%, 10 µM: 3.50 ± 1.42%, n=4, p= 0.0056, Figure 6.1). AraC did not significantly affect cell viability at any concentration tested (Figure 6.1B).

Following the establishment of protocols for the synchronisation of NPCs (Chapter 5) and astrocytes (Figure 6.1), these cells were co-cultured and differentiated over 10 weeks. Their morphology was characterised by ICC (Figure 6.2). $Tuj1^+$ neurons were observed in all cultures, with a low degree of fasciculation and aggregation compared with spontaneous differentiation (Figure 3.3/4, n=12 cs). Astrocytes in co-cultures displayed typical morphology and were $S100\beta^+$ throughout (n=12 cs). Importantly, the ratios of cell types appeared consistent throughout differentiation.

qPCR was used to assess the expression of neuronal-associated genes with cultures (Appendix Figure A9). There was no significant difference in the expression of neuronal TUBB3 and vGAT, when compared to control values of NPCs at Day 0. Expression of astrocytic S100β was significantly increased *cf* control (Control: 0.0004 ± 0.05; S100β: 1.71 ± 0.29, n=3, p= 0.046).

In addition, the baseline activity of this co-culture method was compared to previous models throughout this thesis. In every instance, this co-culture protocol elicited significantly increased values in percentage of active cells *cf* every other protocol (Appendix Figure A12).

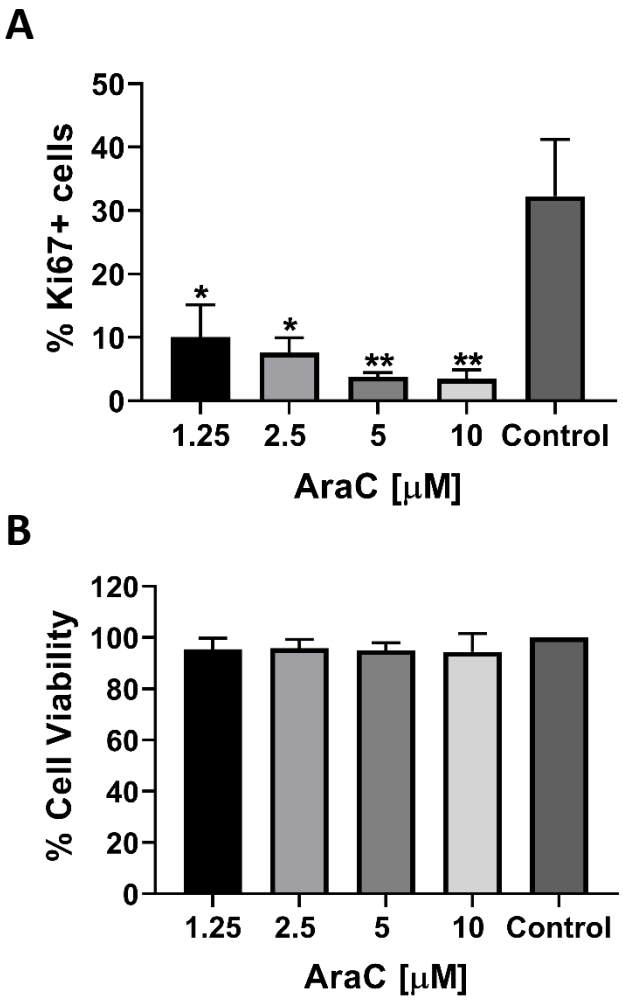

Figure 6.1: Mitotic inhibition of human astrocytes using AraC. Human iPSC-derived astrocytes were plated and incubated for 24 hours, before being treated with 1.25, 2.5, 5 and 10 µM cytosine arabinoside (AraC) for 24 hours. (**A**) Immunocytochemistry was performed to assess for the presence of proliferating astrocytes, using the cell proliferation marker Ki67. (**B**) MTT assay for cell survival to assess the effects of mitotic inhibition on cell survival. N=4. *p< 0.05, **p< 0.01, 1-way ANOVA with Dunnett's multiple comparisons.

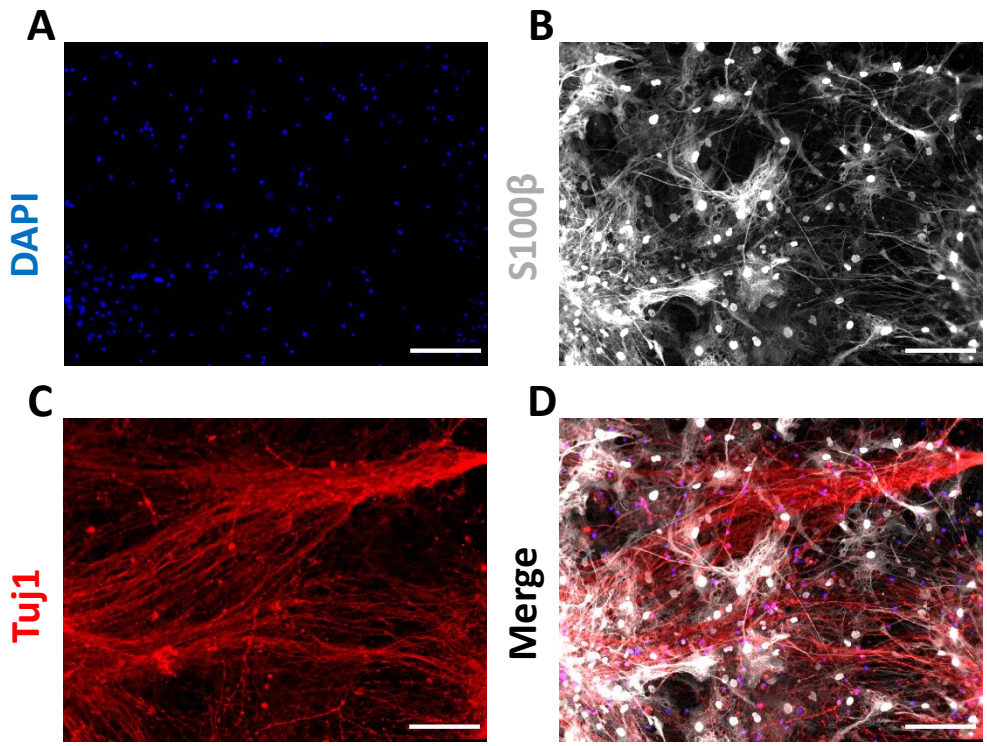

Figure 6.2: Synchronously differentiated co-cultures form morphologically matured astrocytes and neurons. iPSC-derived NPCs were differentiated in SCT media with 10 µM DAPT and co-cultured with AraC-synchronised astrocytes over 10 weeks. Cells were fixed and immunocytochemistry was performed to assess the presence of neural markers. (**A**) Nuclei stained with DAPI (Blue, excitation λ 345 nm, emission λ 455 nm). (**B**) S100β astrocytic staining (Grey, excitation λ 495 nm, emission λ 519 nm). (**C**) Tuj1 neuronal staining (Red, excitation λ 588 nm, emission λ 649 nm). (**D**) Merged image of A,B,C. N=24. Scale bar: 100 µm. 20x magnification.

6.2.2 Network connectivity

A prerequisite of *in vivo* neural activity is the formation of a synaptically-matured neural network (Hill et al., 2012) and indeed, this is especially important for synchronising and eliciting bursts of action potentials in epileptiform activity (Abarbanel, et al., 1996). To this end, the formation of a network using this co-culture method was assessed via the use of 0 Mg and $>K^+$ aCSF. The rapid propagation of calcium activity was observed in both conditions, in every coverslip tested (Figure 6.3/4, n=24). The representative examples presented clearly indicate an origin wherein the calcium signals propagated throughout the culture, stimulating distant cells in both conditions (Supplementary Video files 6.1/6.2).

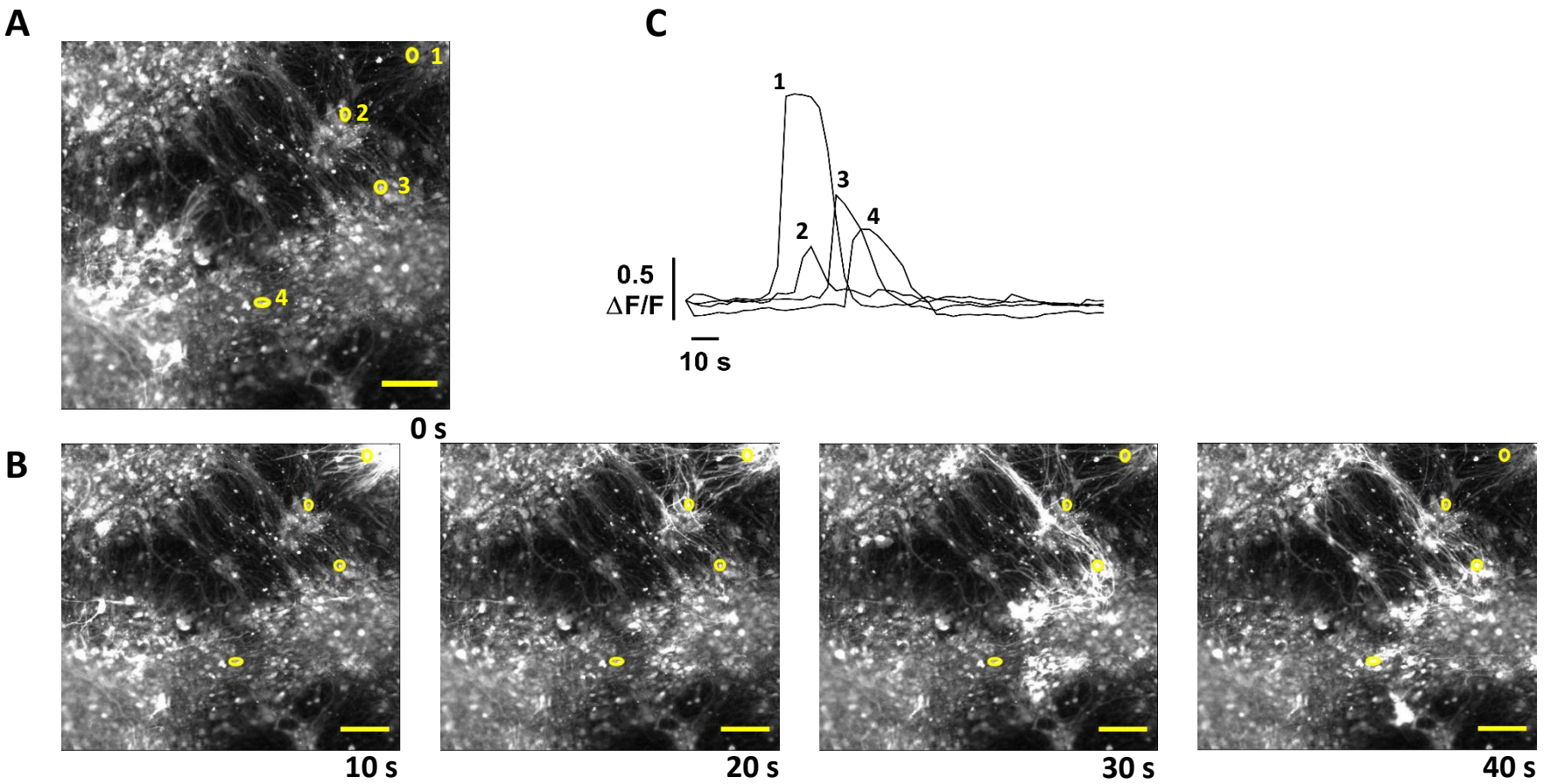

Figure 6.3: Representative example of rapid propagation of calcium waves throughout network during zero-magnesium aCSF perfusion. (**A**) Large image shows fluorescently stained neural cultures, with 4 example somas labelled numerically in yellow at baseline (no calcium activity). (**B**) Calcium waves propagate in sequence from cell 1 through cell 4, shown in 10 second intervals. (**C**) Fluorescence over time traces from each circled cell. Scale bar: 100 µm.

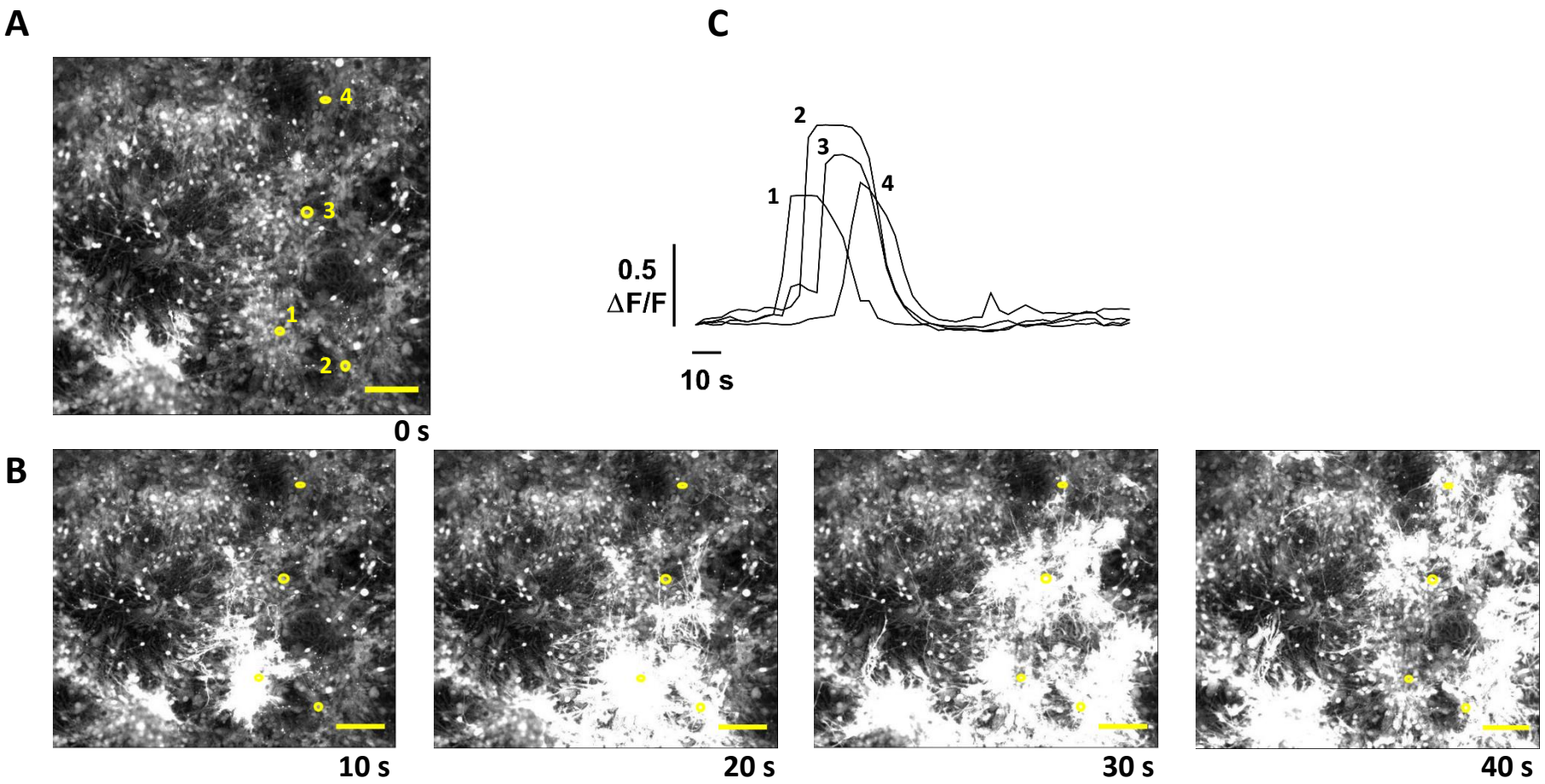

Figure 6.4: Representative example of rapid propagation of calcium waves throughout network during high potassium aCSF perfusion. (**A**) Large image shows fluorescently stained neural cultures, with 4 example somas labelled numerically in yellow at baseline (no calcium activity). (**B**) Calcium waves propagate in sequence from cell 1 through cell 4, shown in 10 second intervals. (**C**) Fluorescence over time traces from each circled cell. Scale bar: 100 µm.

6.2.3 Induction of epileptiform activity in co-cultures

Having determined that spontaneously differentiated cultures and spontaneous co-cultures can produce epileptiform responses (albeit, not reproducibly) to $>K^+$ and 0 Mg aCSF perfusion respectively, these ionic manipulations were selected as the basis for epileptiform experiments. Previously attempted spontaneous and co-culture methods did not elicit epileptiform responses to 4-AP (Chapter 4,5). Furthermore, due to the absence of inhibitory cells, PTX was not tested. In this Chapter, ionic manipulation, followed by the addition of 4-AP was used. This combined method has previously been reported for epileptiform studies (Hongo et al., 2015; Ross et al., 1998, 2000).

The addition of 0 Mg appeared to cause oscillatory activity in some cells within cultures, with large calcium elevations occurring in regular intervals (representative Figure 6.5B). Moreover, perfusion of 0 Mg generated a significant increase in the percentage of active cells (Control: 47.35 ± 9.38%, 0 Mg: 78.25 ± 6.13%, n=12 cs, p= 0.0085, Figure 6.5D), with a further slightly increased response when both 0 Mg aCSF and 100 µM 4-AP were added, compared to control (79.74 ± 3.89%, p= 0.0057, Figure 6.5D). The perfusion of 0 Mg aCSF with 100 µM 4-AP also significantly increased the number of peaks per cell (Control: 1.81 ± 0.27, 0 Mg-4-AP: 2.90 ± 0.25, n=12 cs, p= 0.0072, Figure 6.5E) and R value (Control: 0.24 ± 0.11, 0 Mg-4-AP: 0.59 ± 0.09, n=12 cs, p= 0.0461, Figure 6.5H) However, burst frequency and percentage of synchronised elevations did not increase significantly (Figures 6.5F/G).

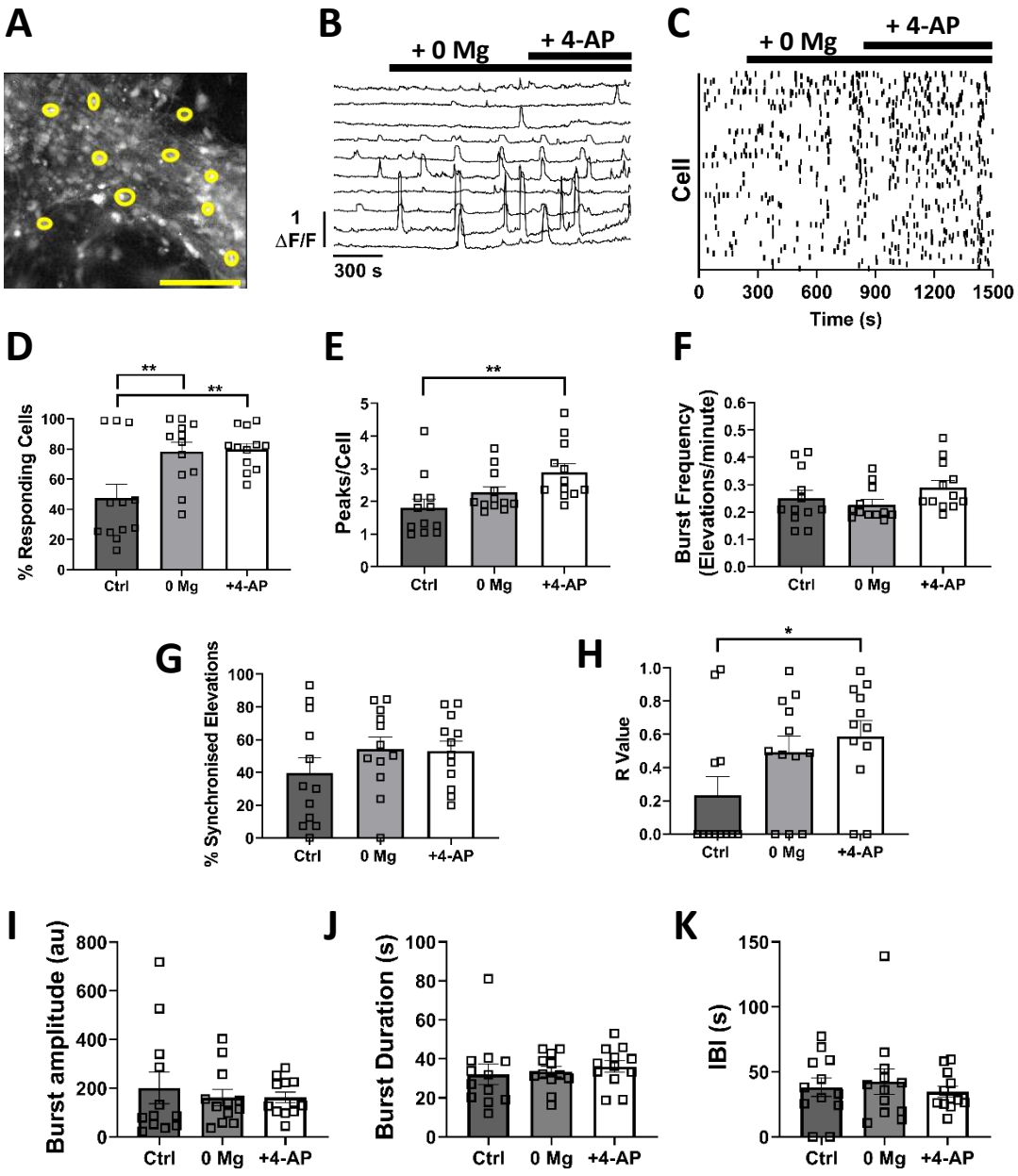

Figure 6.5: Fluorescent calcium imaging responses of co-cultures of human iPSC-derived neurons and astrocytes to zero-magnesium aCSF and 4-aminopyridine perfusion. Neurons and astrocytes were synchronised and cultured independently, before co-culturing at 13 DIV, followed by 10 weeks differentiation. (**A**) Co-cultures were loaded with 5 µM Fluo4-AM for imaging. (**B**) Time-lapse videos were recorded at 0.33 Hz, with representative figures showing 10 example, random fluorescent traces related to yellow regions of interest in (A). (**C**) Representative Raster plot. Spikes were identified manually and plotted over time to identify synchronised events. (**D**) Responding cells were determined as those with ≥ one peak of calcium activity. (**E**) Calcium peaks per active cell. (**F**) Frequency of calcium events per minute. (**G-H**) Quantitative measures of synchrony. (**G**) % synchronised cells relating to (C). (**H**) Average R value. (**I**) Amplitude of calcium events. (**J**) Duration of calcium events. (**K**) Time between calcium events. N=3.*p< 0.05, **p< 0.01, ANOVA with Tukey's multiple comparisons test. Scale bar: 5 µm. Solid black bars in B-C indicate addition of 0 Mg^{2+} aCSF and 100 µM 4-AP.

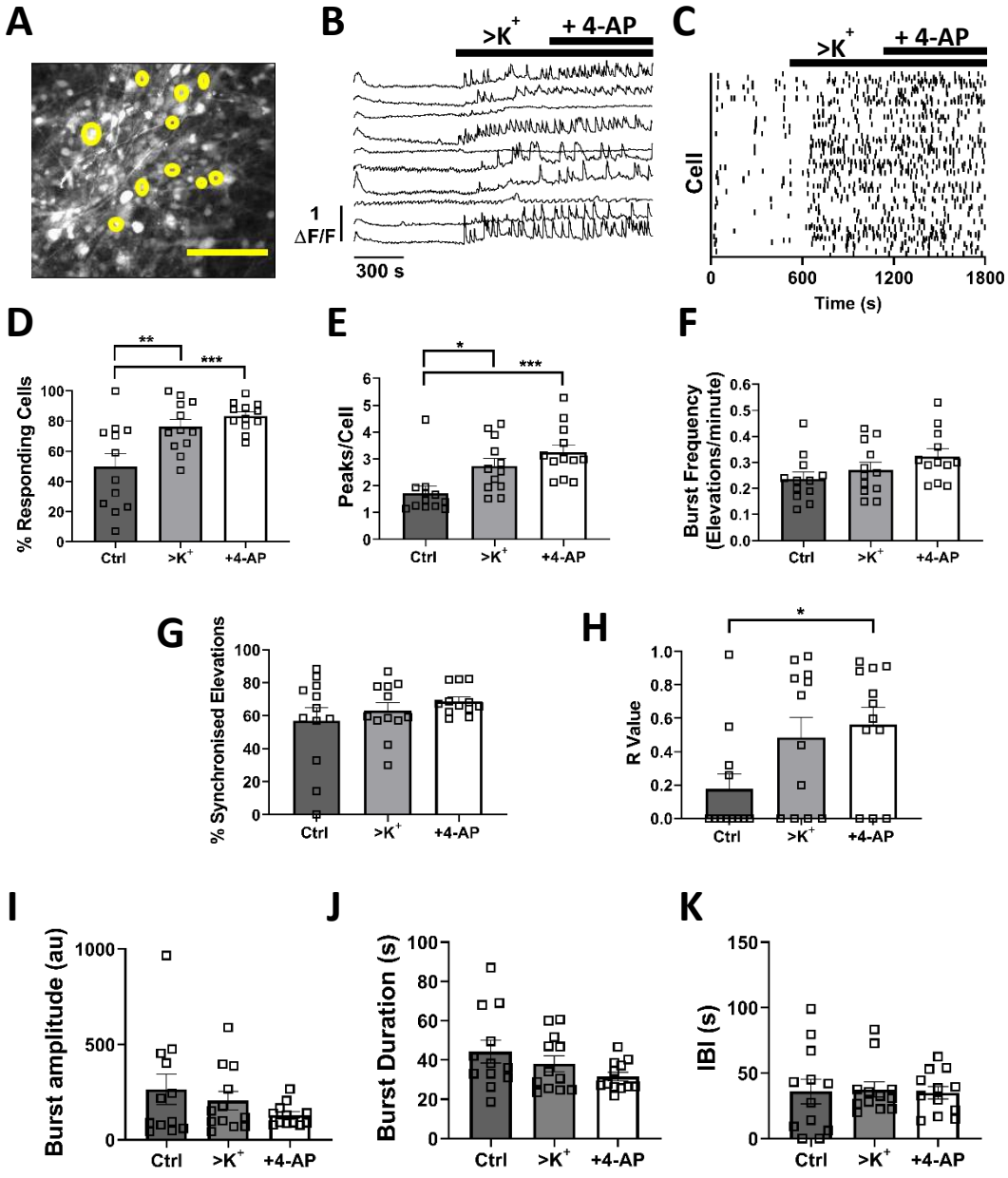

Figure 6.6: Fluorescent calcium imaging responses of co-cultures of human iPSC-derived neurons and astrocytes to elevated potassium aCSF and 4-aminopyridine perfusion. Neurons and astrocytes were synchronised and cultured independently, before co-culturing at 13 DIV, followed by 10 weeks differentiation. (**A**) Co-cultures were loaded with 5 µM Fluo4-AM for imaging. (**B**) Time-lapse videos were recorded at 0.33 Hz, with representative figures showing 10 example, random fluorescent traces related to yellow regions of interest in (A). (**C**) Representative Raster plot. Spikes were identified manually and plotted over time to identify synchronised events. (**D**) Responding cells were determined as those with ≥ one peak of calcium activity. (**E**) Calcium peaks per active cell. (**F**) Frequency of calcium events per minute. (**G-H**) Quantitative measures of synchrony. (**G**) % synchronised cells relating to (C). (**H**) Average R value. (**I**) Amplitude of calcium events. (**J**) Duration of calcium events. (**K**) Time between calcium events. N=3. *p< 0.05, **p< 0.01, ***p< 0.001, ANOVA with Tukey's multiple comparisons test. Scale bar: 5 µm. Solid black bars in B-C indicate addition of $>K^+$ aCSF and 100 µM 4-AP.

The increased cellular and network activity observed from the recordings satisfied the requirements for expanding the range of analyses that could be performed. Burst analysis metrics were all non-significant, however, the duration of a burst and the inter-burst-interval values indicated that perfusion of both manipulations did increase bursting activity to a greater extent that 0 Mg alone (Figures 6.5J-K).

Representative traces from perfusion with high potassium aCSF did not appear to generate oscillatory activity as was seen with perfusion of 0 Mg (Figure 6.6.B). Cellular activity increased in 8/10 traces to produce fluorescence amplitude responses of >0.5ΔF/F and increased spiking activity was also observed (representative, Figure 6.6C). $>K^+$ aCSF significantly increased the percentage of active cells (Control: 49.95 ± 8.35%, $>K^+$: 76.36 ± 4.83%, n=12 cs, p= 0.0077, Figure 6.6.D) and peaks per cell (Control: 1.72 ± 0.26, $>K^+$: 2.74 ± 0.29, n=12 cs, p= 0.0343, Figure 6.6.E). The addition of 100 µM 4-AP elicited significant responses in percentage of responding cells ($>K^+$-4-AP: 83.31 ± 2.73%, n=12 cs, p= 0.0008), peaks per cell ($>K^+$-4-AP: 3.24 ± 0.28, n=12 cs, p= 0.0012) and R value ($>K^+$-4-AP: 0.56 ± 0.11, n=12 cs, p= 0.039). However, there was no significant increase in bursting.

6.2.4 Astrocytic or neuronal calcium activity?

As the co-cultures contained two principal cell types which can both display calcium signalling, further experiments were performed to determine which cell type was responsible for the activity observed. Tetrodotoxin (TTX) was applied to several cultures and its effects are shown in Figure 6.7. TTX significantly reduced the percentage of active cells in all manipulations *cf* baseline control activity (Table 6.2/Figure 6.6B). The peaks per cell values were significantly reduced also (Table 6.6/Figure 6.6C). However, the frequency of bursts did not significantly decrease. Indeed, no significant effects of TTX on burst activity, bursting amplitude and inter-burst-interval (IBI) were observed (Appendix Figure A10).

Table 6.2: Overview of statistical results from one-way ANOVA comparing the effects of TTX addition on percentage of responding cells. ns = not significant. N=7 coverslips from 3 differentiations, Tukey's.

Condition	Mean ± Std. Error	P value
0 Mg Control	44.22 ± 14.09	Ns
0 Mg	82.29 ± 8.18	0.015
0 Mg-4-AP	77.75 ± 6.03	0.033
0 Mg-4-AP-TTX	39.62 ± 5.80	-
>K^+ Control	59.60 ± 7.33	Ns
>K^+	82.11 ± 4.67	0.028
>K^+-4-AP	80.22 ± 3.78	0.034
>K^+-4-AP-TTX	56.09 ± 8.43	-

Table 6.3: Overview of statistical results from one-way ANOVA comparing the effects of TTX addition on peaks per cell. ns = not significant. N=7 coverslips from 3 differentiations.

Condition	Mean ± Std. Error	P value	Post hoc Test
0 Mg Control	1.67 ± 0.26	ns	Dunn's
0 Mg	2.29 ± 0.21	ns	
0 Mg-4-AP	2.86 ± 0.35	0.0049	
0 Mg-4-AP-TTX	1.38 ± 0.11	-	
>K^+ Control	1.57 ± 0.13	ns	Tukey's
>K^+	3.06 ± 0.31	0.0029	
>K^+-4-AP	3.45 ± 0.38	0.0002	
>K^+-4-AP-TTX	1.56 ± 0.16	-	

Alongside TTX studies, the addition of VPA was hypothesised to reduce levels of activity, whilst also giving an indication of the mechanism by which the cultures were eliciting this increased activity. VPA did not produce significant reductions in activity in any metric (Figure 6.8), despite a decrease in percentage of responding cells, peaks per cell and burst frequency, compared with experimental manipulations. Additionally, no significant effect of VPA on burst activity was observed, although a reduction in burst amplitude, increased IBI and decreased burst duration were all observed (Appendix Figure 11A).

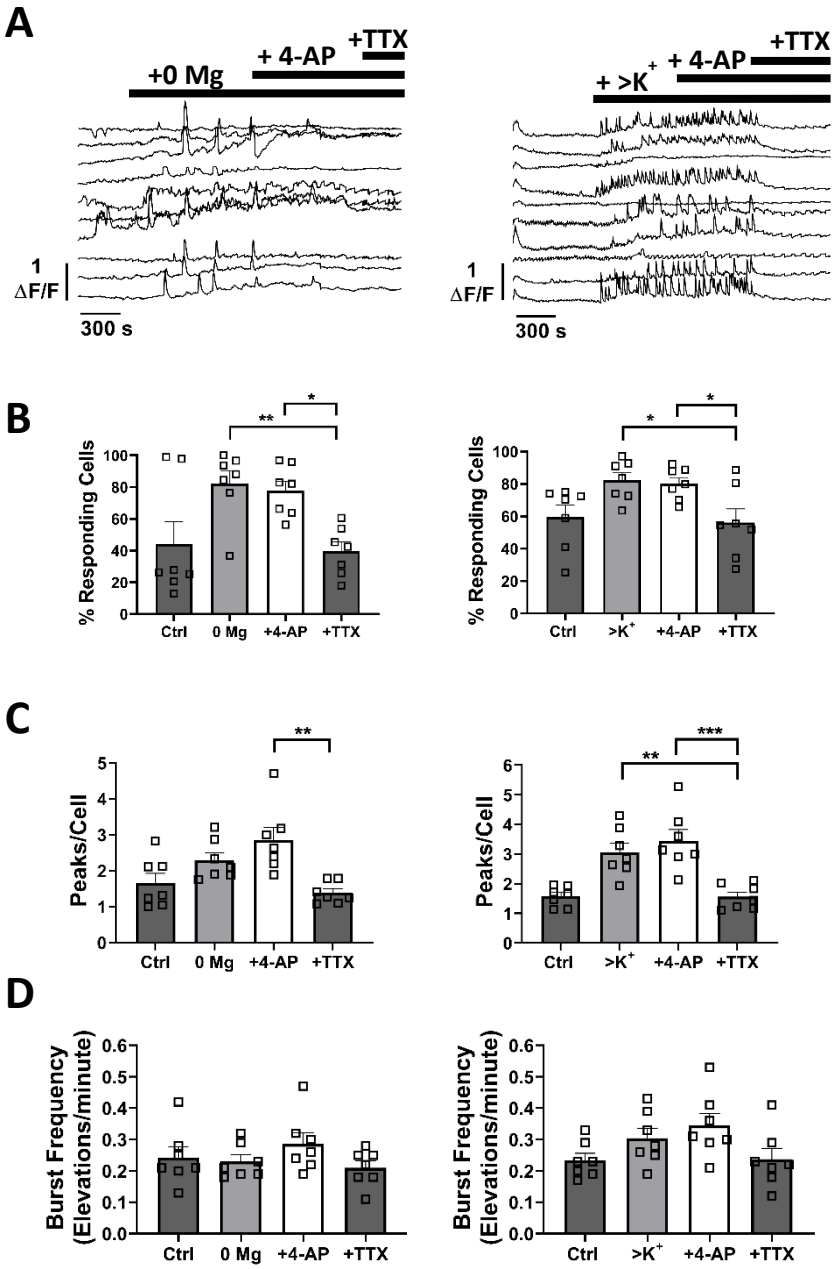

Figure 6.7: Effects of tetrodotoxin perfusion on fluorescent calcium activity of co-cultures of neurons and astrocytes exposed to different pro-ictogenic conditions. Human iPSC-derived neuronal and astrocytic co-cultures were cultured over 10 WIV and treated with various pro-ictogenic perfusions to elicit increased activity, followed by tetrodotoxin (TTX). (**A**) Time-lapse videos were recorded at 0.33 Hz, with representative figures showing 15 example, random fluorescent traces. (**B**) Responding cells were determined as those with ≥ one peak of calcium activity. (**C**) Calcium peaks per active cell. (**D**) Frequency of calcium events per minute. N=3. *p< 0.05, **p< 0.01, ***p< 0.001, ANOVA with Tukey's multiple comparisons test. Scale bar: 5 µm. Solid black bars in A indicate addition of zero magnesium/high potassium aCSF, 100 µM 4-AP and 1 µM TTX.

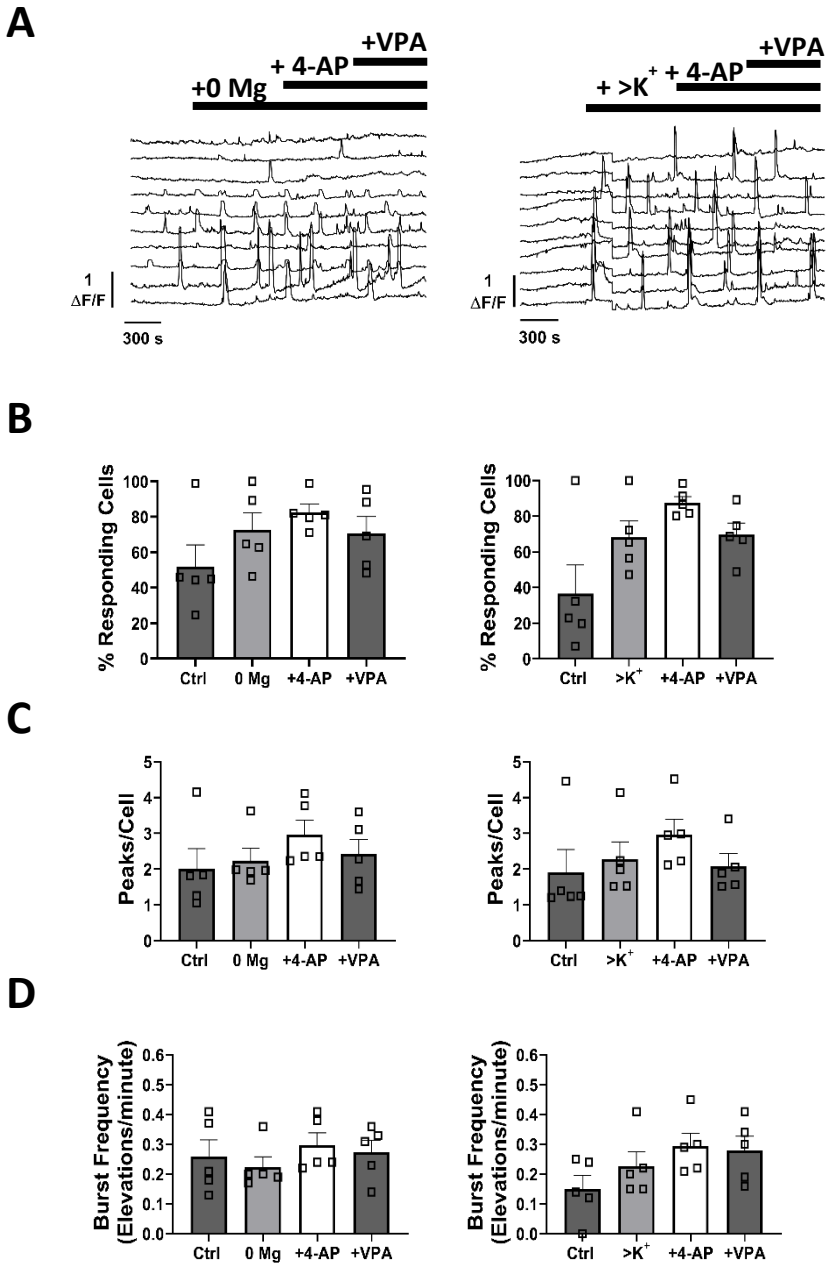

Figure 6.8: Sodium valproate perfusion does not reduce fluorescent calcium activity of co-cultures of neurons and astrocytes exposed to different pro-ictogenic conditions. Human iPSC-derived neuronal and astrocytic co-cultures were cultured over 10 WIV and treated with various pro-ictogenic perfusions to elicit increased activity, followed by valproate (VPA). (**A**) Time-lapse videos were recorded at 0.33 Hz, with representative figures showing 15 example, random fluorescent traces. (**B**) Responding cells were determined as those with ≥ one peak of calcium activity. (**C**) Calcium peaks per active cell. (**D**) Frequency of calcium events per minute. N=3. ANOVA with Tukey's multiple comparisons test. Scale bar: 5 µm. Solid black bars in A indicate addition of zero magnesium/high potassium aCSF, 100 µM 4-AP and 2 mM VPA.

6.2.5 Preliminary characterisation of co-cultures with interneurons

The final series of experiments in this thesis included the addition of human iPSC-derived interneurons to the established co-cultures described (Chapter 6.2). To ensure the survival and incorporation of interneurons into the network, ICC was performed at 10 WIV to assess for the presence of excitatory and inhibitory synapses following seeding of cells. Figure 6.9 shows synaptic puncta of both an excitatory and inhibitory nature (Figure 6.9) which was observed in all three repeats (n=3 coverslips, 1 biological differentiation).

6.2.6 Induction of epileptiform activity in interneuron co-cultures

As the inclusion of interneurons was a final series of experiments, there was unfortunately insufficient time and resources to perform the studies with enough repeats for statistical analysis and to optimise the culture system. As the target of PTX is often interneurons, the cultures were perfused with PTX to observe any effects. PTX appeared to increase the percentage of responding cells, peaks per cell, percentage of synchronised elevations and R value (Figure 6.10). Interestingly, the addition of VPA following PTX perfusion appeared to decrease all measures of activity and synchrony, whilst extending the interval between bursting.

Similar to experiments performed on co-cultures earlier in Section 6.2.3, ionic and pharmacological manipulation was used simultaneously on interneuron co-cultures. 0 Mg and 0 Mg-4-AP both increased every single parameter for activity and synchrony, whilst reducing the IBI (Figure 6.11). In addition, VPA had no effect on percentage of active cells, but did reduce the peaks per cell, bursting frequency and percentage of synchronised elevations.

Finally, perfusion with $>K^+$ and 4-AP also increased percentage of responding cells, peaks per cell and decreased the IBI (Figure 6.12). However, little change was observed for burst frequency, percentage of synchronised elevations or R value.

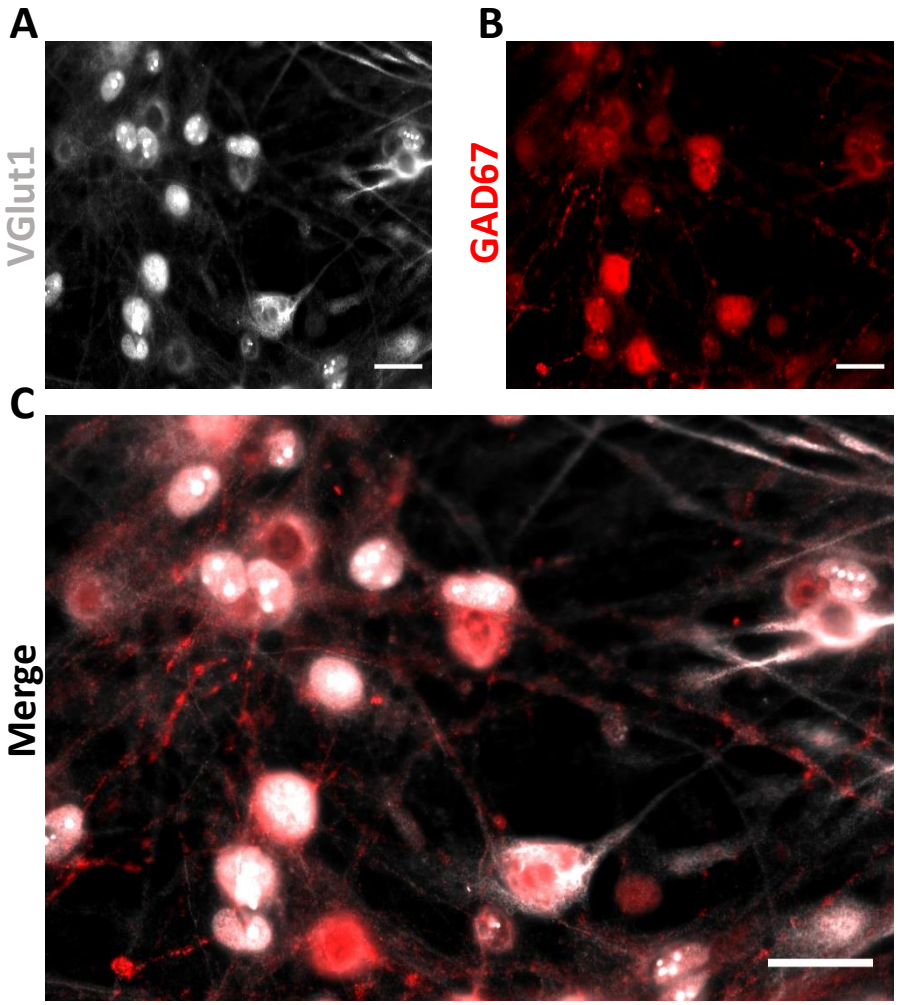

Figure 6.9: Interneuron co-cultures demonstrate the presence of inhibitory synapses. iPSC-derived neural precursors were differentiated in SCT media with 10 µM DAPT and cocultured with AraC-synchronised astrocytes and iPSC-derived interneurons over 10 weeks and immunocytochemistry performed to assess the presence of excitatory and inhibitory synapses. (**A**) Excitatory synapses stained with VGlut1 (Grey, excitation λ 495 nm, emission λ 519 nm). (**B**) Inhibitory synapses stained with GAD67 (Red, excitation λ 588 nm, emission λ 649 nm). (**C**) Merged image of A,B. N=1. Scale bar: 100 µm. 63x magnification.

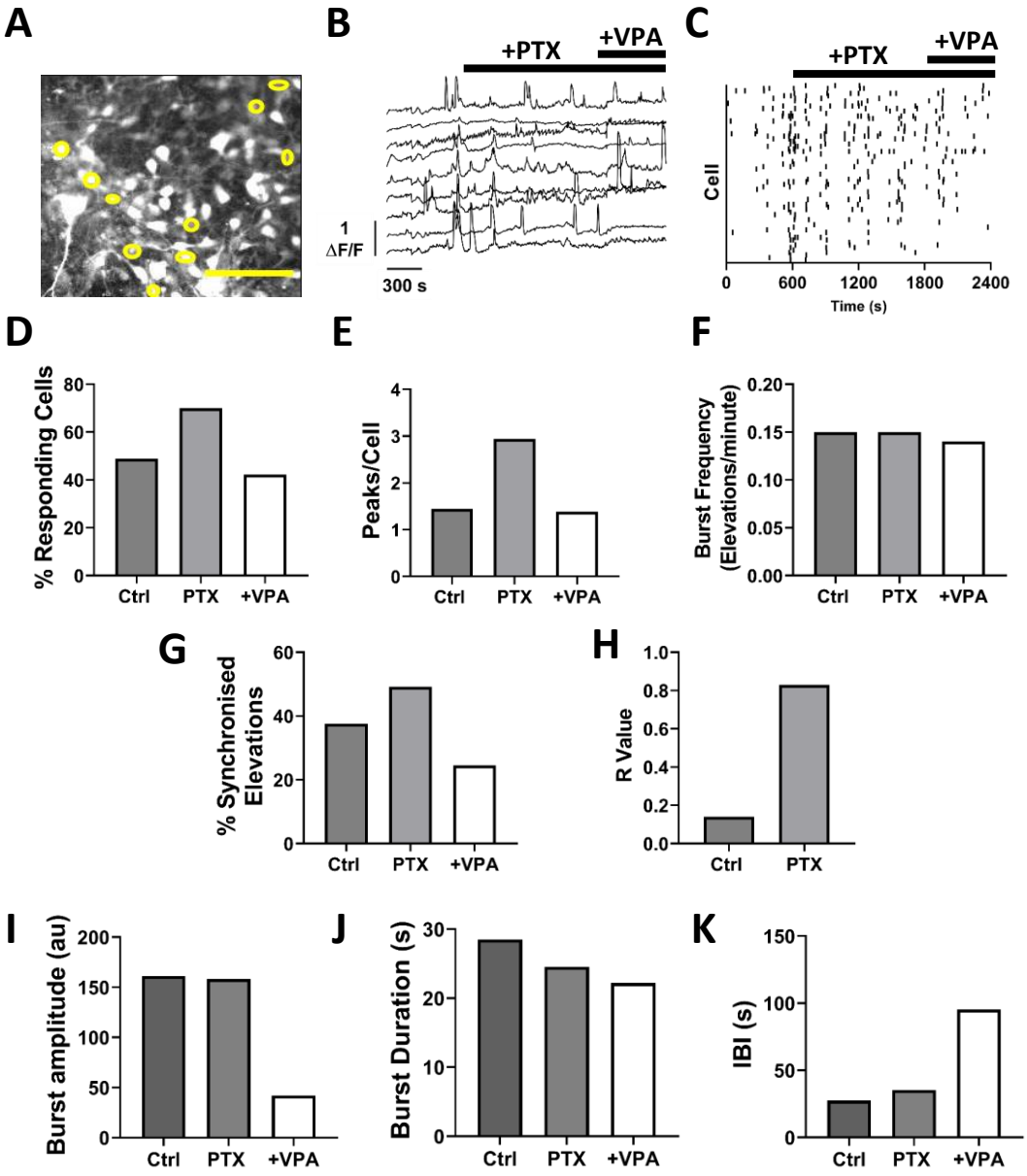

Figure 6.10: Fluorescent calcium imaging responses of co-cultures of human iPSC-derived neurons, astrocytes and interneurons to picrotoxin perfusion. Neurons and astrocytes were synchronised and cultured independently, before co-culturing at 13 DIV alongside addition of interneurons, followed by 10 weeks differentiation. (**A**) Co-cultures were loaded with 5 µM Fluo4-AM for imaging. (**B**) Time-lapse videos were recorded at 0.33 Hz, with representative figures showing 10 example, random fluorescent traces related to yellow regions of interest in (A). (**C**) Representative Raster plot. Spikes were identified manually and plotted over time to identify synchronised events. (**D**) Responding cells were determined as those with ≥ one peak of calcium activity. (**E**) Calcium peaks per active cell. (**F**) Frequency of calcium events per minute. (**G-H**) Quantitative measures of synchrony. (**G**) % synchronised cells relating to (C). (**H**) Average R value. (**I**) Amplitude of calcium events. (**J**) Duration of calcium events. (**K**) Time between calcium events. N=1. Scale bar: 5 µm. Solid black bars in B-C indicate addition of 100 µM PTX and 2 mM sodium valproate.

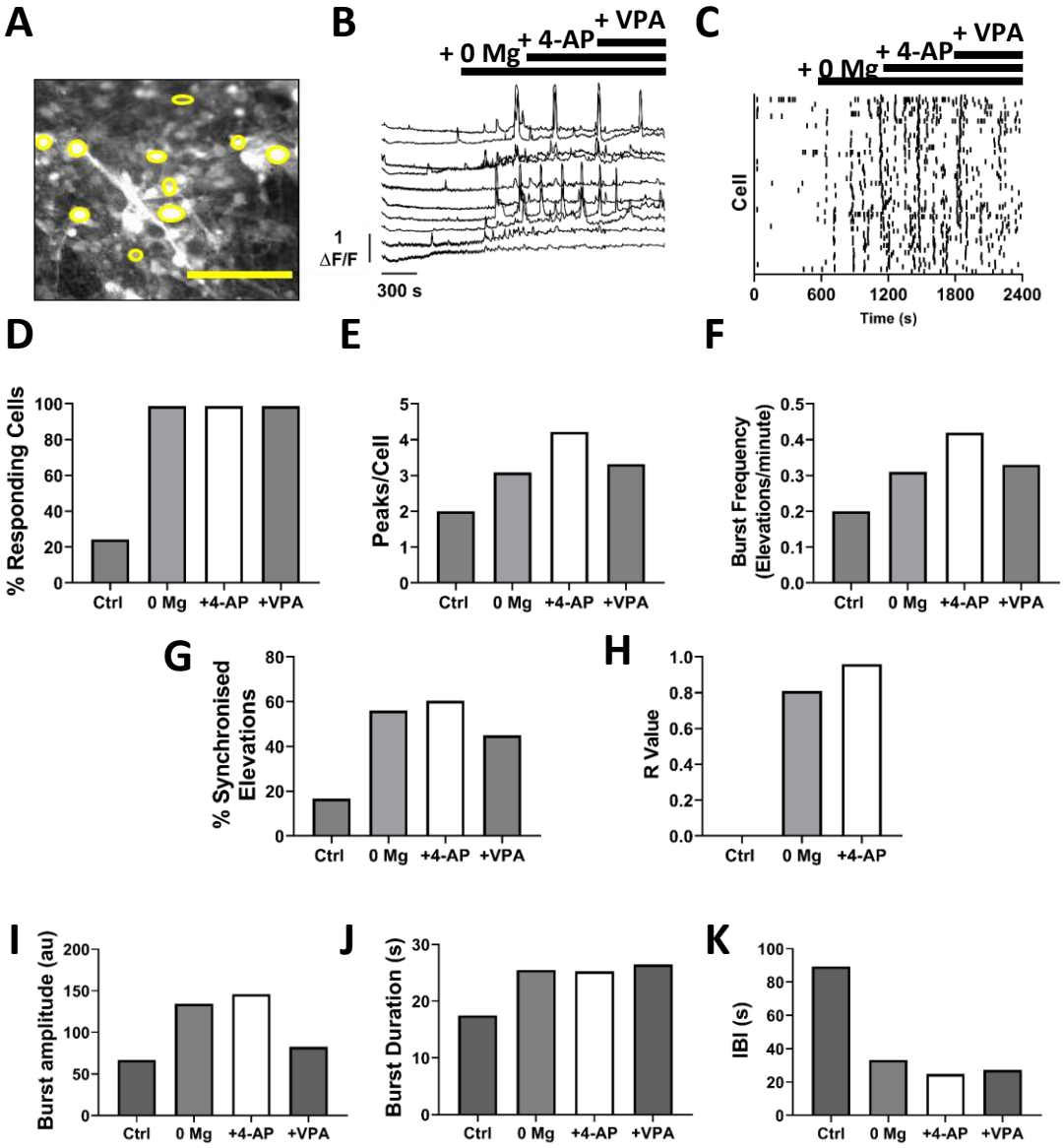

Figure 6.11: Fluorescent calcium imaging responses of co-cultures of human iPSC-derived neurons, astrocytes and interneurons to zero magnesium aCSF and 4-aminopyridine perfusion. Neurons and astrocytes were synchronised and cultured independently, before co-culturing at 13 DIV alongside addition of interneurons, followed by 10 weeks differentiation. (**A**) Co-cultures were loaded with 5 µM Fluo4-AM for imaging. (**B**) Time-lapse videos were recorded at 0.33 Hz, with representative figures showing 10 example, random fluorescent traces related to yellow regions of interest in (A). (**C**) Representative Raster plot. Spikes were identified manually and plotted over time to identify synchronised events. (**D**) Responding cells were determined as those with ≥ one peak of calcium activity. (**E**) Calcium peaks per active cell. (**F**) Frequency of calcium events per minute. (**G-H**) Quantitative measures of synchrony. (**G**) % synchronised cells relating to (C). (**H**) Average R value. (**I**) Amplitude of calcium events. (**J**) Duration of calcium events. (**K**) Time between calcium events. N=1. Scale bar: 5 µm. Solid black bars in B-C indicate addition of zero magnesium aCSF, 100 µM 4-AP and 2 mM sodium valproate.

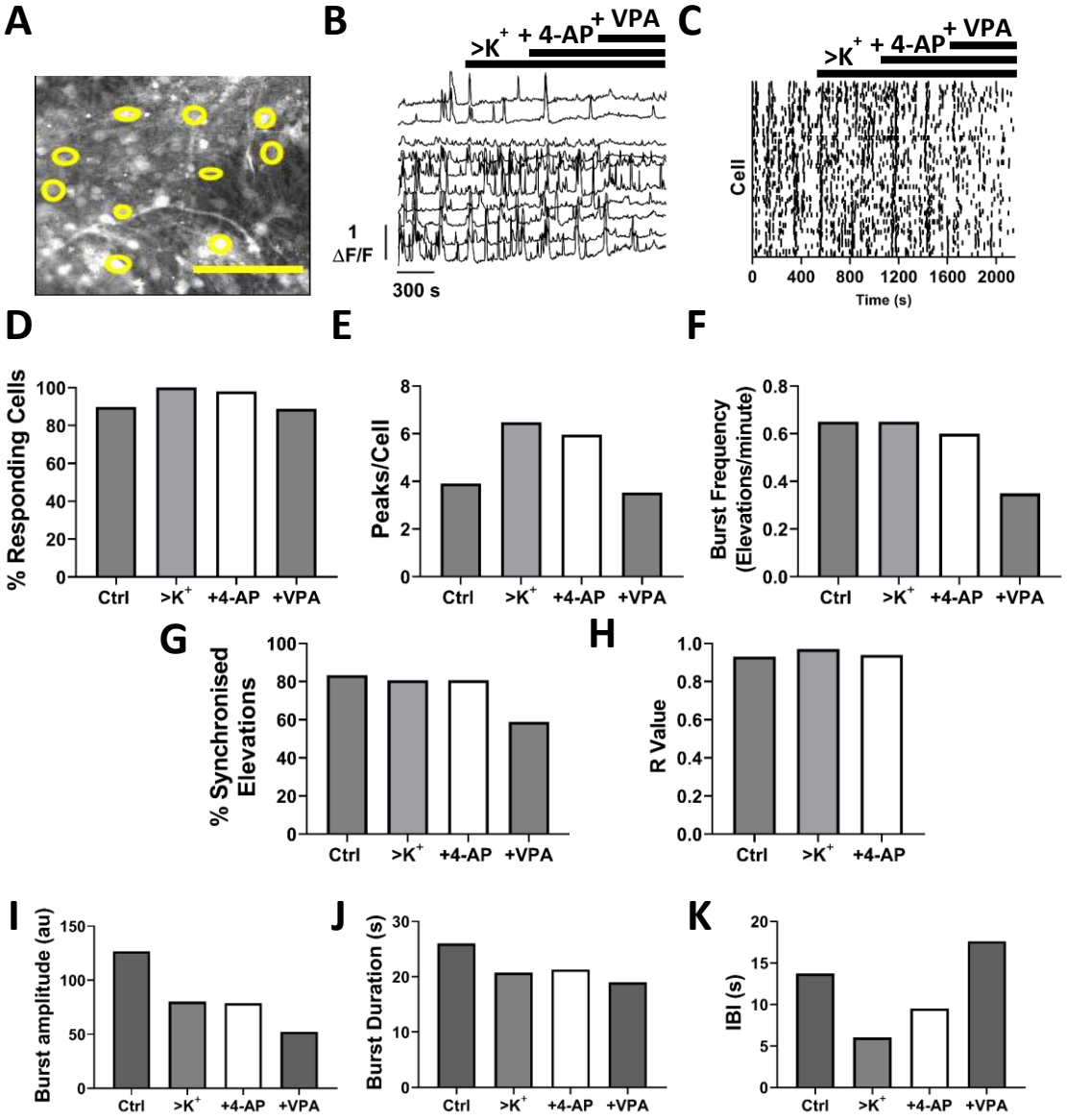

Figure 6.12: Fluorescent calcium imaging responses of co-cultures of human iPSC-derived neurons, astrocytes and interneurons to elevated potassium aCSF and 4-aminopyridine perfusion. Neurons and astrocytes were synchronised and cultured independently, before co-culturing at 13 DIV alongside addition of interneurons, followed by 10 weeks differentiation. (**A**) Co-cultures were loaded with 5 µM Fluo4-AM for imaging. (**B**) Time-lapse videos were recorded at 0.33 Hz, with representative figures showing 10 example, random fluorescent traces related to yellow regions of interest in (A). (**C**) Representative Raster plot. Spikes were identified manually and plotted over time to identify synchronised events. (**D**) Responding cells were determined as those with ≥ one peak of calcium activity. (**E**) Calcium peaks per active cell. (**F**) Frequency of calcium events per minute. (**G-H**) Quantitative measures of synchrony. (**G**) % synchronised cells relating to (C). (**H**) Average R value. (**I**) Amplitude of calcium events. (**J**) Duration of calcium events. (**K**) Time between calcium events. N=1. Scale bar: 5 µm. Solid black bars in B-C indicate addition of high potassium aCSF, 100 µM 4-AP and 2 mM sodium valproate.

6.3 Discussion

In this final experimental chapter, a robust co-culture method has been developed, which responds with increased activity and synchrony to different pro-ictogenic conditions within 10 weeks. Importantly, the baseline percentage of active cells observed from these co-cultures was significantly higher than previously tested models in Chapters 3-5 (Appendix Figure A12).

AraC is an effective mitotic inhibitor for iPSC-derived astrocytes

The results from Chapters 3-5 suggested that the proliferative ability of astrocytes in co-culture models needed to be inhibited. To this end, the mitotic inhibitor AraC was used to synchronise astrocyte cultures and arrest their proliferation (de Rus Jaquet, 2019). As AraC is commonly used as a chemotherapeutic drug (Vincelette & Yun, 2014), and considered a potent anti-proliferative agent, the effect on cell viability was also considered. As it was anticipated that mitotic inhibition could have potentially cytotoxic effects and reduce viability of the astrocytes, a balance had to be struck so that the astrocytic growth was contained, with minimal cytotoxicity. The results indicated that AraC treatment at 10 µM could be applied to cultures of astrocytes to produce the desired effect of containing their growth, as evidence by reduced Ki67 immunostaining, without excessive cell attrition.

Immunostaining was performed throughout differentiation, as for previous Chapters. The consistency of astrocytes and neurons throughout differentiation remained constant, which gives a further, strong indication that the inhibition was successful. As for ICC results in Chapter 3.2, quantitation was not possible. Gene expression analysis performed at 10 WIV showed a significant increase in S100β expression compared with Week 0, which could suggest an increase in numbers of astrocytes themselves, however qualitative visualisation did not indicate that astrocytes had overgrown the culture.

Importantly, an issue observed in spontaneous differentiation, particularly on PORN-laminin was the large degree of fasciculation and the tendency for clusters of somas to form ‘hubs’

throughout the culture (Amin et al., 2016). This was not observed using this co-culture model and is further evidence that the inhibition of both cell types was effective. Of particular significance is that aggregation of previous cultures often resulted in detachment from the culture surface and the ultimate loss of cells. Cultures were successfully differentiated over 10 weeks, demonstrating that co-culturing promotes a more adherent, robust culture, as previously reported (Kuijlaars et al., 2016).

This synchronised co-culture method promotes network formation

Neural networks are essential for seizure generation and are highly suggestive of a matured, connected culture (Spencer, 2002). It has been shown that stored and intracellular calcium are involved in neural network activities such as propagation of calcium waves and that these can increase the rapidity of the spread of calcium via calcium-induced calcium release (Neymotin et al., 2015). As such, calcium imaging was used to determine whether waves of calcium signals were evident and whether they could spread throughout the culture. Both ionically manipulated perfusate condition elicited large waves of calcium activity, which propagated distally from an origin. This provides evidence that the cells in culture had formed an interconnected neural network, as opposed to isolated neurons. The reason behind the formation of reproducible networks is likely due to the inclusion of matured astrocytes in this co-culture model (Halassa & Haydon, 2010). These results agree with those of Kuijlaars et al., (2016) who found co-culture of DAPT-synchronised NPCs with primary human astrocytes promotes neural network formation. However, this group also use synchronised baseline activity as a metric for networks, as it has been demonstrated that developing neural networks exhibit periods of synchronised bursts, mediated by excitatory neurons in iPSC-derived systems which lack a physiologically-relevant interneuronal component (Kirwan et al., 2015). It is important to note, however, that Kuijlaars et al., (2016) demonstrated 'synchronised network activity' at baseline, yet their aCSF recipe did not contain magnesium. This suggests that the activity observed was a result of excitatory ionic manipulation and not of true control (i.e. no manipulation) calcium activity. For

this reason, the propagation of calcium waves was used to determine network connectivity and not synchronised burst activity during development.

Are calcium signals neuronal or astrocytic?

As discussed previously, astrocytes display spontaneous and synchronised calcium activity (Klapper et al., 2019; Pirttimaki et al., 2017). Due to the co-cultures containing both neurons and matured astrocytes, this presented a possibility that the signals observed from calcium imaging could be from astrocytes in culture, as opposed to neurons. Indeed, one could make the link between astrocytic calcium signals and absence of 'typical' electrical activity on MEA recordings both in this Chapter and previous Chapters. Indeed, some cultures displayed what appeared to be oscillatory activity, but with considerably longer times between the oscillations than the wave propagations observed previously. Astrocytes can oscillate and can also influence neuronal oscillations in culture systems, often at a slower pace than that of neurons (Pasti et al., 2001; James Crowe, unpublished data).

In order to distinguish between the two cell types, experiments were performed using tetrodotoxin (TTX), with the aim to inhibit neuronal action potential-mediated activity, which incidentally, provides another metric for assessing network function *in vitro* (Hill et al., 2012; Kasteel & Westerink, 2017). As a result, any signals still observed during TTX application were assumed to be astrocyte-mediated. This method contrasts with those used previously, wherein glutamate was used to distinguish between neuronal and astrocytic cell types (Pickering et al., 2008), however as both cell types in culture can respond to glutamate with increased intracellular calcium activity, this method is ineffective (Bezzi et al., 1998).

The application of an action-potential blocker such as TTX should result in a reduction in neuronal cell and burst activity, with the exception of IBI, which should increase as the cells should fire less often (if at all) (Abe & Terasawa, 2005). It appears that TTX application reduced every parameter assessed, with statistically significant results for some assessments. As a result,

it is likely that most of the individual and network activity observed and reported is either neuronal or is mediated by sodium action potentials, as upon TTX application, propagating waves also ceased. With relevance to calcium waves, the synchronised co-culture platform demonstrated more rapid propagation than those observed in isolated human astrocytic networks (Hill et al., 2012), suggesting that the waves of calcium in this instance, were neuronal. In further support, collaboration with various current and former members of Dr. Rhein Parri's lab group (Aston University, personal communications), patch clamp analysis on both spontaneously differentiated and synchronised co-cultures revealed the ability for neurons in culture to fire action potentials and exhibit electrical activity. The possibility still stands that the calcium activity observed could be astrocytic in nature, but this may be a result of neuronal firing and consequent neurotransmitter release stimulating astrocytes (Agulhon et al., 2008; Fiacco et al., 2007). The inability to effectively distinguish between cell types is a major limitation of this experimental design and is discussed in Chapter 7.

Was activity observed epileptiform?

The rationale behind combining ionic and pharmacological manipulation in this Chapter was that the tendency for previous cultures to appear as if they were reaching a threshold and required only a minor increase in stimulation to fire in a hyperexcitable and hypersynchronous manner was routinely observed. Despite observing increased activity and synchrony (with statistical significance) in each pro-ictogenic condition, a hypersynchronous, hyperactive culture like the isolated repeats in Chapters 4 and 5 was not observed with this model. It could be argued that this is due to the absence of interneurons and it underlines the significant role they play in seizure generation. Irrespective of this, the addition of ionic and pharmacological treatments in tandem often resulted in increased values *cf* ionic manipulation alone and significant increases in activity and synchrony *cf* control. Therefore, the conclusion from this method is that combination of pro-ictogenic conditions excites the system to a greater extent than individual treatments. Again, this is possibly because inhibitory circuits are not present and

thus cannot modulate or mediate the synchronisation typically observed in seizure-like events (Grasse et al., 2013).

Alongside experiments with TTX to attempt to distinguish between neurons and astrocytes, sodium valproate (VPA) was also perfused on several cultures to monitor whether activity reduced. As reviewed in 6.1, VPA can exert effects on GABAergic neurotransmission and various ion channels. VPA appeared to slightly reduce activity, however no parameter assessed was statistically significant. The reason for this could be due to the mechanistic action of VPA: if the action of VPA is based predominantly on GABAergic transmission, the lack of inhibitory input in this system could explain the ineffectiveness of VPA treatment in this instance.

Co-cultures with interneurons display increased activity

The generous donation of commercially available interneurons (James Crowe) provided the basis for the final experiments in this thesis, however, due to time and cost constraints, no repeats could be performed and thus, no statistical analysis. Interneurons were added at a ratio of 1:4 with excitatory neurons, as this ratio has been reported in the human *in vivo* cortex (Sahara et al., 2012). Immunostaining of synapses revealed characteristic punctate VGlut1 excitatory vesicles and $GAD67^{+}$ inhibitory vesicles, not previously seen. These were localised to the soma and along the neurites as previously reported (Gunhanlar et al., 2017).

Interneuronal co-cultures were perfused with PTX, as it was expected that the receptors and cellular targets were now present in the system. Indeed, measures of activity and synchrony were all increased in the presence of PTX, however the burst frequency remained unchanged and burst parameters indicated an unsuccessful epileptiform result. Interestingly, VPA perfusion decreased all measures of activity and synchrony and burst activity, whilst extending IBI, suggesting VPA was effective in reducing PTX-induced neuronal activity. This is possibly due to the effects of VPA on GABA transmission and interneuronal populations (Lauber et al., 2016; Winterer, 2003).

The provisional result with 0 Mg and 4-AP perfusion indicates a successful experiment, with substantially increased activity, synchrony, and burst measures. This combined with visual analysis, the derived traces and the Raster plot were all suggestive of epileptiform activity. Moreover, perfusion with VPA also decreased several parameters of activity, synchrony and burst characteristics. Whilst >K^+ aCSF did increase activity, it displayed no effect on bursting and synchrony, indicating a lack of epileptiform activity. However, in this instance, VPA produced a decrease in every parameter and increased duration between bursts, suggesting it acted successfully upon the culture.

Whilst the results from these preliminary interneuron co-cultures are very promising, there needs to be a significantly increased sample size and appropriate statistical analysis to confirm that interneuron inclusion is necessary for epileptiform activity in the human iPSC-derived neural cultures presented in this Chapter. Furthermore, there was considerable optimisation of ratios, seeding densities and maturation states of the individual cellular components involved in co-culturing methods throughout this thesis. Whilst the ratio of interneurons seeded was similar to that typically observed *in vivo*, further refinement and development of the inhibitory component of *in vitro* models will require lengthy and methodical investigation to generate the most consistent results.

Chapter 7

7: GENERAL DISCUSSION AND FUTURE DIRECTIONS

The main aim of this thesis was to develop and test human iPSC-derived models for preclinical seizure-liability testing and integrate this with a suitable, high-throughput analytical technique. There is a dearth of standard protocols to assemble these cellular platforms, including consideration of growth media, cellular ratios, cell subtypes, donor patients and methods of experimentation, making this aim problematic and challenging. This thesis has compared methods for generating iPSC-derived neural cultures for preclinical seizure-liability testing and has narrowed the choice towards a potentially exciting and productive human culture platform. The most common protocols reported in the literature have been considered and their ability to produce hypersynchronised and hyperactive responses to well-known seizurogenic treatments has been assessed. This Chapter will briefly summarise the experimental findings from previous Chapters, whilst providing a general discussion of the collective results. Limitations of this study, alongside future directions are also addressed.

7.1 Summary of experimental findings

In **Chapter 3**, it was intended to demonstrate the ability of commercially available neural precursor stem cells (NPCs) to differentiate into morphologically and functionally distinct neural subtypes over 18 weeks differentiation. The initial spontaneous differentiation protocol was based on that of the seminal work of Chambers et al., (2009) and Shi et al., (2012a,b) who demonstrated NPCs, in the presence of defined growth medium, could undergo both neurogenesis and gliogenesis. This allowed the formation of the key cellular components of the cortex, along with the ability to exhibit functional activity. In agreement with the scientific literature, spontaneously differentiated cultures displayed developmental markers at the same points in time, with the initial emergence of immunostained neural progenitors and cortical rosettes, radial glia, neurons by 4 WIV, cortical layer markers and astrocyte emergence around

8 WIV, with astrocyte maturation observed post 10 WIV. This was also confirmed by qPCR. These results correlate with the *in vivo* neural development timeline (Mertens et al., 2016), suggestive of a successful differentiation protocol. Furthermore, there was an absence of inhibitory interneuron immunostaining at all timepoints, despite significant increases in vGAT expression, which is further indication of a cortical differentiation.

An important objective of Chapter 3 was to provide evidence of differences in neural growth media, to move closer to standardisation of iPSC protocols for safety pharmacology applications. In Chapter 3, two widely available commercial growth media were directly compared on their ability to influence cultures to generate the above cell types, the speed at which this could be achieved and their subsequent functional activity. The results of this chapter disagree with the scientific literature, where it was shown that SCT media was superior to the standard electrophysiology perfusate 'artificial cerebrospinal fluid' (Bardy et al., 2015). Instead, it was discovered that aCSF produces increased functional responses from cultures and hence, was a more appropriate perfusate for functional recordings.

Chapter 4 sought to build on the findings of Chapter 3 and progress the platform development towards the possible induction of seizure-like activity in the spontaneously developed cultures, using experimental methods which are high-throughput and non-invasive; ideal for toxicity screening (Collins et al., 2017). A novel interrogation of spontaneously derived neural cultures over 18 weeks differentiation was presented, using fluorescent calcium imaging. At various timepoints correlating to key developmental stages (i.e. 4 WIV (arrival of neurons), 8 WIV (arrival of astrocytes), 12 WIV (matured astrocytes, matured culture) and 18 WIV (further maturation)) the ability for spontaneously differentiated cultures to respond to a panel of seizurogenic conditions was explored. Despite many experiments being conducted, in both media, the activity was not epileptiform, with the exception of a single SCT culture which displayed characteristic synchronised and hyperactive bursting calcium activity; indicative of

seizure-like events (Hongo et al., 2015; Pacico & Meur, 2014). However, the overall results of Chapters 3 and 4 suggested cells cultured in SCT media exhibited the greatest activity and responses to seizurogenic manipulations.

Following the morphological and functional characterisation of spontaneous differentiation in two commercially available growth media, in **Chapter 5**, the ability of monocultures of neurons and astrocytes and co-culture models were investigated, in terms of their responses of characteristic epileptiform activity. An optimised protocol for the synchronisation of NPCs was developed in this thesis and following synchronisation, individual neuronal cultures were found to be relatively inactive. Further evidence strongly supported the requirement of astrocytes and neurons to exist in co-culture, in physical contact, as reported previously (Odawara et al., 2014). Neither monoculture platform displayed epileptiform activity and therefore, the co-culturing of both cell types was attempted using two different methods. Epileptiform activity was observed with a spontaneous co-culture model in Chapter 5, albeit not reproducibly; suggesting that co-culture systems have the potential to be used in toxicity screening. A key observation was recorded at this point, with respect to the highly problematic potential for astrocytes to overgrow in late cultures, subsequently reducing activity and neuronal drug responses.

In **Chapter 6** methods were evaluated to control astrocyte proliferation and in collaboration with PhD students from the Coleman, Hill and Parri groups (Aston University), a refined co-culture model was generated, based on previous literature (Kayama et al., 2018; Matsuda et al., 2018; Odawara et al., 2018), wherein the ratios of neurons to astrocytes could be more strictly controlled than in previous co-culture models and spontaneously differentiated cultures (Chapters 3-5). The results were indicative of a functional, heterogeneous model system, although robust epileptiform activity was only episodically observed. Final experiments wherein GABAergic interneurons were added to the culture system, yielded a platform with the capacity to react to a wider range of compounds, some with elevated measures of synchrony, activity

and bursting. In this thesis, evidence for the requirement of astrocytes, neurons and GABAergic interneurons to physically co-exist in culture with consideration of subtype ratios is provided.

7.2 General discussion

7.2.1 Statistical analysis

It is estimated that many biological publications contain errors in their statistical analysis (García-Berthou & Alcaraz, 2004), and thus, care was taken to consult biostatistics expertise to ensure accuracy and reliability. Statistical analysis in this thesis was performed with detailed consideration of several multi-factorial study designs. In many instances (particularly Chapter 3 and 4), it was necessary to perform multiple comparisons, as the primary aim was to compare two growth media and their effect on different drug treatments. A 2-way ANOVA is a parametric test; appropriate for normally distributed data. Parametric tests have higher statistical power than their non-parametric equivalents (Kitchen, 2009), making this a desirable means of determining significant results. However, as biological data is seldom normally distributed, 2-way ANOVA for multiple comparisons presented a challenge. To the author's knowledge no appropriate non-parametric alternative to the 2-way ANOVA is available. The Scheirer-Ray-Hare test (Scheirer et al., 1976) has been used in some situations as a non-parametric alternative, however this test has low statistical power and if applied to the data in this thesis, there was potential to misinterpret the findings. Therefore, non-normally distributed data had to be transformed to enable statistical testing with greater statistical power. Transformations are commonly used in biology to normalise slightly skewed data, enabling scientists to then perform parametric testing (Garcia-Berthou & Alcaraz, 2004). In this thesis, data was transformed using logarithmic methods and this was kept constant for all transformations.

Outliers can be removed from datasets, in the hope that this enables the data to follow a Gaussian (normal) distribution and indeed, this practice is commonly followed. However, particularly in Chapters 4,5 'outliers' provided the most interesting results, demonstrating the cultures' capability to generate hyperexcitable, hypersynchronous activity. In this instance,

removing the outliers would have prevented these important preliminary findings. As a result, it was decided to display all data obtained and then, if necessary, perform transformations to enable 2-way ANOVA. For datasets where the study design permitted 1-way ANOVA (particularly Chapter 6), a suitable non-parametric alternative is allowed, so this data was not adjusted in any way.

7.2.2 What is the ideal culture system for seizure-liability testing?

7.2.2.1 Spontaneous differentiation

As previously stated, the main aim of this thesis was to build an optimal culture method for neurotoxicity testing. Several approaches were attempted, and all assessed using the same broad experimental approach. Spontaneous differentiation revealed the potential for cultures to respond in an epileptiform manner to seizurogenic conditions, however, the data indicated that this is not a reliable or reproducible method of generating this activity. There are several possible explanations for these results. Mature electrical circuits are necessary for normal, oscillatory and seizure activity and human cortical neurogenesis occurs over a period of roughly 100 days (Rabinowicz et al., 1996). Ergo, the neuronal cells and circuits at weeks 4-12 may not be fully matured. Indeed, Amin et al., (2016) assessed their spontaneously differentiated cultures via patch clamp techniques and found that cells fired immature action potentials even at 12 WIV. This is supported by experiments suggesting that the matured network activity of spontaneously differentiated cultures occurs between 8-23 WIV (Kirwan et al., 2015). Due to time constraints of this project, 18 WIV differentiation was an attainable, but nevertheless long duration. However, these reports, combined with the results of Chapter 4, indicate that the activity of most of the cultures was still immature at this timepoint. Relating this to the aim of this thesis, a high-throughput neurotoxicity model which takes over 18 weeks to develop is simply an unrealistic approach (Verstraelen et al., 2014). In agreement, whilst those authors suggest embryoid body protocols generate heterogeneous models, this still takes an

impractically long amount of time (>12 WIV), so therefore, is unsuitable for the purpose of short timeframe toxicity testing (Gunhanlar et al., 2017).

A recurrent theme throughout this thesis is the supportive, developmental and functional roles which astrocytes provide to neurons. In primary rodent cultures, the issue of astrocytic overgrowth is frequently observed over time (Foo, 2013) and the data indicated a similar process was occurring in iPSC-derived cultures, however this could only be observed visually and not quantified. Furthermore, it has been shown in *in vitro* studies that astrocytes tend to grow at the base of culture, invading the culture growth surface, forcing neurons to detach and die (Gilad & Gilad, 1987). In addition, throughout spontaneous cultures, a large degree of neuronal fasciculation was observed, to the point where cells detached from the culture surface and became unstable and ultimately died. *In vivo* developmental studies have confirmed that neuronal fasciculation is a necessary process for providing a scaffold and guide for the migration of developing neurons in the CNS (Bak & Fraser, 2003), hence, initial fasciculation of neurites was a positive result in terms of alignment with the *in vivo* environment. However, the extensive aggregation observed over time is indicative of an incomplete system, wherein the mechanisms behind fasciculation have been able to continue in an uncontrolled manner. It may be that the overgrowth of astrocytes led to this fasciculation, following neuronal detachment from the culture surface.

Ultimately, the lack of responsiveness of spontaneously differentiated cultures may have been due to the variation in cell ratios and the unregulated cell aggregation and overgrowth, which hindered any practical method of determining exactly how many cells of which type were present in the cultures over time. For safety pharmacology applications, variation to this extent is unacceptable and ideally, a system should have physiological ratios of cell types, which do not uncontrollably proliferate or cause the death of neighbouring cells. In conclusion, the author contends that astrocytic overgrowth could explain the lack of reactivity to pro-ictogenic

conditions and relatively low baseline activity observed in later cultures. In addition, the fact that astrocytes do not appear in culture until post W8 differentiation could also provide a reason for this reduced activity, as neurons are less mature than if the physical presence of astrocytes had occurred from a similar time to the initial neuronal plating *in vitro*.

7.2.2.2 Co-culture differentiation

Following from the variation observed from spontaneous differentiation, a more controlled series of methods were attempted, from individual cultures of cell types, to co-culture models. The results from Chapters 3 and 4 indicated that astrocyte overgrowth and neuronal immaturity were likely causative factors in the ineffectiveness of spontaneous differentiation to generate SLE. As such, co-culture methods were employed which seeded neurons and astrocytes together, to provide a supportive, developmental environment for neurons from the initial plating.

To rectify some of the problems with spontaneous differentiation, a synchronisation protocol for neurons in this system was developed, wherein the number of neurons could be more stringently regulated and fewer NPCs would remain to develop into astrocytes. This provided two possibilities for culture systems: firstly, where a defined number of astrocytes would be added to these synchronised neurons and secondly, where a defined number of astrocytes would be added to spontaneously differentiating neurons. The theory behind both being that the presence of astrocytes throughout neuronal development may speed up the maturation process and offer tighter regulation of ratios of cell types, compared with that of spontaneous differentiation. Additionally, the necessity for astrocytes in culture for seizure activity has been reported (Klapper et al., 2019).

Interestingly, the spontaneous co-culture model generated a large synchronised bursting response to $>K^+$ aCSF conditions at 7 WIV, whilst no characteristic epileptiform activity was observed in the synchronised neuron – astrocyte co-cultures. Furthermore, the magnitude of

the seizure-like activity was far greater than that of the response observed for the epileptiform response in the spontaneously differentiated culture (Chapter 4). This suggests that the presence of astrocytes throughout neuronal development led to a more rapidly matured culture, capable of eliciting epileptiform activity and agrees with the scientific literature for rodent (Bradley et al., 2018; Fan et al., 2019) and human iPSC-derived (Ishii et al., 2017; Kuijlaars et al., 2016; Odawara et al., 2016a, 2016b; Tukker et al., 2016, 2018) platforms. However, again this was not reproducible, likely due to the variation previously observed with spontaneous differentiation.

With regards to both co-culture systems from Chapter 5, astrocytic overgrowth was, again, apparent by the end of the differentiation period. Further observation confirmed that the cultures were highly astrocytic, presented as a widespread adherent monolayer. These data suggest that the cells seen over 18 weeks on the culture-ware and MEA chips were astrocytic and that the neurons had diminished to a number which was not compatible with a detectable response. This is supported by the absence of detectable MEA signals, despite a completely adherent monolayer and is reinforced by the appearance of large, astrocytic morphologies from W18 calcium imaging, which can produce calcium responses (Khakh & McCarthy, 2015). Indeed, the calcium responses observed in the cultures which appeared heavily astrocytic were slower and more repetitive than previously observed neuronal signals, which could provide further evidence that the cells being imaged were largely astrocytic; particularly as astrocytic calcium activity typically functions more like that of a pacemaker (Hill et al., 2012).

The experiments with monocultures of neurons and astrocytes have further confirmed reports that neurons and astrocytes must co-exist for a heterogeneous, viable culture system (Odawara et al., 2014; Stogsdill et al., 2017; Taga et al., 2019), particularly as the absence of physical contact with astrocytes (despite neuroprotective growth factors), led to the death of

synchronised neuronal monocultures in all repeats. Astrocytic monocultures demonstrated sporadic calcium activity, but did survive alone essentially indefinitely.

In conclusion, despite the co-cultures of astrocytes and neurons showing the ability to produce epileptiform activity, this method of culturing presents similar issues observed with spontaneous differentiation. This method is still superior to spontaneous differentiation, as epileptiform responses were observed at 7 WIV, far more rapidly than those of spontaneous differentiation. These results are highly indicative of astrocytes influencing the maturation of neurons more rapidly, however, their overgrowth and the continued variation in developing cell type ratios ultimately led to the finding that this culture method was not suitable for the purpose of this thesis.

7.2.2.3 Synchronised astrocytes and neurons in co-culture

The results from Chapters 3-5 indicated that spontaneously differentiating cells are unpredictable in their final culture composition and that at later timepoints, astrocytic overgrowth became a problematic issue. As such, a method for inhibiting astrocytic proliferation in this system was developed, using the chemotherapeutic agent cytosine arabinoside (AraC) (Cheng et al., 2017; de Rus Jacquet, 2019; Schwartzentruber et al., 2017).

This method produced cultures which displayed network activity and significant increases in activity and synchrony to conditions tested. Furthermore, immunostaining and visual observation suggested that by inhibiting the ratios of cell types, this remained constant throughout the differentiation protocol.

This protocol is an amendment of that published previously (Odawara et al., 2018), but with a novel contribution in the inhibition of astrocytes using AraC. Furthermore, the ratio of astrocytes finally chosen was optimised for this individual system, from collaboration with Mr James Crowe (Parri group, Aston University). In further support for this platform, the baseline

activity was significantly increased in synchronised astrocyte-neuronal co-cultures *cf* every preceding model assessed in this thesis (Appendix Figure A12).

Despite generating a functional, integrated and responsive platform, a number of issues still remain. Firstly, the optimisation was performed for this specific cellular model and there is no guarantee that this is applicable more widely, as the data in this thesis has indicated. Secondly and perhaps most importantly, irrespective of the significant increases in epileptiform criteria, statistically significant bursting activity was not observed in this culture system. This is evocative of a missing component in the model to generate a truly controlled, reproducible system.

7.2.3 GABAergic interneurons are vitally important

The findings in this thesis strongly suggests that GABAergic interneurons are required for a heterogeneous, reproducible neural seizure-liability platform.

As discussed in detail in Chapters 1 and 6, GABAergic interneurons (GIN) play critical roles in neural circuits and seizure induction (Sharfman, 2007). Spontaneous differentiation can intermittently produce GIN in monolayer systems (Kirwan, et al., 2015; Shi et al., 2012a) and embryoid body-based protocols (Gunhanlar et al., 2017), particularly in late timepoints in developing cultures. As discussed previously, interneurons do not develop in the cortex, but rather migrate in from the medial ganglionic eminence (Martini et al., 2009) and precise generation of interneurons from NPC involves the use of specific morphogens such as purmorphamine (Liu et al., 2013). As the embryoid-body protocol (Gunhanlar et al., 2017) includes no mention of morphogens, if this is routinely observed with this method, it would be interesting to determine which processes lead to interneuron generation in non-adherent cultures, but unpredictable interneuron generation in adherent cultures. Ultimately, from a toxicity screening standpoint, waiting several months for cultures to *potentially* display interneurons is not feasible and renders this differentiation model unsuitable regardless. Due to apparatus failure and time constraints, sufficient repeats of spontaneously differentiated

cultures at 18 WIV to perform statistical analysis were not possible. vGAT expression in Axol cells was considerably higher than control, which could have been indicative of interneuron emergence at this late point in development.

The proportion of interneurons which develop randomly are likely due to spontaneous differentiation not being 100% efficient (Chambers et al., 2009; Shi et al., 2012b). As discussed above, this presents a problem with variations in cultures in terms of density and final ratios of cell types. The reports of the presence of GIN in spontaneously differentiating cultures, coupled with the variability of spontaneous cultures could explain why some cultures responded with epileptiform activity and *most* did not. Indeed, the co-culture method which produced a hypersynchronous and hyperexcitable response was developed from a spontaneously differentiating neuronal protocol. The irregular, uneven generation of interneurons is likely a causative factor in the inability for most cultures to produce seizure-like activity. With respect to the specific compounds tested, the target of picrotoxin is $GABA_A$ receptors on interneurons (Davidoff & Aprison, 1969), which explains the lack of response to PTX observed. However, there were statistically significant increases in activity in cultures maintained in Axol, in response to PTX, which could indicate the presence of GIN in culture, providing a target for the compound. With regards to 4-aminopyridine, as per Chapter 4, the mechanism of 4-AP seizure-induction includes potassium channel antagonism and interneuronal excitation, via the interneuron-potassium hypothesis (Perreault & Avoli, 1991). These data show that the absence of seizure activity in the presence of 4-AP is also likely to be due to the absence of GIN in this system, and that even if they are present as some data suggests, they are not in sufficient concentration to be reminiscent of the *in vivo* cortical environment.

Furthermore, when considering the bursting parameters for the synchronised astrocytic-neuronal co-culture method, increases in burst activity did not achieve statistical significance. Interneurons are crucial for burst activity (Shin et al., 2010; Velazquez & Carlen, 1999) and their

non-appearance could explain why these metrics were not significantly increased. In conclusion, the unsuccessful generation of seizure-like activity in cultures from all methods is likely due to the absence of GABAergic interneurons, as increased measures of synchrony and activity were observed immediately from preliminary interneuron co-culture experiments. Whilst not conclusive and not statistically verified, the inclusion of interneurons in the established synchronised co-culture protocol in this thesis holds great promise for future seizure-liability testing with human iPSC-derived neural platforms.

7.2.4 Don't stand so close to me

Upon closer inspection of the cultures that responded with epileptiform activity, it was revealed that these cultures were less dense and aggregated than other cultures (Figures 4.13A/5.10A). This was not intentional, and indeed it further highlights the variation in spontaneous culture method outcome. It would appear that this arrangement facilitated the widespread seizure-like activity. This finding prompted closer examination of other cultures and it was found that those with higher activity and drug response were, indeed, less clustered than relatively inactive cultures. The reason for this is unclear but may relate to astrocytic overgrowth as mentioned above. Nevertheless, the precise control of ratios and mitotic inhibition of components did result in less dense co-cultures of synchronised astrocytes and neurons and this discovery most certainly warrants further investigation.

7.3 Limitations of this study and possible solutions

7.3.1 Morphological characterisation

As mentioned previously, quantitation from immunostaining is an imprecise method of obtaining data on ratios of cell types. In fact, this was a limitation of morphological characterisation in Chapters 3-5. The tendency for cultures to aggregate into large 3D hubs meant accurate imaging was very difficult. Arguably, 3-dimensional aggregates could be imaged using Laser confocal microscopy, to generate high resolution z-stacks and indeed, this was explored. Unfortunately, even this approach was found to be unreliable, as there was no

consistency to the degree of aggregation between coverslips, and between aggregates within the same coverslip. This meant that some aggregates were several times the size of others, and in order to generate a fair ratio of antibody-positive cells, each aggregate would have to be considered. For the magnitude of the study and the number of technical and biological repeats, this was unrealistic and not of significantly greater importance than the qualitative results.

To supplement the qualitative immunostaining data and circumvent some of its limitations, qPCR was used to detect gene expression levels. Unfortunately, and due to time constraints, 18 WIV qPCR could not be performed for spontaneous studies. As the trend for neuronal gene expression indicated a decrease over time, the pattern of S100β expression increased over time, after the initial highest timepoint. Perhaps performing additional experiments at W18 would confirm whether S100β expression is further increased, coinciding with the high density of astrocytes seen in final culture. In contrast, performing different experimental procedures, such as single nucleus RNASeq has been used to characterise changing astrocyte phenotypes in disease (Al-Dalahmah et al., 2020).

7.3.2 Multi-electrode array

Despite the prevalence of modern MEA-based methods for assessing neural activity (Hyvärinen et al., 2019; Kayama et al., 2018; Matsuda et al., 2018; Odawara et al., 2018; Taga et al., 2019; Tukker et al., 2016, 2018, 2019; Yokoi et al., 2019), there were several problems identified with the approach using this cellular system. An issue with the MED64 system is the planar MEA chips themselves are considered 'consumables' with limited uses. Initially planar chips coated with platinum were used, however, this has been demonstrated to be toxic to cells (Wissel et al., 2018). In the case of the MEA, platinum coatings repel cells and were subsequently advised against using (personal communication, Alpha Med Scientific). Following this discovery, carbon-coated electrodes were obtained which did increase cell adherence, however electrode degradation and complete destruction of several MEA chips was observed after multiple uses. This signals a product which is not applicable for high-throughput testing applications. Cultures

were also attempted on MEA chips from a competitor company and these were far more robust, with greater adherence noticed. Another limitation is the cost of the MEAs, which provides a significant barrier to the number of cultures that can be attempted before the chips degrade. The application of these chips in this context is, in the author's judgement, not cost effective. There is no doubt that MEA analysis has gained popularity for iPSC-derived toxicity testing, however, significantly more optimisation was required for it to be a possibility for this type of project and due to time constraints, this was not possible. Whilst some experiments were successful and data was generated, a significant number of experiments failed, either from adherence issues, or a lack of activity reported from astrocytic overgrowth.

Analysis of MEA data is possible using software packages from respective companies, however, as these are relatively recent, there is little guidance and no standardisation on analysis of acquired MEA data, meaning there are many subjective analyses published in the scientific literature. Despite the final synchronised co-culture method being successfully adhered in monolayer over 12 WIV, recordings were noisy and random, making analysis impossible. It was hoped that a more standard protocol like the burst analysis protocol developed by Matsuda et al., (2018) could be achieved in this thesis. Ultimately, the adherence issue was a huge limitation and future studies could attempt one of two improvements: firstly, a different MEA system could be used as it may be possible that this cellular system works better with a different experimental system and secondly, a more adherent substrate could be utilised to promote greater adherence. In this thesis, several surface-treatments were attempted as per Amin et al., (2016), however, the use of commercial products were not used, mainly due to the lack of transparency on their composition. A promising avenue is the use of a human laminin substrate 'laminin 521' which was recently found to promote iPSC-derived neural differentiation, cortical integration and synchronisation of burst activity in developing cultures (Hyvärinen et al., 2019). This could bridge the gap between the culture system developed here and the experimental analysis process, to produce future successful recordings.

7.4 Future Directions

Having established a suitable co-culture protocol for seizure-liability studies which can respond to diverse neuroactive conditions with increased synchrony and activity, there are several refinements and future directions to promote the eventual inclusion of this model in pre-clinical seizure-liability testing.

7.4.1 Establishing optimal interneuron ratios

The development of cultures in this thesis proved the necessity for controlling and optimising ratios of neural cell types for the final synchronised co-culture platform. As the interneuronal co-culture was preliminary work, the ratio of interneurons selected was 20% of the neuronal component, as the *in vivo* cortical arrangement suggests GABAergic interneurons account for 20-25% of all cortical neurons (Riedemann, 2019). Extensive optimisation of astrocyte ratios was considered in this thesis (data not shown) and it is likely that the ratio of interneurons would need to be adjusted to produce the prime platform for the desired functional interrogation in future studies.

7.4.2 Optogenetic methods

In this thesis, a novel human iPSC-derived culture system has been developed for seizure-liability testing, using optical fluorescent calcium imaging. The benefits of calcium imaging are multiple, discussed throughout the thesis. Calcium imaging allows for the detection of simultaneous neuronal and astrocytic calcium activity across networks of cells and at the single cell resolution (Hill et al., 2012; Ikegaya et al., 2005). Furthermore, studies have confirmed that calcium imaging is a reliable proxy for seizure activity (Badea et al., 2001; Pacico & Meur, 2014; Smetters et al., 1999). The ability for calcium imaging to detect both neuronal and astrocytic activity, whilst beneficial in many aspects, can also have its limitations. Indeed, the biggest limitation of this study was that the principal technique employed could not differentiate between neuronal calcium activity and astrocytic calcium activity.

Figure 7.1: Visual representation of future directions. After establishment of optimal 2D culture protocols, including ratios of neurons, astrocytes and interneurons, the cultures should then seek to encompass structural properties of the *in vivo* cortex. This may be achieved by 2 photon polymerisation/scaffolding to form 3D, interconnected cultures which are amenable to high-throughput optogenetic and electrophysiological assessment.

Despite experiments performed to selectively stain astrocytes with sulforhodamine, this was unsuccessful (data not shown). Sulforhodamine is a widely used astrocyte marker in microscopy owed to its low phototoxicity and relatively low cytotoxicity. Interestingly, it has recently been demonstrated that sulforhodamine can induce seizure-like events in cortical cultures and as such, even if this method had been successful, it may have negatively influenced the culture activity (Rasmussen et al., 2016). As previously discussed, some cultures displayed typical astrocytic morphology and slow calcium activity, but it is not possible to accurately determine whether that astrocyte is isolated, or whether processes surrounding the astrocyte and

displaying activity have arisen from associated neurons. Not only would being able to visualise each cell type independently show which cells were active and responsive, it would enable research into specific network and astrocyte dynamics within the seizure event.

There now exist several methods to enable this isolation and generate such data. Recent advancements in the development of genetically encoded calcium indicators (GECIs) removes the need for existing fluorescent dye loading (Saber et al., 2018). GECIs, like their traditional counterparts, are non-invasive, but can be targeted to specific neurons or astrocytes, allowing longer duration imaging, without the risk of photo-toxicity (Mank & Griesbeck, 2008) or non-specific cell staining (Rad et al., 2017). Other issues observed with fluorescent dyes such as background fluorescence and non-specific dye loading can be overcome with GECI technology (Mank & Griesbeck, 2008). In addition to GECI, genetically encoded voltage indicators (GEVI) have been in development for decades and allow the recording of membrane potentials and can transduce this voltage change to fluorescence intensity measurements. It is a highly sensitive technique and provides high resolution measurements of spike activity and synaptic communication. Current invasive measurements of membrane potential and voltage imaging are slow, limited to very few cells, technically demanding and incredibly sensitive to biochemical perturbations, which can be induced from photoexcitation using the technique itself (Bando et al., 2019). GEVIs can measure activity in large populations via protein engineering, which couples fluorescent proteins to voltage-sensitive domains (VSDs), microbial rhodopsins or chemogenetic probes. For example, the first use of a GEVI tethered a green fluorescent protein to the VSD of the voltage-gated Shaker potassium channel. As a result, any voltage-dependent alterations to the channel induces changes in the probe fluorescence and the signal amplified, providing significantly greater resolution and the ability to detect action potentials with standard microscopy equipment (Siegel & Isacoff, 1997). Combining these significant advancements in optogenetic methods with iPSC-derived models could provide a new

dimension to PSL and arguably increase the throughput and efficiency of this technique, whilst enabling visualisation of individual cell types in seizure-like activity.

Despite the ionic manipulation of potassium and magnesium in the aCSF, the direct modification of calcium was not explored in this thesis. Lowering the extracellular concentration of Ca^{2+} can induce regular SLE, accompanied by transient decreases in Na^{+} and increases in K^{+} in the extracellular space (Yaari et al., 1983). Low $[Ca^{2+}]_e$ enhances neuronal excitability and can induce spontaneous, synchronised bursts of activity, reminiscent of epileptiform discharges. Calcium influx occurs via voltage gated-calcium channels and *N*-methyl-$_D$-aspartate (NMDA) receptors and during seizure, the $[Ca^{2+}]_e$ decreases far lower than non-convulsing tissue (Blauwblomme et al., 2014; Simons, 1988; Somjen, 2002). This decrease is due to calcium influx into neurons undergoing the seizure activity, which impairs synaptic transmission as there is too little Ca^{2+}_e to sustain the calcium influx. Higher Ca^{2+}_e can enhance synaptic transmission as calcium is available to enter the cell, even though a higher $[Ca^{2+}]_e$ reduces excitability (as the cell is not depolarised). However, this remains to be observed in iPSC-derived models.

7.4.3 3D models and induced neural cells

While human stem cell derived neurons can be routinely produced using well established methods (Chambers et al., 2009; Shi et al., 2012b) the reproducibility of these methods is variable (Hu et al., 2010). The neurons produced are often slow (2–3 months) to exhibit functional properties such as sustained action potential firing and synaptic plasticity. This represents a significant limitation in experimental models and screening platforms. Alternative approaches such as transdifferentiation allow the direct neuronal cell reprogramming to generate different neuronal lineages, termed “induced neurons” (iN; Vierbuchen et al., 2010)) or “induced astrocytes” (iA; Caiazzo et al., 2015). Such iN can be generated within 3–5 weeks after reprogramming and demonstrate physiological action potential firing (Vierbuchen et al., 2010). Furthermore, iA can be produced within 2 weeks (Caiazzo et al., 2015). Whilst these approaches have reduced the time required to generate functional neuronal subtypes, the

efficiency of generating iN cells is often less than 10% (Yang et al., 2011), suggesting that far more development is required to produce a reproducible platform for testing.

A criticism of the use of two-dimensional (2D) human cultures is that they do not reproduce the structure and hierarchical connectivity that is seen in three-dimensional (3D) tissue. An important route to obtain better structural and morphological relevance is to generate iPSC-derived 3D co-cultures such as organoids and spheroids (Figure 7.2), which have been shown to recapitulate early development of the human cortex (Lancaster et al., 2013; Lancaster & Knoblich, 2014a, 2014b; Pasca et al., 2015). While these 3D cultures are useful models for early development and diseased states, they are less able to model complex, later stages of development and lack vasculature (Sun et al., 2018). The use of scaffolds to 'train' cultures to develop into defined structures is an exciting avenue for regenerative medicine and has very recently been demonstrated in our laboratory (Crowe et al., 2020). Overcoming these issues and applying this technology to seizure-liability testing could provide an insight into not only the mechanisms of seizure spread between layers of cortical cells, but possibly identify novel targets and pharmaceuticals. The advent of matured 3D structures would aim to generate layers of the cortex as seen *in vivo* and provide a robust and relevant platform that resembles a human cortex, in terms of both structure and functionality, adding an extra dimension and increased relevance for human seizure-liability testing.

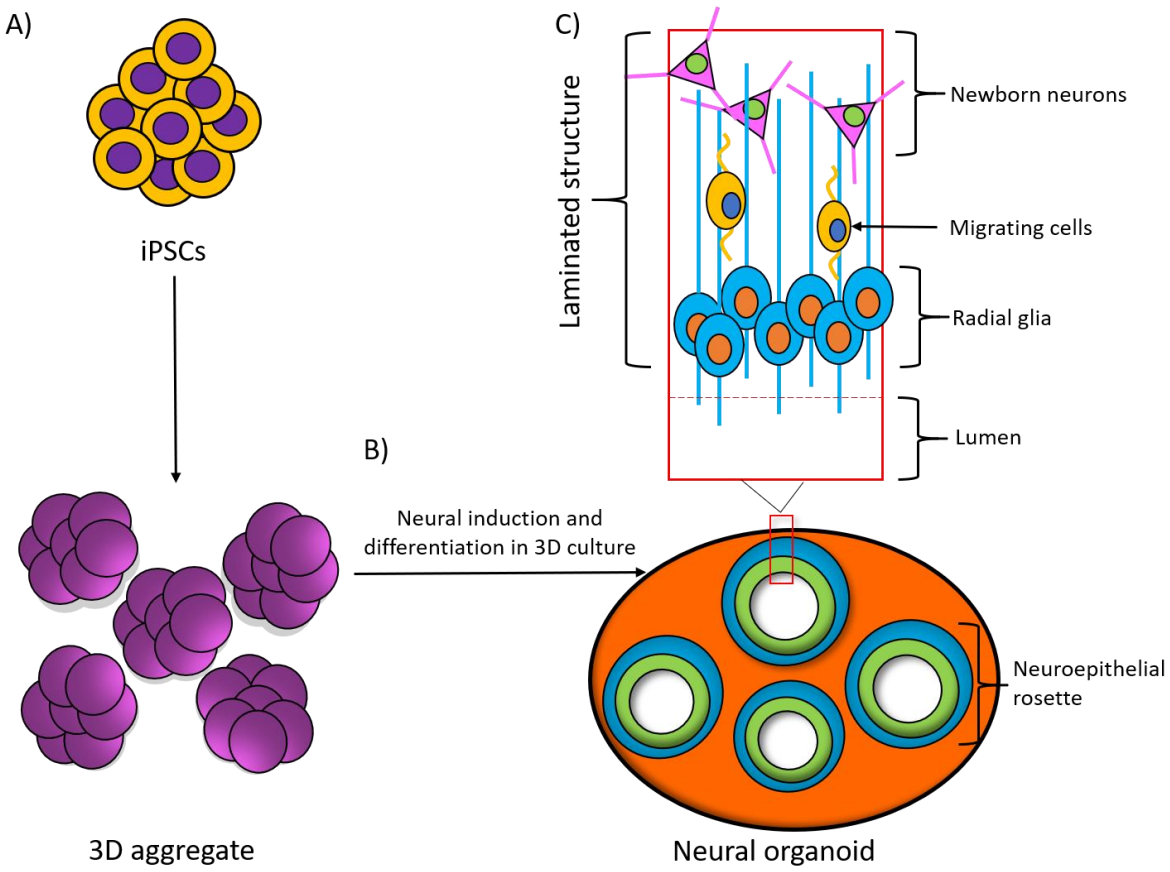

Figure 7.2: 3D culture systems. (A) iPSCs can be spontaneously differentiated within 3D aggregates. (B) 3D aggregates can be further cultured in 3D to develop a neural/cerebral organoid. These organoids recapitulate the developmental processes and structural hierarchy seen in the developing brain. (C) Section of the laminated structure formed within the neural organoid (Grainger et al., 2018).

7.5 Commercial systems

It could be posited that due to the commercial availability of neural cells from iPSC, the generation and co-culturing of individual cell types is redundant. Indeed, there are several benefits to using pre-differentiated neural cultures: these include heterogeneity, presence of all desired cell subtypes and strict quality controls and industrial standards applied. This obviously provides several benefits over the differentiation of cells and batch-to-batch variation that is unavoidable in a research setting, particularly a spontaneous differentiation. However, as these products are commercial outputs, companies are bound by confidentiality with their differentiation methods and methods of mitotic inhibition (if even used). Furthermore, the cost of these cultures is considerable, and quite often, the cells are only suitable for one passage, meaning expansion of cultures for high-throughput testing is incredibly expensive *cf* making ones own cultures. As several companies produce and sell these cultures, this sadly further decreases the likelihood of a 'standard' model system which can be used for screening.

7.6 Concluding remarks

In this thesis, several different culture protocols of human iPSC-derived neurons and astrocytes have been compared, to provide an optimal method for pre-clinical seizure liability testing, which is amenable to high-throughput optical interrogation. It was found that spontaneous differentiation can produce cultures capable of eliciting hyperactive and hypersynchronous bursting activity, typical of seizure-like events, however this method is unreliable and not robust. It was also shown that monocultures of astrocytes and neurons are unsuitable as model systems, and that the interaction between both cell types is necessary for functional maturation, and the ability to respond to diverse neuroactive treatments.

This thesis has provided evidence that co-culturing neurons and astrocytes without mitotic inhibition leads to an overgrowth of glial cells and consequent reductions in cell activity and response to drugs. Therefore, a co-culture model has been produced which controls ratios of neurons and astrocytes to ensure the developing cultures remain constant and responsive. These co-cultures displayed network connectivity and responded to known pro-convulsant conditions with increased activity and synchrony. Preliminary work highlighted the importance of GABAergic interneurons and their ability to form a complete and heterogenous system which can respond to several pro-ictogenic treatments and these are an absolute requirement for *in vitro* neuronal toxicity platforms.

References

Abe, H., & Terasawa, E. (2005). Firing pattern and rapid modulation of activity by estrogen in primate luteinizing hormone releasing hormone-1 neurons. *Endocrinology*, *146*(10), 4312–4320. https://doi.org/10.1210/en.2005-0435

Accardi, M. V., Huang, H., & Authier, S. (2018). Seizure liability assessments using the hippocampal tissue slice: Comparison of non-clinical species. *Journal of Pharmacological and Toxicological Methods*, *93*, 59–68. https://doi.org/10.1016/j.vascn.2017.11.003

Aebersold, M. J., Thompson-Steckel, G., Joutang, A., Schneider, M., Burchert, C., Forró, C., Weydert, S., Han, H., & Vörös, J. (2018). Simple and Inexpensive Paper-Based Astrocyte Co-culture to Improve Survival of Low-Density Neuronal Networks. *Frontiers in Neuroscience*, *12*. https://doi.org/10.3389/fnins.2018.00094

Agulhon, C., Petravicz, J., McMullen, A. B., Sweger, E. J., Minton, S. K., Taves, S. R., Casper, K. B., Fiacco, T. A., & McCarthy, K. D. (2008). What Is the Role of Astrocyte Calcium in Neurophysiology? In *Neuron* (Vol. 59, Issue 6, pp. 932–946). Neuron. https://doi.org/10.1016/j.neuron.2008.09.004

Al-Dalahmah, O., Sosunov, A. A., Shaik, A., Ofori, K., Liu, Y., Vonsattel, J. P., Adorjan, I., Menon, V., & Goldman, J. E. (2020). Single-nucleus RNA-seq identifies Huntington disease astrocyte states. *Acta Neuropathologica Communications*, *8*(1), 19. https://doi.org/10.1186/s40478-020-0880-6

Amin, H., Maccione, A., Marinaro, F., Zordan, S., Nieus, T., & Berdondini, L. (2016). Electrical responses and spontaneous activity of human iPS-derived neuronal networks characterized for 3-month culture with 4096-electrode arrays. *Frontiers in Neuroscience*, *10*(MAR). https://doi.org/10.3389/fnins.2016.00121

Anderson, M. A., Burda, J. E., Ren, Y., Ao, Y., O'Shea, T. M., Kawaguchi, R., Coppola, G., Khakh, B. S., Deming, T. J., & Sofroniew, M. V. (2016). Astrocyte scar formation AIDS central nervous system axon regeneration. *Nature*, *532*(7598), 195–200. https://doi.org/10.1038/nature17623

Anderson, S., & Vanderhaeghen, P. (2014). Cortical neurogenesis from pluripotent stem cells: Complexity emerging from simplicity. In *Current Opinion in Neurobiology* (Vol. 27, pp. 151–157). Elsevier Ltd. https://doi.org/10.1016/j.conb.2014.03.012

Andrews, P. W. (1984). Retinoic acid induces neuronal differentiation of a cloned human embryonal carcinoma cell line in vitro. *Developmental Biology*, *103*(2), 285–293. https://doi.org/10.1016/0012-1606(84)90316-6

Angulo, M. C., Kozlov, A. S., Charpak, S., & Audinat, E. (2004). Glutamate released from glial cells synchronizes neuronal activity in the hippocampus. *Journal of Neuroscience*, *24*(31), 6920–6927. https://doi.org/10.1523/JNEUROSCI.0473-04.2004

Annunziato, L., Boscia, F., & Pignataro, G. (2013). Ionic transporter activity in astrocytes, microglia, and oligodendrocytes during brain ischemia. *Journal of Cerebral Blood Flow and Metabolism : Official Journal of the International Society of Cerebral Blood Flow and Metabolism*, *33*(7), 969–982. https://doi.org/10.1038/jcbfm.2013.44

Authier, S., Arezzo, J., Delatte, M. S., Kallman, M. J., Markgraf, C., Paquette, D., Pugsley, M. K., Ratcliffe, S., Redfern, W. S., Stevens, J., Valentin, J. P., Vargas, H. M., & Curtis, M. J.

(2016). Safety pharmacology investigations on the nervous system: An industry survey. *Journal of Pharmacological and Toxicological Methods*, *81*, 37–46. https://doi.org/10.1016/j.vascn.2016.06.001

Avoli, M., & de Curtis, M. (2011). GABAergic synchronization in the limbic system and its role in the generation of epileptiform activity. In *Progress in Neurobiology* (Vol. 95, Issue 2, pp. 104–132). PMC Canada manuscript submission. https://doi.org/10.1016/j.pneurobio.2011.07.003

Avoli, M., & Jefferys, J. G. R. (2016). Models of drug-induced epileptiform synchronization in vitro. In *Journal of Neuroscience Methods* (Vol. 260, pp. 26–32). Elsevier. https://doi.org/10.1016/j.jneumeth.2015.10.006

Azzarelli, R., Kerloch, T., & Pacary, E. (2015). Regulation of cerebral cortex development by Rho GTPases: Insights from in vivo studies. *Frontiers in Cellular Neuroscience*, *8*(JAN), 445. https://doi.org/10.3389/fncel.2014.00445

Badea, T. C., Badea, T., Goldberg, J., Mao, B., & Yuste, R. (2001). Calcium imaging of epileptiform events with single-cell resolution Melanopsin and ipRGCs View project Cell Type Specification View project Calcium Imaging of Epileptiform Events with Single-Cell Resolution. *Article in Journal of Neurobiology*, *48*(3), 215–227. https://doi.org/10.1002/neu.1052

Bak, M., & Fraser, S. E. (2003). Axon fasciculation and differences in midline kinetics between pioneer and follower axons within commissural fascicles. *Development*, *130*(20), 4999–5008. https://doi.org/10.1242/dev.00713

Bando, Y., Sakamoto, M., Kim, S., Ayzenshtat, I., & Yuste, R. (2019). Comparative Evaluation of Genetically Encoded Voltage Indicators. *Cell Reports*, *26*(3), 802-813.e4. https://doi.org/10.1016/j.celrep.2018.12.088

Bani-Yaghoub, M., Bechberger, J. F., Underhill, T. M., & Naus, C. C. G. (1999). The effects of gap junction blockage on neuronal differentiation of human NTera2/clone D1 cells. *Experimental Neurology*, *156*(1), 16–32. https://doi.org/10.1006/exnr.1998.6950

Bansod, S., Kageyama, R., & Ohtsuka, T. (2017). Hes5 regulates the transition timing of neurogenesis and gliogenesis in mammalian neocortical development. *Development (Cambridge)*, *144*(17), 3156–3167. https://doi.org/10.1242/dev.147256

Baraldi, S., Farrell, F., Benson, J., Diehl, B., Wehner, T., & Kovac, S. (2015). Drop attacks, falls and atonic seizures in the Video-EEG monitoring unit. *Seizure*, *32*, 4–8. https://doi.org/10.1016/j.seizure.2015.08.001

Bardy, C., Van Den Hurk, M., Eames, T., Marchand, C., Hernandez, R. V., Kellogg, M., Gorris, M., Galet, B., Palomares, V., Brown, J., Bang, A. G., Mertens, J., Böhnke, L., Boyer, L., Simon, S., & Gage, F. H. (2015). Neuronal medium that supports basic synaptic functions and activity of human neurons in vitro. *Proceedings of the National Academy of Sciences of the United States of America*, *112*(20), E2725–E2734. https://doi.org/10.1073/pnas.1504393112

Baur, A. M., Gamberger, T. I., Weerda, H. G., Gjuric, M., & Tamm, E. R. (1995). Laminin promotes differentiation, adhesion and proliferation of cell cultures derived from human acoustic nerve schwannoma. *Acta Oto-Laryngologica*, *115*(2), 517–521. https://doi.org/10.3109/00016489509139359

Bedner, P., Dupper, A., Hüttmann, K., Müller, J., Herde, M., Dublin, P., Deshpande, T.,

Schramm, J., Häussler, U., Haas, C., Henneberger, C., Theis, M., & Steinhäuser, C. (2015). Astrocyte uncoupling as a cause of human temporal lobe epilepsy. *Brain : A Journal of Neurology*, *138*. https://doi.org/10.1093/brain/awv067

Ben-Ari, Y., Gaiarsa, J. L., Tyzio, R., & Khazipov, R. (2007). GABA: A pioneer transmitter that excites immature neurons and generates primitive oscillations. In *Physiological Reviews* (Vol. 87, Issue 4, pp. 1215–1284). Physiol Rev. https://doi.org/10.1152/physrev.00017.2006

Benes, F. M., & Berretta, S. (2001). GABAergic interneurons: Implications for understanding schizophrenia and bipolar disorder. *Neuropsychopharmacology*, *25*(1), 1–27. https://doi.org/10.1016/S0893-133X(01)00225-1

Bezzi, P., Carmignoto, G., Pasti, L., Vesce, S., Rossi, D., Rizzini, B. L., Pozzant, T., & Volterra, A. (1998). Prostaglandins stimulate calcium-dependent glutamate release in astrocytes. *Nature*, *391*(6664), 281–285. https://doi.org/10.1038/34651

Bhattacharjee, A., & Kaczmarek, L. K. (2005). For K+ channels, Na+ is the new Ca2+. In *Trends in Neurosciences* (Vol. 28, Issue 8, pp. 422–428). Trends Neurosci. https://doi.org/10.1016/j.tins.2005.06.003

Biedler, J. L., & Schachner, M. (1978). Multiple Neurotransmitter Synthesis by Human Neuroblastoma Cell Lines and Clones. *Cancer Research*, *38*(11 Part 1), 3751–3757.

Binder, D. K., Yao, X., Zador, Z., Sick, T. J., Verkman, A. S., & Manley, G. T. (2006). Increased seizure duration and slowed potassium kinetics in mice lacking aquaporin-4 water channels. *GLIA*, *53*(6), 631–636. https://doi.org/10.1002/glia.20318

Blauwblomme, T., Jiruska, P., & Huberfeld, G. (2014). Mechanisms of ictogenesis. In *International Review of Neurobiology* (Vol. 114, pp. 155–185). Academic Press Inc. https://doi.org/10.1016/B978-0-12-418693-4.00007-8

Bonni, A., Sun, Y., Nadal-Vicens, M., Bhatt, A., Frank, D. A., Rozovsky, I., Stahl, N., Yancopoulos, G. D., & Greenberg, M. E. (1997). Regulation of gliogenesis in the central nervous system by the JAK-STAT signaling pathway. *Science*, *278*(5337), 477–483. https://doi.org/10.1126/science.278.5337.477

Bradley, J. A., Luithardt, H. H., Metea, M. R., & Strock, C. J. (2018). In vitro screening for seizure liability using microelectrode array technology. *Toxicological Sciences*, *163*(1), 240–253. https://doi.org/10.1093/toxsci/kfy029

Broicher, T., Seidenbecher, T., Meuth, P., Munsch, T., Meuth, S. G., Kanyshkova, T., Pape, H. C., & Budde, T. (2007). T-current related effects of antiepileptic drugs and a Ca2+ channel antagonist on thalamic relay and local circuit interneurons in a rat model of absence epilepsy. *Neuropharmacology*, *53*(3), 431–446. https://doi.org/10.1016/j.neuropharm.2007.05.030

Bromfield, E., Cavazos, J., & Sirven, J. (2006). Chapter 1 Basic Mechanisms Underlying Seizures and Epilepsy. *Cerebral Cortex*, 1–11.

Caiazzo, M., Giannelli, S., Valente, P., Lignani, G., Carissimo, A., Sessa, A., Colasante, G., Bartolomeo, R., Massimino, L., Ferroni, S., Settembre, C., Benfenati, F., & Broccoli, V. (2015). Direct conversion of fibroblasts into functional astrocytes by defined transcription factors. *Stem Cell Reports*, *4*(1), 25–36. https://doi.org/10.1016/j.stemcr.2014.12.002

Cain, S. M., & Snutch, T. P. (2013). T-type calcium channels in burst-firing, network synchrony,

and epilepsy. In *Biochimica et Biophysica Acta - Biomembranes* (Vol. 1828, Issue 7, pp. 1572–1578). Biochim Biophys Acta. https://doi.org/10.1016/j.bbamem.2012.07.028

Cammarota, M., Losi, G., Chiavegato, A., Zonta, M., & Carmignoto, G. (2013). Fast spiking interneuron control of seizure propagation in a cortical slice model of focal epilepsy. *Journal of Physiology*, *591*(4), 807–822. https://doi.org/10.1113/jphysiol.2012.238154

Carmignoto, G., & Haydon, P. G. (2012). Astrocyte calcium signaling and epilepsy. In *GLIA* (Vol. 60, Issue 8, pp. 1227–1233). Glia. https://doi.org/10.1002/glia.22318

Chambers, S. M., Fasano, C. A., Papapetrou, E. P., Tomishima, M., Sadelain, M., & Studer, L. (2009). Highly efficient neural conversion of human ES and iPS cells by dual inhibition of SMAD signaling. *Nature Biotechnology*, *27*(3), 275–280. https://doi.org/10.1038/nbt.1529

Chamma, I., Chevy, Q., Poncer, J. C., & Lévi, S. (2012). Role of the neuronal K-Cl co-transporter KCC2 in inhibitory and excitatory neurotransmission. *Frontiers in Cellular Neuroscience*, *6*(JANUARY). https://doi.org/10.3389/fncel.2012.00005

Chandrasekaran, A., Avci, H. X., Ochalek, A., Rösingh, L. N., Molnár, K., László, L., Bellák, T., Téglási, A., Pesti, K., Mike, A., Phanthong, P., Bíró, O., Hall, V., Kitiyanant, N., Krause, K. H., Kobolák, J., & Dinnyés, A. (2017). Comparison of 2D and 3D neural induction methods for the generation of neural progenitor cells from human induced pluripotent stem cells. *Stem Cell Research*, *25*, 139–151. https://doi.org/10.1016/j.scr.2017.10.010

Chang, P., Orabi, B., Deranieh, R. M., Dham, M., Hoeller, O., Shimshoni, J. A., Yagen, B., Bialer, M., Greenberg, M. L., Walker, M. C., & Williams, R. S. B. (2012). The antiepileptic drug valproic acid and other medium-chain fatty acids acutely reduce phosphoinositide levels independently of inositol in Dictyostelium. *DMM Disease Models and Mechanisms*, *5*(1), 115–124. https://doi.org/10.1242/dmm.008029

Chang, P., Walker, M. C., & Williams, R. S. B. (2014). Seizure-induced reduction in PIP3 levels contributes to seizure-activity and is rescued by valproic acid. *Neurobiology of Disease*, *62*(100), 296–306. https://doi.org/10.1016/j.nbd.2013.10.017

Chaudhry, F. A., Reimer, R. J., Bellocchio, E. E., Danbolt, N. C., Osen, K. K., Edwards, R. H., & Storm-Mathisen, J. (1998). The vesicular GABA transporter, VGAT, localizes to synaptic vesicles in sets of glycinergic as well as GABAergic neurons. *Journal of Neuroscience*, *18*(23), 9733–9750. https://doi.org/10.1523/jneurosci.18-23-09733.1998

Chen, P. S., Peng, G. S., Li, G., Yang, S., Wu, X., Wang, C. C., Wilson, B., Lu, R. B., Gean, P. W., Chuang, D. M., & Hong, J. S. (2006). Valproate protects dopaminergic neurons in midbrain neuron/glia cultures by stimulating the release of neurotrophic factors from astrocytes. *Molecular Psychiatry*, *11*(12), 1116–1125. https://doi.org/10.1038/sj.mp.4001893

Chen, Yucui, Stevens, B., Chang, J., Milbrandt, J., Barres, B. A., & Hell, J. W. (2008). NS21: Re-defined and modified supplement B27 for neuronal cultures. *Journal of Neuroscience Methods*, *171*(2), 239–247. https://doi.org/10.1016/j.jneumeth.2008.03.013

Chen, Yuncai, Dubé, C. M., Rice, C. J., & Baram, T. Z. (2008). Rapid loss of dendritic spines after stress involves derangement of spine dynamics by corticotropin-releasing hormone. *Journal of Neuroscience*, *28*(11), 2903–2911. https://doi.org/10.1523/JNEUROSCI.0225-08.2008

Cheng, C., Fass, D. M., Folz-Donahue, K., Macdonald, M. E., & Haggarty, S. J. (2017). Highly

expandable human iPS Cell-Derived neural progenitor cells (NPC) and neurons for central nervous system disease modeling and High-Throughput screening. *Current Protocols in Human Genetics*, *2017*, 1–21. https://doi.org/10.1002/cphg.33

Choi, D. W. (1987). Ionic dependence of glutamate neurotoxicity. *Journal of Neuroscience*, *7*(2), 369–379. https://doi.org/10.1523/jneurosci.07-02-00369.1987

Christopherson, K. S., Ullian, E. M., Stokes, C. C. A., Mullowney, C. E., Hell, J. W., Agah, A., Lawler, J., Mosher, D. F., Bornstein, P., & Barres, B. A. (2005). Thrombospondins are astrocyte-secreted proteins that promote CNS synaptogenesis. *Cell*, *120*(3), 421–433. https://doi.org/10.1016/j.cell.2004.12.020

Chrysafides, S. M., & Sharma, S. (2019). Physiology, Resting Potential. In *StatPearls*. StatPearls Publishing. http://www.ncbi.nlm.nih.gov/pubmed/30855922

Cicardo, V. H., & Torino, A. (1942). Release of potassium by the brain of the dog during electrical stimulation. In *Science* (Vol. 95, Issue 2477, p. 625). https://doi.org/10.1126/science.95.2477.625-a

Clark, A. J., Kaller, M. S., Galino, J., Willison, H. J., Rinaldi, S., & Bennett, D. L. H. (2017). Co-cultures with stem cell-derived human sensory neurons reveal regulators of peripheral myelination. *Brain*, *140*(4), 898–913. https://doi.org/10.1093/brain/awx012

Colas, J. F., & Schoenwolf, G. C. (2001). Towards a cellular and molecular understanding of neurulation. In *Developmental Dynamics* (Vol. 221, Issue 2, pp. 117–145). Dev Dyn. https://doi.org/10.1002/dvdy.1144

Collins, A. R., Annangi, B., Rubio, L., Marcos, R., Dorn, M., Merker, C., Estrela-Lopis, I., Cimpan, M. R., Ibrahim, M., Cimpan, E., Ostermann, M., Sauter, A., Yamani, N. El, Shaposhnikov, S., Chevillard, S., Paget, V., Grall, R., Delic, J., de-Cerio, F. G., … Dusinska, M. (2017). High throughput toxicity screening and intracellular detection of nanomaterials. In *Wiley Interdisciplinary Reviews: Nanomedicine and Nanobiotechnology* (Vol. 9, Issue 1). Wiley-Blackwell. https://doi.org/10.1002/wnan.1413

Cornelissen, F., … P. V.-J. of, & 2013, undefined. (2013). Quantitation of chronic and acute treatment effects on neuronal network activity using image and signal analysis: toward a high-content assay. *Journals.Sagepub.Com*, *18*(7), 807–819. https://doi.org/10.1177/1087057113486518

Coulter, D. A., & Steinhäuser, C. (2015). Role of astrocytes in epilepsy. *Cold Spring Harbor Perspectives in Medicine*, *5*(3). https://doi.org/10.1101/cshperspect.a022434

Crowe, J. A., El-Tamer, A., Nagel, D., Koroleva, A. V., Madrid-Wolff, J., Olarte, O. E., Sokolovsky, S., Estevez-Priego, E., Ludl, A.-A., Soriano, J., Loza-Alvarez, P., Chichkov, B. N., Hill, E. J., Parri, H. R., & Rafailov, E. U. (2020). Development of two-photon polymerised scaffolds for optical interrogation and neurite guidance of human iPSC-derived cortical neuronal networks. *Lab on a Chip*, *20*(10), 1792–1806. https://doi.org/10.1039/c9lc01209e

Dallérac, G., Chever, O., & Rouach, N. (2013). How do astrocytes shape synaptic transmission? Insights from electrophysiology. In *Frontiers in Cellular Neuroscience* (Vol. 7, Issue OCT). Frontiers Media SA. https://doi.org/10.3389/fncel.2013.00159

Daneman, R., & Prat, A. (2015). The blood–brain barrier. *Cold Spring Harbor Perspectives in Biology*, *7*(1). https://doi.org/10.1101/cshperspect.a020412

Darville, H., Poulet, A., Rodet-Amsellem, F., Chatrousse, L., Pernelle, J., Boissart, C., Héron, D., Nava, C., Perrier, A., Jarrige, M., Cogé, F., Millan, M. J., Bourgeron, T., Peschanski, M.,

Delorme, R., & Benchoua, A. (2016). Human Pluripotent Stem Cell-derived Cortical Neurons for High Throughput Medication Screening in Autism: A Proof of Concept Study in SHANK3 Haploinsufficiency Syndrome. *EBioMedicine*, *9*, 293–305. https://doi.org/10.1016/j.ebiom.2016.05.032

Davidoff, R. A., & Aprison, M. H. (1969). Picrotoxin antagonism of the inhibition of interneurons by glycine. *Life Sciences*, *8*(1), 107–112. https://doi.org/10.1016/0024-3205(69)90299-9

de Curtis, M., Uva, L., Gnatkovsky, V., & Librizzi, L. (2018). Potassium dynamics and seizures: Why is potassium ictogenic? In *Epilepsy Research* (Vol. 143, pp. 50–59). Elsevier B.V. https://doi.org/10.1016/j.eplepsyres.2018.04.005

de Graaf-Peters, V. B., & Hadders-Algra, M. (2006). Ontogeny of the human central nervous system: What is happening when? *Early Human Development*, *82*(4), 257–266. https://doi.org/10.1016/j.earlhumdev.2005.10.013

de Rus Jacquet, A. (2019). Preparation and Co-Culture of iPSC-Derived Dopaminergic Neurons and Astrocytes. *Current Protocols in Cell Biology*, *85*(1). https://doi.org/10.1002/cpcb.98

Debanne, D., Thompson, S. M., & Gähwiler, B. H. (2006). A brief period of epileptiform activity strengthens excitatory synapses in the rat hippocampus in vitro. *Epilepsia*, *47*(2), 247–256. https://doi.org/10.1111/j.1528-1167.2006.00416.x

Dhandapani, K. M., Mahesh, V. B., & Brann, D. W. (2003). Astrocytes and Brain Function: Implications for Reproduction. *Experimental Biology and Medicine*, *228*(3), 253–260. https://doi.org/10.1177/153537020322800303

Di Cristo, G., Awad, P. N., Hamidi, S., & Avoli, M. (2018). KCC2, epileptiform synchronization, and epileptic disorders. In *Progress in Neurobiology* (Vol. 162, pp. 1–16). Elsevier Ltd. https://doi.org/10.1016/j.pneurobio.2017.11.002

Diaz Verdugo, C., Myren-Svelstad, S., Aydin, E., Van Hoeymissen, E., Deneubourg, C., Vanderhaeghe, S., Vancraeynest, J., Pelgrims, R., Cosacak, M. I., Muto, A., Kizil, C., Kawakami, K., Jurisch-Yaksi, N., & Yaksi, E. (2019). Glia-neuron interactions underlie state transitions to generalized seizures. *Nature Communications*, *10*(1), 1–13. https://doi.org/10.1038/s41467-019-11739-z

Dichter, M. A. (2009). Emerging Concepts in the Pathogenesis of Epilepsy and Epileptogenesis. In *Archives of Neurology* (Vol. 66, Issue 4, pp. 443–447). https://doi.org/10.1001/archneurol.2009.10

Dichter, M. A., & Brodie, M. J. (1996). New antiepileptic drugs. In *New England Journal of Medicine* (Vol. 334, Issue 24, pp. 1583–1590). N Engl J Med. https://doi.org/10.1056/NEJM199606133342407

Dichter, M. A., & Pollard, J. (2006). Cell Culture Models for Studying Epilepsy. In *Models of Seizures and Epilepsy* (pp. 23–34). Academic Press. https://doi.org/10.1016/B978-012088554-1/50005-0

Dinocourt, C., Petanjek, Z., Freund, T. F., Ben-Ari, Y., & Esclapez, M. (2003). Loss of interneurons innervating pyramidal cell dendrites and axon initial segments in the CA1 region of the hippocampus following pilocarpine-induced seizures. *Journal of Comparative Neurology*, *459*(4), 407–425. https://doi.org/10.1002/cne.10622

Dravet, C., & Bureau, M. (1981). L'epilepsie myoclonique benigne du nourrisson. *Revue d'Electroencephalographie et de Neurophysiologie Clinique*, *11*(3–4), 438–444.

https://doi.org/10.1016/S0370-4475(81)80083-4

Duy, P. Q., David, W. B., & Kahle, K. T. (2019). Identification of KCC2 Mutations in Human Epilepsy Suggests Strategies for Therapeutic Transporter Modulation. *Frontiers in Cellular Neuroscience*, *13*. https://doi.org/10.3389/fncel.2019.00515

Easter, A., Bell, M. E., Damewood, J. R., Redfern, W. S., Valentin, J. P., Winter, M. J., Fonck, C., & Bialecki, R. A. (2009). Approaches to seizure risk assessment in preclinical drug discovery. *Drug Discovery Today*, *14*(17–18), 876–884. https://doi.org/10.1016/j.drudis.2009.06.003

Easter, A., Sharp, T. H., Valentin, J. P., & Pollard, C. E. (2007). Pharmacological validation of a semi-automated in vitro hippocampal brain slice assay for assessment of seizure liability. *Journal of Pharmacological and Toxicological Methods*, *56*(2), 223–233. https://doi.org/10.1016/j.vascn.2007.04.008

Eid, T., Tu, N., Lee, T. S. W., & Lai, J. C. K. (2013). Regulation of astrocyte glutamine synthetase in epilepsy. In *Neurochemistry International* (Vol. 63, Issue 7, pp. 670–681). https://doi.org/10.1016/j.neuint.2013.06.008

El, Y. B., Kanner, S., Barzilai, A., & Hanein, Y. (2018). Activity changes in neuron-Astrocyte networks in culture under the effect of norepinephrine. *PLoS ONE*, *13*(10). https://doi.org/10.1371/journal.pone.0203761

Elkabetz, Y., & Studer, L. (2008). Human ESC-derived neural rosettes and neural stem cell progression. *Cold Spring Harbor Symposia on Quantitative Biology*, *73*, 377–387. https://doi.org/10.1101/sqb.2008.73.052

Englund, M., Hyllienmark, L., & Brismar, T. (2011). Effect of valproate, lamotrigine and levetiracetam on excitability and firing properties of CA1 neurons in rat brain slices. *Cellular and Molecular Neurobiology*, *31*(4), 645–652. https://doi.org/10.1007/s10571-011-9660-y

Escayg, A., & Goldin, A. L. (2010). Sodium channel SCN1A and epilepsy: Mutations and mechanisms. In *Epilepsia* (Vol. 51, Issue 9, pp. 1650–1658). Blackwell Publishing Inc. https://doi.org/10.1111/j.1528-1167.2010.02640.x

Fan, J., Thalody, G., Kwagh, J., Burnett, E., Shi, H., Lewen, G., Chen, S. J., & Levesque, P. (2019). Assessing seizure liability using multi-electrode arrays (MEA). *Toxicology in Vitro*, *55*, 93–100. https://doi.org/10.1016/j.tiv.2018.12.001

Feldberg, W., & Sherwood, S. L. (1957). Effects of calcium and potassium injected into the cerebral ventricles of the cat. *The Journal of Physiology*, *139*(3), 408–416. https://doi.org/10.1113/jphysiol.1957.sp005901

Fiacco, T. A., Agulhon, C., Taves, S. R., Petravicz, J., Casper, K. B., Dong, X., Chen, J., & McCarthy, K. D. (2007). Selective Stimulation of Astrocyte Calcium In Situ Does Not Affect Neuronal Excitatory Synaptic Activity. *Neuron*, *54*(4), 611–626. https://doi.org/10.1016/j.neuron.2007.04.032

Fisher, R. S. (1989). Animal models of the epilepsies. In *Brain Research Reviews* (Vol. 14, Issue 3, pp. 245–278). Brain Res Brain Res Rev. https://doi.org/10.1016/0165-0173(89)90003-9

Fisher, R. S., Cross, J. H., French, J. A., Higurashi, N., Hirsch, E., Jansen, F. E., Lagae, L., Moshé, S. L., Peltola, J., Roulet Perez, E., Scheffer, I. E., & Zuberi, S. M. (2017). Operational classification of seizure types by the International League Against Epilepsy: Position Paper of the ILAE Commission for Classification and Terminology. *Epilepsia*, *58*(4), 522–

530. https://doi.org/10.1111/epi.13670

Fisher, R. S., Scharfman, H. E., & deCurtis, M. (2014). How Can We Identify Ictal and Interictal Abnormal Activity? In *Advances in experimental medicine and biology* (Vol. 813, pp. 3–23). NIH Public Access. https://doi.org/10.1007/978-94-017-8914-1_1

Fisher, R. S., Van Emde Boas, W., Blume, W., Elger, C., Genton, P., Lee, P., & Engel, J. (2005). Epileptic seizures and epilepsy: Definitions proposed by the International League Against Epilepsy (ILAE) and the International Bureau for Epilepsy (IBE). In *Epilepsia* (Vol. 46, Issue 4, pp. 470–472). https://doi.org/10.1111/j.0013-9580.2005.66104.x

Foo, L. C. (2013). Purification and culture of astrocytes. *Cold Spring Harbor Protocols*, *8*(6), 485–487. https://doi.org/10.1101/pdb.top070912

Franceschetti, S., Hamon, B., & Heinemann, U. (1986). The action of valproate on spontaneous epileptiform activity in the absence of synaptic transmission and on evoked changes in [Ca2+]0 and [K+]0 in the hippocampal slice. *Brain Research*, *386*(1–2), 1–11. https://doi.org/10.1016/0006-8993(86)90135-6

Fröhlich, F., Bazhenov, M., Iragui-Madoz, V., & Sejnowski, T. J. (2008). Reviews: Potassium dynamics in the epileptic cortex: New insights on an old topic. In *Neuroscientist* (Vol. 14, Issue 5, pp. 422–433). Howard Hughes Medical Institute. https://doi.org/10.1177/1073858408317955

Funck, V. R., Ribeiro, L. R., Pereira, L. M., de Oliveira, C. V., Grigoletto, J., Della-Pace, I. D., Fighera, M. R., Royes, L. F. F., Furian, A. F., Larrick, J. W., & Oliveira, M. S. (2015). Contrasting effects of Na+, K+-ATPase activation on seizure activity in acute versus chronic models. *Neuroscience*, *298*, 171–179. https://doi.org/10.1016/j.neuroscience.2015.04.031

Gabriel, S., Njunting, M., Pomper, J. K., Merschhemke, M., Sanabria, E. R. G., Eilers, A., Kivi, A., Zeller, M., Meencke, H. J., Cavalheiro, E. A., Heinemann, U., & Lehmann, T. N. (2004). Stimulus and potassium-induced epileptiform activity in the human dentate gyrus from patients with and without hippocampal sclerosis. *Journal of Neuroscience*, *24*(46), 10416–10430. https://doi.org/10.1523/JNEUROSCI.2074-04.2004

García-Berthou, E., & Alcaraz, C. (2004). Incongruence between test statistics and P values in medical papers. *BMC Medical Research Methodology*, *4*(1), 13. https://doi.org/10.1186/1471-2288-4-13

Ghodke-Puranik, Y., Thorn, C. F., Lamba, J. K., Leeder, J. S., Song, W., Birnbaum, A. K., Altman, R. B., & Klein, T. E. (2013). Valproic acid pathway: Pharmacokinetics and pharmacodynamics. *Pharmacogenetics and Genomics*, *23*(4), 236–241. https://doi.org/10.1097/FPC.0b013e32835ea0b2

Gilad, G. M., & Gilad, V. H. (1987). Detachment of cultured neurons from substratum by astrocytic membrane-associated activity. Implications for CNS regeneration? *International Journal of Developmental Neuroscience*, *5*(2). https://doi.org/10.1016/0736-5748(87)90053-0

Giniger, E. (2012). Notch signaling and neural connectivity. In *Current Opinion in Genetics and Development* (Vol. 22, Issue 4, pp. 339–346). NIH Public Access. https://doi.org/10.1016/j.gde.2012.04.003

Gonzalez-Perez, O., Gutierrez-Fernandez, F., Lopez-Virgen, V., Collas-Aguilar, J., Quinones-Hinojosa, A., & Garcia-Verdugo, J. M. (2012). Immunological regulation of neurogenic

niches in the adult brain. *Neuroscience*, *226*, 270–281. https://doi.org/10.1016/j.neuroscience.2012.08.053

Gonzalez-Sulser, A., Wang, J., Motamedi, G. K., Avoli, M., Vicini, S., & Dzakpasu, R. (2011). The 4-aminopyridine in vitro epilepsy model analyzed with a perforated multi-electrode array. *Neuropharmacology*, *60*(7–8), 1142–1153. https://doi.org/10.1016/j.neuropharm.2010.10.007

González, O. C., Shiri, Z., Krishnan, G. P., Myers, T. L., Williams, S., Avoli, M., & Bazhenov, M. (2018). Role of KCC2-dependent potassium efflux in 4-Aminopyridine-induced Epileptiform synchronization. *Neurobiology of Disease*, *109*(Pt A), 137–147. https://doi.org/10.1016/j.nbd.2017.10.011

Goodwani, S., Saternos, H., Alasmari, F., & Sari, Y. (2017). Metabotropic and ionotropic glutamate receptors as potential targets for the treatment of alcohol use disorder. In *Neuroscience and Biobehavioral Reviews* (Vol. 77, pp. 14–31). Elsevier Ltd. https://doi.org/10.1016/j.neubiorev.2017.02.024

Göttlicher, M., Minucci, S., Zhu, P., Krämer, O. H., Schimpf, A., Giavara, S., Sleeman, J. P., Lo Coco, F., Nervi, C., Pelicci, P. G., & Heinzel, T. (2001). Valproic acid defines a novel class of HDAC inhibitors inducing differentiation of transformed cells. *The EMBO Journal*, *20*(24), 6969–6978. https://doi.org/10.1093/emboj/20.24.6969

Graham, V., Khudyakov, J., Ellis, P., & Pevny, L. (2003). SOX2 functions to maintain neural progenitor identity. *Neuron*, *39*(5), 749–765. https://doi.org/10.1016/S0896-6273(03)00497-5

Grainger, A. I., King, M. C., Nagel, D. A., Parri, H. R., Coleman, M. D., & Hill, E. J. (2018). In vitro models for seizure-liability testing using induced pluripotent stem cells. *Frontiers in Neuroscience*, *12*(AUG), 590. https://doi.org/10.3389/fnins.2018.00590

Grasse, D. W., Karunakaran, S., & Moxon, K. A. (2013). Neuronal synchrony and the transition to spontaneous seizures. *Experimental Neurology*, *248*, 72–84. https://doi.org/10.1016/j.expneurol.2013.05.004

Grienberger, C., & Konnerth, A. (2012). Imaging Calcium in Neurons. In *Neuron* (Vol. 73, Issue 5, pp. 862–885). https://doi.org/10.1016/j.neuron.2012.02.011

Gross, R. E., Mehler, M. F., Mabie, P. C., Zang, Z., Santschi, L., & Kessler, J. A. (1996). Bone morphogenetic proteins promote astroglial lineage commitment by mammalian subventricular zone progenitor cells. *Neuron*, *17*(4), 595–606. https://doi.org/10.1016/S0896-6273(00)80193-2

Gunhanlar, N., Shpak, G., van der Kroeg, M., Gouty-Colomer, L. A., Munshi, S. T., Lendemeijer, B., Ghazvini, M., Dupont, C., Hoogendijk, W. J. G., Gribnau, J., de Vrij, F. M. S., & Kushner, S. A. (2017). A simplified protocol for differentiation of electrophysiologically mature neuronal networks from human induced pluripotent stem cells. *Molecular Psychiatry*. https://doi.org/10.1038/mp.2017.56

Gutiérrez, R., & Heinemann, U. (1999). Synaptic reorganization in explanted cultures of rat hippocampus. *Brain Research*, *815*(2), 304–316. https://doi.org/10.1016/S0006-8993(98)01101-9

Gutman, G. A., Chandy, K. G., Grissmer, S., Lazdunski, M., Mckinnon, D., Pardo, L. A., Robertson, G. A., Rudy, B., Sanguinetti, M. C., Stühmer, W., & Wang, X. (2005). International Union of Pharmacology. LIII. Nomenclature and molecular relationships of

voltage-gated potassium channels. In *Pharmacological Reviews* (Vol. 57, Issue 4, pp. 473–508). Pharmacol Rev. https://doi.org/10.1124/pr.57.4.10

Halassa, M. M., & Haydon, P. G. (2010). Integrated Brain Circuits: Astrocytic Networks Modulate Neuronal Activity and Behavior. *Annual Review of Physiology*, *72*(1), 335–355. https://doi.org/10.1146/annurev-physiol-021909-135843

Hanaya, R., & Arita, K. (2016). The new antiepileptic drugs: Their neuropharmacology and clinical indications. In *Neurologia Medico-Chirurgica* (Vol. 56, Issue 5, pp. 205–220). Japan Neurosurgical Society. https://doi.org/10.2176/nmc.ra.2015-0344

Hedegaard, A. (2019). *Using human induced pluripotent stem cells to reveal astrocyte-neuron interactions in health and disease*. Oxford.

Hedrich, U. B. S., Liautard, C., Kirschenbaum, D., Pofahl, M., Lavigne, J., Liu, Y., Theiss, S., Slotta, J., Escayg, A., Dihné, M., Beck, H., Mantegazza, M., & Lerche, H. (2014). Impaired action potential initiation in GABAergic interneurons causes hyperexcitable networks in an epileptic mouse model carrying a human Nav1.1 mutation. *Journal of Neuroscience*, *34*(45), 14874–14889. https://doi.org/10.1523/JNEUROSCI.0721-14.2014

Herculano-Houzel, S. (2014). The glia/neuron ratio: How it varies uniformly across brain structures and species and what that means for brain physiology and evolution. In *GLIA* (Vol. 62, Issue 9, pp. 1377–1391). John Wiley and Sons Inc. https://doi.org/10.1002/glia.22683

Herzog, B., Pellet-Many, C., Britton, G., Hartzoulakis, B., & Zachary, I. C. (2011). VEGF binding to NRP1 is essential for VEGF stimulation of endothelial cell migration, complex formation between NRP1 and VEGFR2, and signaling via FAK Tyr407 phosphorylation. *Molecular Biology of the Cell*, *22*(15), 2766–2776. https://doi.org/10.1091/mbc.E09-12-1061

Hill, E. J., Jiménez-González, C., Tarczyluk, M., Nagel, D. A., Coleman, M. D., & Parri, H. R. (2012). NT2 derived neuronal and astrocytic network signalling. *PLoS ONE*, *7*(5). https://doi.org/10.1371/journal.pone.0036098

Hill, E., Nagel, D., Parri, R., & Coleman, M. (2016). Stem cell-derived astrocytes: are they physiologically credible? *Journal of Physiology*, *594*(22), 6595–6606. https://doi.org/10.1113/JP270658

Home Office. (2018). *Annual statistics of scientific procedures on living animals: Great Britain 2018*. https://www.gov.uk/government/uploads/system/uploads/attachment_data/file/327854/spanimals13.pdf

Hongo, Y., Takasu, K., Ikegaya, Y., Hasegawa, M., Sakaguchi, G., & Ogawa, K. (2015). Heterogeneous effects of antiepileptic drugs in an in vitro epilepsy model - a functional multineuron calcium imaging study. *European Journal of Neuroscience*, *42*(2), 1818–1829. https://doi.org/10.1111/ejn.12945

Hsiao, M. C., Yu, P. N., Song, D., Liu, C. Y., Heck, C. N., Millett, D., & Berger, T. W. (2015). An in vitro seizure model from human hippocampal slices using multi-electrode arrays. *Journal of Neuroscience Methods*, *244*, 154–163. https://doi.org/10.1016/j.jneumeth.2014.09.010

Hubbard, J. A., & Binder, D. K. (2016). Astrocytes and Epilepsy. In *Astrocytes and Epilepsy*. Elsevier Inc. https://doi.org/10.1016/C2014-0-03100-0

Hubbard, J. A., Hsu, M. S., Seldin, M. M., & Binder, D. K. (2015). Expression of the astrocyte water channel aquaporin-4 in the mouse brain. *ASN Neuro*, *7*(5), 175909141560548. https://doi.org/10.1177/1759091415605486

Huberfeld, G., Blauwblomme, T., & Miles, R. (2015). Hippocampus and epilepsy: Findings from human tissues. *Revue Neurologique*, *171*(3), 236–251. https://doi.org/10.1016/j.neurol.2015.01.563

Hyvärinen, T., Hyysalo, A., Kapucu, F. E., Aarnos, L., Vinogradov, A., Eglen, S. J., Ylä-Outinen, L., & Narkilahti, S. (2019). Functional characterization of human pluripotent stem cell-derived cortical networks differentiated on laminin-521 substrate: comparison to rat cortical cultures. *Scientific Reports*, *9*(1), 1–15. https://doi.org/10.1038/s41598-019-53647-8

ICH. (2000). INTERNATIONAL CONFERENCE ON HARMONISATION OF TECHNICAL REQUIREMENTS FOR REGISTRATION OF PHARMACEUTICALS FOR HUMAN USE. *Database.Ich.Org*. https://database.ich.org/sites/default/files/S7A_Guideline.pdf

Igelström, K. M., Shirley, C. H., & Heyward, P. M. (2011). Low-magnesium medium induces epileptiform activity in mouse olfactory bulb slices. *Journal of Neurophysiology*, *106*(5), 2593–2605. https://doi.org/10.1152/jn.00601.2011

Ikegaya, Y., Le Bon-Jego, M., & Yuste, R. (2005). *Large-scale imaging of cortical network activity with calcium indicators*. https://doi.org/10.1016/j.neures.2005.02.004

Isaev, D., Ivanchick, G., Khmyz, V., Isaeva, E., Savrasova, A., Krishtal, O., Holmes, G. L., & Maximyuk, O. (2012). Surface charge impact in low-magnesium model of seizure in rat hippocampus. *Journal of Neurophysiology*, *107*(1), 417–423. https://doi.org/10.1152/jn.00574.2011

Ishii, M. N., Yamamoto, K., Shoji, M., Asami, A., & Kawamata, Y. (2017). Human induced pluripotent stem cell (hiPSC)-derived neurons respond to convulsant drugs when co-cultured with hiPSC-derived astrocytes. *Toxicology*, *389*, 130–138. https://doi.org/10.1016/j.tox.2017.06.010

Jana, M., Jana, A., Pal, U., & Pahan, K. (2007). A simplified method for isolating highly purified neurons, oligodendrocytes, astrocytes, and microglia from the same human fetal brain tissue. *Neurochemical Research*, *32*(12), 2015–2022. https://doi.org/10.1007/s11064-007-9340-y

Jiang, C., & Haddad, G. G. (1991). Effect of anoxia on intracellular and extracellular potassium activity in hypoglossal neurons in vitro. *Journal of Neurophysiology*, *66*(1), 103–111. https://doi.org/10.1152/jn.1991.66.1.103

Jiruska, P., de Curtis, M., Jefferys, J. G. R., Schevon, C. A., Schiff, S. J., & Schindler, K. (2013). Synchronization and desynchronization in epilepsy: Controversies and hypotheses. In *Journal of Physiology* (Vol. 591, Issue 4, pp. 787–797). https://doi.org/10.1113/jphysiol.2012.239590

Johannessen, C. U., & Johannessen, S. I. (2003). Valproate: Past, present, and future. In *CNS Drug Reviews* (Vol. 9, Issue 2, pp. 199–216). John Wiley & Sons, Ltd. https://doi.org/10.1111/j.1527-3458.2003.tb00249.x

Johnstone, A. F. M., Gross, G. W., Weiss, D. G., Schroeder, O. H. U., Gramowski, A., & Shafer, T. J. (2010). Microelectrode arrays: A physiologically based neurotoxicity testing platform for the 21st century. In *NeuroToxicology* (Vol. 31, Issue 4, pp. 331–350).

https://doi.org/10.1016/j.neuro.2010.04.001

Jones, E. V., Cook, D., & Murai, K. K. (2012). A neuron-astrocyte co-culture system to investigate astrocyte-secreted factors in mouse neuronal development. *Methods in Molecular Biology*, *814*, 341–352. https://doi.org/10.1007/978-1-61779-452-0_22

Jung, Y. W., Hysolli, E., Kim, K. Y., Tanaka, Y., & Park, I. H. (2012). Human induced pluripotent stem cells and neurodegenerative disease: Prospects for novel therapies. In *Current Opinion in Neurology* (Vol. 25, Issue 2, pp. 125–130). https://doi.org/10.1097/WCO.0b013e3283518226

Kasteel, E. E. J., & Westerink, R. H. S. (2017). Comparison of the acute inhibitory effects of Tetrodotoxin (TTX) in rat and human neuronal networks for risk assessment purposes. *Toxicology Letters*, *270*, 12–16. https://doi.org/10.1016/j.toxlet.2017.02.014

Kayama, T., Suzuki, I., Odawara, A., Sasaki, T., & Ikegaya, Y. (2018). Temporally coordinated spiking activity of human induced pluripotent stem cell-derived neurons co-cultured with astrocytes. *Biochemical and Biophysical Research Communications*, *495*(1), 1028–1033. https://doi.org/10.1016/j.bbrc.2017.11.115

Khakh, B. S., & McCarthy, K. D. (2015). Astrocyte calcium signaling: From observations to functions and the challenges therein. *Cold Spring Harbor Perspectives in Biology*, *7*(4). https://doi.org/10.1101/cshperspect.a020404

Kim, S., Lehtinen, M. K., Sessa, A., Zappaterra, M. W., Cho, S. H., Gonzalez, D., Boggan, B., Austin, C. A., Wijnholds, J., Gambello, M. J., Malicki, J., LaMantia, A. S., Broccoli, V., & Walsh, C. A. (2010). The Apical Complex Couples Cell Fate and Cell Survival to Cerebral Cortical Development. *Neuron*, *66*(1), 69–84. https://doi.org/10.1016/j.neuron.2010.03.019

Kim, T. G., Yao, R., Monnell, T., Cho, J. H., Vasudevan, A., Koh, A., Peeyush, K. T., Moon, M., Datta, D., Bolshakov, V. Y., Kim, K. S., & Chung, S. (2014). Efficient specification of interneurons from human pluripotent stem cells by dorsoventral and rostrocaudal modulation. *Stem Cells*, *32*(7), 1789–1804. https://doi.org/10.1002/stem.1704

Kirwan, P., Turner-Bridger, B., Peter, M., Momoh, A., Arambepola, D., Robinson, H. P. C., & Livesey, F. J. (2015). Development and function of human cerebral cortex neural networks from pluripotent stem cells in vitro. *Development (Cambridge)*, *142*(18), 3178–3187. https://doi.org/10.1242/dev.123851

Kitchen, C. M. R. (2009). Nonparametric vs Parametric Tests of Location in Biomedical Research. In *American Journal of Ophthalmology* (Vol. 147, Issue 4, pp. 571–572). NIH Public Access. https://doi.org/10.1016/j.ajo.2008.06.031

Klaft, Z. J., Hollnagel, J. O., Salar, S., Calişkan, G., Schulz, S. B., Schneider, U. C., Horn, P., Koch, A., Holtkamp, M., Gabriel, S., Gerevich, Z., & Heinemann, U. (2016). Adenosine A1 receptor-mediated suppression of carbamazepine-resistant seizure-like events in human neocortical slices. *Epilepsia*, *57*(5), 746–756. https://doi.org/10.1111/epi.13360

Klapper, S. D., Garg, P., Dagar, S., Lenk, K., Gottmann, K., & Nieweg, K. (2019). Astrocyte lineage cells are essential for functional neuronal differentiation and synapse maturation in human iPSC-derived neural networks. *GLIA*, *67*(10), 1893–1909. https://doi.org/10.1002/glia.23666

Kodandaramaiah, S. B., Franzesi, G. T., Chow, B. Y., Boyden, E. S., & Forest, C. R. (2012). Automated whole-cell patch-clamp electrophysiology of neurons in vivo. *Nature*

Methods, *9*(6), 585–587. https://doi.org/10.1038/nmeth.1993

Koseki, N., Deguchi, J., Yamashita, A., Miyawaki, I., & Funabashi, H. (2014). Establishment of a novel experimental protocol for drug-induced seizure liability screening based on a locomotor activity assay in zebrafish. In *Journal of Toxicological Sciences* (Vol. 39, Issue 4). Japanese Society of Toxicology. https://doi.org/10.2131/jts.39.579

Kreir, M., Van Deuren, B., Versweyveld, S., De Bondt, A., Van den Wyngaert, I., Van der Linde, H., Lu, H. R., Teuns, G., & Gallacher, D. J. (2018). Do in vitro assays in rat primary neurons predict drug-induced seizure liability in humans? *Toxicology and Applied Pharmacology*, *346*, 45–57. https://doi.org/10.1016/j.taap.2018.03.028

Kuijlaars, J., Oyelami, T., Diels, A., Rohrbacher, J., Versweyveld, S., Meneghello, G., Tuefferd, M., Verstraelen, P., Detrez, J. R., Verschuuren, M., De Vos, W. H., Meert, T., Peeters, P. J., Cik, M., Nuydens, R., Brône, B., & Verheyen, A. (2016). Sustained synchronized neuronal network activity in a human astrocyte co-culture system. *Scientific Reports*, *6*. https://doi.org/10.1038/srep36529

Kumar, K. K., Aboud, A. A., & Bowman, A. B. (2012). The potential of induced pluripotent stem cells as a translational model for neurotoxicological risk. In *NeuroToxicology* (Vol. 33, Issue 3, pp. 518–529). https://doi.org/10.1016/j.neuro.2012.02.005

Lancaster, M. A., & Knoblich, J. A. (2014a). Organogenesisin a dish: Modeling development and disease using organoid technologies. In *Science* (Vol. 345, Issue 6194). American Association for the Advancement of Science. https://doi.org/10.1126/science.1247125

Lancaster, M. A., & Knoblich, J. A. (2014b). Generation of cerebral organoids from human pluripotent stem cells. *Nature Protocols*, *9*(10), 2329–2340. https://doi.org/10.1038/nprot.2014.158

Lancaster, M. A., Renner, M., Martin, C. A., Wenzel, D., Bicknell, L. S., Hurles, M. E., Homfray, T., Penninger, J. M., Jackson, A. P., & Knoblich, J. A. (2013). Cerebral organoids model human brain development and microcephaly. *Nature*, *501*(7467), 373–379. https://doi.org/10.1038/nature12517

Lange, S. C., Bak, L. K., Waagepetersen, H. S., Schousboe, A., & Norenberg, M. D. (2012). Primary cultures of astrocytes: Their value in understanding astrocytes in health and disease. In *Neurochemical Research* (Vol. 37, Issue 11, pp. 2569–2588). NIH Public Access. https://doi.org/10.1007/s11064-012-0868-0

Larsen, B. R., Stoica, A., & MacAulay, N. (2016). Managing brain extracellular K+ during neuronal activity: The physiological role of the Na+/K+-ATPase subunit isoforms. In *Frontiers in Physiology* (Vol. 7, Issue APR). Frontiers Media S.A. https://doi.org/10.3389/fphys.2016.00141

Lattanzi, S., Brigo, F., Trinka, E., Zaccara, G., Cagnetti, C., Del Giovane, C., & Silvestrini, M. (2018). Efficacy and Safety of Cannabidiol in Epilepsy: A Systematic Review and Meta-Analysis. In *Drugs* (Vol. 78, Issue 17, pp. 1791–1804). Springer International Publishing. https://doi.org/10.1007/s40265-018-0992-5

Lauber, E., Filice, F., & Schwaller, B. (2016). Prenatal valproate exposure differentially affects parvalbumin-expressing neurons and related circuits in the cortex and striatum of mice. *Frontiers in Molecular Neuroscience*, *9*(DEC2016). https://doi.org/10.3389/fnmol.2016.00150

Lee, T. S., Bjørnsen, L. P., Paz, C., Kim, J. H., Spencer, S. S., Spencer, D. D., Eid, T., & Lanerolle,

N. C. (2006). GAT1 and GAT3 expression are differently localized in the human epileptogenic hippocampus. *Acta Neuropathologica*, *111*(4), 351–363. https://doi.org/10.1007/s00401-005-0017-9

Lein, P. J., Barnhart, C. D., & Pessah, I. N. (2011). Acute hippocampal slice preparation and hippocampal slice cultures. *Methods in Molecular Biology*, *758*, 115–134. https://doi.org/10.1007/978-1-61779-170-3_8

Lerche, H., Biervert, C., Alekov, A. K., Schleithoff, L., Lindner, M., Klingler, W., Bretschneider, F., Mitrovic, N., Jurkat-Rott, K., Bode, H., Lehmann-Horn, F., & Steinlein, O. K. (1999). A reduced K+ current due to a novel mutation in KCNQ2 causes neonatal convulsions. *Annals of Neurology*, *46*(3), 305–312. https://doi.org/10.1002/1531-8249(199909)46:3<305::AID-ANA5>3.0.CO;2-5

Leresche, N., Parri, H. R., Erdemli, G., Guyon, A., Turner, J. P., Williams, S. R., Asprodini, E., & Crunelli, V. (1998). On the action of the anti-absence drug ethosuximide in the rat and cat thalamus. *Journal of Neuroscience*, *18*(13), 4842–4853. https://doi.org/10.1523/jneurosci.18-13-04842.1998

Lerma, J. (2003). Roles and rules of kainate receptors in synaptic transmission. *Nature Reviews Neuroscience*, *4*(6), 481–495. https://doi.org/10.1038/nrn1118

Lesage, F. (2003). Pharmacology of neuronal background potassium channels. In *Neuropharmacology* (Vol. 44, Issue 1, pp. 1–7). Elsevier Ltd. https://doi.org/10.1016/S0028-3908(02)00339-8

Lévesque, M., Herrington, R., Hamidi, S., & Avoli, M. (2016). Interneurons spark seizure-like activity in the entorhinal cortex. *Neurobiology of Disease*, *87*, 91–101. https://doi.org/10.1016/j.nbd.2015.12.011

Librizzi, L., Losi, G., Marcon, I., Sessolo, M., Scalmani, P., Carmignoto, G., & De Curtis, M. (2017). Interneuronal network activity at the onset of seizure-like events in entorhinal cortex slices. *Journal of Neuroscience*, *37*(43), 10398–10407. https://doi.org/10.1523/JNEUROSCI.3906-16.2017

Lischka, F. W., Efthymiou, A., Zhou, Q., Nieves, M. D., McCormack, N. M., Wilkerson, M. D., Sukumar, G., Dalgard, C. L., & Doughty, M. L. (2018). Neonatal mouse cortical but not isogenic human astrocyte feeder layers enhance the functional maturation of induced pluripotent stem cell-derived neurons in culture. *GLIA*, *66*(4), 725–748. https://doi.org/10.1002/glia.23278

Liu, J., Saponjian, Y., Mahoney, M. M., Staley, K. J., & Berdichevsky, Y. (2017). Epileptogenesis in organotypic hippocampal cultures has limited dependence on culture medium composition. *PLoS ONE*, *12*(2). https://doi.org/10.1371/journal.pone.0172677

Liu, Yan, Liu, H., Sauvey, C., Yao, L., Zarnowska, E. D., & Zhang, S. C. (2013). Directed differentiation of forebrain GABA interneurons from human pluripotent stem cells. *Nature Protocols*, *8*(9), 1670–1679. https://doi.org/10.1038/nprot.2013.106

Liu, Yanan, Yan, Y., Inagaki, Y., Logan, S., Bosnjak, Z. J., & Bai, X. (2017). Insufficient astrocyte-derived brain-derived neurotrophic factor contributes to propofol-induced neuron death through Akt/Glycogen Synthase Kinase 3β/Mitochondrial Fission Pathway. *Anesthesia and Analgesia*, *125*(1), 241–254. https://doi.org/10.1213/ANE.0000000000002137

Loboda, A., & Armstrong, C. M. (2001). Resolving the gating charge movement associated with late transitions in K channel activation. *Biophysical Journal*, *81*(2), 905–916.

https://doi.org/10.1016/S0006-3495(01)75750-5

Löscher, W. (1981). Correlation between alterations in brain GABA metabolism and seizure excitability following administration of GABA aminotransferase inhibitors and valproic acid-a re-evaluation. *Neurochemistry International*, *3*(6), 397–404. https://doi.org/10.1016/0197-0186(81)90060-7

Löscher, Wolfgang. (2002). Basic pharmacology of valproate: A review after 35 years of clinical use for the treatment of epilepsy. In *CNS Drugs* (Vol. 16, Issue 10, pp. 669–694). Springer. https://doi.org/10.2165/00023210-200216100-00003

Lossin, C. (2009). A catalog of SCN1A variants. In *Brain and Development* (Vol. 31, Issue 2, pp. 114–130). Brain Dev. https://doi.org/10.1016/j.braindev.2008.07.011

Lutzu, S., & Castillo, P. E. (2020). Modulation of NMDA Receptors by G-protein-coupled receptors: Role in Synaptic Transmission, Plasticity and Beyond. In *Neuroscience*. Elsevier Ltd. https://doi.org/10.1016/j.neuroscience.2020.02.019

Ma, N.-X., Yin, J.-C., & Chen, G. (2019). Transcriptome Analysis of Small Molecule–Mediated Astrocyte-to-Neuron Reprogramming. *Frontiers in Cell and Developmental Biology*, *7*(May), 82. https://doi.org/10.3389/fcell.2019.00082

Mack, C. M., Lin, B. J., Turner, J. D., Johnstone, A. F. M., Burgoon, L. D., & Shafer, T. J. (2014). Burst and principal components analyses of MEA data for 16 chemicals describe at least three effects classes. *NeuroToxicology*, *40*, 75–85. https://doi.org/10.1016/j.neuro.2013.11.008

Magloire, V., Cornford, J., Lieb, A., Kullmann, D. M., & Pavlov, I. (2019). KCC2 overexpression prevents the paradoxical seizure-promoting action of somatic inhibition. *Nature Communications*, *10*(1), 1–13. https://doi.org/10.1038/s41467-019-08933-4

Malik, N., & Rao, M. S. (2013). A review of the methods for human iPSC derivation. *Methods in Molecular Biology*, *997*, 23–33. https://doi.org/10.1007/978-1-62703-348-0_3

Mank, M., & Griesbeck, O. (2008). Genetically encoded calcium indicators. In *Chemical Reviews* (Vol. 108, Issue 5, pp. 1550–1564). https://doi.org/10.1021/cr078213v

Manuel, M. N., Mi, D., Masonand, J. O., & Price, D. J. (2015). Regulation of cerebral cortical neurogenesis by the Pax6 transcription factor. In *Frontiers in Cellular Neuroscience* (Vol. 9). Frontiers Research Foundation. https://doi.org/10.3389/fncel.2015.00070

Maragakis, N. J., Dietrich, J., Wong, V., Xue, H., Mayer-Proschel, M., Rao, M. S., & Rothstein, J. D. (2004). Glutamate Transporter Expression and Function in Human Glial Progenitors. *GLIA*, *45*(2), 133–143. https://doi.org/10.1002/glia.10310

Marik, S. A., Yamahachi, H., McManus, J. N. J., Szabo, G., & Gilbert, C. D. (2010). Axonal dynamics of excitatory and inhibitory neurons in somatosensory cortex. *PLoS Biology*, *8*(6). https://doi.org/10.1371/journal.pbio.1000395

Maroof, A. M., Keros, S., Tyson, J. A., Ying, S. W., Ganat, Y. M., Merkle, F. T., Liu, B., Goulburn, A., Stanley, E. G., Elefanty, A. G., Widmer, H. R., Eggan, K., Goldstein, P. A., Anderson, S. A., & Studer, L. (2013). Directed differentiation and functional maturation of cortical interneurons from human embryonic stem cells. *Cell Stem Cell*, *12*(5), 559–572. https://doi.org/10.1016/j.stem.2013.04.008

Marrion, N. V., & Tavalin, S. J. (1998). Selective activation of Ca2+-activated K+ channels by co-localized Ca2+ channels in hippocampal neurons. *Nature*, *395*(6705), 900–905.

https://doi.org/10.1038/27674

Martin, D. P., Wallace, T. L., & Johnson, E. M. (1990). Cytosine arabinoside kills postmitotic neurons in a fashion resembling trophic factor deprivation: Evidence that a deoxycytidine-dependent process may be required for nerve growth factor signal transduction. *Journal of Neuroscience*, *10*(1), 184–193. https://doi.org/10.1523/jneurosci.10-01-00184.1990

Martini, F. J., Valiente, M., Bendito, G. L., Szabó, G., Moya, F., Valdeolmillos, M., & Marín, O. (2009). Biased selection of leading process branches mediates chemotaxis during tangential neuronal migration. *Development*, *136*(1), 41–50. https://doi.org/10.1242/dev.025502

Matsuda, N., Odawara, A., Katoh, H., Okuyama, N., Yokoi, R., & Suzuki, I. (2018). Detection of synchronized burst firing in cultured human induced pluripotent stem cell-derived neurons using a 4-step method. *Biochemical and Biophysical Research Communications*, *497*(2), 612–618. https://doi.org/10.1016/j.bbrc.2018.02.117

Mayer, M. L., Westbrook, G. L., & Guthrie, P. B. (1984). Voltage-dependent block by Mg2+ of NMDA responses in spinal cord neurones. *Nature*, *309*(5965), 261–263. https://doi.org/10.1038/309261a0

McConnell, E. R., McClain, M. A., Ross, J., LeFew, W. R., & Shafer, T. J. (2012). Evaluation of multi-well microelectrode arrays for neurotoxicity screening using a chemical training set. *NeuroToxicology*, *33*(5), 1048–1057. https://doi.org/10.1016/j.neuro.2012.05.001

McCormick, D. A., & Contreras, D. (2001). On The Cellular and Network Bases of Epileptic Seizures. *Annual Review of Physiology*, *63*(1), 815–846. https://doi.org/10.1146/annurev.physiol.63.1.815

Mergenthaler, P., Lindauer, U., Dienel, G. A., & Meisel, A. (2013). Sugar for the brain: The role of glucose in physiological and pathological brain function. In *Trends in Neurosciences* (Vol. 36, Issue 10, pp. 587–597). Trends Neurosci. https://doi.org/10.1016/j.tins.2013.07.001

Mertens, J., Marchetto, M. C., Bardy, C., & Gage, F. H. (2016). Evaluating cell reprogramming, differentiation and conversion technologies in neuroscience. In *Nature Reviews Neuroscience* (Vol. 17, Issue 7, pp. 424–437). Nature Publishing Group. https://doi.org/10.1038/nrn.2016.46

Moser, V. C. (2011). Functional Assays for Neurotoxicity Testing. *Toxicologic Pathology*, *39*(1), 36–45. https://doi.org/10.1177/0192623310385255

Mostert, M. M. C., Van De Pol, M., Van Echten, J., Olde Weghuis, D., Geurts Van Kessel, A., Oosterhuis, J. W., & Looijenga, L. H. J. (1996). Fluorescence in situ hybridization-based approaches for detection of 12p overrepresentation, in particular i(12p), in cell lines of human testicular germ cell tumors of adults. *Cancer Genetics and Cytogenetics*, *87*(2), 95–102. https://doi.org/10.1016/0165-4608(95)00233-2

Murray, S. A., Morgan, J. L., Kane, C., Sharma, Y., Heffner, C. S., Lake, J., & Donahue, L. R. (2010). Mouse gestation length is genetically determined. *PLoS ONE*, *5*(8). https://doi.org/10.1371/journal.pone.0012418

Nagao, M., Sugimori, M., & Nakafuku, M. (2007). Cross Talk between Notch and Growth Factor/Cytokine Signaling Pathways in Neural Stem Cells. *Molecular and Cellular Biology*, *27*(11), 3982–3994. https://doi.org/10.1128/mcb.00170-07

Nagelhus, E. A., Mathiisen, T. M., & Ottersen, O. P. (2004). Aquaporin-4 in the central nervous system: Cellular and subcellular distribution and coexpression with KIR4.1. *Neuroscience*, *129*(4), 905–913. https://doi.org/10.1016/j.neuroscience.2004.08.053

Nelson, B. R., Hartman, B. H., Georgi, S. A., Lan, M. S., & Reh, T. A. (2007). Transient inactivation of Notch signaling synchronizes differentiation of neural progenitor cells. *Developmental Biology*, *304*(2), 479–498. https://doi.org/10.1016/j.ydbio.2007.01.001

Neske, G.T., Patrick, S.L., & Connors, B.W. (2015). Contributions of Diverse Excitatory and Inhibitor Neurons to Recurrent Network Activity in Cerebral Cortex. *Journal of Neuroscience, 35*(3): 1089-1105. https://doi.org/10.1523/JNEUROSCI.2279-14.2015

Newland, C. F., & Cull-Candy, S. G. (1992). On the mechanism of action of picrotoxin on GABA receptor channels in dissociated sympathetic neurones of the rat. *The Journal of Physiology*, *447*(1), 191–213. https://doi.org/10.1113/jphysiol.1992.sp018998

Neymotin, S. A., McDougal, R. A., Sherif, M. A., Fall, C. P., Hines, M. L., & Lytton, W. W. (2015). Neuronal calcium wave propagation varies with changes in endoplasmic reticulum parameters: A computer model. In *Neural Computation* (Vol. 27, Issue 4, pp. 898–924). MIT Press Journals. https://doi.org/10.1162/NECO_a_00712

Nguyen, J. V., Soto, I., Kim, K. Y., Bushong, E. A., Oglesby, E., Valiente-Soriano, F. J., Yang, Z., Davis, C. H. O., Bedont, J. L., Son, J. L., Wei, J. O., Buchman, V. L., Zack, D. J., Vidal-Sanz, M., Ellisman, M. H., & Marsh-Armstrong, N. (2011). Myelination transition zone astrocytes are constitutively phagocytic and have synuclein dependent reactivity in glaucoma. *Proceedings of the National Academy of Sciences of the United States of America*, *108*(3), 1176–1181. https://doi.org/10.1073/pnas.1013965108

Nicholas, C. R., Chen, J., Tang, Y., Southwell, D. G., Chalmers, N., Vogt, D., Arnold, C. M., Chen, Y. J. J., Stanley, E. G., Elefanty, A. G., Sasai, Y., Alvarez-Buylla, A., Rubenstein, J. L. R., & Kriegstein, A. R. (2013). Functional maturation of hPSC-derived forebrain interneurons requires an extended timeline and mimics human neural development. *Cell Stem Cell*, *12*(5), 573–586. https://doi.org/10.1016/j.stem.2013.04.005

Nichols, J. M., & Kaplan, B. L. F. (2020). Immune Responses Regulated by Cannabidiol. *Cannabis and Cannabinoid Research*, *5*(1), 12–31. https://doi.org/10.1089/can.2018.0073

Nikolic, L., Nobili, P., Shen, W., & Audinat, E. (2019). Role of astrocyte purinergic signaling in epilepsy. *Glia*, glia.23747. https://doi.org/10.1002/glia.23747

Niu, W., Zang, T., Smith, D.K., Vue, T.Y., Zou, Y., Bachoo, R., Johnson, J.E., & Zhang, C.L. (2015). SOX2 Reprograms Resident Astorcytes into Neural Progenitors in the Adult Brain. *Stem Cell Reports*, *4*(5): 780-794. https://doi.org/10.1016/j.stemcr.2015.03.006

Oberheim, N. A., Takano, T., Han, X., He, W., Lin, J. H. C., Wang, F., Xu, Q., Wyatt, J. D., Pilcher, W., Ojemann, J. G., Ransom, B. R., Goldman, S. A., & Nedergaard, M. (2009). Uniquely hominid features of adult human astrocytes. *Journal of Neuroscience*, *29*(10), 3276–3287. https://doi.org/10.1523/JNEUROSCI.4707-08.2009

Odawara, A., Katoh, H., Matsuda, N., & Suzuki, I. (2016a). Induction of long-term potentiation and depression phenomena in human induced pluripotent stem cell-derived cortical neurons. *Biochemical and Biophysical Research Communications*, *469*(4), 856–862. https://doi.org/10.1016/j.bbrc.2015.12.087

Odawara, A., Katoh, H., Matsuda, N., & Suzuki, I. (2016b). Physiological maturation and drug responses of human induced pluripotent stem cell-derived cortical neuronal networks in

long-term culture. *Scientific Reports*, *6*. https://doi.org/10.1038/srep26181

Odawara, A., Matsuda, N., Ishibashi, Y., Yokoi, R., & Suzuki, I. (2018). Toxicological evaluation of convulsant and anticonvulsant drugs in human induced pluripotent stem cell-derived cortical neuronal networks using an MEA system. *Scientific Reports*, *8*(1), 1–11. https://doi.org/10.1038/s41598-018-28835-7

Odawara, A., Saitoh, Y., Alhebshi, A. H., Gotoh, M., & Suzuki, I. (2014). Long-term electrophysiological activity and pharmacological response of a human induced pluripotent stem cell-derived neuron and astrocyte co-culture. *Biochemical and Biophysical Research Communications*, *443*(4), 1176–1181. https://doi.org/10.1016/j.bbrc.2013.12.142

OECD. (2006). *Test Guidelines for the Chemicals*. http://www.oecd.org/env/ehs/testing/oecdguidelinesforthetestingofchemicals.htm

Olsen, R., & DeLorey, T. (2012). Cellular Neurochemistry and Neural Membranes. In G. Siegel, B. Agranoff, R. Albers, S. Fisher, & M. Uhler (Eds.), *Basic Neurochemistry: Molecular, Cellular and Medical Aspects* (6th ed., pp. 3–234). https://books.google.com/books?id=Af0IyHtGCMUC&pgis=1

Otaegi, G., Yusta-Boyo, M. J., Vergaño-Vera, E., Méndez-Gómez, H. R., Carrera, A. C., Abad, J. L., González, M., De la Rosa, E. J., Vicario-Abejón, C., & De Pablo, F. (2006). Modulation of the Pl 3-kinase-Akt signalling pathway by IGF-I and PTEN regulates the differentation of neural stem/precursor cells. *Journal of Cell Science*, *119*(13), 2739–2748. https://doi.org/10.1242/jcs.03012

Pacico, N., & Meur, A. M. Le. (2014). New in vitro phenotypic assay for epilepsy: Fluorescent measurement of synchronized neuronal calcium oscillations. *PLoS ONE*, *9*(1). https://doi.org/10.1371/journal.pone.0084755

Packard, A. I., Lin, B., & Schwob, J. E. (2016). Sox2 and Pax6 play counteracting roles in regulating neurogenesis within the murine olfactory epithelium. *PLoS ONE*, *11*(5). https://doi.org/10.1371/journal.pone.0155167

Pak, changhui, Pak, C., Grieder, S., Yang, N., Zhang, Y., Wernig, M., & Sudhof, T. (2018). Rapid generation of functional and homogeneous excitatory human forebrain neurons using Neurogenin-2 (Ngn2). *Protocol Exchange*. https://doi.org/10.1038/protex.2018.082

Park, I. H., Arora, N., Huo, H., Maherali, N., Ahfeldt, T., Shimamura, A., Lensch, M. W., Cowan, C., Hochedlinger, K., & Daley, G. Q. (2008). Disease-Specific Induced Pluripotent Stem Cells. *Cell*, *134*(5), 877–886. https://doi.org/10.1016/j.cell.2008.07.041

Parri, R., & Crunelli, V. (2003). An astrocyte bridge from synapse to blood flow. In *Nature Neuroscience* (Vol. 6, Issue 1, pp. 5–6). Nature Publishing Group. https://doi.org/10.1038/nn0103-5

Pasca, A. M., Sloan, S. A., Clarke, L. E., Tian, Y., Makinson, C. D., Huber, N., Kim, C. H., Park, J. Y., O'Rourke, N. A., Nguyen, K. D., Smith, S. J., Huguenard, J. R., Geschwind, D. H., Barres, B. A., & Pasca, S. P. (2015). Functional cortical neurons and astrocytes from human pluripotent stem cells in 3D culture. *Nature Methods*, *12*(7), 671–678. https://doi.org/10.1038/nmeth.3415

Pasti, L., Zonta, M., Pozzan, T., Vicini, S., & Carmignoto, G. (2001). Cytosolic Calcium Oscillations in Astrocytes May Regulate Exocytotic Release of Glutamate. In *Soc Neuroscience*. https://www.jneurosci.org/content/21/2/477.short

Paul, S. M., Mytelka, D. S., Dunwiddie, C. T., Persinger, C. C., Munos, B. H., Lindborg, S. R., & Schacht, A. L. (2010). How to improve RD productivity: The pharmaceutical industry's grand challenge. In *Nature Reviews Drug Discovery* (Vol. 9, Issue 3, pp. 203–214). Nature Publishing Group. https://doi.org/10.1038/nrd3078

Pena, F., & Tapia, R. (2000). Seizures and neurodegeneration induced by 4-aminopyridine in rat hippocampus in vivo: Role of glutamate- and GABA-mediated neurotransmission and of ion channels. *Neuroscience*, *101*(3), 547–561. https://doi.org/10.1016/S0306-4522(00)00400-0

Perea, G., Navarrete, M., & Araque, A. (2009). Tripartite synapses: astrocytes process and control synaptic information. In *Trends in Neurosciences* (Vol. 32, Issue 8, pp. 421–431). Trends Neurosci. https://doi.org/10.1016/j.tins.2009.05.001

Perreault, P., & Avoli, M. (1991). Physiology and pharmacology of epileptiform activity induced by 4-aminopyridine in rat hippocampal slices. *Journal of Neurophysiology*, *65*(4), 771–785. https://doi.org/10.1152/jn.1991.65.4.771

Perriot, S., Mathias, A., Perriard, G., Canales, M., Jonkmans, N., Merienne, N., Meunier, C., El Kassar, L., Perrier, A. L., Laplaud, D. A., Schluep, M., Déglon, N., & Du Pasquier, R. (2018). Human Induced Pluripotent Stem Cell-Derived Astrocytes Are Differentially Activated by Multiple Sclerosis-Associated Cytokines. *Stem Cell Reports*, *11*(5), 1199–1210. https://doi.org/10.1016/j.stemcr.2018.09.015

Perucca, E., French, J., & Bialer, M. (2007). Development of new antiepileptic drugs: challenges, incentives, and recent advances. In *Lancet Neurology* (Vol. 6, Issue 9, pp. 793–804). Lancet Neurol. https://doi.org/10.1016/S1474-4422(07)70215-6

Pfrieger, F. W., & Barres, B. A. (1997). Synaptic efficacy enhanced by glial cells in vitro. *Science*, *277*(5332), 1684–1687. https://doi.org/10.1126/science.277.5332.1684

Pickering, M., Pickering, B. W., Murphy, K. J., & O'Connor, J. J. (2008). Discrimination of cell types in mixed cortical culture using calcium imaging: A comparison to immunocytochemical labeling. *Journal of Neuroscience Methods*, *173*(1), 27–33. https://doi.org/10.1016/j.jneumeth.2008.05.014

Pirttimaki, T. M., Sims, R. E., Saunders, G., Antonio, S. A., Codadu, N. K., & Parri, H. R. (2017). Astrocyte-mediated neuronal synchronization properties revealed by false gliotransmitter release. *Journal of Neuroscience*, *37*(41), 9859–9870. https://doi.org/10.1523/JNEUROSCI.2761-16.2017

Pitkänen, A. (2010). Therapeutic approaches to epileptogenesis - Hope on the horizon. *Epilepsia*, *51*(SUPPL. 3), 2–17. https://doi.org/10.1111/j.1528-1167.2010.02602.x

Prat, A., Biernacki, K., Wosik, K., & Antel, J. P. (2001). Glial cell influence on the human blood-brain barrier. *GLIA*, *36*(2), 145–155. https://doi.org/10.1002/glia.1104

Pruunsild, P., Bengtson, C. P., & Bading, H. (2017). Networks of Cultured iPSC-Derived Neurons Reveal the Human Synaptic Activity-Regulated Adaptive Gene Program. *Cell Reports*, *18*(1), 122–135. https://doi.org/10.1016/j.celrep.2016.12.018

Quraishi, I. H., Stern, S., Mangan, K. P., Zhang, Y., Ali, S. R., Mercier, M. R., Marchetto, M. C., McLachlan, M. J., Jones, E. M., Gage, F. H., & Kaczmarek, L. K. (2019). An Epilepsy-Associated KCNT1 Mutation Enhances Excitability of Human iPSC-Derived Neurons by Increasing Slack KNa Currents. *The Journal of Neuroscience : The Official Journal of the Society for Neuroscience*, *39*(37), 7438–7449. https://doi.org/10.1523/JNEUROSCI.1628-

18.2019

Rabinowicz, T., De Courten-Myers, G. M., Petetot, J. M. C., Xi, G., & De Los Reyes, E. (1996). Human cortex development: Estimates of neuronal numbers indicate major loss late during gestation. *Journal of Neuropathology and Experimental Neurology*, *55*(3), 320–328. https://doi.org/10.1097/00005072-199603000-00007

Rahmati, N., Hoebeek, F. E., Peter, S., & De Zeeuw, C. I. (2018). Chloride homeostasis in neurons with special emphasis on the olivocerebellar system: Differential roles for transporters and channels. In *Frontiers in Cellular Neuroscience* (Vol. 12). Frontiers Media S.A. https://doi.org/10.3389/fncel.2018.00101

Raimondo, J. V., Burman, R. J., Katz, A. A., & Akerman, C. J. (2015). Ion dynamics during seizures. In *Frontiers in Cellular Neuroscience* (Vol. 9, Issue OCTOBER). Frontiers Research Foundation. https://doi.org/10.3389/fncel.2015.00419

Raponi, E., Agenes, F., Delphin, C., Assard, N., Baudier, J., Legraverend, C., & Deloulme, J. C. (2007). S100B expression defines a state in which GFAP-expressing cells lose their neural stem cell potential and acquire a more mature developmental stage. *GLIA*, *55*(2), 165–177. https://doi.org/10.1002/glia.20445

Rash, B. G., & Grove, E. A. (2007). Patterning the dorsal telencephalon: A role for sonic hedgehog? *Journal of Neuroscience*, *27*(43), 11595–11603. https://doi.org/10.1523/JNEUROSCI.3204-07.2007

Rasmussen, R., Nedergaard, M., & Petersen, N. C. (2016). Sulforhodamine 101, a widely used astrocyte marker, can induce cortical seizure-like activity at concentrations commonly used. *Scientific Reports*, *6*(1), 1–9. https://doi.org/10.1038/srep30433

Rassendren, F., & Audinat, E. (2016). Purinergic signaling in epilepsy. *Journal of Neuroscience Research*, *94*(9), 781–793. https://doi.org/10.1002/jnr.23770

Rhee, H. J., Shaib, A. H., Rehbach, K., Brose, N., Br€, O., & Rhee, J. S. (2019). An Autaptic Culture System for Standardized Analyses of iPSC-Derived Human Neurons. *CellReports*, *27*, 2212-2228.e7. https://doi.org/10.1016/j.celrep.2019.04.059

Riedemann, T. (2019). Diversity and function of somatostatin-expressing interneurons in the cerebral cortex. In *International Journal of Molecular Sciences* (Vol. 20, Issue 12). MDPI AG. https://doi.org/10.3390/ijms20122952

Robain, O., Barbin, G., Billette de Villemeur, T., Jardin, L., Jahchan, T., & Ben-Ari, Y. (1994). Development of mossy fiber synapses in hippocampal slice culture. *Developmental Brain Research*, *80*(1–2), 244–250. https://doi.org/10.1016/0165-3806(94)90109-0

Robinton, D. A., & Daley, G. Q. (2012). The promise of induced pluripotent stem cells in research and therapy. In *Nature* (Vol. 481, Issue 7381, pp. 295–305). https://doi.org/10.1038/nature10761

Rocktäschel, P., Sen, A., & Cader, M. Z. (2019). High glucose concentrations mask cellular phenotypes in a stem cell model of tuberous sclerosis complex. *Epilepsy and Behavior*, *101*. https://doi.org/10.1016/j.yebeh.2019.106581

Rogawski, M. A. (1992). The NMDA Receptor, NMDA Antagonists and Epilepsy Therapy: A Status Report. *Drugs*, *44*(3), 279–292. https://doi.org/10.2165/00003495-199244030-00001

Rogawski, M. A., Löscher, W., & Rho, J. M. (2016). Mechanisms of action of Antiseizure Drugs

and the Ketogenic diet. *Cold Spring Harbor Perspectives in Medicine*, *6*(5), 28. https://doi.org/10.1101/cshperspect.a022780

Ross, F. M., Brodie, M. J., & Stone, T. W. (1998). Modulation by adenine nucleotides of epileptiform activity in the CA3 region of rat hippocampal slices. *British Journal of Pharmacology*, *123*(1), 71–80. https://doi.org/10.1038/sj.bjp.0701586

Ross, F. M., Gwyn, P., Spanswick, D., & Davies, S. N. (2000). Carbenoxolone depresses spontaneous epileptiform activity in the CA1 region of rat hippocampal slices. *Neuroscience*, *100*(4), 789–796. https://doi.org/10.1016/S0306-4522(00)00346-8

Rothstein, J. D., Dykes-Hoberg, M., Pardo, C. A., Bristol, L. A., Jin, L., Kuncl, R. W., Kanai, Y., Hediger, M. A., Wang, Y., Schielke, J. P., & Welty, D. F. (1996). Knockout of glutamate transporters reveals a major role for astroglial transport in excitotoxicity and clearance of glutamate. *Neuron*, *16*(3), 675–686. https://doi.org/10.1016/S0896-6273(00)80086-0

Rubio, C., Rubio-Osornio, M., Retana-Marquez, S., Lopez, M., Custodio, V., & Paz, C. (2012). In Vivo Experimental Models of Epilepsy. *Central Nervous System Agents in Medicinal Chemistry*, *10*(4), 298–309. https://doi.org/10.2174/187152410793429746

Rudy, B., Fishell, G., Lee, S. H., & Hjerling-Leffler, J. (2011). Three groups of interneurons account for nearly 100% of neocortical GABAergic neurons. *Developmental Neurobiology*, *71*(1), 45–61. https://doi.org/10.1002/dneu.20853

Ruppersberg, J. P., Kitzing, E. V., & Schoepfer, R. (1994). The mechanism of magnesium block of nmda receptors. *Seminars in the Neurosciences*, *6*(2), 87–96. https://doi.org/10.1006/smns.1994.1012

Saber, W. A., Gasparoli, F. M., Dirks, M. G., Gunn-Moore, F. J., & Antkowiak, M. (2018). All-optical assay to study biological neural networks. *Frontiers in Neuroscience*, *12*(JUL). https://doi.org/10.3389/fnins.2018.00451

Sadler, T. W. (2005). Embryology of neural tube development. *American Journal of Medical Genetics - Seminars in Medical Genetics*, *135 C*(1), 2–8. https://doi.org/10.1002/ajmg.c.30049

Sahara, S., Yanagawa, Y., O'Leary, D. D. M., & Stevens, C. F. (2012). The fraction of cortical GABAergic neurons is constant from near the start of cortical neurogenesis to adulthood. *Journal of Neuroscience*, *32*(14), 4755–4761. https://doi.org/10.1523/JNEUROSCI.6412-11.2012

Sampath, D., Cortes, J., Estrov, Z., Du, M., Shi, Z., Andreeff, M., Gandhi, V., & Plunkett, W. (2006). Pharmacodynamics of cytarabine alone and in combination with 7-hydroxystaurosporine (UCN-01) in AML blasts in vitro and during a clinical trial. *Blood*, *107*(6), 2517–2524. https://doi.org/10.1182/blood-2005-08-3351

Sato, K., Akaishi, T., Matsuki, N., Ohno, Y., & Nakazawa, K. (2007). β-Estradiol induces synaptogenesis in the hippocampus by enhancing brain-derived neurotrophic factor release from dentate gyrus granule cells. *Brain Research*, *1150*(1), 108–120. https://doi.org/10.1016/j.brainres.2007.02.093

Scharfman, H. E. (2007). The neurobiology of epilepsy. In *Current Neurology and Neuroscience Reports* (Vol. 7, Issue 4, pp. 348–354). https://doi.org/10.1007/s11910-007-0053-z

Scheirer, C., Ray, W., Biometrics, N. H.-, & 1976, U. (1976). The analysis of ranked data derived from completely randomized factorial designs. *JSTOR*. https://www.jstor.org/stable/2529511?casa_token=EHJWOlr22egAAAAA:VrfQP1Gp9Zhx

Nps8XGP1rGa9ewpQYXDB2scZ5d1_AnxcNCNgTV6bM6-UZQBc_rDOglziMSYcsWvQiyhb5PrZfiLEKlD9764J-9EWPkWMQiKrkNHZqGA

Schick, V., Majores, M., Engels, G., Spitoni, S., Koch, A., Elger, C. E., Simon, M., Knobbe, C., Blümcke, I., & Becker, A. J. (2006). Activation of Akt independent of PTEN and CTMP tumor-suppressor gene mutations in epilepsy-associated Taylor-type focal cortical dysplasias. *Acta Neuropathologica*, *112*(6), 715–725. https://doi.org/10.1007/s00401-006-0128-y

Schwartzentruber, J., Foskolou, S., Kilpinen, H., Rodrigues, J., Alasoo, K., Knights, A., Patel, M., Goncalves, A., Ferreira, R., Benn, C. L., Wilbrey, A., Bictash, M., Impey, E., Cao, L., Lainez, S., Loucif, A. J., Whiting, P. J., Gutteridge, A., & Gaffney, D. (2017). Molecular and functional variation in iPSC-derived sensory neurons. *Molecular and Functional Variation in IPSC-Derived Sensory Neurons*, 095943. https://doi.org/10.1101/095943

Schwarz, N., Hedrich, U. B. S., Schwarz, H., Harshad, P. A., Dammeier, N., Auffenberg, E., Bedogni, F., Honegger, J. B., Lerche, H., Wuttke, T. V., & Koch, H. (2017). Human Cerebrospinal fluid promotes long-term neuronal viability and network function in human neocortical organotypic brain slice cultures. *Scientific Reports*, *7*(1). https://doi.org/10.1038/s41598-017-12527-9

Seidel, D., Jahnke, H. G., Englich, B., Girard, M., & Robitzki, A. A. (2017). In vitro field potential monitoring on a multi-microelectrode array for the electrophysiological long-term screening of neural stem cell maturation. *Analyst*, *142*(11), 1929–1937. https://doi.org/10.1039/c6an02713j

Semple, B. D., Blomgren, K., Gimlin, K., Ferriero, D. M., & Noble-Haeusslein, L. J. (2013). Brain development in rodents and humans: Identifying benchmarks of maturation and vulnerability to injury across species. In *Progress in Neurobiology* (Vols. 106–107, pp. 1–16). NIH Public Access. https://doi.org/10.1016/j.pneurobio.2013.04.001

Sepehri Rad, M., Choi, Y., Cohen, L. B., Baker, B. J., Zhong, S., Storace, D. A., & Braubach, O. R. (2017). Voltage and Calcium Imaging of Brain Activity. In *Biophysical Journal* (Vol. 113, Issue 10, pp. 2160–2167). Biophysical Society. https://doi.org/10.1016/j.bpj.2017.09.040

Serio, A., Bilican, B., Barmada, S. J., Ando, D. M., Zhao, C., Siller, R., Burr, K., Haghi, G., Story, D., Nishimura, A. L., Carrasco, M. A., Phatnani, H. P., Shum, C., Wilmut, I., Maniatis, T., Shaw, C. E., Finkbeiner, S., & Chandran, S. (2013). Astrocyte pathology and the absence of non-cell autonomy in an induced pluripotent stem cell model of TDP-43 proteinopathy. *Proceedings of the National Academy of Sciences of the United States of America*, *110*(12), 4697–4702. https://doi.org/10.1073/pnas.1300398110

Shaltouki, A., Peng, J., Liu, Q., Rao, M. S., & Zeng, X. (2013). Efficient generation of astrocytes from human pluripotent stem cells in defined conditions. *Stem Cells*, *31*(5), 941–952. https://doi.org/10.1002/stem.1334

Shi, Y., Kirwan, P., & Livesey, F. J. (2012). Directed differentiation of human pluripotent stem cells to cerebral cortex neurons and neural networks. *Nature Protocols*, *7*(10), 1836–1846. https://doi.org/10.1038/nprot.2012.116

Shi, Y., Kirwan, P., Smith, J., Robinson, H. P. C., & Livesey, F. J. (2012). Human cerebral cortex development from pluripotent stem cells to functional excitatory synapses. *Nature Neuroscience*, *15*(3), 477–486. https://doi.org/10.1038/nn.3041

Shih, J. J., Tatum, W. O., & Rudzinski, L. A. (2013). New drug classes for the treatment of partial onset epilepsy: Focus on perampanel. In *Therapeutics and Clinical Risk Management* (Vol.

9, Issue 1, pp. 285–293). Dove Press. https://doi.org/10.2147/TCRM.S37317

Shin, D. S. H., Yu, W., Fawcett, A., & Carlen, P. L. (2010). Characterizing the persistent CA3 interneuronal spiking activity in elevated extracellular potassium in the young rat hippocampus. *Brain Research*, *1331*, 39–50. https://doi.org/10.1016/j.brainres.2010.03.023

Shipley, M. M., Mangold, C. A., & Szpara, M. L. (2016). Differentiation of the SH-SY5Y human neuroblastoma cell line. *Journal of Visualized Experiments*, *2016*(108). https://doi.org/10.3791/53193

Siegel, M. S., & Isacoff, E. Y. (1997). A genetically encoded optical probe of membrane voltage. *Neuron*, *19*(4), 735–741. https://doi.org/10.1016/S0896-6273(00)80955-1

Simons, T. J. B. (1988). Calcium and neuronal function. In *Neurosurgical Review* (Vol. 11, Issue 2, pp. 119–129). Springer-Verlag. https://doi.org/10.1007/BF01794675

Smetters, D., Majewska, A., & Yuste, R. (1999). Detecting action potentials in neuronal populations with calcium imaging. *Methods: A Companion to Methods in Enzymology*, *18*(2), 215–221. https://doi.org/10.1006/meth.1999.0774

Smirnova, L., Block, K., Sittka, A., Oelgeschläger, M., Seiler, A. E. M., & Luch, A. (2014). MicroRNA profiling as tool for in vitro developmental neurotoxicity testing: The case of sodium valproate. *PLoS ONE*, *9*(6). https://doi.org/10.1371/journal.pone.0098892

Solenov, E., Watanabe, H., Manley, G. T., & Verkman, A. S. (2004). Sevenfold-reduced osmotic water permeability in primary astrocyte cultures from AQP-4-deficient mice, measured by a fluorescence quenching method. *American Journal of Physiology - Cell Physiology*, *286*(2 55-2). https://doi.org/10.1152/ajpcell.00298.2003

Somjen, G. G. (2002). Ion regulation in the brain: Implications for pathophysiology. In *Neuroscientist* (Vol. 8, Issue 3, pp. 254–267). SAGE Publications Inc. https://doi.org/10.1177/1073858402008003011

Soto, F., Bleckert, A., Lewis, R., Kang, Y., Kerschensteiner, D., Craig, A. M., & Wong, R. O. L. (2011). Coordinated increase in inhibitory and excitatory synapses onto retinal ganglion cells during development. *Neural Development*, *6*(1), 1–15. https://doi.org/10.1186/1749-8104-6-31

Soubannier, V., Maussion, G., Chaineau, M., Sigutova, V., Rouleau, G., Durcan, T., & Stifani, S. (2019). Characterization of human iPSC-derived astrocytes with potential for disease modeling and drug discovery. *BioRxiv*, 2019.12.28.890012. https://doi.org/10.1101/2019.12.28.890012

Spencer, S. S. (2002). Neural networks in human epilepsy: Evidence of and implications for treatment. *Epilepsia*, *43*(3), 219–227. https://doi.org/10.1046/j.1528-1157.2002.26901.x

Stafstrom, C. E. (2007). Persistent Sodium Current and Its Role in Epilepsy. *Epilepsy Currents*, *7*(1), 15–22. https://doi.org/10.1111/j.1535-7511.2007.00156.x

Stafstrom, C. E., & Carmant, L. (2015). Seizures and epilepsy: An overview for neuroscientists. *Cold Spring Harbor Perspectives in Biology*, *7*(5), 1–19. https://doi.org/10.1101/cshperspect.a022426

Staley, K. J., & Dudek, F. E. (2006). Interictal Spikes and Epileptogenesis. *Epilepsy Currents*, *6*(6), 199–202. https://doi.org/10.1111/j.1535-7511.2006.00145.x

Stasiukyniene, V., Pilvinis, V., Reingardiene, D., & Janauskaite, L. (2009). Epileptic seizures in

critically ill patients. In *Medicina* (Vol. 45, Issue 6, pp. 501–507). Kauno Medicinos Universitetas. https://doi.org/10.3390/medicina45060066

Steinlein, O. K., Lerche, H., Jurkat-Rott, K., Lehmann-Horn, F., & Steinlein, O. K. (2001). Ion channels and epilepsy. *American Journal of Medical Genetics*, *106*(2), 146–159. https://doi.org/10.1002/ajmg.1582

Stogsdill, J. A., Ramirez, J., Liu, D., Kim, Y. H., Baldwin, K. T., Enustun, E., Ejikeme, T., Ji, R. R., & Eroglu, C. (2017). Astrocytic neuroligins control astrocyte morphogenesis and synaptogenesis. *Nature*, *551*(7679), 192–197. https://doi.org/10.1038/nature24638

Sun, A. X., Ng, H. H., & Tan, E. K. (2018). Translational potential of human brain organoids. *Annals of Clinical and Translational Neurology*, *5*(2), 226–235. https://doi.org/10.1002/acn3.505

Sun, X., & Kaufman, P. D. (2018). Ki-67: more than a proliferation marker. In *Chromosoma* (Vol. 127, Issue 2, pp. 175–186). Springer Science and Business Media Deutschland GmbH. https://doi.org/10.1007/s00412-018-0659-8

Sünwoldt, J., Bosche, B., Meisel, A., & Mergenthaler, P. (2017). Neuronal culture microenvironments determine preferences in bioenergetic pathway use. *Frontiers in Molecular Neuroscience*, *10*. https://doi.org/10.3389/fnmol.2017.00305

Sypert, G. W., & Ward, A. A. (1974). Changes in extracellular potassium activity during neocortical propagated seizures. *Experimental Neurology*, *45*(1), 19–41. https://doi.org/10.1016/0014-4886(74)90097-1

Taga, A., Dastgheyb, R., Habela, C., Joseph, J., Richard, J., Gross, S. K., Lauria, G., Lee, G., Haughey, N., & Maragakis, N. J. (2019). Role of Human-Induced Pluripotent Stem Cell-Derived Spinal Cord Astrocytes in the Functional Maturation of Motor Neurons in a Multielectrode Array System. *STEM CELLS Translational Medicine*, *8*(12), 1272–1285. https://doi.org/10.1002/sctm.19-0147

Takahashi, K., & Yamanaka, S. (2006). Induction of Pluripotent Stem Cells from Mouse Embryonic and Adult Fibroblast Cultures by Defined Factors. *Cell*, *126*(4), 663–676. https://doi.org/10.1016/j.cell.2006.07.024

Tang, F., Hartz, A. M. S., & Bauer, B. (2017). Drug-resistant epilepsy: Multiple hypotheses, few answers. In *Frontiers in Neurology* (Vol. 8, Issue JUL). Frontiers Media S.A. https://doi.org/10.3389/fneur.2017.00301

Tang, X., Zhou, L., Wagner, A. M., Marchetto, M. C. N., Muotri, A. R., Gage, F. H., & Chen, G. (2013). Astroglial cells regulate the developmental timeline of human neurons differentiated from induced pluripotent stem cells. *Stem Cell Research*, *11*(2), 743–757. https://doi.org/10.1016/j.scr.2013.05.002

Tarczyluk, M. A., Nagel, D. A., Rhein Parri, H., Tse, E. H. Y., Brown, J. E., Coleman, M. D., & Hill, E. J. (2015). Amyloid β 1-42 induces hypometabolism in human stem cell-derived neuron and astrocyte networks. *Journal of Cerebral Blood Flow and Metabolism*, *35*(8), 1348–1357. https://doi.org/10.1038/jcbfm.2015.58

Tchieu, J., Calder, E. L., Guttikonda, S. R., Gutzwiller, E. M., Aromolaran, K. A., Steinbeck, J. A., Goldstein, P. A., & Studer, L. (2019). NFIA is a gliogenic switch enabling rapid derivation of functional human astrocytes from pluripotent stem cells. *Nature Biotechnology*, *37*(3), 267–275. https://doi.org/10.1038/s41587-019-0035-0

TCW, J., Wang, M., Pimenova, A. A., Bowles, K. R., Hartley, B. J., Lacin, E., Machlovi, S. I.,

Abdelaal, R., Karch, C. M., Phatnani, H., Slesinger, P. A., Zhang, B., Goate, A. M., & Brennand, K. J. (2017). An Efficient Platform for Astrocyte Differentiation from Human Induced Pluripotent Stem Cells. *Stem Cell Reports*, *9*(2), 600–614. https://doi.org/10.1016/j.stemcr.2017.06.018

Thurman, D. J., Beghi, E., Begley, C. E., Berg, A. T., Buchhalter, J. R., Ding, D., Hesdorffer, D. C., Hauser, W. A., Kazis, L., Kobau, R., Kroner, B., Labiner, D., Liow, K., Logroscino, G., Medina, M. T., Newton, C. R., Parko, K., Paschal, A., Preux, P. M., … Wiebe, S. (2011). Standards for epidemiologic studies and surveillance of epilepsy. *Epilepsia*, *52*(SUPPL. 7), 2–26. https://doi.org/10.1111/j.1528-1167.2011.03121.x

Tian, G. F., Azmi, H., Takano, T., Xu, Q., Peng, W., Lin, J., Oberheim, N. A., Lou, N., Wang, X., Zielke, H. R., Kang, J., & Nedergaard, M. (2005). An astrocytic basis of epilepsy. *Nature Medicine*, *11*(9), 973–981. https://doi.org/10.1038/nm1277

Tonekaboni, S. H., EBRAHIMI, A., BALI, M. K. B., OTAGHSARA, S. M. T., HOUSHMAND, M., NASEHI, M. M., TAGHDIRI, M. M., & MOGHADDASI, M. (2013). Sodium Channel Gene Mutations in Children with GEFS+ and Dravet Syndrome: A Cross Sectional Study. *Iranian Journal of Child Neurology*, *7*(2), 31–36. http://www.ncbi.nlm.nih.gov/pubmed/24665294%0Ahttp://www.pubmedcentral.nih.gov/articlerender.fcgi?artid=PMC3943035

Tosetti, P., Taglietti, V., & Toselli, M. (1998). Functional changes in potassium conductances of the human neuroblastoma cell line SH-SY5Y during in vitro differentiation. *Journal of Neurophysiology*, *79*(2), 648–658. https://doi.org/10.1152/jn.1998.79.2.648

Toyomoto, M., Inoue, S., Ohta, K., Kuno, S., Ohta, M., Hayashi, K., & Ikeda, K. (2005). Production of NGF, BDNF and GDNF in mouse astrocyte cultures is strongly enhanced by a cerebral vasodilator, ifenprodil. *Neuroscience Letters*, *379*(3), 185–189. https://doi.org/10.1016/j.neulet.2004.12.063

Traynelis, S. F., & Dingledine, R. (1988). Potassium-induced spontaneous electrographic seizures in the rat hippocampal slice. *Journal of Neurophysiology*, *59*(1), 259–276. https://doi.org/10.1152/jn.1988.59.1.259

Treiman, D. M. (2001). GABAergic mechanisms in epilepsy. *Epilepsia*, *42*(SUPPL. 3), 8–12. https://doi.org/10.1046/j.1528-1157.2001.042Suppl.3008.x

Trevelyan, A. J., & Schevon, C. A. (2013). How inhibition influences seizure propagation. In *Neuropharmacology* (Vol. 69, pp. 45–54). Neuropharmacology. https://doi.org/10.1016/j.neuropharm.2012.06.015

Trevelyan, A. J., Sussillo, D., Watson, B. O., & Yuste, R. (2006). Modular propagation of epileptiform activity: Evidence for an inhibitory veto in neocortex. *Journal of Neuroscience*, *26*(48), 12447–12455. https://doi.org/10.1523/JNEUROSCI.2787-06.2006

Trevelyan, A. J., Sussillo, D., & Yuste, R. (2007). Feedforward inhibition contributes to the control of epileptiform propagation speed. *Journal of Neuroscience*, *27*(13), 3383–3387. https://doi.org/10.1523/JNEUROSCI.0145-07.2007

Tukker, A. M., De Groot, M. W. G. D. M., Wijnolts, F. M. J., Kasteel, E. E. J., Hondebrink, L., & Westerink, R. H. S. (2016). Is the time right for in vitro neurotoxicity testing using human iPSC-derived neurons? *Limav.Org*. https://doi.org/10.14573/altex.1510091

Tukker, A. M., Wijnolts, F. M. J., de Groot, A., & Westerink, R. H. S. (2018). Human iPSC-derived neuronal models for in vitro neurotoxicity assessment. *NeuroToxicology*, *67*, 215–225.

https://doi.org/10.1016/j.neuro.2018.06.007

Tukker, A. M., Wijnolts, F. M. J., de Groot, A., Wubbolts, R. W., & Westerink, R. H. S. (2019). In vitro techniques for assessing neurotoxicity using human IPSC-derived neuronal models. In *Neuromethods* (Vol. 145, pp. 17–35). Humana Press Inc. https://doi.org/10.1007/978-1-4939-9228-7_2

Tyson, J. A., Goldberg, E. M., Maroof, A. M., Xu, Q., Petros, T. J., & Anderson, S. A. (2015). Duration of culture and sonic hedgehog signaling differentially specify PV versus SST cortical interneuron fates from embryonic stem cells. *Development (Cambridge)*, *142*(7), 1267–1278. https://doi.org/10.1242/dev.111526

Ueno, S., Bracamontes, J., Zorumski, C., Weiss, D. S., & Steinbach, J. H. (1997). Bicuculline and gabazine are allosteric inhibitors of channel opening of the GABA(A) receptor. *Journal of Neuroscience*, *17*(2), 625–634. https://doi.org/10.1523/JNEUROSCI.17-02-00625.1997

Uusisaari, M., Smirnov, S., Voipio, J., & Kaila, K. (2002). Spontaneous epileptiform activity mediated by GABAA receptors and gap junctions in the rat hippocampal slice following long-term exposure to GABAB antagonists. *Neuropharmacology*, *43*(4), 563–572. https://doi.org/10.1016/S0028-3908(02)00156-9

Vaillend, C., Mason, S. E., Cuttle, M. F., & Alger, B. E. (2002). Mechanisms of neuronal hyperexcitability caused by partial inhibition of Na+-K+-ATPases in the rat CA1 hippocampal region. *Journal of Neurophysiology*, *88*(6), 2963–2978. https://doi.org/10.1152/jn.00244.2002

Valdivia, P., Martin, M., LeFew, W. R., Ross, J., Houck, K. A., & Shafer, T. J. (2014). Multi-well microelectrode array recordings detect neuroactivity of ToxCast compounds. *NeuroToxicology*, *44*, 204–217. https://doi.org/10.1016/j.neuro.2014.06.012

Vardi, R., Goldental, A., Sardi, S., Sheinin, A., & Kanter, I. (2016). Simultaneous multi-patch-clamp and extracellular-array recordings: Single neuron reflects network activity. *Scientific Reports*, *6*, 36228–36228. https://doi.org/10.1038/srep36228

Vargas-Caballero, M., & Robinson, H. P. C. (2003). A slow fraction of Mg2+ unblock of NMDA receptors limits their contribution to spike generation in cortical pyramidal neurons. *Journal of Neurophysiology*, *89*(5), 2778–2783. https://doi.org/10.1152/jn.01038.2002

Vaughan, C. J., & Delanty, N. (2003). Pathophysiology of Acute Symptomatic Seizures. *Seizures*, 007–023. https://doi.org/10.1385/1-59259-094-2:007

Velazquez, J. L. P., & Carlen, P. L. (1999). Synchronization of GABAergic interneuronal networks during seizure-like activity in the rat horizontal hippocampal slice. *European Journal of Neuroscience*, *11*(11), 4110–4118. https://doi.org/10.1046/j.1460-9568.1999.00837.x

Verheyen, A., Diels, A., Dijkmans, J., Oyelami, T., Meneghello, G., Mertens, L., Versweyveld, S., Borgers, M., Buist, A., Peeters, P., & Cik, M. (2015). Using Human iPSC-Derived Neurons to Model TAU Aggregation. *PLOS ONE*, *10*(12), e0146127. https://doi.org/10.1371/journal.pone.0146127

Verstraelen, P., Pintelon, I., Nuydens, R., Cornelissen, F., Meert, T., & Timmermans, J. P. (2014). Pharmacological characterization of cultivated neuronal networks: Relevance to synaptogenesis and synaptic connectivity. *Cellular and Molecular Neurobiology*, *34*(5), 757–776. https://doi.org/10.1007/s10571-014-0057-6

Vierbuchen, T., Ostermeier, A., Pang, Z. P., Kokubu, Y., Südhof, T. C., & Wernig, M. (2010). Direct conversion of fibroblasts to functional neurons by defined factors. *Nature*,

463(7284), 1035–1041. https://doi.org/10.1038/nature08797

Vincelette, N. D., & Yun, S. (2014). Assessing the Mechanism of Cytarabine-Induced Killing in Acute Leukemia. *Blood*, *124*(21), 5210–5210. https://doi.org/10.1182/blood.v124.21.5210.5210

Volman, V., Bazhenov, M., & Sejnowski, T. J. (2012). Computational models of neuron-astrocyte interaction in epilepsy. *Frontiers in Computational Neuroscience*, *6*(AUGUST), 58. https://doi.org/10.3389/fncom.2012.00058

Volterra, A., Liaudet, N., & Savtchouk, I. (2014). Astrocyte Ca2+ signalling: An unexpected complexity. In *Nature Reviews Neuroscience* (Vol. 15, Issue 5, pp. 327–335). Nature Publishing Group. https://doi.org/10.1038/nrn3725

von Bartheld, C. S., Bahney, J., & Herculano-Houzel, S. (2016). The search for true numbers of neurons and glial cells in the human brain: A review of 150 years of cell counting. In *Journal of Comparative Neurology* (Vol. 524, Issue 18, pp. 3865–3895). Wiley-Liss Inc. https://doi.org/10.1002/cne.24040

Wallace, R. H., Scheffer, I. E., Barnett, S., Richards, M., Dibbens, L., Desai, R. R., Lerman-Sagie, T., Lev, D., Mazarib, A., Brand, N., Ben-Zeev, B., Goikhman, I., Singh, R., Kremmidiotis, G., Gardner, A., Sutherland, G. R., George, A. L., Mulley, J. C., & Berkovic, S. F. (2001). Neuronal sodium-channel β1-subunit mutations in generalized epilepsy with febrile seizures plus. *American Journal of Human Genetics*, *68*(4), 859–865. https://doi.org/10.1086/319516

Wallace, Robyn H., Wang, D. W., Singh, R., Scheffer, I. E., George, A. L., Phillips, H. A., Saar, K., Reis, A., W.johnson, E., Sutherland, G. R., Berkovic, S. F., & Mulley, J. C. (1998). Febrile seizures and generalized epilepsy associated with a mutation in the Na+-channel β1 subunit gene SCN1B. *Nature Genetics*, *19*(4), 366–370. https://doi.org/10.1038/1252

Wang, D. D., & Kriegstein, A. R. (2009). Defining the role of GABA in cortical development. *Journal of Physiology*, *587*(9), 1873–1879. https://doi.org/10.1113/jphysiol.2008.167635

Wang, F. wu, Hao, H. bo, Zhao, S. dou, Zhang, Y. min, Liu, Q., Liu, H. juan, Liu, S. ming, Yuan, Q. huan, Bing, L. jun, Ling, E. A., & Hao, A. jun. (2011). Roles of activated astrocyte in neural stem cell proliferation and differentiation. *Stem Cell Research*, *7*(1), 41–53. https://doi.org/10.1016/j.scr.2011.03.004

Wasserstrom, J. A., & Salata, J. J. (1988). Basis for tetrodotoxin and lidocaine effects on action potentials in dog ventricular myocytes. *The American Journal of Physiology*, *254*(6 Pt 2), H1157-66. https://doi.org/10.1152/ajpheart.1988.254.6.H1157

Wenzel, M., Hamm, J. P., Peterka, D. S., & Yuste, R. (2017). Reliable and Elastic Propagation of Cortical Seizures In Vivo. *Cell Reports*, *19*(13), 2681–2693. https://doi.org/10.1016/j.celrep.2017.05.090

Wetherington, J., Serrano, G., & Dingledine, R. (2008). Astrocytes in the Epileptic Brain. In *Neuron* (Vol. 58, Issue 2, pp. 168–178). Neuron. https://doi.org/10.1016/j.neuron.2008.04.002

Wickham, J., Brödjegård, N. G., Vighagen, R., Pinborg, L. H., Bengzon, J., Woldbye, D. P. D., Kokaia, M., & Andersson, M. (2018). Prolonged life of human acute hippocampal slices from temporal lobe epilepsy surgery. *Scientific Reports*, *8*(1), 1–13. https://doi.org/10.1038/s41598-018-22554-9

Wickham, Jenny, Corna, A., Schwarz, N., Uysal, B., Layer, N., Honegger, J. B., Wuttke, T. V.,

Koch, H., & Zeck, G. (2020). Human Cerebrospinal Fluid Induces Neuronal Excitability Changes in Resected Human Neocortical and Hippocampal Brain Slices. *Frontiers in Neuroscience*, *14*, 283. https://doi.org/10.3389/fnins.2020.00283

Will, Y., McDuffie, J. E., Olaharski, A. J., & Jeffy, B. D. (2016). Drug Discovery Toxicology: From Target Assessment to Translational Biomarkers. In *Drug Discovery Toxicology: From Target Assessment to Translational Biomarkers*. https://doi.org/10.1002/9781119053248

Winterer, G. (2003). Valproate and GABAergic System Effects [2]. In *Neuropsychopharmacology* (Vol. 28, Issue 11, pp. 2050–2051). European Association for Cardio-Thoracic Surgery. https://doi.org/10.1038/sj.npp.1300245

Wissel, K., Brandes, G., Pütz, N., Angrisani, G. L., Thieleke, J., Lenarz, T., & Durisin, M. (2018). Platinum corrosion products from electrode contacts of human cochlear implants induce cell death in cell culture models. *PLoS ONE*, *13*(5). https://doi.org/10.1371/journal.pone.0196649

Woehrling, E. K., Hill, E. J., & Coleman, M. (2010). Evaluation of the Importance of Astrocytes When Screening for Acute Toxicity in Neuronal Cell Systems. *Springer*, *17*(2), 103–113. https://doi.org/10.1007/s12640-009-9084-3

Woehrling, E. K., Hill, E. J., Nagel, D., & Coleman, M. D. (2013). Brain-derived neurotrophic factor as an indicator of chemical neurotoxicity: An animal-free CNS cell culture model. *ATLA Alternatives to Laboratory Animals*, *41*(6), 503–511. https://doi.org/10.1177/026119291304100613

Woehrling, E. K., Hill, E. J., Torr, E. E., & Coleman, M. (2011). Single-Cell ELISA and Flow Cytometry as Methods for Highlighting Potential Neuronal and Astrocytic Toxicant Specificity Toxicity of drugs and antioxidants View project Development of three-dimensional (3D) neuronal network derived from iPSCs with defined biological architecture View project. *Springer*, *19*(3), 472–483. https://doi.org/10.1007/s12640-010-9202-2

Woehrling, E. K., James Hill, E., Coleman, M., Woehrling, E., & Hill, E. (2007). Development of a neurotoxicity test-system, using human post-mitotic, astrocytic and neuronal cell lines in co-culture PBPK modelling in special populations View project Toxicity of drugs and antioxidants View project Development of a neurotoxicity test-system, using human post-mitotic, astrocytic and neuronal cell lines in co-culture. *Elsevier*. https://doi.org/10.1016/j.tiv.2007.04.011

Woehrling, E. K., Zilz, T. R., & Coleman, M. D. (2006). The toxicity of hexanedione isomers in neural and astrocytic cell lines. *Environmental Toxicology and Pharmacology*, *22*(3), 249–254. https://doi.org/10.1016/j.etap.2005.12.010

Wojcik, S. M., Rhee, J. S., Herzog, E., Sigler, A., Jahn, R., Takamori, S., Brose, N., & Rosenmund, C. (2004). An essential role for vesicular glutamate transporter 1 (VGLUT1) in postnatal development and control of quantal size. *Proceedings of the National Academy of Sciences of the United States of America*, *101*(18), 7158–7163. https://doi.org/10.1073/pnas.0401764101

Wolff, A. C., Domchek, S. M., Davidson, N. E., Sacchini, V., & McCormick, B. (2014). 91 - Cancer of the Breast. In J. E. Niederhuber, J. O. Armitage, J. H. Doroshow, M. B. Kastan, & J. E. Tepper (Eds.), *Abeloff's Clinical Oncology (Fifth Edition)* (Fifth Edit, pp. 1630-1692.e9). Content Repository Only! https://doi.org/https://doi.org/10.1016/B978-1-4557-2865-7.00091-6

Wong, E. H. F., Yocca, F., Smith, M. A., & Lee, C. M. (2010). Challenges and opportunities for drug discovery in psychiatric disorders: The drug hunters' perspective. In *International Journal of Neuropsychopharmacology* (Vol. 13, Issue 9, pp. 1269–1284). Oxford Academic. https://doi.org/10.1017/S1461145710000866

Wong, R. C. B., Lim, S. Y., Hung, S. S. C., Jackson, S., Khan, S., Van Bergen, N. J., De Smit, E., Liang, H. H., Kearns, L. S., Clarke, L., Mackey, D. A., Hewitt, A. W., Trounce, I. A., & Pébay, A. (2017). Mitochondrial replacement in an iPSC model of Leber's hereditary optic neuropathy. *Aging*, *9*(4), 1341–1350. https://doi.org/10.18632/aging.101231

Wu, X., Chen, P. S., Dallas, S., Wilson, B., Block, M. L., Wang, C. C., Kinyamu, H., Lu, N., Gao, X., Leng, Y., Chuang, D. M., Zhang, W., Lu, R. B., & Hong, J. S. (2008). Histone deacetylase inhibitors up-regulate astrocyte GDNF and BDNF gene transcription and protect dopaminergic neurons. *International Journal of Neuropsychopharmacology*, *11*(8), 1123–1134. https://doi.org/10.1017/S1461145708009024

Xicoy, H., Wieringa, B., & Martens, G. J. M. (2017). The SH-SY5Y cell line in Parkinson's disease research: a systematic review. In *Molecular Neurodegeneration* (Vol. 12, Issue 1, pp. 1–11). BioMed Central Ltd. https://doi.org/10.1186/s13024-017-0149-0

Xu, Q., Guo, L., Moore, H., Waclaw, R. R., Campbell, K., & Anderson, S. A. (2010). Sonic Hedgehog Signaling Confers Ventral Telencephalic Progenitors with Distinct Cortical Interneuron Fates. *Neuron*, *65*(3), 328–340. https://doi.org/10.1016/j.neuron.2010.01.004

Xu, Q., Wonders, C. P., & Anderson, S. A. (2005). Sonic hedgehog maintains the identity of cortical interneuron progenitors in the ventral telencephalon. *Development*, *132*(22), 4987–4998. https://doi.org/10.1242/dev.02090

Xu, W. S., Parmigiani, R. B., & Marks, P. A. (2007). Histone deacetylase inhibitors: Molecular mechanisms of action. In *Oncogene* (Vol. 26, Issue 37, pp. 5541–5552). Nature Publishing Group. https://doi.org/10.1038/sj.onc.1210620

Yaari, Y., Konnerth, A., & Heinemann, U. (1983). Spontaneous epileptiform activity of ca1 hippocampal neurons in low extracellular calcium solutions. *Experimental Brain Research*, *51*(1), 153–156. https://doi.org/10.1007/BF00236813

Yaari, Y., Konnerth, A., & Heinemann, U. (1986). Nonsynaptic epileptogenesis in the mammalian hippocampus in vitro. II. Role of extracellular potassium. *Journal of Neurophysiology*, *56*(2), 424–438. https://doi.org/10.1152/jn.1986.56.2.424

Yang, N., Ng, Y. H., Pang, Z. P., Südhof, T. C., & Wernig, M. (2011). Induced neuronal cells: How to make and define a neuron. In *Cell Stem Cell* (Vol. 9, Issue 6, pp. 517–525). NIH Public Access. https://doi.org/10.1016/j.stem.2011.11.015

Ye, H., & Kaszuba, S. (2017). Inhibitory or excitatory? Optogenetic interrogation of the functional roles of GABAergic interneurons in epileptogenesis. *Journal of Biomedical Science*, *24*(1). https://doi.org/10.1186/s12929-017-0399-8

Yokoi, R., Okabe, M., Matsuda, N., Odawara, A., Karashima, A., & Suzuki, I. (2019). Impact of sleep–wake-associated neuromodulators and repetitive low-frequency stimulation on human iPSC-derived neurons. *Frontiers in Neuroscience*, *13*(MAY). https://doi.org/10.3389/fnins.2019.00554

Yu, J., Vodyanik, M. A., Smuga-Otto, K., Antosiewicz-Bourget, J., Frane, J. L., Tian, S., Nie, J., Jonsdottir, G. A., Ruotti, V., Stewart, R., Slukvin, I. I., & Thomson, J. A. (2007). Induced

pluripotent stem cell lines derived from human somatic cells. *Science*, *318*(5858), 1917–1920. https://doi.org/10.1126/science.1151526

Yusuf, M., Leung, K., Morris, K. J., & Volpi, E. V. (2013). Comprehensive cytogenomic profile of the in vitro neuronal model SH-SY5Y. *Neurogenetics*, *14*(1), 63–70. https://doi.org/10.1007/s10048-012-0350-9

Zhang, B., & Wong, M. (2012). Pentylenetetrazole-induced seizures cause acute, but not chronic, mTOR pathway activation in rat. *Epilepsia*, *53*(3), 506–511. https://doi.org/10.1111/j.1528-1167.2011.03384.x

Zhang, S. (2014). Sox2, a key factor in the regulation of pluripotency and neural differentiation. *World Journal of Stem Cells*, *6*(3), 305. https://doi.org/10.4252/wjsc.v6.i3.305

Zhang, Y., Yu, Z., Jiang, D., Liang, X., Liao, S., Zhang, Z., Yue, W., Li, X., Chiu, S. M., Chai, Y. H., Liang, Y., Chow, Y., Han, S., Xu, A., Tse, H. F., & Lian, Q. (2016). iPSC-MSCs with High Intrinsic MIRO1 and Sensitivity to TNF-α Yield Efficacious Mitochondrial Transfer to Rescue Anthracycline-Induced Cardiomyopathy. *Stem Cell Reports*, *7*(4), 749–763. https://doi.org/10.1016/j.stemcr.2016.08.009

Zhu, Q., Naegele, J. R., & Chung, S. (2018). Cortical GABAergic Interneuron/Progenitor Transplantation as a Novel Therapy for Intractable Epilepsy. *Frontiers in Cellular Neuroscience*, *12*, 167. https://doi.org/10.3389/fncel.2018.00167

Appendix

A1: Achievements throughout PhD

Publications

Coleman, Michael & **Grainger, Alastair** & Parri, Harri & Hill, Eric. *In vitro human stem cell mediated CNS platforms: progress and challenges.* in Induced Pluripotent Stem Cells – Novel Concepts", Ed. Birbrair A., in press, in the series Advances in Stem Cell Biology, Elsevier Science.

Elsworthy, Richard & **Grainger, Alastair** & Fisher, Emily & Alqattan, Sarah & Hill, Eric & Aldred, Sarah. Amyloid-β precursor protein processing and oxidative stress are altered in human iPSC-derived neuron and astrocyte co-cultures carrying presenilin-1 gene mutations. In Press. Frontiers in Neuroscience.

Karikari, Thomas & Nagel, David & **Grainger, Alastair** & Bland, Charlotte & Hill, Eric & Moffat, Kevin. (2019). Preparation of stable tau oligomers for cellular and biochemical studies. Analytical Biochemistry. 566. 67-74.

Karikari, Thomas & Nagel, David & **Grainger, Alastair** & Bland, Charlotte & Crowe, James & Hill, Eric & Moffat, Kevin. (2019). Distinct Conformations, Aggregation and Cellular Internalization of Different Tau Strains. Frontiers in Cellular Neuroscience. 13. 296. 10.3389/fncel.2019.00296.

Grainger, Alastair & King, Marianne & Nagel, David & Parri, Harri & Coleman, Michael & Hill, Eric. (2018). In vitro Models for Seizure-Liability Testing Using Induced Pluripotent Stem Cells. Frontiers in Neuroscience. 12. 590. 10.3389/fnins.2018.00590.

Grainger, Alastair. (2017). Using neural stem cells for safety pharmacology studies. Blog post. https://www.axolbio.com/blog/guest-post-using-neural-stem-cells-for-safety-pharmacology-studies

Qualifications

- Postgraduate certificate in teaching and learning in higher education course completed. Grade: Distinction
- Achieved certification of fellowship of the Higher Education Authority

Awards

- British Neuroscience Association travel bursary for Conference Poster presentation in Dublin 2019 (£200)
- PrimerDesign Silver award

A2: Supplementary results

This Appendix contains a series of supplementary figures and graphs which are referred to in the main text.

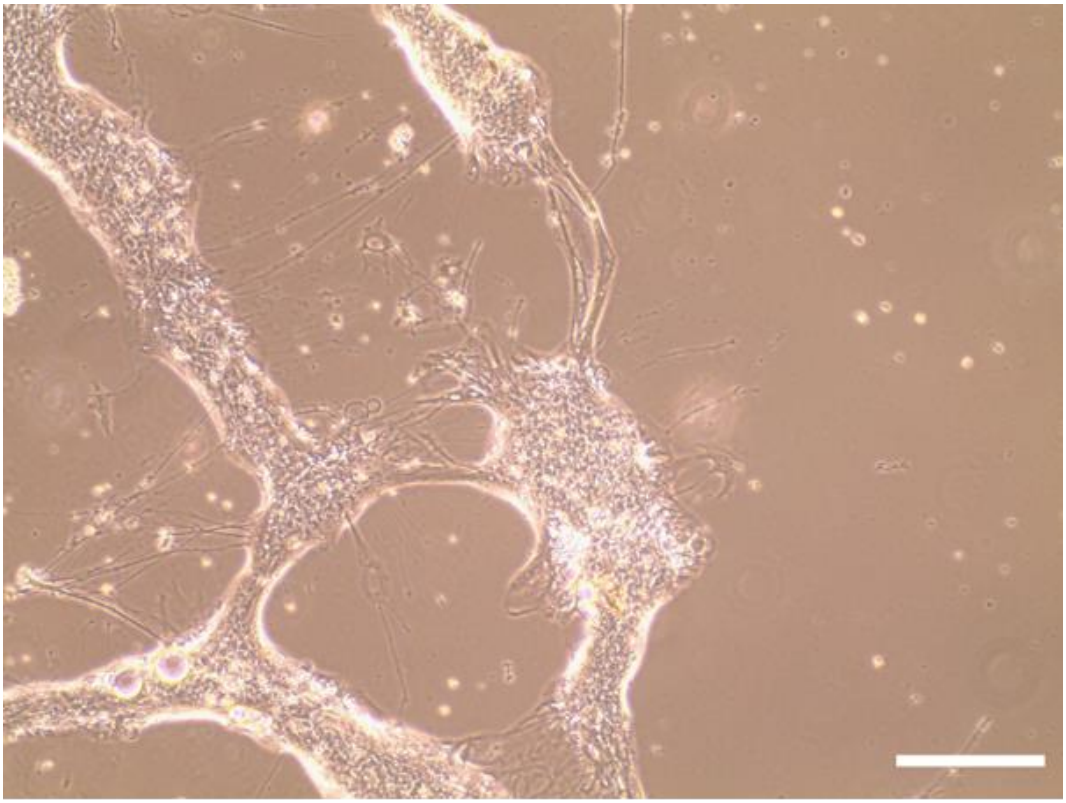

Figure A1: Representative figures showing detachment of neurons in SCT media at 18 WIV. Cells cultured in SCT media formed extensive fasciculation of neurites and detached from the culture surface, with widespread death observed. N=3. Scale bar: 250 µM.

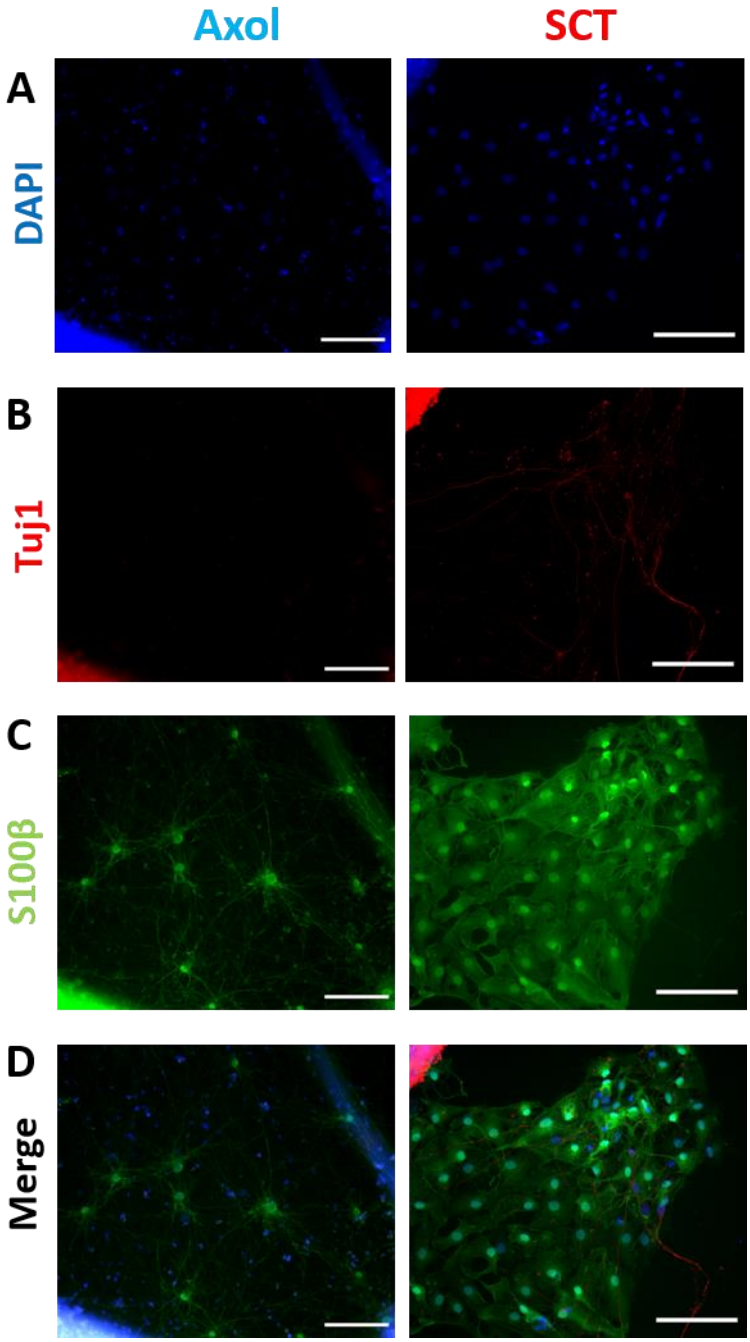

Figure A2: Spontaneously differentiated cultures at 18 WIV are heavily astrocytic. Neural cultures were differentiated in either Axol legacy or SCT BrainPhys media over 18 weeks and immunocytochemistry was performed to assess the relative quantities of neurons (Tuj1) and astrocytes (S100β in culture). (A) Nuclei stained with DAPI (Blue, excitation λ 345 nm, emission λ 455 nm). (B) Tuj1 neuronal staining (Red, excitation λ 588 nm, emission λ 649 nm). (C) S100β astrocyte staining (Green, excitation λ 495 nm, emission λ 519 nm). (D) Merged image of A,B,C. N=3. Scale bar: 100 µm.

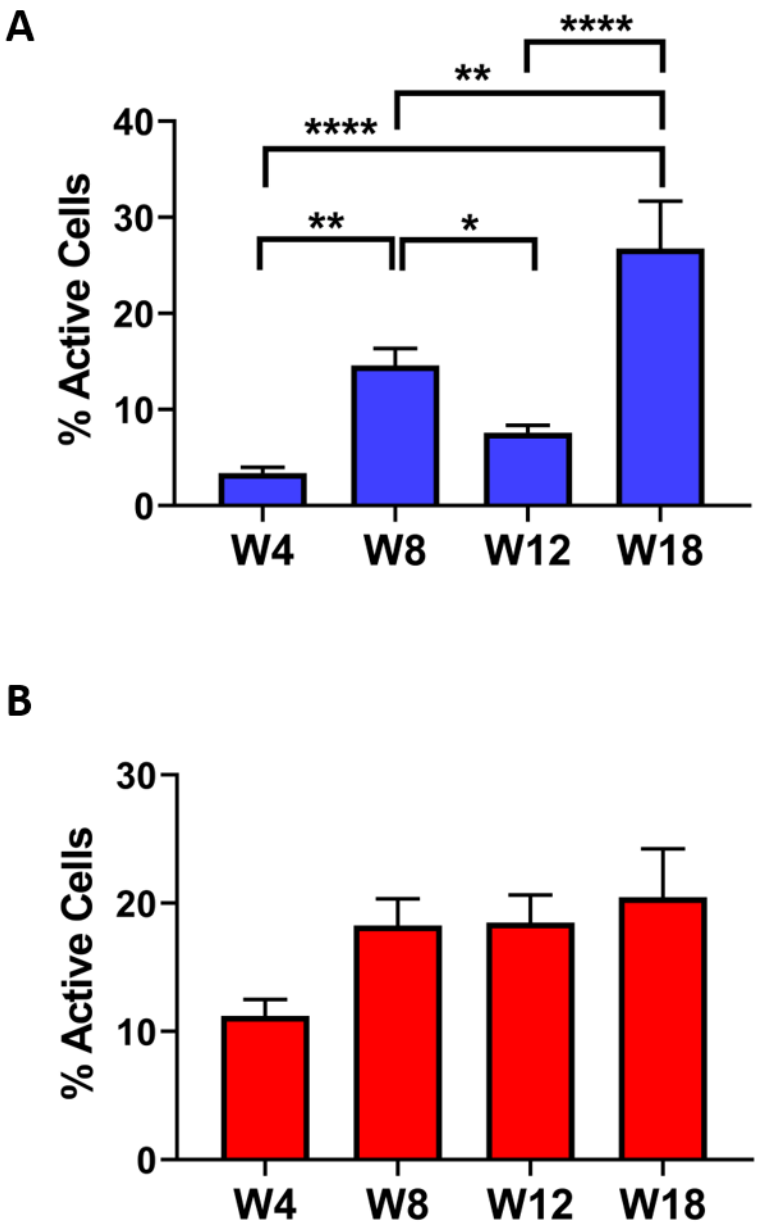

Figure A3: Activity over time of spontaneously differentiated cultures in Axol and SCT differentiation media. Neural cultures were differentiated in either Axol legacy or SCT BrainPhys media over 18 weeks and assessed intermittently for functional activity using fluorescent (Fluo4-AM) calcium imaging in aCSF perfusion. Active cells were determined as those with a minimum of one peak of calcium-mediated activity (peak > 3x s.d. baseline noise). (A) Axol-cultured cells over time (Blue). (B) SCT-cultured cells over time (Red). Data is displayed as mean ± SEM. N=3. *$p < 0.05$, **$p< 0.01$, ****$p< 0.0001$, one-way ANOVA with Tukey's.

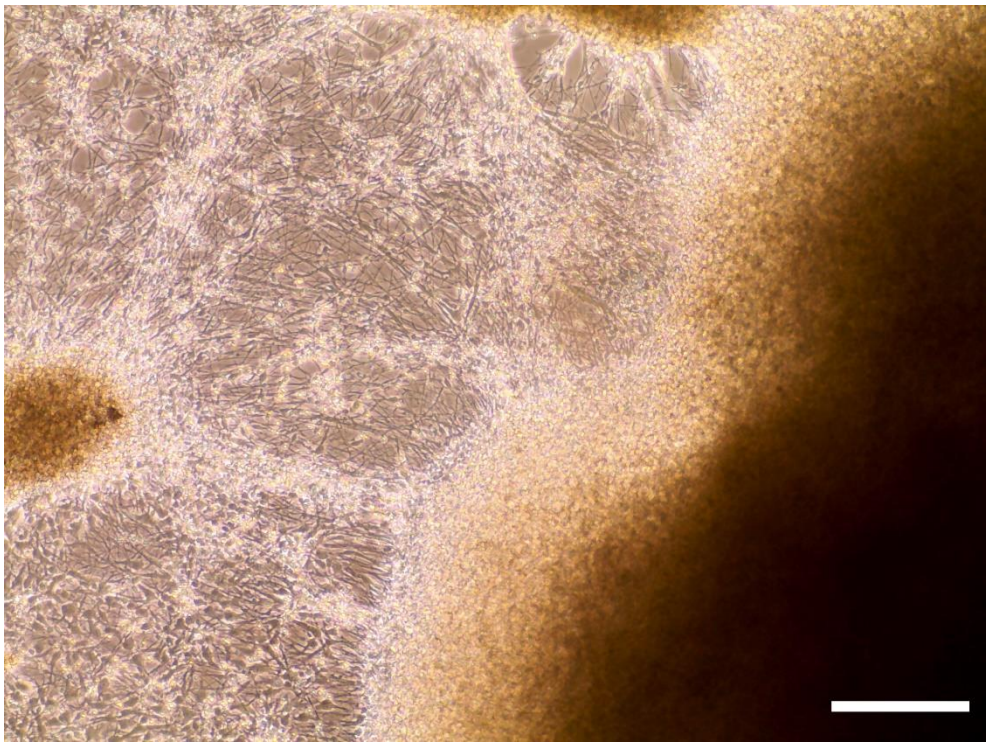

Figure A4: Spontaneously differentiated cultures at 18 WIV form large aggregates and clustering of cell bodies. Representative image of cultures differentiated over 18 WIV. Widespread clumping was observed in both Axol and SCT-cultured cells. N=3, both media conditions. Scale bar: 250 µM.

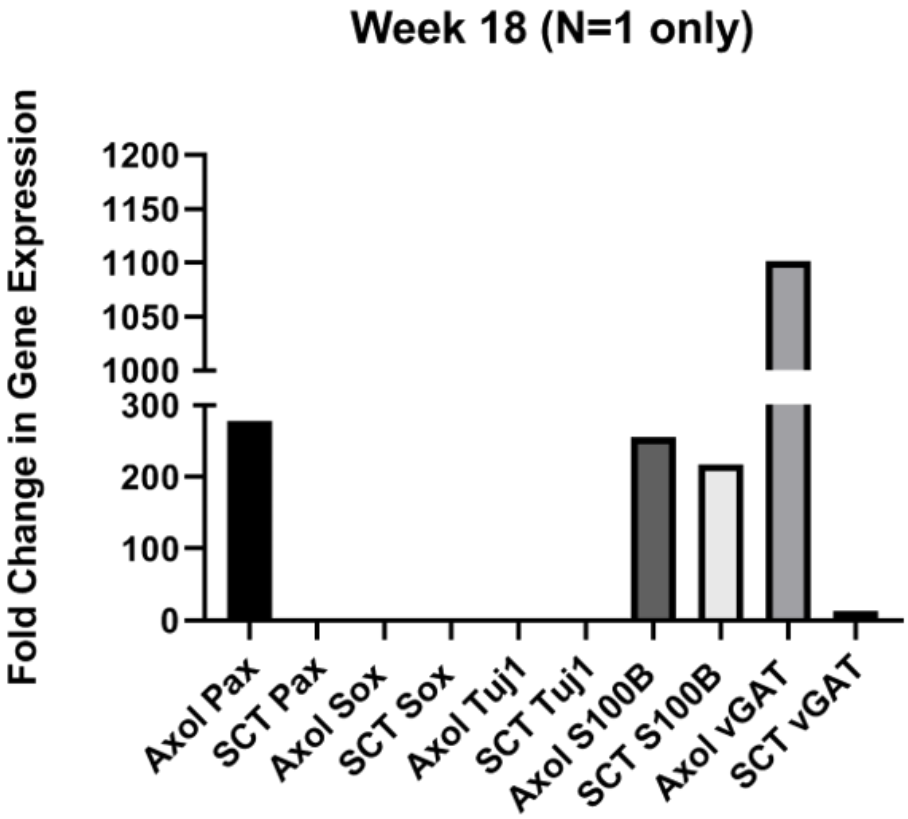

Figure A5: Spontaneously differentiated cultures in Axol express S100β and vGAT at 18 WIV. iPSC-derived neural precursors were differentiated in Axol or SCT media over 18 weeks and qPCR performed to assess the expression of neural progenitors Pax and Sox, neuronal cells (Tuj1), astrocytes (S100β) and inhibitory amino acid transporter vGAT. Fold change in expression is displayed as mean ± SEM. N=1.

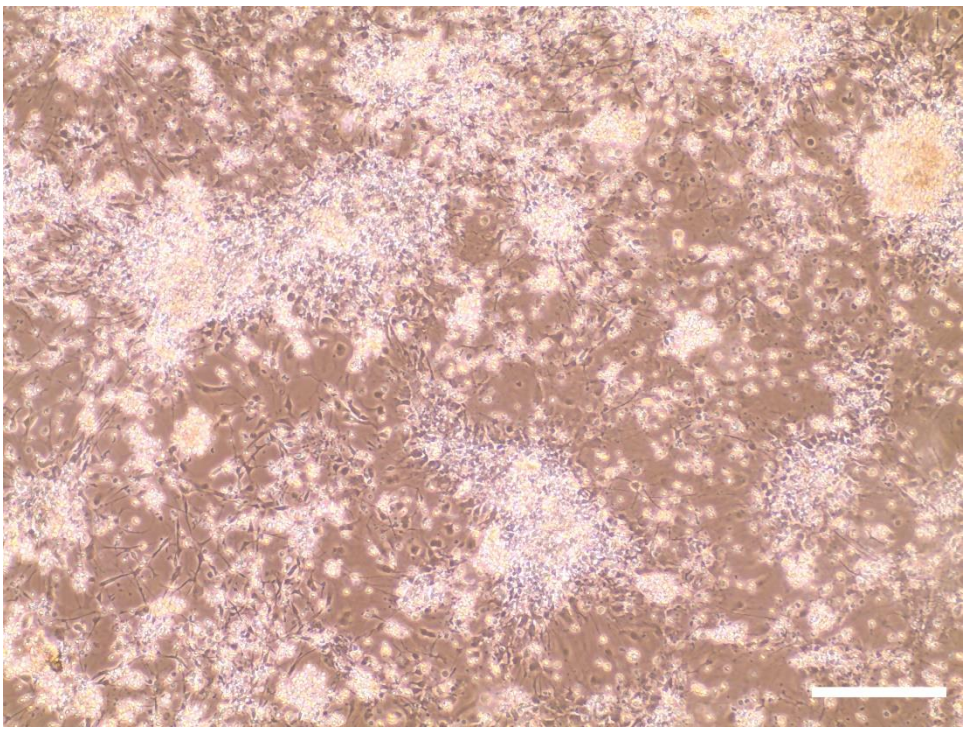

Figure A6: Representative figures showing detachment of DAPT-synchronised neurons at 7 WIV. NPCs cultured in sync media formed extensive fasciculation of neurites and detached from the culture surface, with widespread death observed. N=3. Scale bar: 250 μM.

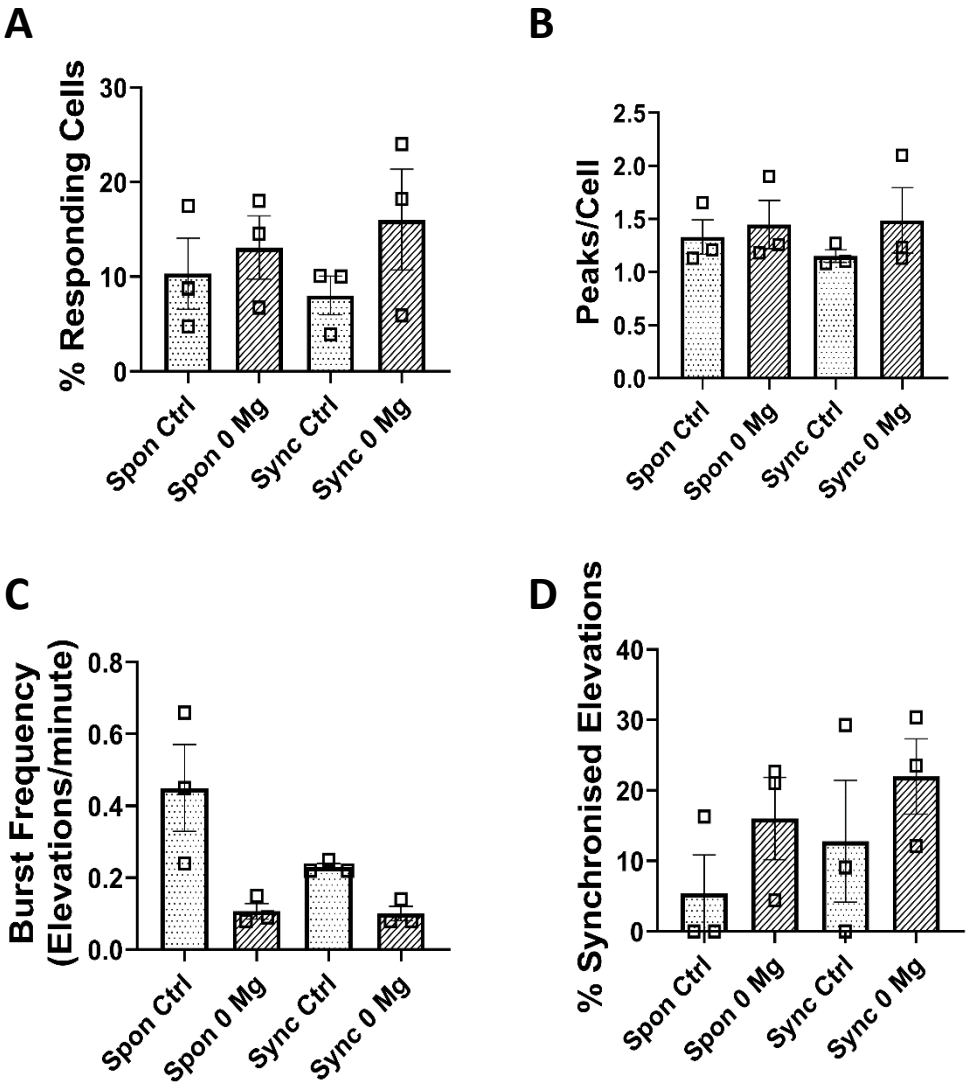

Figure A7: Zero-magnesium aCSF has no effect on 18 WIV co-cultures. Cultures were loaded with 5 µM Fluo4-AM for fluorescent calcium imaging. (A) Responding cells were determined as those with ≥ one peak of calcium activity. (B) Calcium peaks per active cell. (C) Frequency of calcium events per minute. (D) Percentage of synchronised cells of total active cells. N=3. 2-way ANOVA with Tukey's multiple comparisons.

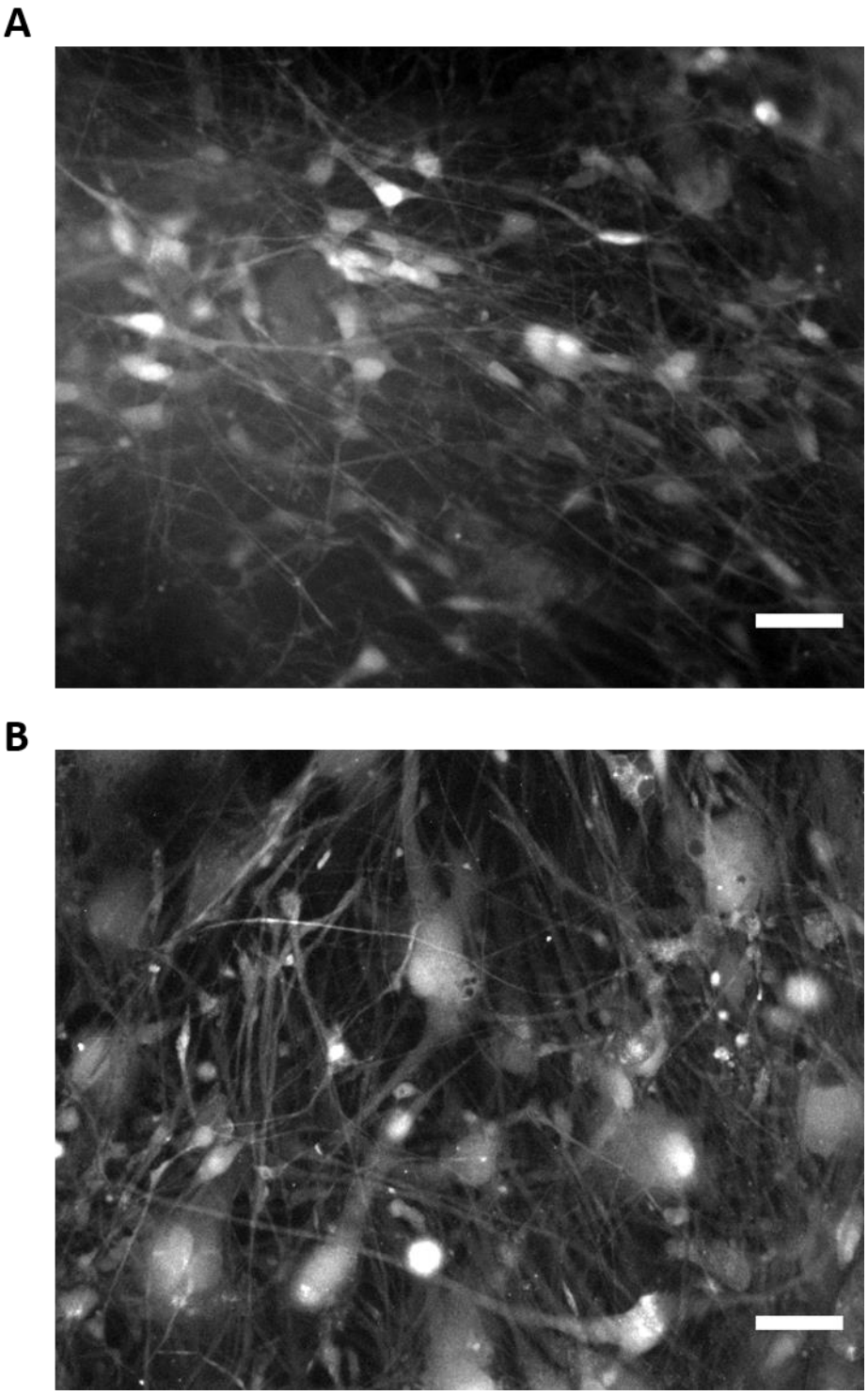

Figure A8: Example Synchronised and Spontaneous co-cultures show cells with astrocytic morphology. Spontaneous and synchronous co-cultures were differentiated over 18 WIV and fluorescent (Fluo4-AM) calcium imaging performed. Images were taken from the loaded cultures. **(A)** Synchronous co-cultures loaded with 5 µM Fluo4-AM appeared to display astrocytic processes and morphology. (B) Spontaneous co-cultures show large, characteristic astrocyte morphology. N=3. Scale bar: 10 µM.

A

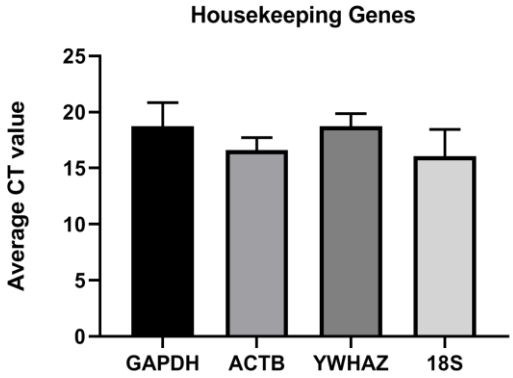

Gene	Mean	S.D.
GAPDH	18.74	2.114
Act	16.61	1.110
YWHAZ	18.73	1.122
18S	16.05	2.402

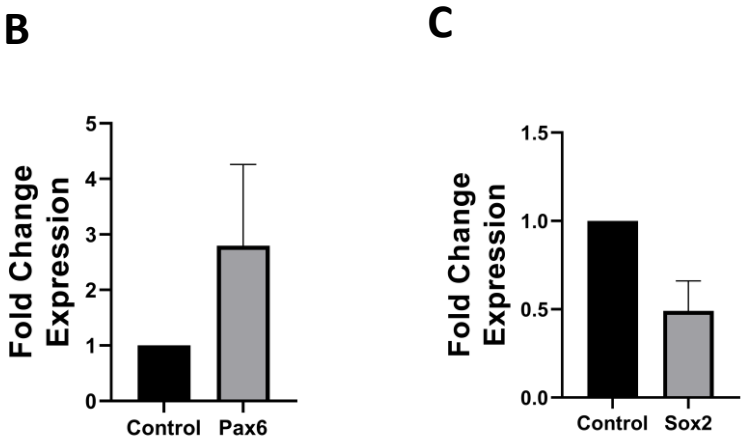

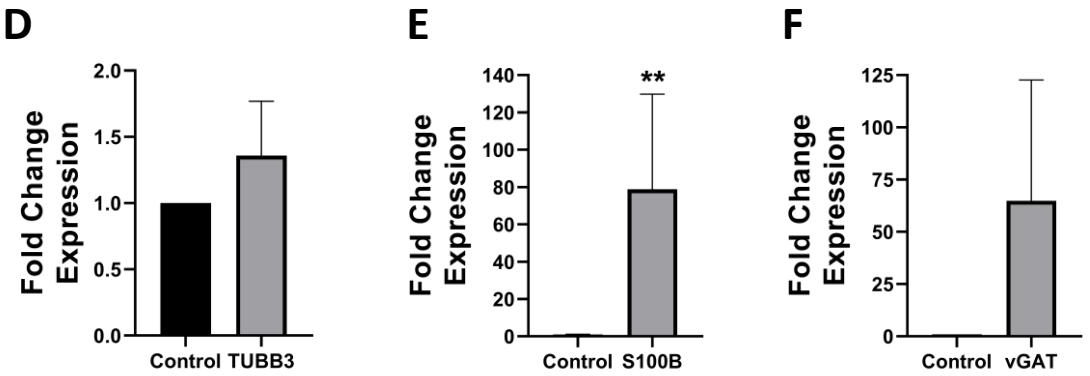

Figure A9: Housekeeping genes for endogenous controls and gene expression analysis of synchronised neuronal and astrocytic co-cultures. Top: Four endogenous control genes were tested to determine a suitable control for all qPCR analysis within the thesis. (**A**) Average Ct value for each housekeeping gene, with its corresponding mean value and standard deviation. Bottom: Co-cultures of synchronised neurons and astrocytes were differentiated over 12 WIV and qPCR was performed to assess the expression of progenitor genes Pax6 (**B**) and Sox2 (**C**), neuronal TUBB3 (**D**), astrocytic S100β (**E**) and inhibitory neuronal marker vGAT (**F**). Data is displayed as mean ± SEM. N=3. **p< 0.01, T-test.

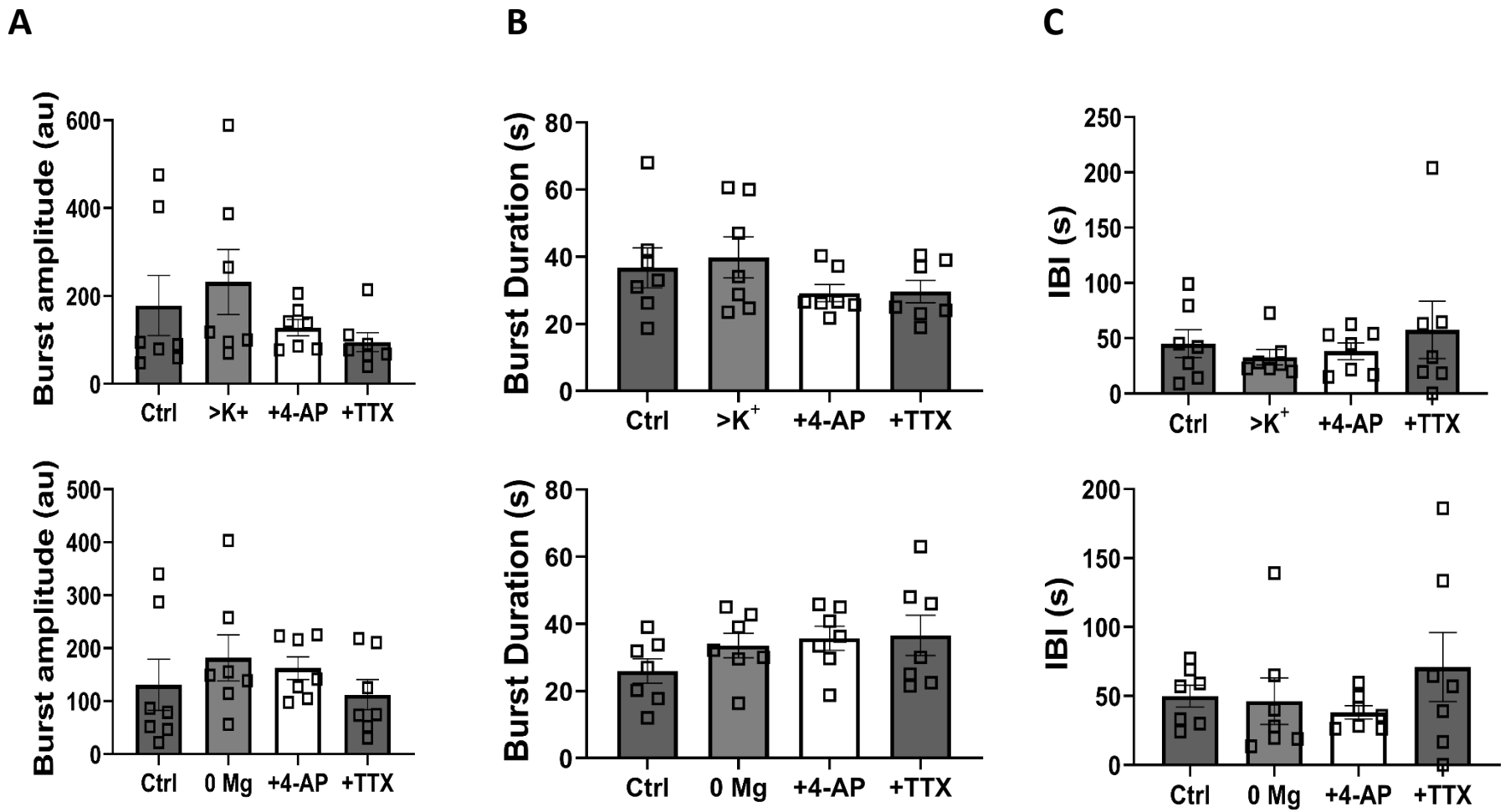

Figure A10: Tetrodotoxin perfusion effects on bursting activity in co-cultures of neurons and astrocytes exposed to different pro-ictogenic conditions. Human iPSC-derived neuronal and astrocytic co-cultures were cultured over 12 WIV and treated with various pro-ictogenic perfusions to elicit increased activity, followed by TTX. (**A**) Amplitude of calcium bursts. (**B**) Duration of calcium bursts. (**C**) Time between calcium bursts. N=3. 1-way ANOVA with Tukey's

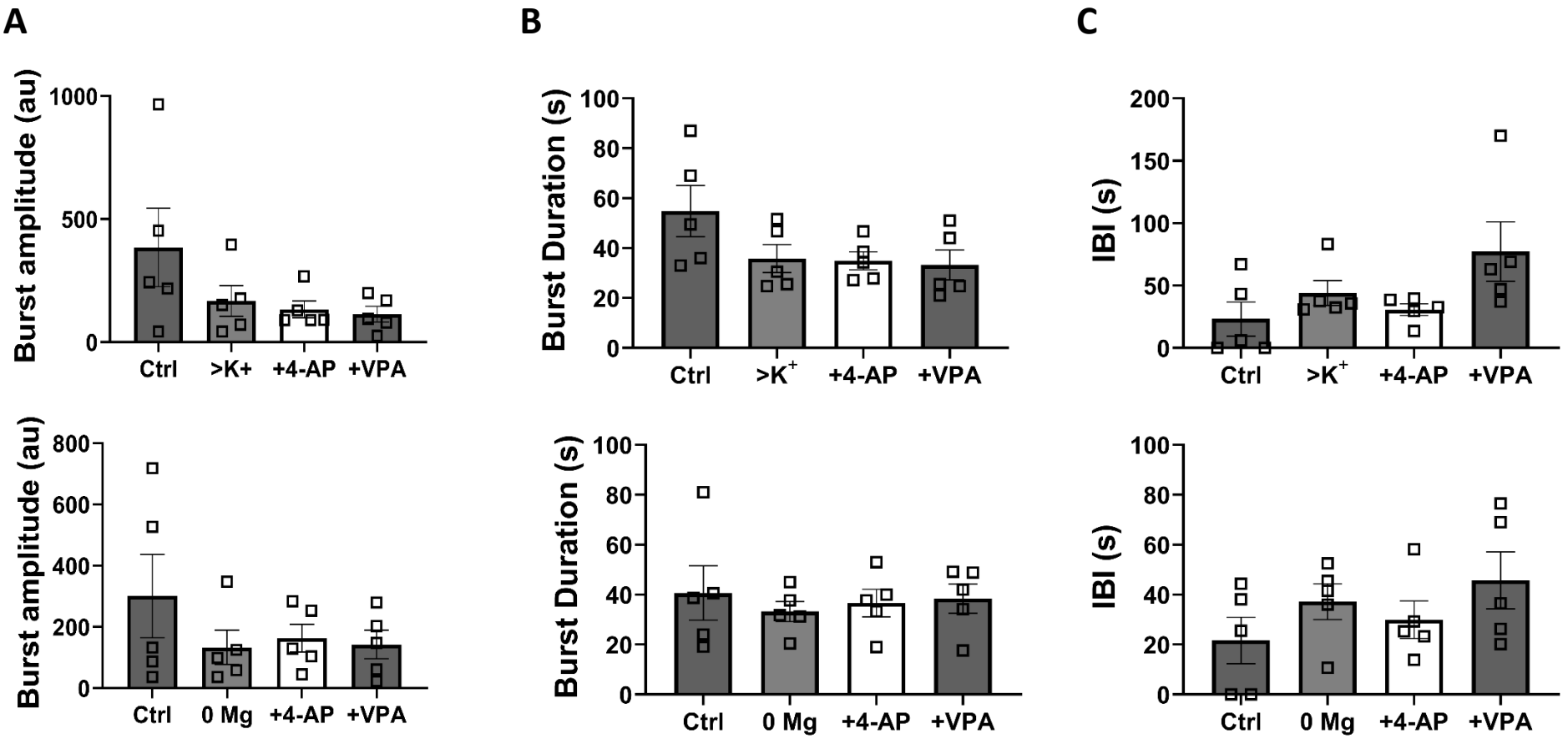

Figure A11: Sodium valproate perfusion effects on bursting activity in co-cultures of neurons and astrocytes exposed to different pro-ictogenic conditions. Human iPSC-derived neuronal and astrocytic co-cultures were cultured over 12 WIV and treated with various pro-ictogenic perfusions to elicit increased activity, followed by VPA. (**A**) Amplitude of calcium events. (**B**) Duration of calcium bursts. (**C**) Time between calcium bursts. N=3. 1-way ANOVA with Tukey's multiple comparisons.

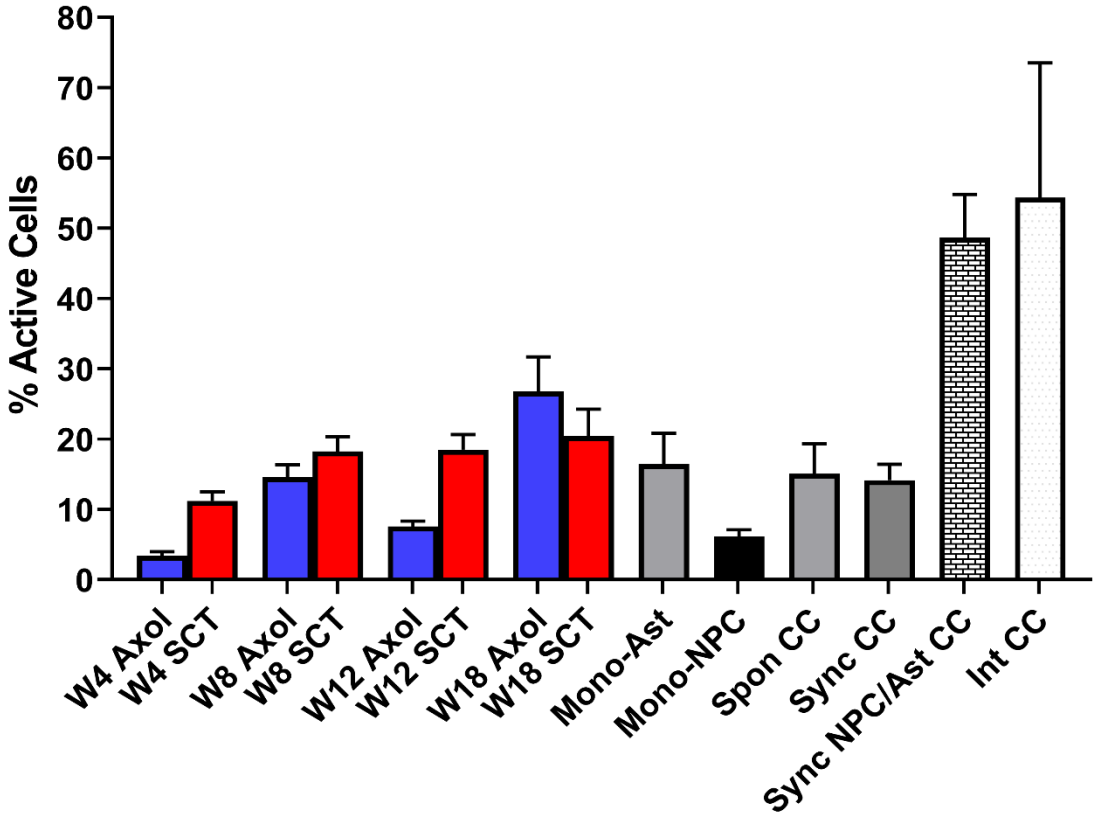

Culture Condition	% Active Cells Mean ± SEM	P-value from T-test
Axol W4 Spon	3.4 ± 0.58	<0.0001
SCT W4 Spon	11.22 ± 1.27	<0.0001
Axol W8 Spon	14.57 ± 1.77	<0.0001
SCT W8 Spon	18.25 ± 2.09	<0.0001
Axol W12 Spon	7.59 ± 0.75	<0.0001
SCT W12 Spon	18.50 ± 2.14	<0.0001
Axol W18 Spon	26.76 ± 4.93	0.007
SCT W18 Spon	20.47 ± 3.77	0.0001
Astrocyte mono	16.45 ± 4.36	0.0001
NPC mono	6.15 ± 0.94	<0.0001
Spon CC	15.07 ±4.27	0.007
Sync CC	14.19 ± 2.22	0.006
Sync astrocytes and NPC CC	48.65 ± 6.14	-

Figure 12A: Overall comparison. Percentage of active cells for every culture method tested in this thesis. Statistics in the lower table were calculated individually using t-test, purely to present the significantly increased activity observed in the co-culture method employed in Chapter 6.